eIF2B Bodies and their Role in the Control of

Protein Synthesis

Karl Francis Norris

A Thesis submitted in partial fulfillment of the

requirements of Sheffield Hallam University for the

degree of Doctor of Philosophy

June 2018

Dedication

In memory of James Norris - my Dad, who, when there was a difficult task at hand,

always said:

'… Will it kill you?'…

Well… Nearly… But not quite. I hope you are proud.

Contents

List of Figures

List of Tables

Abbreviations

α	Alpha
β	Beta
δ	Delta
Δ	Delta (delete)
γ	Gamma
ε	Epsilon
μ	Micro (prefix)
3-AT	3-amino-1,2,4-triazole
4E-BP	eIF4E-binding protein
A	Absorbance (prefix)
AA	Amino acids
ADP	Adenosine diphosphate
AMP-PNP	Adenylyl-imidodiphosphate
ATP	Adenosine triphosphate
BCA	Bicinchoninic acid assay
bp	Base pair
BSA	Bovine serum albumin
CD	Cytoplasmic domain
COP	Coat protein complex
CTD	C terminus domain
DEPC	Diethylpyrocarbonate
dH$_2$O	Deionised water
DNA	Deoxyribonucleic acid
dNTP	deoxynucleoside triphosphate
eIF	Eukaryotic initiation factor
ER	Endoplasmic reticulum
FRAP	Fluorescence recovery after photobleaching
GCD	General control derepressible
GCN	General control nonderepressible
GDF	GDI displacement factor
GDI	GDP dissociation inhibitor
GDP	Guanosine diphosphate
GEF	Guanine nucleotide exchange factor
GFP	Green fluorescent protein
GTP	Guanosine triphosphate
LB	Luri-Bertani
LDS	Lithium dodecyl sulfate
m	Monomeric (prefix)
M	Molar

m	Milli (prefix)
MP	Membrane protein
mRNA	Messenger RNA
OD	Optical density
OE-PCR	Overlap extension polymerase chain reaction
ONPG	2-Nitrophenyl β-D-galactopyranoside
P-bodies	Processing bodies
P:M	Polysome monosome ratio
PCR	Polymerase chain reaction
PI	phosphatidylinositol
PI(4)P	phosphatidylinositol 4-phosphate phosphatase
PI4K	PI 4-kinase
Ptdins(4)P	phosphatidylinositol 4-phosphate
qPCR	Quantitative polymerase chain reaction
RFP	Red fluorescent protein
RNA	Ribonucleic acid
SC	Synthetic complete
SCD	Synthetic complete dextrose
SDS	Sodium dodecyl sulfate
t½	Half time
TMD	Transmembrane domain
TOPO	Topoisomerase
TOR	Target of rapamycin
uORF	Upstream open reading frame
VLFA	Very long fatty acid chain
VWM	Vanishing white matter
WT	Wild type

Abstract

The eukaryotic initiation factor 2B (eIF2B) serves as a vital control point within translation initiation. eIF2B initiates translation by exchanging GDP for GTP on eIF2. However, this mechanism may be attenuated in response to cellular stress by the phosphorylation of eIF2, which paradoxically enhances the translation of stress-specific mRNA to instigate a stress response. Autosomal recessive mutations within eIF2B result in the disease leukoencephalopathy with vanishing white matter (VWM). Current models of VWM disease suggest that abnormal eIF2B results in the cell being in a constant state of stress. However, previous biochemical studies have illustrated that VWM mutations not only decrease the catalytic activity of eIF2B, but can increase activity or not affect it at all. Furthermore, changes in the activity eIF2B do not correlate with disease severity. These observations suggest that there may be additional characteristics of eIF2B contributing to VWM pathogenesis which remain to be elucidated.

In this study, we investigated whether the localisation of eIF2B to eIF2B bodies was integral for function. Using the yeast *S. cerevisiae,* we show that the regulatory subunit eIF2Bα is required for localisation. Interestingly, catalytic mutations in eIF2Bα localised eIF2B to several smaller foci, termed microbodies. *In vivo* FRAP analysis highlighted that eIF2 shuttles through microbodies slower than eIF2B bodies, indicating that localisation to eIF2B bodies may be required for full eIF2B activity. Surprisingly, phenotypes from eIF2Bα VWM missense mutations were highly variable in localisation, possibly recapitulating variable phenotypes observed in humans.

The putative membrane proteins Mst27p, Erp4p and Sac1p have been shown to associate with eIF2B. We therefore investigated whether they were required for the formation of eIF2B bodies. Deletion of membrane proteins did not significantly alter eIF2B localisation. Surprisingly however, deletion of the PI(4)P Sac1p reduced rates of translation initiation independently of eIF2B, highlighting a link between membrane integrity and translational control.

Acknowledgements

Coladas fo life) and have changed a work-a-holic into someone who now wants to try

and experience as much as I can. For that, and everything else, I am eternally grateful.

1. Introduction

1.1. General Introduction

Gene expression is coordinated by the processes of transcription and translation which is facilitated by various types of ribonucleic acids (RNA). Transcribed and processed in the nucleus before being exported into the cytosol, messenger RNA (mRNA) facilitates the flow of genetic information from DNA to protein. Once synthesised and exported to the cytosol, mRNA can be degraded, stored or translated depending on the integrity of the transcript as well as cellular conditions. During steady-state conditions the ribosome is recruited to the mRNA to synthesise the desired protein. In times of cellular stress however, transcripts can be translationally silenced and stored via translocation to stress granules. Alternatively, mRNAs may be targeted for degradation by localisation to processing bodies (P-bodies). Thus, the cellular production of proteins is an intricately regulated process that demonstrates layers of organisation, allowing cells to adapt and change the translatome in a quick, efficient and organised manner.

Under normal conditions, mRNA transcripts may undergo concurrent rounds of translation which is facilitated and controlled by eukaryotic initiation factors (eIFs). One of the key initiation factors is the guanine nucleotide exchange factor (GEF) eIF2B which controls the initiation of translation by regulating levels of GTP-bound eIF2. This initial event is subject to regulation in response to several cellular stresses, subsequently halting global protein synthesis allowing the cell to focus on reinstating cellular homeostasis. Intriguingly, inherited autosomal recessive mutations within any subunit of eIF2B are thought to result in constitutive stress responses which cause the fatal disease leukoencephalopathy with vanishing white matter (VWM).

In 2005, Campbell *et al.,* observed a new layer of translational organisation where eIF2B localised to discrete cytoplasmic foci termed eIF2B bodies. eIF2 also co-localised to these eIF2B bodies leading to the suggestion that eIF2B bodies were sites at which eIF2B function is controlled and regulated. Despite eIF2B's pivotal role in translation initiation, the exact purpose of the eIF2B body and how and why it is assembled remains unclear. In the last 10 years, high resolution structures of eIF2B have been solved which may help uncover how the eIF2B body is formed, providing novel insights into the role of the eIF2B body and its implication for disease. In this thesis, the role of eIF2B bodies in the regulation of translation initiation is further investigated with a particular focus on its implication to disease.

1.2. Protein synthesis

Translation is the process where genetic information is decoded from mRNA into polypeptide chains, and comprises a series of sub-processes; initiation, elongation, termination and ribosome recycling. In all living systems, protein synthesis is facilitated by the RNA/protein machinery known as the ribosome. In eukaryotes, the small 40S subunit and the large 60S subunit complete the 80S ribosome which contains three transfer RNA (tRNA) binding sites: the A, P and E sites. Aminoacyl-tRNAs pre-emptively occupy the A site, while the elongating peptide chain or peptidyl-tRNA exists in the P site. Finally, uncharged or deacylated-tRNAs exit through the E site. During translation initiation, where most mechanisms of translational control exist, the 80S ribosome is assembled at the 'start' of the open reading frame with the first aminoacyl-tRNA in sequence at the P site. The ribosome subsequently moves across the mRNA in a 5'-3' direction during the elongation step, adding an amino acid each time an aminoacyl-tRNA senses a complementary codon until a stop codon is reached. Finally, the

ribosome is removed from the mRNA, or alternatively, the ribosome may reinitiate to undergo further rounds of translation.

1.2.1. Synthesis of messenger RNA (mRNA)

In eukaryotes, genes are transcribed from template DNA to mRNA in the process of transcription. During transcription, the mRNA is capped at the 5' end, non-coding introns are spliced out and a polyadenoside (poly-A) tail is added to the 3' end. These co-transcriptional modifications enhance the stability of mRNA and play important roles in translation initiation.

Transcription is initiated by general transcription factors which facilitate the recruitment of RNA polymerase II (Pol II) . As soon as the 5' triphosphorylated end of the pre-cursor mRNA (pre-mRNA) emerges from Pol II, a three-step enzymatic reaction occurs which results in the acquisition of a 5' 7-methyl guanoside (7meGpppN) residue(Proudfoot et al., 2002). This unique base resists 3'-5' exonucleases and requires specialist decapping enzymes, thereby enhancing the half-life of the mRNA. A nuclear cap binding complex associates with the 5' cap until the processed mRNA is exported into the cytosol. The nuclear cap binding complex is replaced by the cytosolic cap binding protein eIF4E which plays an important role in translation initiation and translation regulation (Visa et al., 1996, Fortes et al., 2000).

Interrupting sequences, known as introns, may be spliced out of mRNA cotranscriptionally or post-transcriptionally. The subsequent coding sequences, known as exons, are ligated back together by two transesterification reactions to produce the spliced mRNA(Wachtel and Manley, 2009). Introns may be retained in some cases which allow a pool pre-mRNA to be maintained within the nucleus, ready to be quickly processed and exported to meet instances of high demand. Alternatively, specific

introns may be allowed to persist or exons may be spliced out, giving rise to multiple proteins from a single gene.

The final processing event of mRNA, the addition of the poly-A tail, is closely linked to the termination of transcription. Cleavage is dependent on highly conserved AU-rich sequences present at the 3' end of the pre-mRNA (Zhao et al., 1999). Following cleavage, a poly-A tail is added to the 3' of the mRNA by the polyadenlyate polymerase (Pap1p in yeast) (Wahle and Ruegsegger 1999). Poly-A binding proteins (Nab2p and Pab1p in yeast) associate with the poly-A tail before the fully matured mRNA is exported into the cytoplasm (Dunn et al., 2005, Hector et al., 2002). The poly-A tail is an important addition to pre-mRNA as it enhances mRNA stability and plays important roles in translation initiation.

1.2.2. Translation initiation

For the translation of mRNA transcripts to occur, the 40S and 60S ribosomal subunits must be assembled onto the mRNA at the beginning of the ORF to initiate translation. Under normal conditions, the bulk of protein synthesis is mediated by eukaryotic initiation factors (eIFs) which directly or indirectly interact with the 5' 7meGpppN cap. Cap-dependent translation is therefore estimated to account for 95 % of proteins synthesised (Merrick, 2004).

1.2.2.1.   Cap-dependent translation

The initiation of cap-dependent translation is the most complex and regulated process within translation, requiring the coordinated efforts of 10 eIFs **(Table 1.1, Fig.1.1)**. The cytosolic cap binding protein eIF4E associates with the 5' end of the mRNA which further recruits eIF4G and eIF4A, completing the eIF4F cap binding complex. eIF4A is a DEAD box ATP-dependent RNA helicase that unravels secondary

structures in the 5' untranslated region (UTR), promoting ribosome recruitment (Svitkin et al., 2001). eIF4G primarily serves as a scaffold, binding both eIF4E and eIF4A as well as the poly(A)-binding protein (PABP) present at the 3' end of the transcript (Tarun and Sachs, 1996). These interactions subsequently produce the closed loop complex which is thought to enhance ribosome re-initiation (Wells et al., 1998). Once the mRNA is unwound, eIF4G acts as a bridge by interacting with eIF3, allowing the 43S pre-initiation complex (PIC) to be stably loaded onto the mRNA.

In the first step, eIF2 bound to GTP recruits the initiator methionyl tRNA (Met-tRNA$_i^{Met}$) to form a ternary complex (TC). eIFs 1, 3 and 5 associate with the TC to form the intermediary multifactor complex (MFC) (Sokabe et al., 2012). Mediated by eIF1A, the 40S ribosomal subunit is then loaded on to the MFC to produce the 43S PIC (Asano et al., 2000). Interactions between eIF4G and eIF3 lead to the loading of the 43S PIC onto the 5' UTR of the mRNA (LeFebvre et al., 2006), which subsequently scans in a 5'-3' direction to find the optimal AUG 'start' codon (in yeast: (A/U)A(A/C)AA(A/C)AUGUC(U/C)) (Miyasaka, 1999), delivering the 40S ribosome subunit complexed with the initiator tRNA at the beginning of the ORF. Following AUG recognition, the GTPase accelerating protein (GAP), eIF5, hydrolyses the GTP that is bound to eIF2, promoting the release of the initiating factors (Unbehaun et al., 2004). In addition, eIF5 also forms a complex with the subsequent GDP bound eIF2 providing GDP displacement inhibition (GDI), which prevents spontaneous events of translation initiation (Singh et al., 2006). When bound with GTP, the GAP eIF5B mediates the binding of the large 60S subunit to the small 40S subunit. Auto-hydrolysis promotes the release of eIF5B-GDP, thereby completing the assembly of the 80S ribosome.

For subsequent rounds of translation initiation to occur, eIF2 must be recycled and converted back from the inactive GDP binary complex to the active GTP bound complex (Pavitt, 2005). This process is facilitated by the multi-functioning initiation factor, eIF2B, which consists of five subunits that are classified into two groups (Pavitt et al., 1998). The eIF2B subunits α, β and δ are considered regulatory subunits whilst γ and ε are considered catalytic subunits. All five subunits are highly conserved throughout eukaryotes and share significant homology within their groups (Pavitt et al., 1997) **(Fig. 1.2)**. For instance, eIF2Bγ and ε share similarities between pyrophosphorylases suggesting that they both have the capacity to bind GTP (Gomez and Pavitt, 2000). Contrary to this, mass spectrometry data showed that GTP readily binds to eIF2Bγ, but not to eIF2Bε (Gordiyenko et al., 2014). Therefore, the role of eIF2Bγ could be to provide the necessary energy for GEF activity or bind the GTP that eIF2Bε places on eIF2. eIF2Bγ has been shown to be important for eIF2B's GDI displacement factor (GDF) activity, which frees GDP bound eIF2 from eIF5 (Jennings et al., 2013). Exclusive to eIF2Bε are several phosphorylation sites and a catalytic domain that contains two aromatic/acidic residue-rich regions (known as AA boxes) which bind GDP bound eIF2 for GTP exchange to occur (Gomez et al., 2002, Boesen et al., 2004). The dual specific tyrosine kinase (DYRK), glycogen synthase kinase 3 (GSK3) and casein kinases (CK) 1 and 2 may phosphorylate eIF2Bε at various positions to reduce the catalytic activity of eIF2B in response to insulin and nutrient limiting conditions (Welsh et al., 1998, Woods et al., 2001). Similarly, eIF2B activity can be inhibited by the phosphorylation of eIF2 which subsequently interacts with another binding domain in the regulatory subunits of eIF2B.

Table 1.1 - eukaryotic initiation factors

Figure 1.1 - Initiation of translation in eukaryotes. The eIF4F-cap binding complex, consisting of eIF4E, 4A and 4G as well as Pab1p associate with the mRNA producing a closed loop complex. A ternary complex of GDP-bound eIF2 and Met-tRNA$_i^{Met}$ recruits addition factors including the 40S ribosome, forming the 43S PIC. The 43S PIC is loaded onto the closed mRNA, which subsequently scans for the optimal AUG start codon. Upon recognising the start of the ORF, eIF2-GTP is hydrolysed and the initiation factors are released, allowing the 60S ribosome subunit to be recruited, completing the 80S ribosome. GDP-bound eIF2 is recycled by eIF2B for concurrent rounds of initiation.
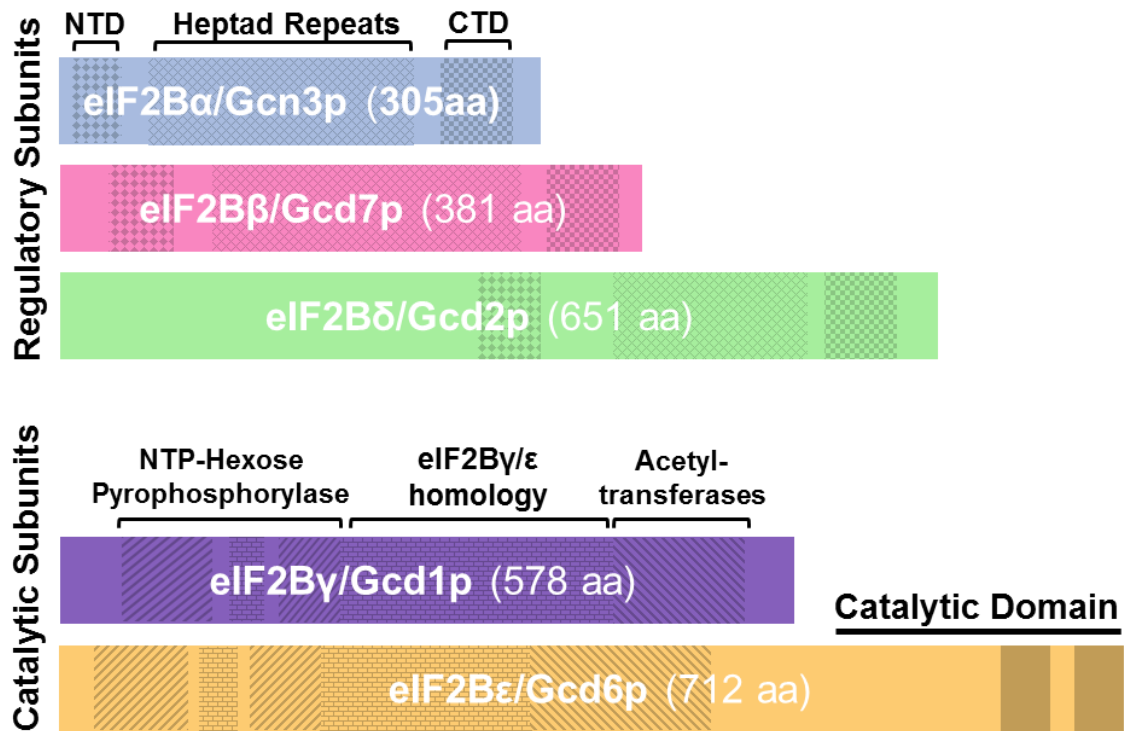
Figure 1.2 - Homology between the subunits of eIF2B in *S. cerevisiae*. The regulatory subunits eIF2Bα, β and δ share several heptad repeats as well as homologous NTDs and CTDs. The catalytic subunits share homology with each other, pyrophosphorylases and acetyl-transferases.

1.2.2.1.1. Regulation of translation initiation through eIF2B

Translation is a resource-heavy process that can place an unnecessary burden on the cell in times of cellular stress. Whilst proliferating, it is estimated that a yeast cell synthesises 13,000 proteins per second, accounting for approximately 76% of the cell's total energy expenditure (von der Haar, 2008, Wang and Zhang, 2011). Subsequently, eukaryotes have adapted responses that reduce or reprogramme global protein synthesis in an attempt to focus resources on neutralising the stress. These mechanisms not only ease the burden of protein synthesis, but ensure the cell can adapt before irreversible damage occurs.

In addition to controlling the initiation of translation via GDP/GTP exchange on eIF2, eIF2B also serves as a vital control point where protein synthesis can be regulated in response to several stimuli. eIF2B's substrate, eIF2, is a heterotrimeric G-protein consisting of the three subunits α, β and γ. In times of cellular stress, eIF2α kinases phosphorylate serine 51 within eIF2α (eIF2α-P) (Rowlands et al., 1988), which binds eIF2Bα instead of eIF2Bε. eIF2-P has also been shown to bind eIF2B with much higher affinity than the non-phosphorylated counterpart, thus allowing eIF2B to be regulated rapidly (Sudhakar et al., 1999). Interestingly, eIF2B was recently shown to exist as a decameric complex comprising of a regulatory $\alpha_2\beta_2\delta_2$ core flanked by two εγ catalytic dimers at opposing sides (**Fig. 1.3**) (Gordiyenko et al., 2014, Wortham et al., 2014, Kashiwagi et al., 2016). In yeast, all of the subunits of eIF2B are essential with the exception of eIF2Bα (Gcn3p in *S. cerevisiae*). Intriguingly, the loss of eIF2Bα prevents eIF2B regulation and also destabilises the decamer into two eIF2Bεγδβ heterotetramers (Wortham et al., 2014). Although eIF2Bα is not required for cellular growth in yeast, irreparable cellular damage will occur should homeostasis deviate. In

mammals however, the destabilisation of the decameric complexes decreases catalytic activity by 50 % (Williams et al., 2001, Wortham et al., 2014)

Following cellular stress and eIF2α-P-eIF2Bα interaction, a conformational change subsequently attenuates the catalytic activity of eIF2B, reducing levels of TCs and consequently inhibiting global protein synthesis. This reduction in TC formation paradoxically enhances the translation of stress-specific mRNAs, therefore allowing a stress response to occur (Hinnebusch, 1997).

In yeast, general control nonderepressible 2 (Gcn2p) represents the sole eIF2α kinase which responds to the classical cellular stress, amino acid starvation. Following the inhibition of eIF2B, the transcriptional activator Gcn4p is paradoxically translated, instigating a transcriptional programme that upregulates genes involved in amino acid biosynthesis (**Fig. 1.4**) (Natarajan et al., 2001). Under normal conditions, Gcn4p is repressed by the presence of four upstream open reading frames in the 5' UTR (Hinnebusch, 1997). When TCs are abundant, 43S PICs initiate at uORF1 which is subsequently translated. Post-termination 40S subunits reinitiate after uORF1, binding further TCs before reaching the inhibitory uORF4. Here, the ribosome disassociates from the mRNA preventing the ribosome from reaching the true ORF (Hinnebusch, 1997). Under stressful conditions however, fewer TCs are available which allows uORF4 to be bypassed by a phenomenon referred to as 'leaky scanning' (Wang and Rothnagel, 2004). Binding a TC at the true ORF induces the expression of Gcn4p. This mechanism allows specific proteins to persist despite reduced protein synthesis to provide a stress-response that returns homeostatic conditions.

During the 1990s, studies in the yeast *S. cerevisiae* underlined how sensitive the balance is between a decrease in GTP bound eIF2 and the initiation of a stress

response (Hannig et al., 1990). For instance, mutations within the yeast eIF2Bα (known as Gcn3p) initiated the translation (or derepression) of *GCN4*. These mutations, dubbed general control nonderepressible constitutive (GCN3[c]) mutations, reduced GEF activity which mimicked eIF2B-eIF2-P binding, a situation that should only occur when the cell is under stress.

In yeast, eIF2B is also subject to regulation in response to fusel alcohols which are produced during amino acid scarcity (Eden et al., 2001). Naturally occurring alleles within the catalytic subunit eIF2Bγ have shown to increase (S180) or decrease (P180) the cell's translational resistance to butanol (Ashe et al., 2001). Interestingly, additional mutations within eIF2Bα were discovered that also produces a resistant phenotype (Taylor et al., 2010). However, eIF2B is regulated independent of eIF2α-P in response to butanol, thus Gcn4p expression in this instance is independent of an eIF2α kinase.

In addition to amino acid starvation, mammals have also adapted similar responses to viral infection, ER stress and haem deficiency which are sensed by protein kinase R (PKR), PKR-like endoplasmic reticulum kinase (PERK) and haem control repressor (HCR), respectively (Dey et al., 2005). Analogous to Gcn4p in yeast, the mammalian activating transcription factor 4 (ATF4) is specifically translated following the build-up of unfolded proteins in the ER, subsequently leading to the unfolded protein response (UPR) (Vattem and Wek, 2004). ATF4 contains two uORFs and induces a transcriptional programme that upregulates the chaperones required to fold nascent proteins within the ER. GADD34 is also expressed, which when properly folded in the ER, provides negative feedback allowing translation to be resumed (Novoa et al., 2001).
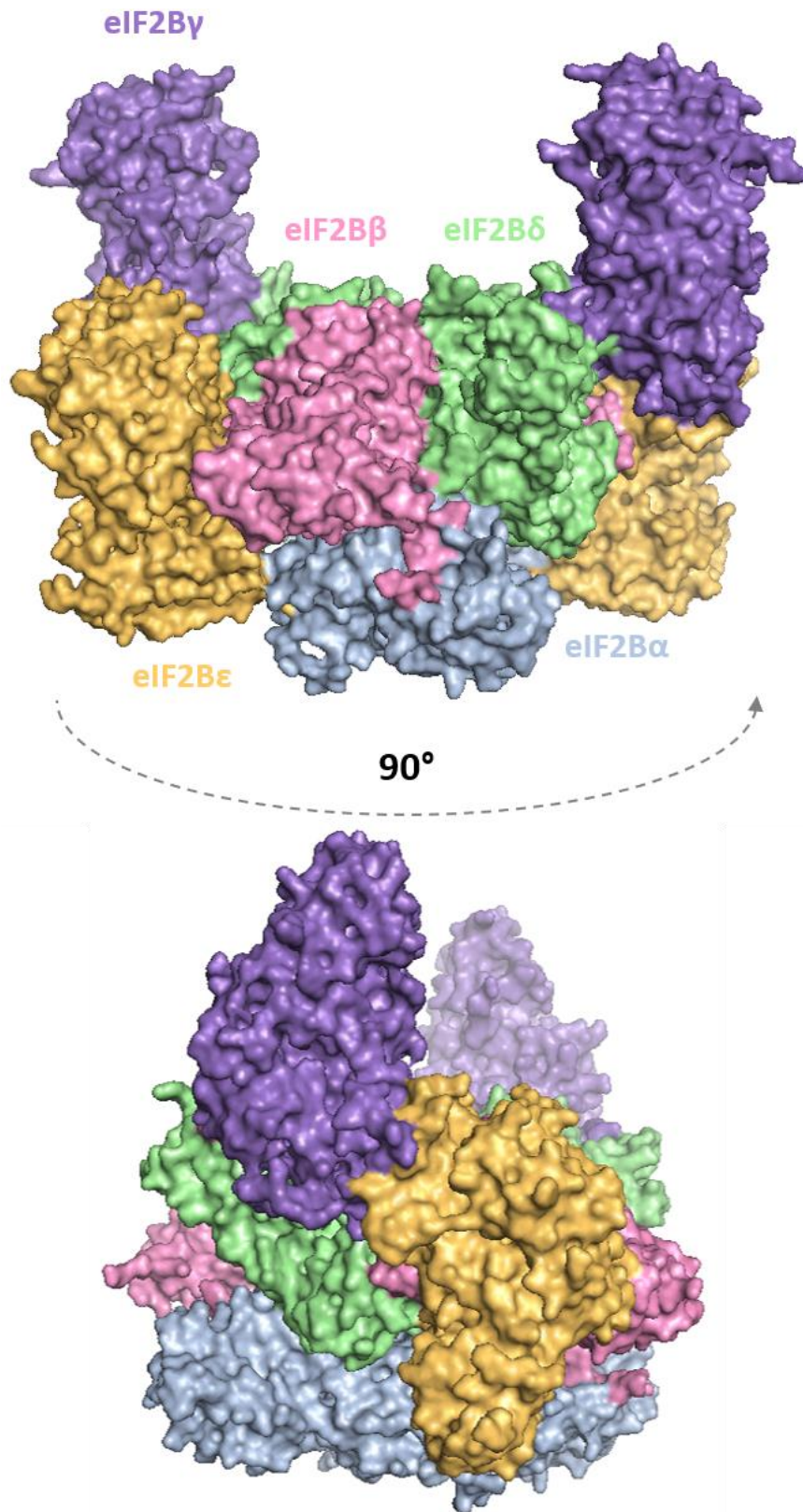
Figure 1.3 - The decameric crystal structure of eIF2B. Two heterotetrameric eIF2Bεγβδ complexes are stabilised by a homodimer of eIF2Bα. In the decameric holocomplex, a regulatory core is flanked by two catalytic domains on opposing sides.
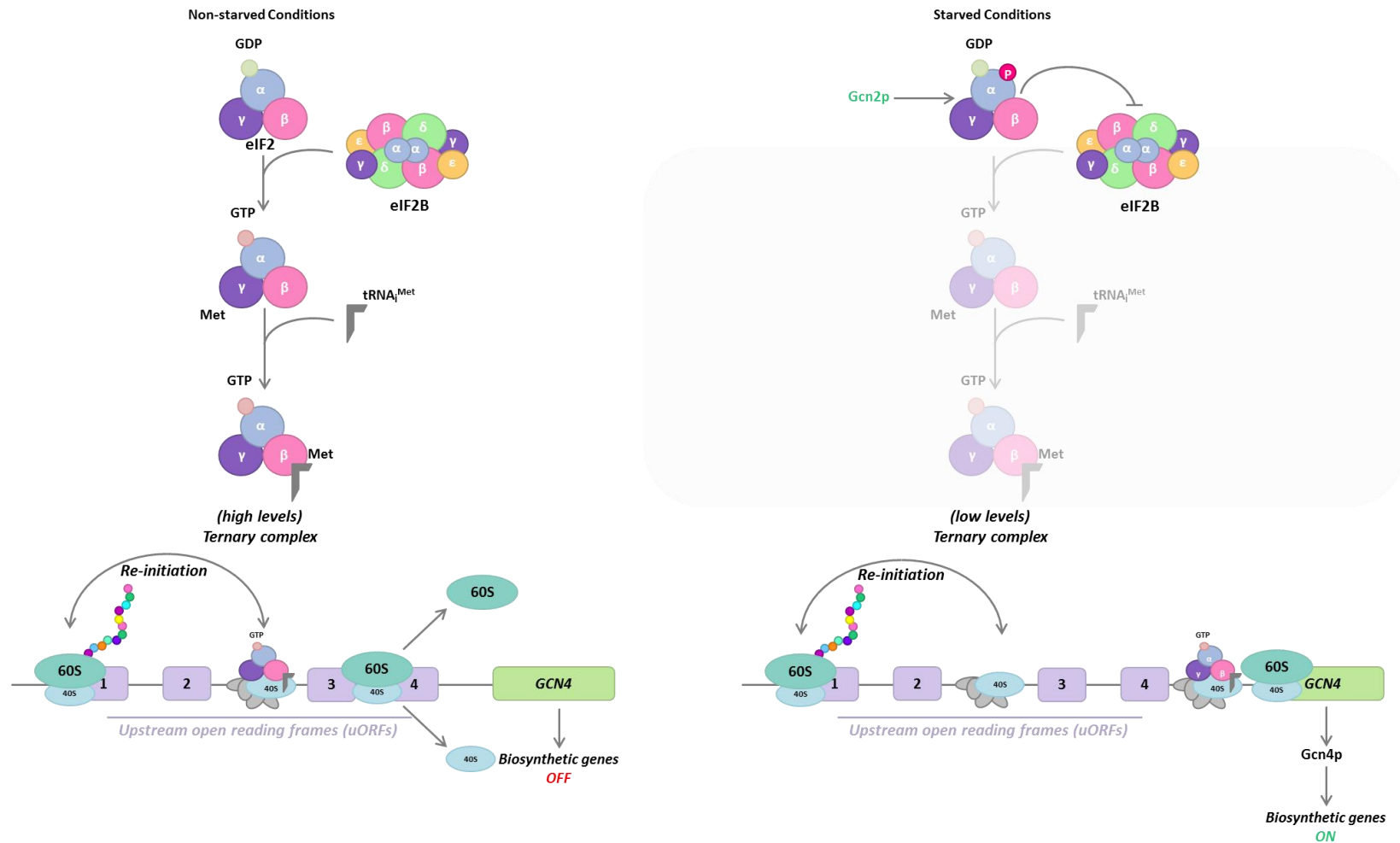
Figure 1.4 - Regulation of Gcn4p expression by uORFs. Gcn4p expression is regulated by the presence of four uORFs in mRNA's. Under normal conditions with high levels of TCs, ribosomes translate uORF1 and reinitiate afterwards. If the ribosome recruits another TC before uORF4, the ribosomes will disassociate. Under stressed conditions with low levels of TC, there is less chance for the ribosome to recruit another TC before uORF4, allowing the ribosome to reach and translate the true ORF.

1.2.2.1.2. Regulation of translation initiation through 4E-BPs

In addition to regulation via eIF2B, translation initiation may also be subject to regulation by eIF4E-binding proteins (4E-BPs) following cellular stresses, such as heat shock or oxidative stress (Pham et al., 2000, Sukarieh et al., 2009). 4E-BPs compete with eIF4G for a shared binding motif on eIF4E (Pause et al., 1994), therefore preventing the formation of the closed loop complex (Haghighat et al., 1995). This control of translation initiation via 4E-BPs is dependent upon the phosphorylation status of the 4E-BPs at several serine/threonine residues (Pyronnet et al., 1999, Holz et al., 2005). During steady-state conditions, the 4E-BPs are phosphorylated by the mammalian target of rapamycin complex 1 (mTORC1) in response to nutrients or growth factors. In this phosphorylated state the 4E-BPs are unable to bind eIF4E, allowing translation initiation to continue (Holz et al., 2005). However under stressed conditions that inhibits mTOR activity, hypo-phosphorylation results in the attenuation of eIF4F-cap binding complexes, consequently preventing the loading of 43S PICs. In mammals, three 4E-BPs exist: 4E-BP1, 2 and 3, whereas two 4E-BPs exist in yeast: Caf20p and Eap1p.

Published data suggests that Caf20p and Eap1p regulate the expression of specific subsets of mRNA spanning hundreds of transcripts, thus 4E-BPs play a large role in reprogramming the translatome following a cellular stress (Cridge et al., 2010). Interestingly, global RNA-binding protein immunoprecipitation sequencing (RIP-seq) showed that Caf20p and Eap1p can bind mRNA transcripts in an eIF4E-independent manner, although the specific mechanism remains unclear (Castelli et al., 2015). The activation of 4E-BPs elicit different stress responses to eIF2α kinases, for instance 4E-BPs do not instigate the expression of the stress-specific mRNA Gcn4p. Interestingly

however, Eap1p may repress Gcn4p expression when TOR is inactivated under rapamycin treatment or extreme stresses (Matsuo et al., 2005), suggesting cross-talk between the two major regulating mechanisms of translation. Both Caf20p and Eap1p can enhance the binding of specialist de-capping enzymes or mediate the association of RNA processing enzymes required for mRNA decay (Ferraiuolo et al., 2005). Moreover, mRNAs can be translationally silenced by translocation to stress-granules in a 4E-BP dependent manner (Fujimura et al., 2012), where mRNA is thought to be stored until cellular homeostasis is restored.

1.2.2.2. Initiation and regulation of cap-independent translation

Initially discovered in the picornavirus, cap-independent translation requires the presence of internal ribosome entry sites (IRES) (Jang et al., 1988, Pelletier and Sonenberg, 1988). Highly structured IRES elements present in the 5' non-coding region (NCR) bypass the host-cells defensive regulatory mechanisms (*i.e.* PKR) and directly recruit ribosomal subunits to initiate translation (Kaminski et al., 1990, Pestova et al., 1996). Although IRES were thought to be unique to viruses, subsequent studies discovered similar IRES elements in eukaryotic mRNA transcripts that encode proteins involved in cellular differentiation, apoptosis and stress responses (Komar and Hatzoglou, 2005). IRES-mediated ribosome recruitment was thought to be independent of initiation factors. However, recent studies have shown that eIF4G and the PABP can enhance mRNA expression by several orders of magnitude in both mammals and yeast (Smith et al., 2017, Gilbert et al., 2007).

1.2.3. Translation elongation

Following initiation, several ribosomes may be elongating along an mRNA at any given time, giving rise to polyribosomes or polysomes. During the elongation step, the 80S ribosome moves along the ORF in a 5'-3' direction catalysing the synthesis of nascent polypeptide chains. Aminoacyl-tRNA selection as well as ribosome movement is mediated by eukaryotic elongation factors (eEFs). GTP bound eEF1A forms a complex with aminoacyl-tRNA which enters the A site. Complementary base pairing between the mRNA codon and the aminoacyl-tRNA anti-codon induces a conformational change which instigates the hydrolysis of eEF1A. Released GDP bound eEF1A is recycled by the GEF enzyme eEF1B for concurrent rounds of tRNA selection (Kapp and Lorsch, 2004).

The peptidyl transferase centre (PTC) of the ribosome catalyses the formation of a peptide bond between the amino acid in the A site and the elongating polypeptide in the P site. This reaction subsequently results in a deacylated-tRNA in the P site whilst the elongating peptide is temporarily transferred to the A site. A ratchet-like motion reorganises the ribosome by translocating the peptidyl-tRNA (with the elongating peptide) to the P site (Ben-Shem et al., 2010), whilst deacylated-tRNA moves to the E site. With the A site empty, another round of aminoacyl-tRNA selection may begin. Ribosome translocation is facilitated by the hydrolysis of GTP by eEF2 which can be inhibited by cycloheximide resulting in stalled ribosomes (Rodnina et al., 1997, Schneider-Poetsch et al., 2010). Specific to yeast, the release of deacylated-tRNA is dependent upon the hydrolysis of ATP which is mediated by eEF3 (Triana-Alonso et al., 1995). The essential elongation factor eEF3 is a ribosome-dependent ATPase that can bind both ATP and ADP, and has also been shown to interact with eEF1A to stimulate aminoacyl-tRNA recruitment (Kamath and Chakraburtty, 1989, Anand et al., 2003).

1.2.4. Translation termination and re-initiation

Translation enters the termination stage once the ribosome encounters one of three stop codons: UAG, UGA or UAA. The eukaryotic release factors (eRF) 1 and 3 (Sup35p and Sup45p in yeast) work together to release the polypeptide chain and recycle the ribosome for concurrent rounds of translation (Urakov et al., 2006). The tRNA-shaped eRF1 forms a complex with GTP bound eRF3 which directs eRF1 into the A site of the ribosome (Bertram et al., 2000). Ribosome interaction promotes the hydrolysis and release of eRF3 from eRF1, allowing the ATPase Rli1p to be recruited (Salas-Marco and Bedwell, 2004, Preis et al., 2014). The interaction of Rli1p induces a

conformational change within eRF1 that allows the N-terminal domain to interact with the stop codon, consequently promoting the hydrolysis and release of the complete polypeptide chain.

Following termination and the release of the polypeptide chain, the ribosome may be recycled for the translation of other mRNA, or reinitiated for the translation of the same transcript. The latter scenario is suggested to be dependent upon the closed loop complex (described in section 1.2.1.1.) which could release ribosomal subunits in close proximity to the start codon. Ribosomes are disassembled by Rli1p following the hydrolysis of ATP (Preis et al., 2014). Rli1p is also important for ribosome re-initiation as its deletion leads to abnormal re-initiation nearby start codons (Shoemaker and Green, 2011). In mammals, the individual activity of Ligatin or the complex of MCT-1 and DENR may promote ribosome release and re-initiation (Skabkin et al., 2010). Although yeast orthologues have been described for all three human proteins (Tma64p, Tma20p and Tma22p, respectively), their function remains unknown. This suggests that ribosome re-initiation is conserved throughout eukaryotes and that Tma64p, Tma20p and Tma22p may also be required for stress-specific re-initiation mechanisms (Dever et al., 2016), such as those that regulate *GCN4* transcripts (see section 1.2.1.1.1.).

1.3.   Subcellular organisation of translation

Once a newly synthesised mRNA is delivered to the cytosol, it may be silenced and transported to a specific location within the cell before translation occurs. This mechanism enhances the efficiency of protein synthesis by expressing the encoded protein in a spatial region. Under cellular stress, the inhibition of protein synthesis by 4E-BPs/eIF2α kinases can promote the translocation of transcripts to specific

cytoplasmic granules. Stress granules and processing bodies (P-bodies) are thought to store or degrade specific subsets of mRNA transcripts. In addition, the localisation of the key translation initiation factor eIF2B to specific cytoplasmic foci has been show to control and regulate its function. Together, these observations demonstrate that translation is a highly organised process within the cellular cytoplasm during steady-state growth and during instances of regulation following cellular stress.

1.3.1. Localisation of mRNA

It is estimated that each mRNA transcript can be used to synthesise between 4000-5000 molecules of the encoded protein (Ghaemmaghami et al., 2003, Lu et al., 2007). The localisation of proteins can be important for function, especially in the context of biochemical reactions as a large amount of energy would be required to localise these proteins to the required region. Alternatively, the cell localises the mRNA transcript and synthesises proteins at the required site, resulting in a much more energy efficient process **(Fig. 1.5)**.

The best described example of mRNA localisation is the *ASH1* mRNA which is solely expressed in daughter cells during cellular division in yeast (Bertrand et al., 1998, Sil and Herskowitz, 1996). During transcription of *ASH1*, the RNA-binding protein She2p recognises four cis-acting elements within the emerging transcript (Landers et al., 2009). Once delivered to the cytoplasm, *ASH1* expression is instantly silenced by the presence of She2p which also mediates the recruitment of additional translocation factors, including the motor protein Myo4p. The *ASH1* transcript subsequently transits along actin filaments to be relocated at the tip of the bud where Ash1p protein is required to transcriptionally repress the homothallic switching (HO) endonuclease (Sil and Herskowitz, 1996). Thus, the HO endonuclease is exclusively present in the mother

cell where it mediates the switching of the cells mating type by rearranging the genomic MAT locus.

This mechanism is highly conserved in mammals whereby the spatial organisation of mRNAs is vital for embryo development and synaptic plasticity. Moreover, mRNA localisation is also important for the development and function of organelles, including peroxisome biogenesis in yeast (Zipor et al., 2009). However, in times of cellular stress, the spatially distributed mRNA transcripts may become aggregated into RNA granules which serve to store messages for when homeostasis returns, or for the degradation of redundant transcripts.

Figure 1.5 - Localisation of mRNA in budding Yeast. Following the export of mRNA, some transcripts are instantly silenced and transported to a specific cytoplasmic location where the encoded protein is translated. By synthesising the protein at their required sub-cellular site, the proteins do not need to be transported, resulting in a much more energy efficient mechanism. Such examples include *ASH1* which is transported to the bud tip, Peroxin mRNA which are transported to peroxisomes and a whole class of mRNA which are localised to the mitochondria (Zipor et al., 2009, Saint-Georges et al., 2008).

1.3.2. P-bodies

Processing bodies (P-bodies) are highly conserved RNA granules that are thought to promote the storage and degradation of translationally-repressed mRNAs following various cellular stresses (Sheth and Parker, 2003, Cougot et al., 2004). Although the complete configuration of P-bodies is yet to be fully elucidated, they are characterised by a core set of fundamental proteins that are involved in mRNA decay, such as proteins that promote decapping, Lsm1-7p (Tharun and Parker, 2001), the decapping complex: Dcp1p/Dcp2p (van Dijk et al., 2002, Eystathioy et al., 2003), as well as the 5'-3' exoribonuclease Xrn2p (Bashkirov et al., 1997). Additionally, eIF4E, eIF4G and Pab1p also localise to P-bodies in yeast (Hoyle et al., 2007). As decay factors actively repress mRNA translation, the presence of initiation factors suggest that they may compete for transcripts in a dynamic cycle (Hoyle and Ashe, 2008).

1.3.3. Stress granules

Similar to P-bodies, stress granules are another class of cytoplasmic RNA granule that is conserved across the eukarya domain, and form in response to cellular stress. Although P-bodies and stress granules both contain eIF4E, eIF4G and Pab1p, stress granules contain additional initiation factors such as eIF2, eIF3 and eIF4A as well as 40S ribosomal subunits (Kedersha et al., 2002). Therefore, under cellular stress, it is thought that stress granules may be sites where stalled 48S PICs are stored in addition to other mRNA.

The attenuation of eIF4A can lead to the formation of stress granules, which occurs through an unclear mechanism in response to glucose starvation (Castelli et al., 2011). Furthermore, stress granules can also form in response to environmental

stresses that result in the phosphorylation of eIF2α. Experiments using an eIF2α phosphomimetic mutant (S51D) and a nonphosphorylatable mutant (S51A) either induced or reduced stress granule formation, respectively (Kedersha et al., 2002). In mammals, the attenuation of eIF2B activity promotes the T-cell restricted intracellular antigen-1 (TIA-1) and the TIA-1 related protein (TIAR) to recruit transcripts to stress granules (Gilks et al., 2004, Kedersha et al., 1999). The organisation and localisation of mRNA transcripts can therefore be intrinsically linked to eIF2B activity which may be controlled at another cytoplasmic locale.

1.3.4. eIF2B bodies

As highlighted in section 1.2.1.1.1, eIF2B controls the initiation of translation by recycling eIF2-GDP as well as serving as a vital control point in response to cellular stress. Using the model organism *S. cerevisiae*, Campbell *et al.,* observed that eIF2B localised to a specific cytoplasmic focus, termed the eIF2B body (Campbell et al., 2005). The G-protein eIF2 co-localised with eIF2B bodies, although, under normal conditions eIF2 did not remain static. Interestingly, the use of fluorescence recovery after photobleaching (FRAP) highlighted that eIF2B remains resident within the foci while eIF2 shuttles through, allowing GDP-GTP exchange to occur (Campbell et al., 2005). The initiating Met-tRNA$_i^{Met}$ does not co-localise to eIF2B bodies, nor does any other translation initiation factor (Campbell et al., 2005). Therefore, the eIF2B body does not serve as sites for TC, MFC or 43S PIC formation.

Whether the eIF2B body contains mRNA transcripts is unknown. Although the composition of eIF2B bodies may be different to the aforementioned RNA granules, they all respond to translational control and therefore maintain the organisation of translation (**Fig. 1.6**). Using FRAP analysis, Campbell *et al.,* showed the rate of eIF2

shuttling could be used to measure the GEF activity of eIF2B *in vivo*. In the presence of constitutively active Gcn2p mutants as well as an eIF2Bε mutant F250L, the cycling of eIF2 decreased significantly, highlighting that the use of FRAP could be used to gain more insightful measurements where *in vitro* biochemical assays have been predominantly used (Campbell et al., 2005).

In mammals, several sub-types of eIF2B bodies exist whereby the increasing size of the foci correlates with the number of subunits present (Hodgson et al., 2018). Subsequently and in-line with *in vitro* biochemical assays, FRAP analyses of mammalian eIF2B bodies highlighted that changes in the cycling of eIF2 is dependent on the subunits present (**Hodgson** et al., 2018). In yeast however, the eIF2B body is a singular aggregate that contains all five subunits of eIF2B, thus it is likely that the eIF2B body contains decameric complexes in yeast (Campbell et al., 2005, Gordiyenko et al., 2014, Wortham et al., 2014). These differences are likely to be explained by the higher eukaryote requiring more complex control to fine-tune the requirements of higher rates of protein synthesis.

In yeast, the only other known factor required for the integrity of the eIF2B body is the initiation factor associated of 38 kDa protein (Ifa38p) (Browne et al., 2013). The very-long fatty acid (VLFA) elongase enzyme, Ifa38p does not have a specific role in translational control or initiation, but was shown to interact with both catalytic subunits of eIF2B (Browne et al., 2013). Gene deletion subsequently resulted in the fragmentation of the eIF2B body to several smaller foci. The authors concluded that the differential localisation of eIF2B did not affect rates of translation initiation. Therefore, Ifa38p could be required to maintain the stability of the eIF2B body,

although the current authors note that the cycling of eIF2 through these foci was not directly compared.

Other features of the eIF2B foci have been described in yeast. The aggregated eIF2B displays a filamentous structure which may be affected by changes in cytosolic pH (Petrovska et al., 2014). However, the eIF2B body represents the congregation of 40% of the cells total eIF2B, thus GDP and GTP exchange as well as regulation can presumably occur elsewhere in the cytoplasm (Campbell et al., 2005). Thus, the specific role of the eIF2B body remains unclear, but could have important implications for vanishing white matter disease.
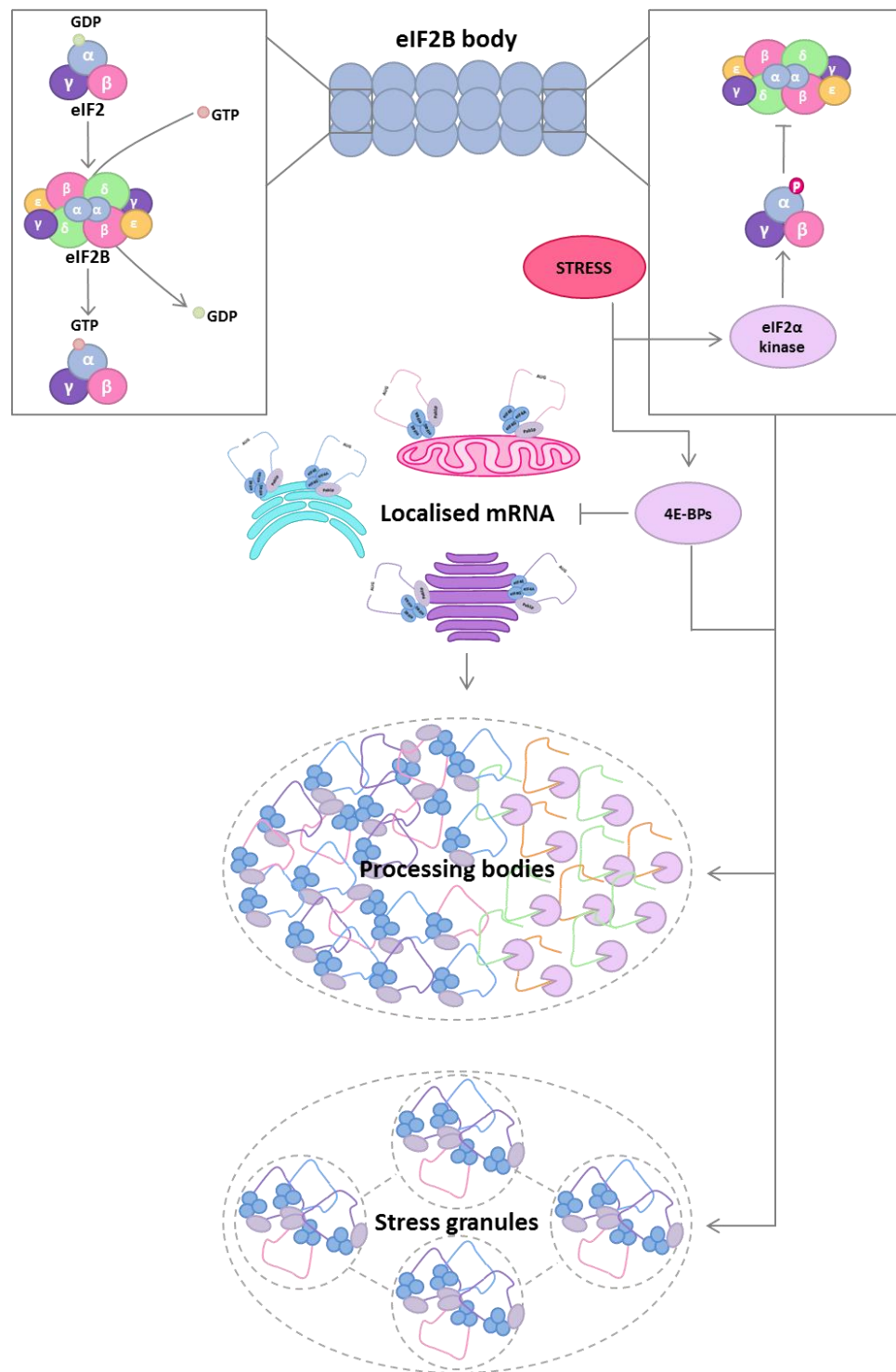
Figure 1.6 - Organisation and regulation of protein synthesis. Translation consists of distinctive cytoplasmic foci where mRNA and translation initiation factors can congregate under steady-state growth or rate-limiting stress conditions. eIF2B localises to eIF2B bodies, where eIF2 shuttles through for GDP-GTP exchange, or alternatively, where eIF2α-P may attenuate eIF2B GEF activity. Inhibition of translation can translocate mRNA to P-bodies which may target specific transcripts for degradation. Alternatively, transcripts may localise to stress granules to be stored until cellular homeostasis is restored.

1.4. Leukoencephalopathy with Vanishing White Matter disease

Translation is a core cellular process in all organisms, hence only a small number of diseases are attributable to protein synthesis. The most prominent of these diseases is the complex neurological disorder leukoencephalopathy with vanishing white matter disease (VWM). VWM, also known as childhood ataxia with central nervous system hypomyelination (CACH), arises through autosomal recessive mutations within any subunit of eIF2B (Leegwater et al., 2001). A hallmark feature of VWM is the progressive loss of white matter, which is replaced by cerebral spinal fluid (CSF) (Schiffmann et al., 2012). Although VWM is regarded as the most prevalent childhood leukodystrophy, it is relatively rare with a limited number of cases recorded (Bugiani et al., 2010). Interestingly though, approximately 161 unique mutations have been documented across all five eIF2B subunits so far, contributing to the complexity of VWM as well as the variability observed in clinical presentation (Pavitt and Proud, 2009, Shimada et al., 2015, Zhang et al., 2015). From over 30 years of research, there is definitive evidence to suggest that the root cause lies within eIF2B's intrinsic role as a cellular hub to control translation in response to stress (Pavitt and Proud, 2009). However, observations from biochemical experiments do not fully agree with this model (Wortham and Proud, 2015). Moreover, published data has highlighted that there is no genotype-phenotype correlation, leading to the idea that there may be other unknown functions or features of eIF2B not fully understood (van der Lei et al., 2010, Liu et al., 2011).

1.4.1. Disease onset and current diagnosis

VWM is defined as a chronic progressive disease that can advance rapidly in its most severe antenatal form or more slowly in the adolescent form (Schiffmann et al., 2012). Affected individuals may rapidly deteriorate following acute traumas, such as head trauma, febrile infection or acute fright (van der Knaap et al., 1997, Fogli et al., 2004a, Kaczorowska et al., 2006). Adverse symptoms may manifest shortly after the traumatic event (van der Knaap et al., 1997). There are many symptoms associated with VWM, including migraines, psychiatric symptoms, kidney ataxia and seizures (van der Knaap et al., 1997). Clinical presentation of VWM strongly correlates with the severity of the disease **(Table 1.2)** (Pavitt and Proud, 2009). Whilst episodes of rapid deterioration are not restricted to the three traumas previously mentioned, they are the most common as a consequence of inherent environmental factors (*e.g.* head trauma following a fall). Currently, there is no direct link to explain why intercurrent trauma exacerbates the condition. One hypothesis that has been suggested is that each of these traumas further impairs eIF2B's catalytic activity via regulatory mechanisms responding to cellular stress.

The most severe forms generally manifest antenatally, congenitally or during early childhood (van der Knaap et al., 2003). Milder forms can develop between the ages of 1-5 years and from 5 years onwards. Individuals with congenital or antenatal forms do not survive past a year, in contrast to those with adolescent onset who generally live considerably longer (van der Knaap et al., 2003, Fogli et al., 2004a). One exception is a mutation commonly found in the Cree and Chippewayan population indigenous to North America (Fogli et al., 2002). The R195H mutation within eIF2Bε,

also known as the Cree mutation, causes onset to occur around 3 months after birth, with affected infants rarely living past the second year of life (Fogli et al., 2002).

Diagnosis of VWM is primarily achieved through mass resonance imagining (MRI; **Fig. 1.7**). The hallmark signs are cystic degeneration and cavitation of the white matter surrounding the cerebral hemisphere which is replaced by cerebral spinal fluid. Following radiological imaging, suspected VWM patients are genotyped to determine whether aberrant eIF2B genes (*EIF2B1-5*) are present (Schiffmann et al., 2012).

Table 1.2 VWM Disease Severity

*Age in years, unless otherwise stated.

Figure 1.7 - Comparison of MRI images from VWM and non-VWM brain. Proton density weighted images illustrate the extent of white matter loss within affected individuals. T2 weighted images show that the white matter is replaced by cerebral spinal fluid, indicated by the intense white signal (Leegwater et al., 2001).

1.4.2. Aetiology of VWM disease

A wide variety of eIF2B mutations have been described, including missense, nonsense, insertions, deletions and splicing errors (**Fig. 1.8**) (Pavitt and Proud, 2009). Indeed, mutations that result in a frame shift or a premature stop codon produce the most severe phenotypes which have never been observed in the homozygous state and are likely to be incompatible with life (Pavitt and Proud, 2009, Pronk et al., 2006). Instead, severe mutations are generally found to coexist with a missense mutation (Pavitt and Proud, 2009). In the compound heterozygous state, both mutations may influence the progression of the disease, although some individual mutations are known to confer a severe phenotype whether they are in the homozygous or compound heterozygous state (*e.g.* eIF2Bε R195H/Cree mutation) (Takano et al., 2015, van der Lei et al., 2010).

The majority of mutations found within patients within eIF2B are missense. The catalytic subunit, eIF2Bε, contains the most mutations and harbours the most frequent amino acid substitution: R113H (Pronk et al., 2006). One study predicted another mutation (eIF2Bβ V85E) to be the most frequent throughout the Japanese population despite a low cohort number (5 patients) (Shimada et al., 2015). The R113H mutation is found in 20 % of all VWM cases and has been reported in both homozygous and compound heterozygous states (Pronk et al., 2006). In a genotype-phenotype correlation study, patients that were homozygous for R113H were found to have a milder disease progression than those who were compound heterozygous for R113H (van der Lei et al., 2010). Whilst statistically relevant, there was high variance indicating other influencing factors.

Missense mutations have also been identified that are yet to be found homozygously. The catalytic domain, present within eIF2Bε, harbours very few amino acid residues that are mutated. It is likely that it is spared because mutations within this domain would result in the loss of GEF activity. Interestingly, the four amino acid substitutions that are present within the catalytic domain have never been observed in the homozygous state (Pronk et al., 2006, Pavitt and Proud, 2009). Severe missense mutations have also been documented within the regulatory domains (*e.g.* eIF2Bβ V316D), which are likely to impact on eIF2B's decameric conformation (Richardson et al., 2004).

Most VWM mutations change amino acid residues that are instrumental to the structure and integrity of eIF2B, impacting on its ability to carry out its role (**Fig. 1.8**). As mentioned earlier, the regulatory subunit eIF2Bα and the catalytic subunit eIF2Bε both contain putative binding sites for eIF2 (Mohammad-Qureshi et al., 2007). Although the three remaining subunits partially bind eIF2, they do influence and enhance eIF2B's activity.

The regulatory subunits share large segments of homology, including a large amount of homologous heptad repeats and a C-terminal domain that are important for dimerization (Pavitt et al., 1997). A VWM mutation, V183F, was recently shown to prevent eIF2Bα homodimerisation and subsequently resulted in decreased GEF activity (Wortham et al., 2014, Wortham and Proud, 2015). Another eIF2Bα VWM mutation, N208V, increased GEF activity during recent biochemical testing (Wortham and Proud, 2015). This particular VWM mutation is in a region that binds eIF2α-P under cellular stress, although no significant decrease of eIF2α-P binding was found. Interestingly, the P278R mutation does not decrease or increase GEF activity, nor does it alter

eIF2B's ability to bind eIF2α-P (Wortham and Proud, 2015). Hence, how P278R produces the VWM phenotype is unknown. A low number of mutations exist within eIF2Bα, with ≤1% of VWM patients characterised with them (Pronk et al., 2006). This observation could very well be a testament as to how vital the subunit is to other, yet unknown, functions.

eIF2Bβ and δ contain many more VWM mutations than eIF2Bα. A large proportion of mutations occur throughout the heptad repeats, whilst the N and C-terminal domains are relatively spared (Pronk et al., 2006). Crystallography experiments have shown that these two subunits form a heterodimer which is in line with observations from biochemical experiments on the eIF2Bβ V316D VWM mutation. This particular mutation abolishes the eIF2Bδ subunit from the eIF2B complex (Kashiwagi et al., 2014, Richardson et al., 2004). Introduction of the equivalent eIF2Bβ mutation in yeast (V341D) produced the most detrimental phenotype in comparison to a small subset of other eIF2Bβ VWM mutations (Richardson et al., 2004). Although the severity of V316D is yet to be recorded in human patients, prior experimental evidence has shown that the severity of eIF2B missense mutations may not necessarily correlate with the severity of VWM (Fogli et al., 2004b, Liu et al., 2011).

The presence of eIF2Bβ stabilises the interactions between the regulatory subunits while eIF2Bδ stabilises the catalytic core. In addition to eIF2Bβ V316D affecting eIF2Bδ recruitment, G329V, another eIF2Bβ VWM mutation, prevents eIF2Bα interacting with the remaining complex (Liu et al., 2011). eIF2B complexes cannot form in the presence of the eIF2Bδ VWM mutations, R357W and R483W, although eIF2Bγε dimers are still able to form, lacking all the regulatory subunits. These observations

suggest that eIF2Bδ serves as a bridge between the regulatory core and the catalytic subunits (Liu et al., 2011).

Akin to the regulatory subunits; eIF2Bγ and ε also share large segments of homology with one another (Pronk et al., 2006). In contrast to eIF2Bε, eIF2Bγ is relatively small and contains fewer VWM mutations. eIF2Bε incurs many mutations that have not been observed within eIF2Bγ, suggesting a potential hotspot for mutations within the genomic DNA (Gomez and Pavitt, 2000). Many biochemical studies have shown eIF2Bε VWM mutations to reduce the GEF activity by up to 70 % (Liu et al., 2011, Fogli et al., 2004b). Interestingly, the Cree mutation (R195H), which consistently produces a severe phenotype and is not located within the catalytic domain, decreases the GEF activity by 30 % (Fogli et al., 2004a). In contrast, the R113H eIF2Bε VWM mutation, also reduces GEF activity by 30 %, but is associated with a milder disease progression (Fogli et al., 2004a).

Figure 1.8 - The broad spectrum of eIF2B VWM mutations in Humans. Over 153 VWM mutations have been described within the subunits of eIF2B collectively. Of note are the α and ε subunits which represent the subunits with the least and most mutations respectively. eIF2Bε contains over half of total VWM mutations, however the catalytic domain is relatively spared (Shimada et al., 2015).

1.4.3. Cellular and molecular pathogenesis of VWM

Whilst VWM mutations are ubiquitously expressed throughout all cells, glial cells are generally more impeded than any other cell type. There are several pathological signs of VWM, including an increase in the number of proliferating cells as well as an increase in the number of apoptotic cells. A notable feature of oligodendrocytes is a foam-like appearance which is possibly characteristic of undeveloped cells (Bugiani et al., 2011). Proteomic, transcriptomic and histopathological studies have revealed that the maturation of glia is somewhat delayed (Bugiani et al., 2011, Marom et al., 2011). It is likely that the immature glia cannot function properly under the impaired conditions conferred by a deficit in protein synthesis, especially considering that oligodendrocytes require a high rate of protein synthesis for myelination (Baumann and Pham-Dinh, 2001).

As described in section 1.2.1.1.1, the translation of *ATF4* is derepressed following a build-up of unfolded proteins within the ER (Vattem and Wek, 2004). The subsequent stress response prevents the synthesis of nascent proteins, as well as concomitantly upregulating the chaperones needed to fold proteins (Walter and Ron, 2011). The hyper-induction of ATF4 is a notable feature of VWM and could explain why further insults exacerbate the condition (Kantor et al., 2005, van Kollenburg et al., 2006). As mentioned previously, there is no direct evidence currently explaining why VWM patients are liable to rapid episodes of deterioration. However one explanation is that these additional stresses cause already impaired oligodendrocytes to release a key component of myelin, subsequently promoting apoptosis (Baumann and Pham-Dinh, 2001). Oxidative stress, infection, inflammatory mediators and head injury are all

known to potentiate sphingomyelinase, an enzyme that breaks sphingomyelin down into ceramide and lipids (Singh et al., 1998, Schenck et al., 2007). The presence of ceramide within the cytoplasm promotes apoptosis and oligodendrocyte loss (McTigue and Tripathi, 2008).
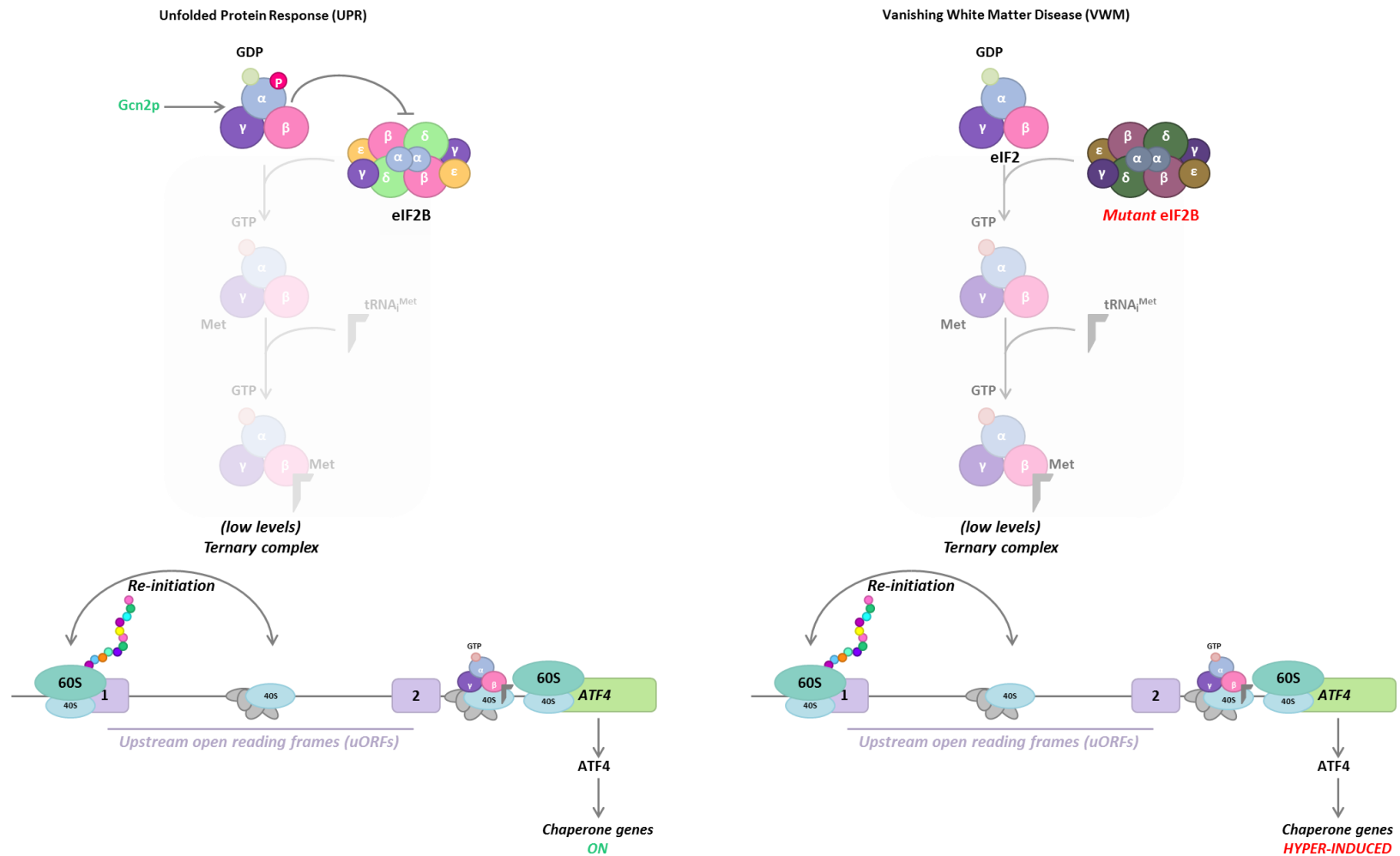
Figure 1.9 - Hyper-induction of *ATF4* in VWM disease. When there is a build-up of nascent proteins in the ER, global protein synthesis is inhibited and *ATF4* is specifically expressed for the unfolded protein response (UPR) to occur. However, the rate of protein synthesis is reduced when eIF2B is mutated, resulting in the constant expression of *ATF4*, which is normally regulated by two uORFs.

1.4.4. Current models of VWM disease

eIF2B is undoubtedly one of the most complex GEF enzymes in nature, comprising of five subunits which form a complex that exerts multiple functions. Over the last 30 years, *in vitro* and *in vivo* experiments utilising cell lines, animal models and *S. cerevisiae* have investigated the underlying mechanism behind VWM disease (Pavitt and Proud, 2009). It is generally accepted that abnormal eIF2B reduces rates of global protein synthesis which concomitantly enhances the translation of stress-specific mRNAs. Cells are therefore in a constant state of stress, hindering cellular differentiation and development (Pavitt and Proud, 2009, Bugiani et al., 2011). This hypothesis also explains why further trauma exacerbates the condition leading to rapid deterioration. However, there are some inconsistencies that cannot be explained by current models of eIF2B.

The current model of VWM disease presumes that the decline in the catalytic activity of eIF2B correlates with the severity of the disease. Contrary to this, independent studies have shown that there is no genotype-phenotype correlation (van der Lei et al., 2010, Liu et al., 2011). In addition, *in vitro* biochemical assays found no differences in eIF2B's catalytic activity (<30%) when in the presence of moderate or severe mutations (Liu et al., 2011). Using similar assays, other mutations have been shown to enhance the GEF activity of eIF2B or not affect it at all (Wortham and Proud, 2015). Hence, the current model of VWM disease cannot explain these discrepancies which could imply that there are features yet to be described of VWM disease, or alternatively, functions of eIF2B yet to be highlighted.

A characteristic of eIF2B that remains to be fully understood is the role of eIF2B bodies. eIF2B's substrate, eIF2, co-localises with the eIF2B body and may shuttle

through or accumulate within foci depending on cellular conditions. However, this eIF2B body only represents a portion of the cells total eIF2B, thus whether localisation enhances the various activities of eIF2B remains to be shown (Campbell et al., 2005). In addition, how the eIF2B body is formed and whether VWM mutations affect the subcellular localisation of eIF2B also remains unknown. Mis-localisation of proteins is well-documented in human disease, especially considering that the subcellular localisation of proteins is usually crucial to their biochemical function. Accordingly, additional studies investigating the function of the eIF2B body as well as the formation of the macromolecular structure may help shed light on the contradictions highlighted in this section. Subsequently, these data could substantiate hypotheses which may explain the variable phenotypes observed within VWM sufferers.

1.5. Project overview

In the following chapters, experiments were carried out to further elucidate how eIF2B bodies are formed, with a particular focus on the eIF2Bα subunit. eIF2B localisation was investigated in the presence of well-characterised mutations that either affect the catalytic activity of eIF2B or its ability to regulate global protein synthesis. To determine whether localisation may have a role in disease, VWM mutations were additionally generated and characterised. A particular theme in these studies was to try and maintain the cellular or *in vivo* environment. Therefore, the localisation of eIF2B was most analysed via live-cell imaging methods.

Previously published data has shown that other proteins are required for the formation of eIF2B bodies, but that are not necessarily involved in translation initiation or translational control. Similarly, the putative membrane proteins Mst27p, Erp4p and Sac1p have been shown to associate with eIF2B (Babu et al., 2012). Thus, their role in

eIF2B body formation as well translation initiation and translational control was also investigated.

2. Methods

2.1.   Culture conditions

2.1.1. Yeast strains and culture conditions

The *Saccharomyces cerevisiae* strain W303-1A was used throughout this study and strain genotypes are detailed in Table 2.2. Strains were either generated by homologous recombination as previously described, or by mating yeast strains (see section 2.5).

Yeast strains were typically grown in rich YPD media (1 % (w/v) Yeast extract, 2 % (w/v) Bacto Peptone and 2 % (w/v) glucose) or in minimal synthetic complete media (SCD; 0.17 % (w/v) Yeast nitrogen base without amino acids, 0.5 % (w/v) ammonium sulphate, 2 % (w/v) glucose). SCD was supplemented with either all essential amino acids or amino acids with specific dropouts (Formedium) depending on the genotype of the strain. In liquid media, strains were incubated at 30 °C with agitation (180 RPM). When grown on solid media, YPD or SCD media was supplemented with 2 % (w/v) agar.

2.1.2. Analysis of yeast growth rates

Individual colonies of yeast strains were inoculated in appropriate media and cultivated overnight at 30 °C with agitation (180 RPM). Overnight starter cultures were back-diluted to an OD_{600} of 0.2 and incubated at 30 °C with agitation. Growth was measured hourly using a Genesys 10S UV-VIS spectrophotometer (ThermoFisher Scientific) or by using a CLARIOstar platereader (BMG Labtech). When using the plate-reader, 200 µl of the diluted culture was pipetted into a 96 well-plate (ThermoFisher Scientific) which was incubated at 30 °C with agitation.

2.1.3. Bacterial strains and culture conditions

Escherichia coli (*E. coli*) background strain DH5α was routinely used for the amplification of plasmids. For site directed mutagenesis, XL10-Gold Ultracompetent *E. coli* was used to amplify mutant plasmids (Agilent). For cloning and sub-cloning, XL1-Blue competent *E. coli* (Agilent) were used to amplify recombinant DNA. Bacteria were grown in Luri-Bertani (LB) media (1 % (w/v) Bacto tryptone, 0.5 % (w/v) Yeast extract, 10 mM NaCl). For bacterial growth on solid media at 37 °C, LB was supplemented with 2 % (w/v) agar.

2.1.4. Antibiotics and drug supplements

Stock solutions of carbenicillin and kanamycin (Formedium) were prepared in distilled H_2O (dH_2O) at a concentration of 100 mg/ml and used in media at a final concentration of 50 µg/ml. Cycloheximide (Calbiochem) was dissolved in Diethylpyrocarbonate (DEPC) treated dH_2O as a 10 mg/ml stock and used at a final concentration of 100 µg/ml.

2.2. General DNA manipulation

2.2.1. Purification of plasmid DNA from bacterial cells

Plasmid DNA was isolated from bacterial cultures using a GeneJET plasmid miniprep kit (ThermoFisher Scientific) as per manufacturer's instructions. The plasmids used in this study are detailed in Table 2.3.

2.2.2. Genomic DNA extraction from yeast cells

Overnight starter cultures were pelleted by centrifugation (Eppendorf 5804 R) at 2500 x g for 3 minutes, before the media was removed and the DNA was extracted

using a MasterPure Yeast DNA purification kit (Cambio) as per manufacturer's instructions. The only modification to this protocol was that the precipitated DNA was dissolved in sterile dH$_2$O and not Tris-EDTA (TE) buffer.

2.2.3. Amplification of DNA via polymerase chain reaction

Polymerase chain reaction (PCR) was routinely used to amplify deletion cassettes using a Roche Expand High Fidelity kit (Sigma-Aldrich). Verification of genomic substitutions and colony PCR was carried out using TrueStart Taq polymerase (ThermoFisher Scientific). Oligonucleotides (Sigma-Aldrich) used throughout this study are listed in Table 2.4.

PCR reactions typically consisted of 1X buffer (without MgCl$_2$), 2.5 mM MgCl$_2$, 2.5 mM dNTP mix, 2 U of polymerase, 0.2 µM of appropriate primers and 2 µl of a 1 in 100 diluted DNA template. Sterile dH$_2$O was added to a final volume of 50 µl. PCR reactions were subjected to the reaction conditions in Table 2.1 by a Techne TC-312 thermocycler.

Table 2.1 - Typical PCR programme

PCR Step		Time (seconds)	Temperature (°C)
Initial denaturation		120	95
30 cycles	Denaturation	30	95
	Annealing	30	54-56
	Extension	60 / 1kb	68 High Fid / 72 TrueStart
Final extension		300	*As above*

2.2.4. Agarose gel electrophoresis

Amplified PCR products were typically separated through a 1 % (w/v) agarose gel containing 1 X TAE buffer (1.85 M Tris, 45 mM EDTA and 1 M Glacial acetic acid). To facilitate the visualisation of DNA fragments, 0.5 µg/ml ethidium bromide was used as an 'in-gel' stain. The presence of a GeneRuler 1 kB DNA ladder facilitated the identification of PCR products, which was pre-mixed with 1 X DNA loading dye (ThermoFisher Scientific). Agarose gels were visualised using a NuGenius UV gel imaging system (Syngene).

2.2.5. Site directed mutagenesis

Site directed mutagenesis was performed using the QuikChange II XL kit (Agilent) as instructed by the manufacturers with slight modifications. To increase the efficiency of bacterial transformations with mutated plasmid DNA, reactions were concentrated to 1/5th the volume by ethanol precipitation after the *Dpn*I digestion step. To precipitate the DNA, 0.1 volume NaAc (3M, pH 5.2) and 2 volumes of cold 100 % (v/v) ethanol (-20 °C) were added to the digestion reactions and incubated at -20 °C for 1 hour. The DNA was pelleted by centrifugation at 17000 x g for 15 minutes. The supernatant was removed and the DNA was washed once in cold 70 % (v/v) ethanol before being centrifuged again for 5 minutes. The supernatant was removed and the pellet was allowed to air dry at room temperature for 10 minutes. DNA was resuspended in 10 µl sterile dH$_2$O and stored at 4 °C until transformation.

To isolate the mutagenic plasmids, the concentrated DNA was transformed into bacteria. XL10-Gold Ultracompetent *E. coli* were thawed on ice before 50 µl aliquots were transferred into sterile microcentrifuge tubes. The concentrated plasmid DNA was incubated with the competent *E. coli* for 1 hour on ice, before being heat-shocked

in a water bath at 42 °C for 90 seconds. Bacterial cells were then placed on ice for 2 minutes. Cells were allowed to recover in 1 ml of SOC media (ThermoFisher Scientific) for 1 hour at 37 °C with agitation (180 RPM). Following recovery, bacterial cells were gently pelleted by centrifugation at 2000 $x\,g$ for 5 minutes. 1 ml of supernatant was removed before the cells were resuspended and spread onto appropriate solid selection media, which was incubated at 37 °C overnight.

Plasmid DNA was isolated from a number of colonies as described in section 2.3.1, and Sanger sequenced gene-wide as described in section 2.4.4.

2.2.6. Transformation of yeast with PCR product/plasmid DNA

Yeast strains were transformed with plasmids and PCR products by the LiOAc TRAFO method, as previously described (Gietz, 2014). Strains were cultivated in 50 ml of media until an OD_{600} 0.6 was reached at 30 °C. Cells were pelleted by centrifugation at 2500 $x\,g$ for 3 minutes and the media was decanted. The cells were washed in sterile dH_2O before being pelleted again. Following the removal of the water, the cells were resuspended in 100 mM sterile LiOAc and divided into 50 µl aliquots. Cells were pelleted once more by a microcentrifuge at 17000 $x\,g$ for 10 seconds before the LiOAc was removed. A 300 µl transformation mix was sequentially added on top of the cells, consisting of 38.0 % (w/v) polyethylene glycol, 100 mM LiOAc and 0.46 mg/ml single-stranded DNA of salmon sperm. Before use, 10 mg/ml of DNA from salmon sperm was heated to 95˚C for 5 minutes before being snap-cooled on ice for 10 minutes. The PCR product, plasmid DNA or sterile dH_2O (negative control) was added to corresponding tubes. Transformation mixtures were vortexed vigorously to resuspended the cells before incubation at 30 °C for 1 hour with agitation. Cells were then heat-shocked at 42 °C for 20 minutes. Cells that were transformed with plasmid DNA were quickly

pelleted at 17000 x g for 15 seconds before being resuspended in dH$_2$O and spread onto solid media for selection. Genomically altered cells that were transformed with a PCR product were incubated in 2 ml YPD overnight, before being pelleted and spread on to solid media for selection. Agar plates were incubated in a static 30 °C incubator for 48 hours.

2.3.   Cloning of DNA

2.3.1. Over-lap extension PCR

To produce Mst27p, Erp4p and Sac1p protein fusions with the fluorophore mKate2, one-step over-lap extension PCR (OE-PCR) was performed as previously described (Bryksin and Matsumura, 2010). PCR conditions were mostly similar to section 2.2.3 using the Roche High Fidelity polymerase system with slight modifications. In OE-PCR, the concentration of primers and template DNA was halved to accommodate two plasmids and four primers. The PCR programme remained mostly unchanged with the exception of 60 °C annealing temperature.

Following the amplification of PCR products and the separation via agarose gel electrophoresis, the corresponding DNA fragment was excised and purified using a GeneJet PCR purification kit (ThermoFisher Scientific) as per manufacturer's instructions.

2.3.2. Cloning into TOPO TA pYES2.1 vector

Purified mKate2 gene fusions were cloned into a TOPO TA pYES2.1 *GAL1* vector (ThermoFisher Scientific) as per manufacturer's instructions. Subsequent ligation reactions were transformed into bacteria as described in section 2.3.5. Following overnight selection on LB agar plates at 37 °C, colonies were resuspended in sterile

dH$_2$O which served as template DNA in a PCR reaction to determine colonies that were positive for recombinant DNA. DNA fragments from colony PCR were visualised by agarose gel electrophoresis. Plasmid DNA was isolated from positive colonies and Sanger sequenced prior to use.

2.3.3. Sub-cloning into pSF-TEF1 vector

The *SAC1-mKATE2* cassette was sub-cloned into a *pSF-TEF1-CEN6ARS4* vector (Oxford genetics). As the *SAC1-mKATE2* cassette already contained the canonical and optimal start codon, an AUG start codon was removed from the vector by *Kpn*I restriction digest (New England Biolabs) at 37 °C for 1 hour. The digested vector was visualised by agarose gel electrophoresis, and the corresponding vector fragment was excised and purified as in section 2.3.1. The vector was ligated using 8000 U of T4 DNA ligase (New England Biolabs) supplemented with 1 X T4 DNA ligase buffer. The reaction was left overnight at room temperature, before being transformed into bacteria as previously described in section 2.2.5. To confirm the removal of the start codon, plasmid DNA was purified from selected colonies and digested with *Nco*I (New England Biolabs), which was subsequently visualised via agarose gel electrophoresis. An undigested plasmid was taken forward and used to sub-clone *SAC1-mKATE2*.

The *SAC1-mKATE2* cassette was digested out of the pYES2.1 vector by incubation with *Ssp*I and *Xba*I for 1 hour at 37 °C. Similarly, the *pSF-TEF1-CEN6ARS4* vector lacking any start codon was digested by *Eco*RV and *Xba*I. Restriction enzymes were heat-inactivated at 80 °C for 20 minutes before DNA fragments were visualised and purified by agarose gel electrophoresis. To increase the efficiency of ligation, the purified DNA fragment and vector were both concentrated to 1/5th of the original volume by ethanol precipitation (see section 2.2.5). The *SAC1-mKATE2* cassette was

incubated with the linearised vector at a molar ratio of 5:1. The ligation reaction included 1X T4 DNA ligase buffer and 8000 U T4 DNA ligase which were subsequently incubated at room temperature overnight. The ligation reaction was then transformed into bacteria (see section 2.2.5) and incubated overnight. Colony PCR (see section 2.3.2) was used to identify colonies that contained recombinant DNA. Plasmid DNA containing recombinant *SAC1-mKATE2* was isolated and Sanger sequenced gene-wide prior to use.

2.3.4. Sanger sequencing

Sanger sequencing was performed by Source Biosciences (UK) using an Applied BioSystems 3730 DNA analyser with PeakTrace analysis software. A quality value limit of 20 was used which calls bases with 99 % confidence. The Staden software package (V2.0.0b9) was used to analyse chromatograms. Sequences were identified through NCBI Nucleotide-Blast.

2.4. Strain construction

2.4.1. Cross mating yeast strains

To cross yeast strains, single colonies of *Mat a* and *Mat α* strains were inoculated into the same 5 ml of YPD which was incubated overnight at 30 °C. Cells were pelleted by centrifugation at 2500 *x g* for 3 minutes before being washed in sterile dH$_2$O. Cells were pelleted once more and resuspended in 1 ml of sterile dH$_2$O before 50 µl was spread onto appropriate selection plates, which was incubated overnight at 30 °C.

2.4.2. Tetrad dissection

Selected diploid cells were spread onto solid sporulation media (0.1 % (w/v) Yeast extract, 0.05 % (w/v) glucose and 100 mM KOAc) and incubated at 30 °C for 5 days to induce sporulation. Several yeast colonies were resuspended in 50 µl of 1 M sorbitol and 1 mg/ml lyticase (Sigma-Aldrich) and incubated for 15 minutes at 37 °C. The reaction was slowed by the addition of 400 µl sterile dH_2O which was aliquoted onto solid YPD media and allowed to dry. To isolate single spores, tetrads were dissected using a Singer MSM System microscope (Abelson et al., 2004). Isolated tetrads were incubated for 2 days at 30 °C. To determine genotypes, the dissected tetrads were replica plated using velveteen cloths onto appropriate selection media and incubated at 30 °C for 2 days.

2.4.3. Mating type assay

The mating types of yeast strains were determined using the *Mat α* tester (yMK50) and the *Mat a* tester (yMK51). Each tester strain was cultivated overnight in YPD media. 150 µl of the culture was spread onto solid YPD media and allowed to dry. The isolated haploid cells were replica plated onto these plates and incubated at 30 °C for 2 days. Cells with a *Mat a* mating type inhibit the growth of *Mat α* cells (yMK50). Conversely, cells with a *Mat α* mating type inhibit the growth of *Mat a* cells (yMK51).

2.5. Protein analysis

2.5.1. Extraction of protein from yeast

Yeast strains were cultivated in 15 ml of media until an OD_{600} of 1 was reached. Cells were pelleted by centrifugation at 2500 *x g* for 3 minutes and the media was discarded. The cells were washed in ice-cold 1 X lysis buffer (30 mM Hepes KOH pH 7.4,

100 mM KOAc, 10 mM MgOAc and 1 mM PMSF) and pelleted in a microcentrifuge at 2500 $x\ g$ for 3 minutes, before the supernatant was discarded. Cells were resuspended in 1 X lysis before adding 100 µl acid-washed glass beads (Sigma-Aldrich). Cells were vortexed for 15 seconds and then placed on ice for 45 seconds. The glass bead beating step was repeated for a total of 6 cycles, with the final cycle lasting 20-30 seconds. Cellular fragments were pelleted by centrifugation at 17000 $x\ g$ for 15 minutes at 4 °C. The supernatant was transferred to a fresh microcentrifuge tube and 10 µl was aliquoted for quantification. Protein extracts were stored at -20 °C and defrosted on ice prior to use.

2.5.2. LacZ assay

LacZ assays were carried out to assess the expression levels of Gcn4p-LacZ as previously described (Hinnebusch, 1985). Strains were cultivated in appropriate media until an OD_{600} 0.7 was reached. Protein extracts were made as in the above section. 20 µl of crude protein extract was incubated in 980 µl 1X Z buffer (65 mM Na_2HPO_4, 45 mM NaH_2PO_4, 10 mM KCl, 1 mM $MgSO_4$) supplemented with 2 mg/ml Ortho-Nitrophenyl-β-galactoside (ONPG). The reaction was incubated at 30 °C with agitation (180 RPM) for 30 minutes before being stopped by the addition of 1M sodium carbonate. Absorbances were measured at OD_{420} in a Genesys 10S UV-VIS spectrophotometer. Miller units were calculated by using the following formula:

Miller units = 1000 x (Absorbance OD_{420} / (Volume x Time (mins) x OD_{600}))

The Miller units were calculated and normalised to the concentration of protein extracts, which was determined by BCA assay.

2.5.3. Quantification of protein extracts

The concentration of protein extracts was determined using the Bicinchoninic Acid (BCA) assay. A BCA working stock was made by adding 4 % copper sulphate to BCA (Sigma-Aldrich) at a ratio of 1:25. Bovine serum albumin (BSA) standards, ranging from 0.1 mg/ml to 4 mg/ml, were prepared in 1X lysis buffer. Protein extracts and BSA standards were aliquoted into 96-well plates. The BCA working stock was then added to the protein extracts/BSA standards at a ratio of 1:20. Following an incubation of 30 minutes at room temperature, absorbances were determined using a Victor^2 1420 multi-label counter (Wallac) at a wavelength of 560nm.

2.5.4. Western blotting

For the analysis of proteins via Western blotting, 30 µg of protein extract was boiled in 1X RunBlue LDS sample buffer (Expedeon) at 95 °C for 5 minutes. Boiled cell lysates were then separated through a 4-20 % gradient RunBlue SDS protein gel (Expedeon) in the presence of 1X RunBlue SDS-Tris-Tricine running buffer. The examination of protein molecular weights was facilitated by the presence of Chameleon duo pre-stained protein ladder (LiCor).

Separated proteins were transferred onto a nitrocellulose membrane (0.2 µm pore, ThermoFisher Scientific) in the presence of cold transfer buffer (25 mM Tris, 192 mM Glycine and 10 % (v/v) methanol). Following transfer, the nitrocellulose membrane was blocked for 1 hour in TBST buffer (50 mM Tris, 150 mM NaCl and 0.05 % (v/v) Tween-20) containing 5 % skimmed milk powder (Marvel). The membrane was washed three times in TBST for 10 minutes per wash, before incubating with the primary antibody overnight at 4 °C. The Rabbit Gcn3p antibody was gifted by Prof. Graham Pavitt (University of Manchester, UK) and used at a 1:1000 dilution. The

Mouse Pab1p antibody was gifted by Prof. Mark Ashe (University of Manchester, UK) and used at a 1:5000 dilution. Following primary antibody incubation, the membrane was washed three times and incubated with a near-infrared 680 anti-Mouse antibody and a near-infrared 800 anti-Rabbit antibody (LiCor). Both secondary antibodies were used at a 1:1000 dilution. The membrane was washed three times in TBST before imaging on a LiCor Odyssey Scanner.

2.6. Microscopy

2.6.1. Live-cell imaging and quantification of eIF2B localisation

Strains were cultivated in media at 30 °C until they reached an OD_{600} of 0.6. Cultures were placed on a 1 % (w/v) poly-L-lysine coated slide (ThermoFisher, UK) and visualised on a Zeiss LSM 510 confocal microscope using a 63 x plan-apochromat oil objective lens. To image GFP, an argon laser (488 nm) was typically used at 50 % capacity. To image RFP, a helium laser (543 nm) was used at 75 % capacity. Images were analysed either using Zeiss 2009 software or the National Institutes of Health (NIH) ImageJ software. For each strain/mutant analysed, the localisation of eIF2B was assessed for 100 cells per replicate.

2.6.2. Fluorescent recovery after photobleaching (FRAP)

FRAP was performed to measure the shuttling of eIF2α-GTP through eIF2B foci as previously described by (Campbell et al., 2005). Cytoplasmic foci were imaged and bleached using the argon laser at full capacity. Following the pre-bleach and bleach steps, the recovery of eIF2B into the cytoplasmic was followed by taking iterative images every 1.8 seconds for 25 cycles. 25 cells were analysed for each replicate.

Fluorescence recovery was normalised to the total fluorescence of the cell. Background fluorescence was also measured and subtracted from fluorescence recovery. Normalised data was fitted to a one-phase association curve to find mobile eIF2 and half-time recovery. A rate of recovery was calculated from the one-phase association curves by dividing the plateau by the rate constant (k). The eIF2 content of cytoplasmic foci was determined using NIH ImageJ software.

2.7. Sucrose density gradient analysis

2.7.1. Extract preparation

Yeast strains were typically cultivated in 150 ml of media which was separated into 50 ml aliquots. Ice cold cycloheximide (final conc. 0.1 mg/ml) was added to one 50 ml aliquot and then placed in iced-water for 30 minutes. The remaining were pelleted at 2500 x g for 3 minutes and resuspended in SCD lacking amino acids or glucose, before being incubated for either 30 minutes or 10 minutes respectively. Ice cold cycloheximide was added to the final aliquots and following a 30 minute incubation in ice-water, polysome extracts were prepared.

To extract the polysomes, cultures were pelleted at 2500 x g for 3 minutes at 4 °C and washed in 1 X lysis buffer (10 mM HEPES.KOH, pH 7.4, 2 mM MgOAc, 0.1 M KOAc, 0.1 mg/mL cycloheximide and 0.5 mM dithithreitol in DEPC treated distilled water). Cells were lysed by vortexing for 20 seconds in the presence of 1X lysis buffer and glass beads before being incubated back on ice-water for 40 seconds, vortexing cycles were performed 6 times. The lysed cells were pelleted by centrifugation at 8000 x g for 10 minutes at 4 °C. The supernatant was transferred to a fresh pre-chilled microcentrifuge tube which was stored at -80 °C to prevent degradation prior to use.

2.7.2. Preparation of sucrose density gradients

Varied concentrations of sucrose ranging from 15-50 % were prepared from a 60 % (w/v) DEPC treated sucrose stock and 10X polysome buffer (100mM Tris acetate, pH 7.4, 700 mM NH_4OAc, 40 mM MgOAc) as detailed in Table #. To generate a gradient, 2.25ml of each solution was sequentially dispensed into open-top 12.0 ml pollyallomer centrifuge tubes (Seton Scientific), starting with the 50 % (w/v) sucrose solution and ending with the 15 % (w/v) solution. Each layer was snap-frozen in liquid nitrogen before the next layer was added. Sucrose gradients were stored at -80 °C and thawed overnight at 4 °C prior to use.

2.7.3. Sedimentation of extracts on polysome gradients

The concentration of polysome extracts was determined using a NanoDrop 1000 spectrophotometer (ThermoFisher Scientific). 2.5 A_{260} units of extract were layered on top of sucrose gradients. Sucrose gradients were centrifuged using a Th-641 swing-out rotor in a Sorvall WX Ultracentrifuge for 150 minutes at 4 °C. Polysomes were measured by upward displacement using 60 % (w/v) sucrose; gradients were displaced using a fractionator that was connected to a UV-vis detector which measured polysomes at 254nm. Monosomes/polysomes were measured and compared using NIH ImageJ software.

2.7.4. Statistical analysis

To determine statistical significance between the various groups within each data set, a shapiro wilk test was performed to test for normality. Data was considered to be parametric when $p < 0.05$. However, all data was found to be non-parametric.

Various groups was compared to each other using the Kruskal-Wallis test followed by a

Conover Inman posthoc test.

Table 2.2 Yeast strains used in this study

Name	Genotype	Source
yMK50	*Mat a*	Campbell strain collection
yMK51	*Mat α*	Campbell strain collection
yMK467	*Mat α, ura3-52, leu2-3,112, gcn2::LEU2*	Campbell strain collection
yMK880	*Mat α, ADE2, his3-11,15, leu2-3,112, trp1-1, ura3-1, can1-100, GCD1-P180-GFP::G418*	Campbell strain collection
yMK883	*Mat α, ADE2, his3-11,15, leu2-3,112, trp1-1, ura3-1, can1-100, GCD1-P180 SUI2-GFP::G418*	Campbell strain collection
yMK1330	*Mat α, ADE2, his3-11,15, leu2-3,112, trp1-1, ura3-1, can1-100, GCD1-P180, SUI2-GFP::G418, gcn3::URA3*	Campbell strain collection
yMK1402	*Mat α, ADE2, his3-11,15, leu2-3,112, trp1-1, ura3-1, can1-100, GCD1-P180-GFP::G418, gcn3::LEU2*	Campbell strain collection
ySC14	*Mat α, ADE2, his3-11,15, leu2-3,112, trp1-1, ura3-1, can1-100, GCD1-P180-GFP::G418 mst27::URA3*	This study
ySC16	*Mat α, ADE2, his3-11,15, leu2-3,112, trp1-1, ura3-1, can1-100, GCD1-P180, SUI2-GFP::G418, gcn3::LEU2*	This study
ySC18	*Mat a, ADE2, his3-11,15, leu2-3,112, trp1-1, ura3-1, can1-100, GCD1-S180-GFP::G418 sac1::LEU2*	This study
ySC31	*Mat α, ADE2, his3-11,15, leu2-3,112, trp1-1, ura3-1, can1-100, GCD1-P180-GFP::G418 erp4::URA3*	This study
ySC85	*Mat α, ADE2, his3-11,15, leu2-3,112, trp1-1, ura3-1, can1-100, GCD1-P180, GCN4-LacZ-TRP1*	This study
ySC86	*Mat α, ADE2, his3-11,15, leu2-3,112, trp1-1, ura3-1, can1-100, GCD1-P180, GCN4-LacZ-TRP1, gcn3::HIS3*	This study
ySC97	*Mat α, ADE2, his3-11,15, leu2-3,112, trp1-1, ura3-1, can1-100, GCD1-P180, sac1::LEU2*	This study

ySC98	*Mat α, ADE2, his3-11,15, leu2-3,112, trp1-1, ura3-1, can1-100, GCD1-P180, sac1::LEU2, gcn3::HIS3*	This study
ySC99	*Mat a, ADE2, his3-11,15, leu2-3,112, trp1-1, ura3-1, can1-100, GCD1-P180, GCN4-LacZ-TRP1*	This study
ySC100	*Mat a, ADE2, his3-11,15, leu2-3,112, trp1-1, ura3-1, can1-100, GCD1-P180, GCN4-LacZ-TRP1, gcn3::HIS3*	This study

Table 2.3 Plasmids used in this study

Name	Genotype	Source
BSC078	*p[mKATE2]*	Addgene; (Lee et al., 2013)
BSC087	*p[GAL1-ERP4-mKATE2 2μ]*	This study
BSC088	*p[GAL1-MST27-mKATE2 2μ]*	This study
BSC090	*p[GAL1-SAC1-mKATE2 2μ]*	This study
BSC091	*p[GAL1-MST27 2μ]*	Harvard Medical School
BSC093	*p[GAL1-ERP4 2μ]*	Harvard Medical School
BSC094	*p[GAL1-SAC1 2μ]*	Harvard Medical School
BSC116	*p[GCN3 K111E URA3 CEN6ARS4]*	This study
BSC117	*p[GCN3 V184D URA3 CEN6ARS4]*	This study
BSC118	*p[GCN3 F240V URA3 CEN6ARS4]*	This study
BSC119	*p[GCN3 Y274C URA3 CEN6ARS4]*	This study
BSC128	*p[TEF1-SAC1-mKATE2 CEN6ARS4]*	This study
pAV1108	*p[GCN3(T41A) URA3 2μ]*	(Pavitt et al., 1997)
pAV1109	*p[GCN3(E44V)URA3 2μ]*	(Pavitt et al., 1997)
pAV1110	*p[GCN3(E44K)URA3 2μ]*	(Pavitt et al., 1997)
pAV1111	*p[GCN3(F73L) URA3 2μ]*	(Pavitt et al., 1997)
pAV1112	*p[GCN3(N80D) URA3 2μ]*	(Pavitt et al., 1997)
pAV1113	*p[GCN3(F240I) URA3 2μ]*	(Pavitt et al., 1997)
pAV1115	*pGCN3 (T291P) URA3 2μ]*	(Pavitt et al., 1997)
pAV1116	*p[GCN3 (S293R) URA3 2μ]*	(Pavitt et al., 1997)
pAV1117	*p[GCN3 URA3 2μ]*	(Pavitt et al., 1997)
pAV1170	*p[GCN3 URA3 CEN]*	(Hannig et al., 1990)
pAV1239	*p[GCN3(AA2526VV) URA3 CEN]*	(Hannig et al., 1990)
pAV1240	*p[GCN3(A26T) URA3 CEN]*	(Hannig et al., 1990)

pAV1241	*p[GCN3(R104K) URA3 CEN]*	(Hannig et al., 1990)
pAV1242	*p[GCN3(V295F) URA3 CEN]*	(Hannig et al., 1990)
pAV1243	*p[GCN3(D71N) URA3 CEN]*	(Hannig et al., 1990)
pAV1244	*p[GCN3(E199K) URA3 CEN]*	(Hannig et al., 1990)
pAV1268	*p[GCN3(303//305Δ) URA3 CEN]*	(Hannig et al., 1990)
pAV1729	*p[GCN4 leader-lacZ-TRP1]*	(Hinnebusch, 1985)
pAV1769	*p[GCN3 URA3 CEN6ARS4]*	(Richardson et al., 2004)
pAV1778	*p[GCN3(N209Y) URA3 CEN6ARS4]*	(Richardson et al., 2004)
pRS423	*p[HIS3]*	(Christianson et al., 1992)
pRS424	*p[URA3]*	(Christianson et al., 1992)
pRS425	*p[LEU2]*	(Christianson et al., 1992)

Table 2.4 - Oligonucleotides used in this study.

Name	Purpose	Sequence
Mst27DelF	Amplification of deletion cassette used to delete the *MST27* gene.	CACAGAGACAATCAGGAATACTATAGTCATAGACGATAC AAGGTATATATTGGTCGCAGATTGTACTGAGAGTGC
Mst27DelR		GATTATATATCATACTCTAGTTTATGTTCGCTTTACGTATG GCAGTGTCTCTAAGCTGTGCGGTATTTCACACCG
Mst27DelVF	External verification primers, designed to avoid *MST28*.	GATGTTAGAGGAAGCTGAAGTG
Mst27DelVR		TGCTGCTTGAAAGTCTCTGC
Erp4DelF	Amplification of deletion cassette used to delete the *ERP4* gene.	CGAGCGCTAGTGAAGTTTTTTCATAAATATATATTCCCAA TCATCGCTAGGAATTGCAGATTGTACTGAGAGTGC
Erp4DelR		AGTGCCTTCCCCTTAGCACAGCTGATCCAACAATTTTAAG AGCTTGAAAAGCAACCTGTGCGGTATTTCACACCG
Erp4DelVF	External verification primers to confirm *ERP4* deletion.	TGTGCTCTCTCAAGTGCC
Erp4DelVR		TGGACAATGGTTGTTTGTGGCC
Sac1DelF	Amplification of deletion cassette to delete the *SAC1* gene.	ATCCCTATAACAGTAACGATAATATTTATATACACGTATA TTTTCTCGTCTAGATGCAGATTGTACTGAGAGTGC
Sac1DelR		TCGGTTTTACGTTTTGGATTTACAATAATCATCATTTTATC ACATATAGAACTCACTGTGCGGTATTTCACACCG
Sac1DelVF	External verification primers to confirm *SAC1* deletion.	TCGTGCCCTTTAAGTGTTGC
Sac1DelVR		ACCAGGGACGATGCTGAAAA
Gcn3DelF	Amplification of deletion cassette to delete the *GCN3* gene.	TAATTGATAGAAAGAATTTTAAAAGTCCTACGTATACCA GAAATCGAGAGGAAGGGCAGATTGTACTGAGAGTGC
Gcn3DelR		GCGCTTTTTCTCCTTTTCTATTAAGTCATTGCGTGCATATA TTATGTGATTTTTTCTGTGCGGTATTTCACACCG
Gcn3DelVF	External verification primers to confirm *GCN3* deletion.	ACGTATACCAGAAATCGAGAGGA
Gcn3DelVR		ACTGATGTCTGATGCTGTTCT
Ura3VF	Internal verification primers used to verify gene deletions.	GGGATGCTAAGGTAGAGGGTG
Ura3VR		CCCGCAGAGTACTGCAATTTGA

Leu2VF	Internal verification primers used to verify gene deletions.	CACCGTTCCAGAAGTGCAAA
Leu2VR		CATGGCGGCAGAATCAATCA
K111E_F	Internal primers used for site directed mutagenesis.	CAAAAAATCGCGTAACGAGATTGCAGAAATAGG
K111E_R		CCTATTTCTGCAATCTCGTTACGCGATTTTTTG
V184D_F	Internal primers used for site directed mutagenesis.	GTCGATAGCGCGGATGGAGCGGTAATC
V184D_R		GATTACCGCTCCATCCGCGCTATCGAC
F240V_F	Internal primers used for site directed mutagenesis.	CACAAATTTGTTCGTATGGTTCCATTGTCTTCAGATG
F240V_R		CATCTGAAGACAATGGAACCATACGAACAAATTTGTG
Y274C_F	Internal primers used for site directed mutagenesis.	CCCACGATCGACTGTACCGCCCAAGAA
Y274C_R		TTCTTGGGCGGTACAGTCGATCGTGGG
Mst27F		ATGCAGACCCCTCTAGAAAGTACC
Mst27mKR	Primers used in OE-PCR to create *MST27-mKATE2* gene fusions.	CACCGTCACCTTCCGTCTTTTTAAGAAGCGCATCGAT
mKMst27F		CTTAAAAAGACGGAAGGTGACGGTGCTGGTTTAATTAAC ATG
Erp4F		ATGCGCGTTTTTACTTTGATTGCGATT
Erp4mKR	Primers used in OE-PCR to create *ERP4-mKATE2* gene fusions.	CACCGTCACCTACGTAGTTTTTTTGGCGACTGGTAAAAA AG
mKErp4F		CCAAAAAAACTACGTAGGTGACGGTGCTGGTTTAATTAA CATG
Sac1F		ATGACAGGTCCAATAGTGTACGTTC
Sac1mKR	Primers used in OE-PCR to create *SAC1-mKATE2* gene fusions.	CACCGTCACCATCTCTTTTTAAAGGATCCGGCTTGGAA
mKSac1F		GATCCTTTAAAAAGAGATGGTGACGGTGCTGGTTTAATT AACATG
mKate2R	*mKATE2* primer used in OE-PCR to create gene fusions	GGTGACGGTGCTGGTTTAATTAACATGGT

3. eIF2Bα is required for the formation of eIF2B bodies

3.1. Introduction

Various cytoplasmic foci such as P-bodies and stress granules have been well documented to play roles in the storage and fate of mRNAs. Whilst mRNA transcripts and various translation initiation factors are known components of these foci, eIF2B mainly localises to eIF2B bodies (Campbell et al., 2005). The importance of eIF2B bodies with respect to translational control is still unclear. Thus, important questions remain: why localise eIF2B to one singular cytoplasmic body? Which eIF2B subunit is responsible for such localisation? Is localisation important for the functional properties of eIF2B?

The main aim of this chapter was to gain insight into how eIF2B forms eIF2B bodies. Recently, the eIF2B body was shown to exhibit features indicative of a filamentous structure (Petrovska et al., 2014). Indeed, a hallmark of filamentous aggregates is their progression from single molecules to macromolecules, which display intrinsic organisation often incorporating intermediate structures. In their initial study describing eIF2B bodies in the yeast *S. cerevisiae*, Campbell *et al.*, (2005) showed all eIF2B subunits to co-localise. Since one uniform eIF2B body was present within each cell, it is likely that the decameric complex is formed prior to localisation.

eIF2B consists of five different subunits that are divided into two categories based on their function. The α, β and δ subunits are regulatory subunits whilst γ and ε are catalytic. In humans and yeast, eIF2B exists as a decamer comprising two εγδβ heterotetramers stabilised by an α-α homodimer (Wortham et al., 2014). Over the last 10 years, several structural studies investigating eIF2B's crystal structure as well as

subunit interactions and stoichiometry have been published. Taken together, they imply that eIF2Bα may play a key role in the formation of eIF2B bodies.

Recent evidence has provided the first model on how the decameric structure may be formed with eIF2Bα entering last (Wortham et al., 2016). Wortham *et al.,* identified that all eIF2B subunits, except eIF2Bα, are stochastically regulated (**Fig. 3.1**). Stable expression of eIF2Bε relies on similar levels of γ to be co-expressed; correspondingly eIF2Bδ requires similar levels of eIF2Bεγ and β (Wortham et al., 2016). Any surpluses are degraded by the ubiquitin-proteasome system. This study indicated that the eIF2B holocomplex may be built around the catalytic subunits, with eIF2Bβδ entering second to form an eIF2Bεγβδ tetramer. Finally, the eIF2Bα$_2$ dimer then binds two tetramers to complete the decameric holocomplex. In line with this model, observations from crystallography and mass spectrometry highlighted ε-β and γ-δ interactions primarily stabilise the tetrameric subcomplex which is unable to dimerise in the absence of eIF2Bα (Wortham et al., 2014) (Kashiwagi et al., 2016).

Under physiological conditions eIF2Bα homodimerises at its C-terminus (Kashiwagi et al., 2016). Interestingly, experiments with higher concentrations of purified protein have shown eIF2Bα to aggregate and even to form octamers (Bogorad et al., 2014). Although these experiments were performed *in vitro* using purified recombinant proteins, similar experiments with eIF2Bβ using physiological and high concentrations showed that it is indeed a monomer, highlighting that the ability of eIF2Bα to form complexes was not an experimental artefact (Bogorad et al., 2014). It is plausible that these experiments are representative of *in vivo* conditions, with physiological conditions representing eIF2Bα forming the decamer and higher concentrations representing eIF2Bα forming eIF2B bodies, therefore contributing to

the overall organisation of the eIF2B complex as previously described, and potentially eIF2B body formation thereafter.

Within this chapter, experiments were undertaken to test the hypothesis that eIF2Bα (Gcn3p in *S. cerevisiae*) is required for the aggregation of eIF2B to form eIF2B body.
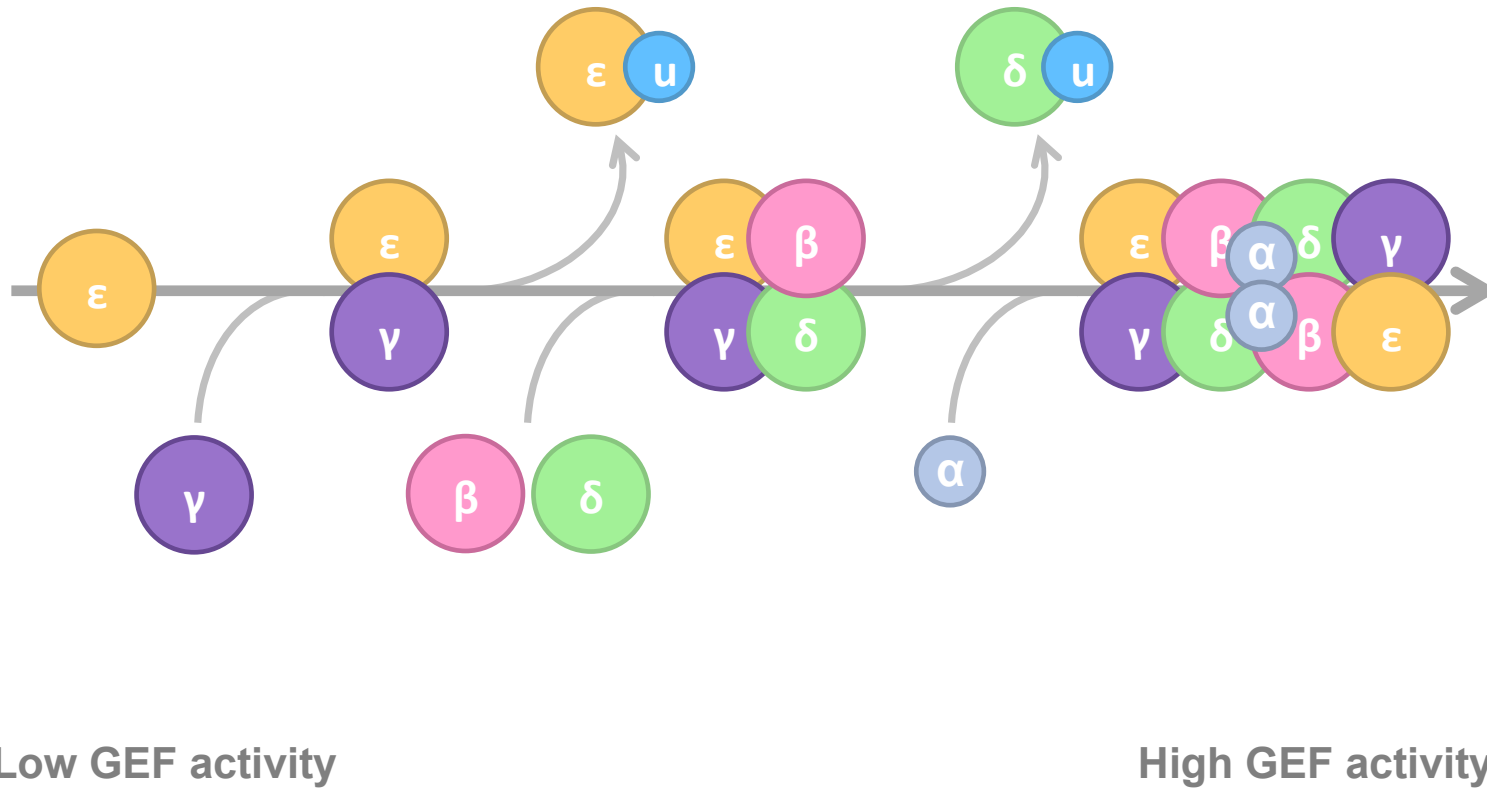
Figure 3.1 eIF2B subunits are stochastically expressed. eIF2Bγ relies on stable expression of the ε subunit, whilst eIF2Bδ relies on stable expression of the β subunit in addition to eIF2Bεγ. Any abundances are degraded by the ubiquitin-proteasome system. These observations provide the basis for the first model on how eIF2B may be assembled, with eIF2Bα binding two eIF2Bεγβδ tetramers to form the complete decameric complex. Whilst some of these subcomplexes are yet to be observed in vivo¸ in vitro biochemical testing shows eIF2B activity to increase as more subunits enter the complex, thus in support of this model.

3.1.1. eIF2Bα is required for the formation of eIF2B bodies

In their original study identifying eIF2B bodies, Campbell *et al.,* (2005) showed eIF2B and eIF2 to co-localise within eIF2B bodies. Using a number of strategies to alter the GEF activity of eIF2B, results suggested that these cytoplasmic foci where sites were eIF2B activity can be controlled and regulated. These eIF2B bodies can be seen in **Figure 3.2A**. Live-cell imaging was carried out on individual strains containing GFP tagged *GCD1* (eIF2Bγ) or *SUI2* (eIF2α), which were generated prior to this study (Campbell et al., 2005). Although eIF2B bodies were visible in exponentially growing cultures, they were not present in every cell. Therefore, to examine the prevalence of the eIF2B body phenotype, a minimum of 100 GFP tagged *GCD1* (eIF2Bγ) cells were assessed based upon eIF2B localisation (**Fig. 3.2B**). It was identified that 55.8% of cells formed eIF2B bodies. Intriguingly, eIF2B also localised to multiple foci instead of the singular eIF2B body, although this was a rare occurrence (1.8%).

To investigate whether eIF2Bα was responsible for the formation of eIF2B bodies, eIF2B localisation was determined in strains *gcn3::LEU2 GCD1-GFP* (yMK1402) and *gcn3::LEU2 SUI2-GFP* (ySC16). yMK1402 was generated prior to this study. The *URA3* cassette within *gcn3::URA3 SUI2-GFP* (yMK1330) was replaced with *LEU2* to enable complementation by *URA3* based plasmids. To substitute amino acid markers, homologous recombination was performed as described in 2.3.6.

Both strains were analysed to investigate whether eIF2Bα/Gcn3p is required for eIF2B body formation. Live-cell imaging of cells lacking Gcn3p showed eIF2Bγ to be dispersed throughout the cytoplasm (**Fig. 3.2A**). Quantitation of this dispersed phenotype is shown in **Figure 3.2B**.

In-order to confirm that this dispersal was due to the lack of Gcn3p, *gcn3Δ* strains were transformed with low copy (Cen) and high copy (2µ) plasmids containing wild-type *GCN3,* complete with its canonical promoter. Localisation was rescued in the presence of Gcn3p (**Fig 3.2A**). Exogenously expressed *GCN3* from a low copy Cen plasmid showed a similar localisation pattern to wild-type with 48.5 % of cells containing eIF2B bodies (**Fig 3.2B**). Again like the wild-type, a very small proportion of cells containing multiple smaller eIF2B foci were present (1.1 %). eIF2B bodies were also rescued when *GCN3* was over-expressed on a high copy 2µ plasmid. In contrast to wild-type however, there was a decrease in the number of cells with eIF2B bodies (31 %) and an increase in the number of cells displaying dispersed eIF2B (63.2 %). Interestingly, instances of multiple foci also increased slightly (5.4 %). Although this was not significant, it suggested that *GCN3* over-expression may be detrimental to eIF2B localisation. Nevertheless, these experiments showed that eIF2Bα is required for the formation of eIF2B bodies.
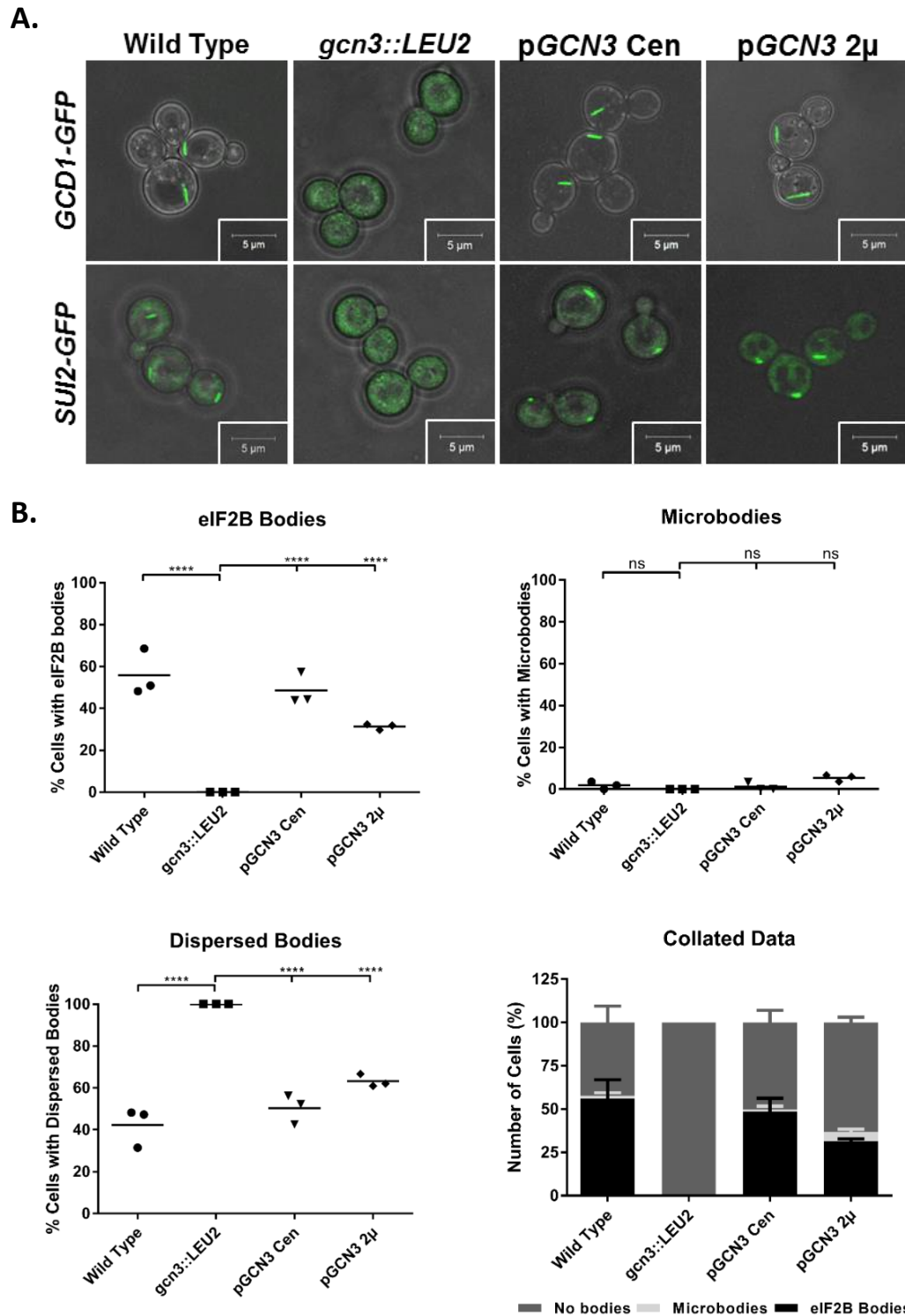
Figure 3.2 eIF2Bα is required for eIF2B body formation. (A) Confocal microscopy of GCD1-yeGFP (yMK880), SUI2-yeGFP (yMK883), GCD1-yeGFP gcn3::LEU2 (yMK1402) and SUI2-yeGFP gcn3::LEU2 (ySC16). Null strains were transformed with a low copy Cen plasmid (pAV1170) or a high copy 2μ plasmid (pAV1117) both containing WT GCN3. (B) A minimum of 100 cells were counted and assessed as to whether eIF2B bodies were present, dispersed or localised to microbodies. Overnight cultures were diluted in SCD media to 0.2 OD_{600} and incubated at 30°C with shaking until exponential growth was reached. n=3, error bars are representative of SD, ns = not significant, * P=<0.05, ** P=<0.01, *** P=<0.001, **** P=<0.0001.

3.1.2. Characterisation of *gcn3Δ* cells growth

Although Gcn3p/eIF2Bα is required for the regulatory function of eIF2B, it is not essential for cellular growth in yeast (Pavitt et al., 1997). In contrast, over expression of Gcn3p has been shown to be toxic to cells, slowing growth dramatically (Yoshikawa et al., 2011). To ensure our background strain behaved similarly, therefore allowing comparisons with previous work, growth curves were generated for the wild-type and *gcn3Δ* strains as well as the cells expressing *GCN3* exogenously on low or high copy plasmids (**Fig. 3.3**). In line with previous data, deletion of *gcn3* did not impact upon cellular growth and *gcn3Δ* cells grew at a similar rate as wild-type cells. In addition, when *GCN3* was exogenously expressed from a low copy plasmid, cell growth was not affected however, the high copy counterpart dramatically decreased cellular growth rate, confirming previous observations (Yoshikawa et al., 2011).
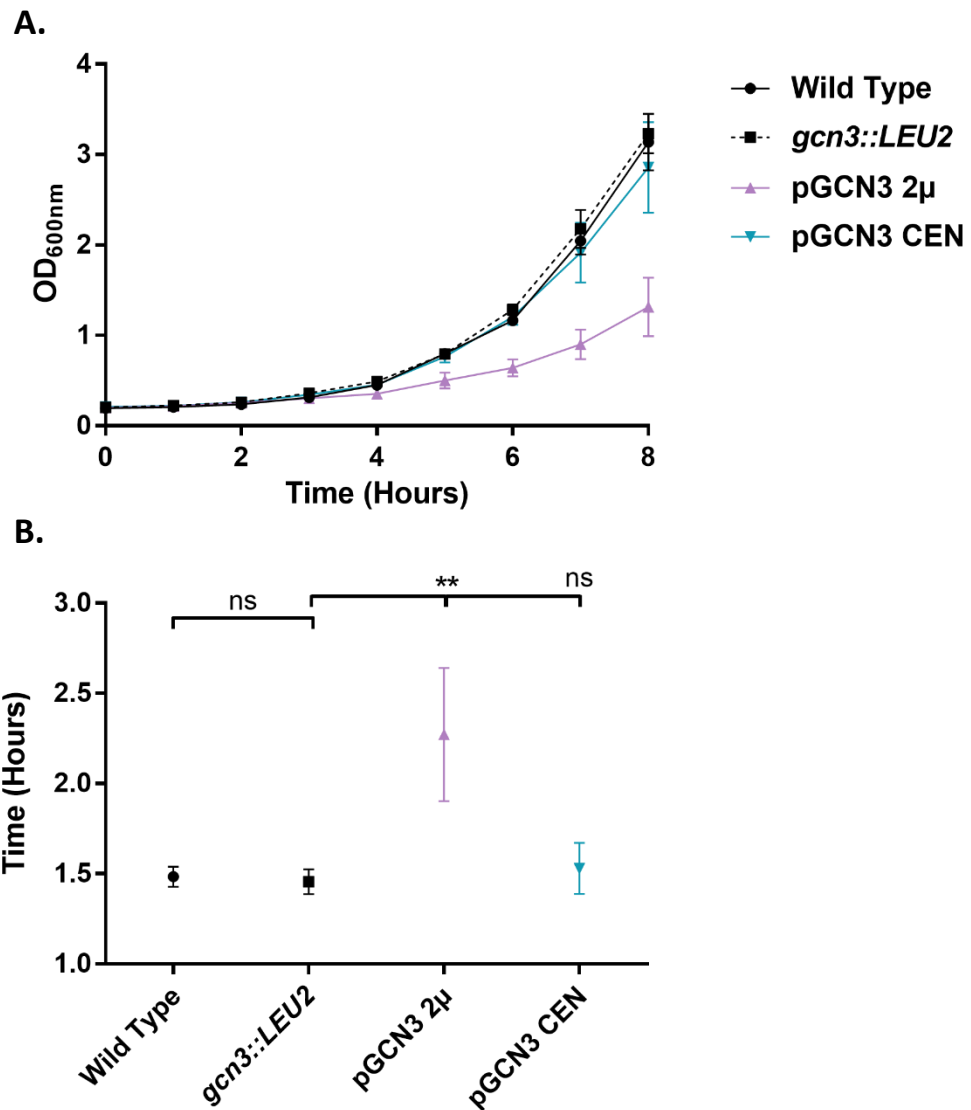
Figure 3.3 Deletion of eIF2Bα does not impact growth. Overnight cultures were diluted to 0.2 OD_{600} in fresh SCD media before incubation at 30°C with shaking. Growth was monitored over eight hours, n=3, error bars are representative of SD.

3.1.3. Characterisation of eIF2B dependent regulation in cells lacking *gcn3*

To assess the efficiency of translation initiation in cells deleted for *gcn3*, or exogenously expressing *GCN3*, polysome analysis was carried out. Under optimal growth conditions, most mRNAs are actively translated. During these steady-state conditions, mRNAs may have several ribosomes attached that are at various stages of translation. This results in the accumulation of ribosomes on mRNA transcripts, giving rise to polyribosomes or polysomes (**Fig. 3.4**). When translation initiation is inhibited however, ribosomes are unable to undergo concurrent rounds of translation, subsequently leading them to 'run-off' mRNAs resulting in an increase of 80S monosomes.

One of the classic cellular stresses which inhibits protein synthesis is amino acid depletion. In yeast, Gcn2p responds to amino acid starvation by phosphorylating serine 51 on eIF2α (Sui2p in *S. cerevisiae*). In its phosphorylated state eIF2 binds more tightly to eIF2B inhibiting the GEF activity and subsequently decreasing translation initiation and global protein synthesis (see section 1.2.1.1.1). eIF2Bα contains the binding site for phosphorylated eIF2 and is crucial to eIF2B's ability to respond to this stress. Deleting *gcn3* therefore renders eIF2B insensitive to eIF2α-P, preventing the sequestration of translation initiation. To ensure the *gcn3Δ* strain used here displayed a similar phenotype, polysome profiling was used to analyse whether cells lacking *gcn3* could respond to amino acid starvation (**Fig. 3.5**). As a control, glucose starvation was included as an eIF2B-independent stress which is a potent inhibitor of translation initiation. In line with previous observations, amino acid starvation lead to ribosomal 'run-off' within all wild-types expressing *GCN3*, indicated by the increase in the 80S monosome peak (**Fig. 3.5A**). Quantification of the area underneath the monosome and

polysome peaks revealed that the polysome:monosome (P:M) ratio decreased by around 50 % (**Fig. 3.5B**). Consistent with previous findings, the P:M ratio did not change in response to amino acid starvation within the *gcn3* null strain, indicating that these cells are unable to respond to eIF2B-dependent regulation.
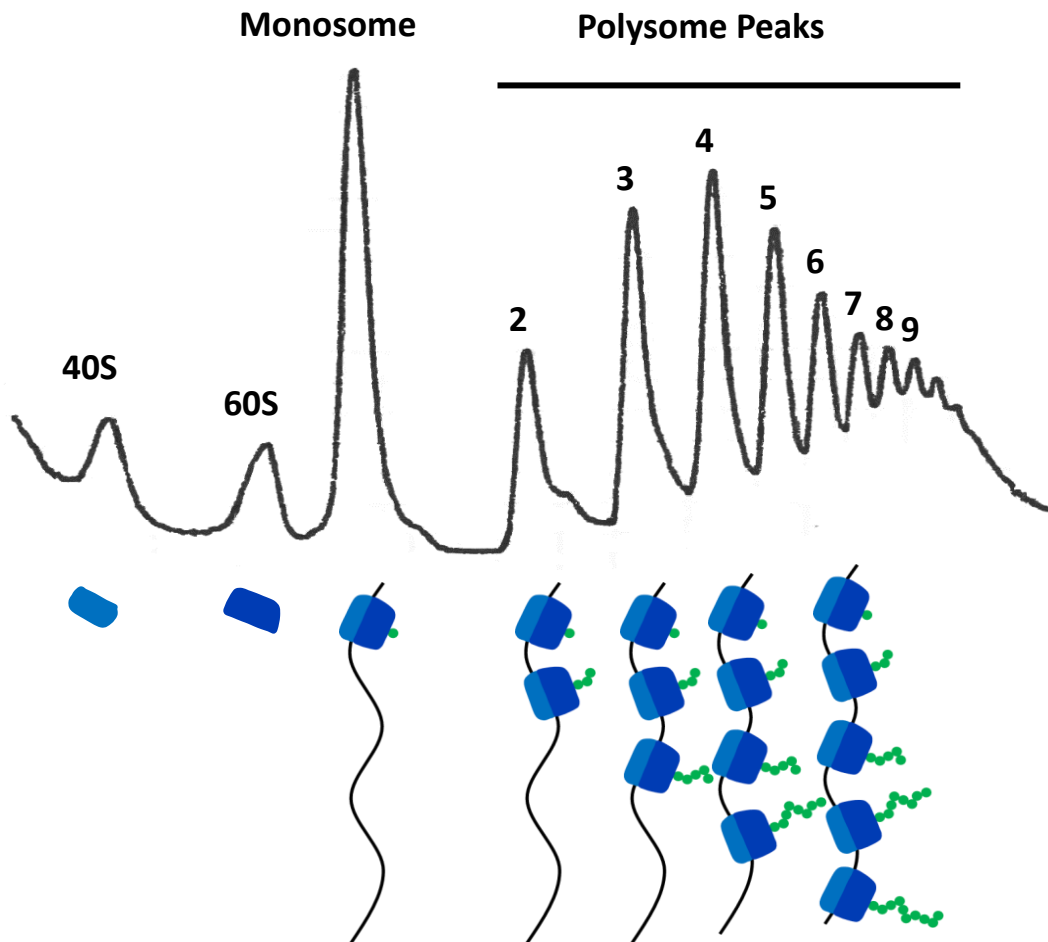
Figure 3.4 Schematic of polysome profiling traces. Following the addition of cycloheximide, ribosomes decoding mRNA become stalled. Cell extracts are then separated on a sucrose gradient before being passed through a UV detector to produce a polysome trace. With the exception of the 40S and 60S peaks, the peaks relate to the number of ribosomes attached to any given mRNA. As efficient translation can be attributed to multiple ribosomes translating along mRNAs, the area underneath the monosome peak can be compared to the polysome peaks to calculate a polysome/monosome ratio which can be compared to evaluate translational control and translation initiation.
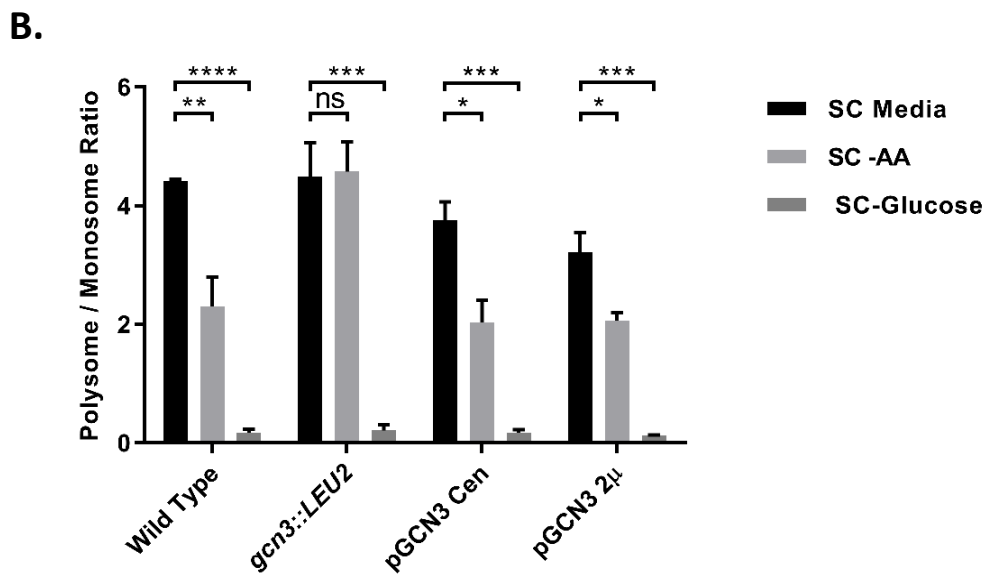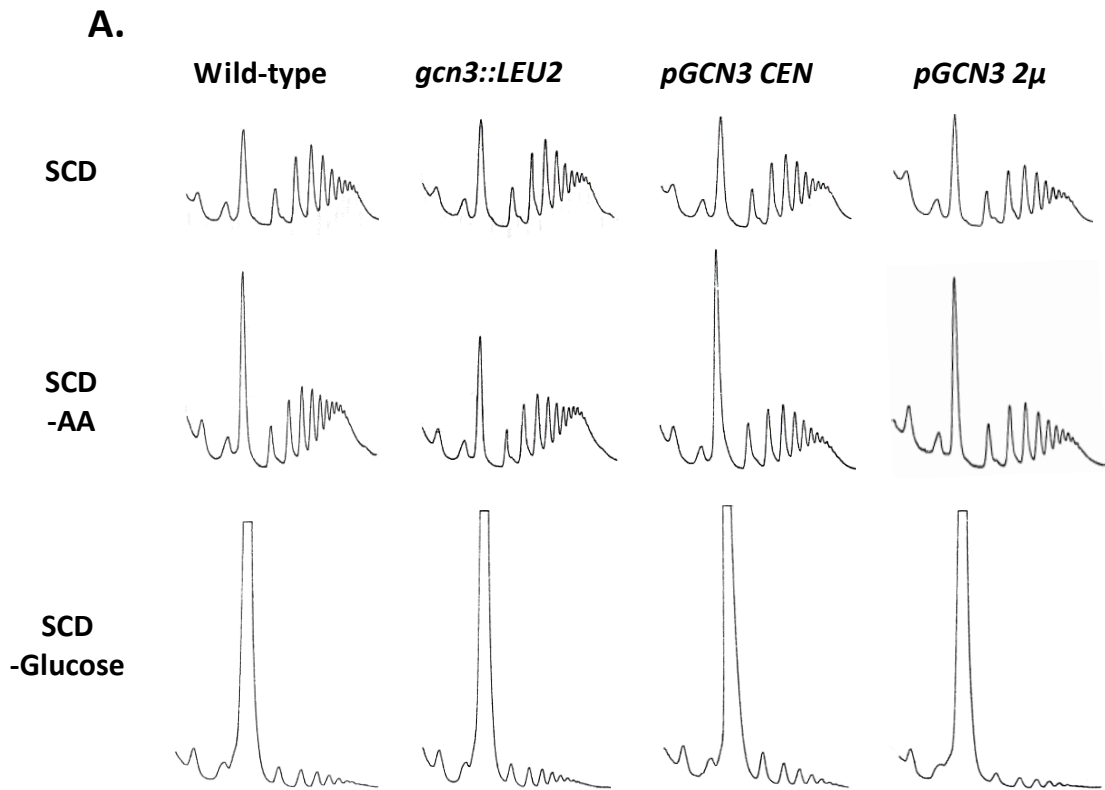
Figure 3.5 Deletion of eIF2Bα prevents eIF2B from responding to amino acid starvation. (A) Polysome profiles of GCD1-yeGFP (yMK880), GCD1-yeGFP gcn3::LEU2 (yMK1402) as well as yMK1402 containing exogenous WT GCN3 on low copy Cen (pAV1170) or high copy 2μ plasmids (pAV1117). (B) The area underneath the monosome peak and polysome peaks were quantified using ImageJ to find the polysome/monosome ratio. Overnight starter cultures were diluted to 0.2 OD_{600} in SCD media and incubated at 30°C with shaking until exponential growth was reached. Cultures were divided, pelleted and resuspended in media lacking amino acids or glucose, and incubated at 30°C for 30 minutes and 10 minutes respectively. n=3, error bars are representative of SD, ns = not significant, * P=<0.05, ** P=<0.01, *** P=<0.001, **** P=<0.0001.

3.1.4. eIF2Bα mutations alter the localisation of eIF2B

Having established eIF2Bα to be essential for the formation of eIF2B bodies, we wished to further investigate the role of eIF2Bα in the formation of eIF2B bodies. To achieve this, a series of previously published Gcn3p mutants were characterised. These mutants were originally generated by Hannig *et al.,* (1990) and Pavitt *et al.,* (1997) and gave two distinct phenotypes that either affected the regulatory or catalytic activities of eIF2B. Both types of mutations influence Gcn4p expression and therefore the stress response (see section 1.2.1.1.1). Regulatory mutations (initially coined general control nonderepressible (Gcn⁻) mutations) prevent eIF2B from binding eIF2α-P in response to cellular stress (Pavitt et al., 1997), thus Gcn4p expression cannot be induced preventing the cell from producing a stress response. Catalytic mutations (initially coined general control derepressible (Gcd⁻) mutations) decrease eIF2Bs ability to exchange GDP for GTP on eIF2, reducing global protein synthesis which leads to the constitutive expression of Gcn4p (Hannig et al., 1990). The *gcn3* catalytic and regulatory mutants were originally generated via random mutagenesis using the low copy (Cen) and high copy (2μ) *GCN3* plasmids as respective templates, which were characterised during section 3.1.1.

All *gcn3* regulatory and catalytic mutations used in this study were sequenced prior to any analyses to ensure additional mutations were not present. The mutations are shown in **Figure 3.6**, modelled on the eIF2Bα homodimer from *Schizosaccharomyces pombe* (Kashiwagi et al., 2016)*.* Highlighted in blue are catalytic mutants whilst regulatory mutants are coloured purple. Interestingly, the Gcn3p regulatory mutants are mostly located on the distal face where eIF2Bβ and δ docking sites exist. Although the Gcn3p catalytic mutants seem to be in close proximity to

these pockets, they are mostly located further away and therefore may affect intra-

residue interactions instead.
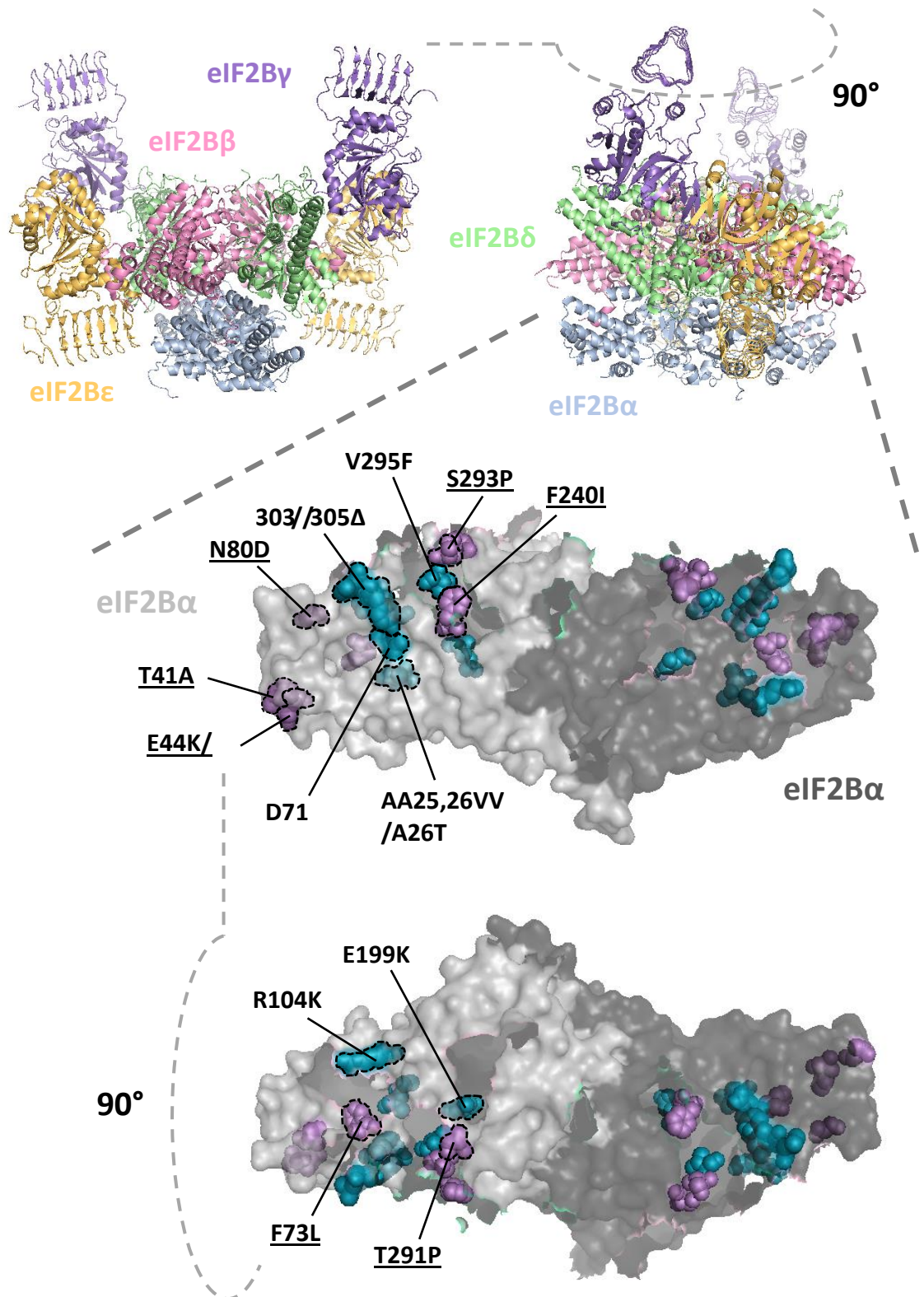
Figure 3.6 Structural schematic highlighting eIF2Bα mutations. To observe their effect on eIF2B localisation, a series of regulatory (purple and underlined) and catalytic (turquoise) mutations were introduced into the deletion strain. Mutated amino acids are modelled on crystal structure data derived from *Schizosaccharomyces pombe* (Kashiwagi et al., 2016).

3.1.4.1.   Phenotypic confirmation of *gcn3* regulatory mutants

Previously, the Gcn3p regulatory mutants were characterised by their growth on 3-amino-1,2,4-triazole (3-AT) which instigates a stress response that is dependent upon eIF2B regulation (Pavitt et al., 1997). Accordingly, Gcn3p regulatory mutations were unable to grow in the presence of 3-AT. Therefore, eIF2B was unable to be regulated in the presence of these mutations. Here, growth curves and polysome profiles were generated for three *gcn3* regulatory mutants to confirm the mutant phenotype. The regulatory mutants E44V, N80D and T291P were chosen as polysome profiles are yet to be published.

To investigate whether the regulatory mutants grew similarly to previously published data, plasmids containing the E44V, N80D and T291P mutants were transformed into the *GCD1-GFP gcn3::LEU2* strain. Growth curves were generated over 16 hours at 30˚C (**Fig. 3.7**). *GCN3* expressed on a high-copy plasmid exhibited a similar growth defect to data generated previously within this study (**Fig. 3.3**). All three *gcn3* regulatory mutants exhibited slower growth rates than the high-copy wild-type plasmid, with N80D and T291P growing similarly, whilst E44V grew the slowest.

Akin to *gcn3Δ* cells, *gcn3* regulatory mutants render cells unresponsive to amino acid stress and cannot produce a stress response by inhibiting translation initiation (Pavitt et al., 1997). To confirm this for the mutations used here, polysome profiles were generated (**Fig. 3.8**). P:M ratios of the wild-type as well as the *gcn3* null strain are included for comparison (data from **Fig. 3.5**). All three regulatory mutants failed to respond to amino acid starvation and could not inhibit translation initiation. The regulatory mutants still responded to eIF2B independent regulation however, as P:M ratios decreased across all mutants under glucose starvation. These data confirm

previous observations that the Gcn3p regulatory mutations cannot induce eIF2B-dependent regulation.
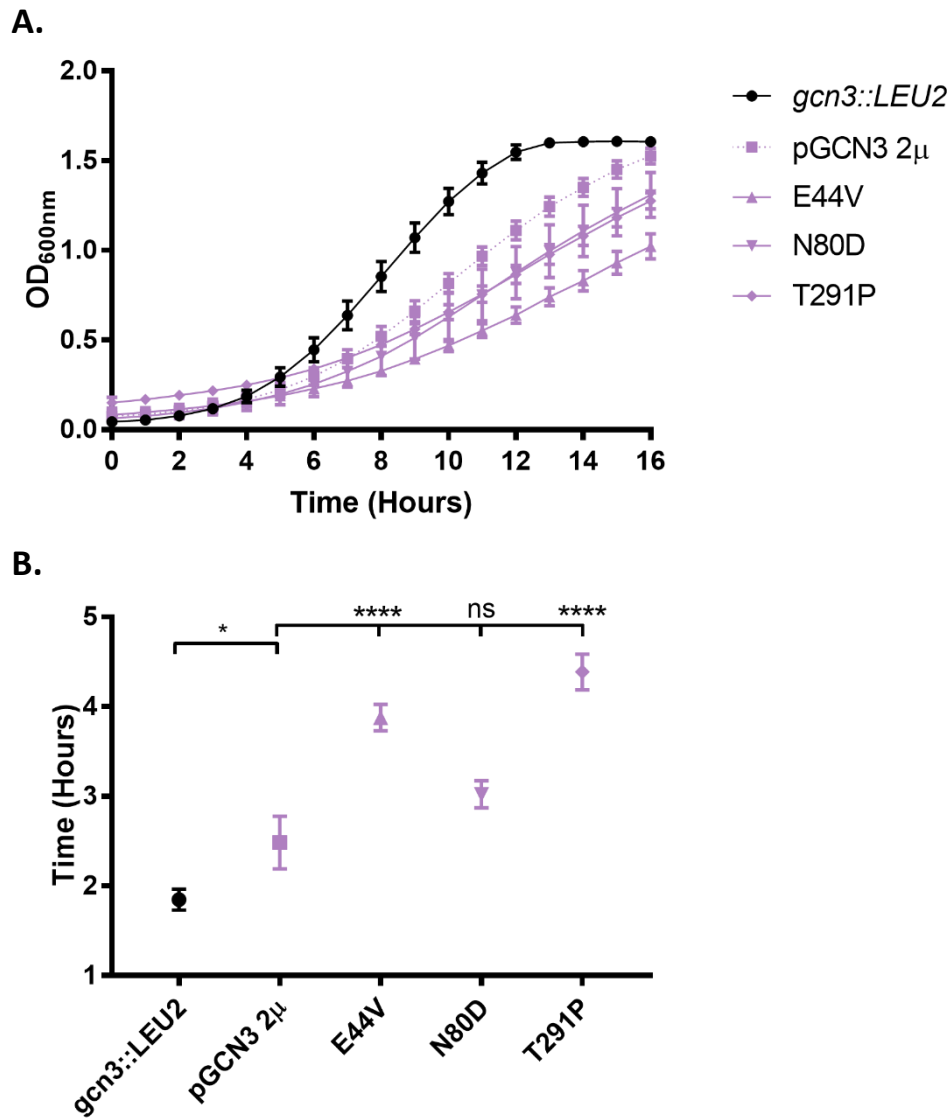
Figure 3.7 eIF2Ba regulatory mutants grow similarly to the wild-type plasmid. Overnight starter cultures were diluted to 0.1 OD_{600} in fresh SCD media before being incubated at 30°C with shaking. Growth was monitored over thirty hours in a 96-well plate; results shown the mean of three values from one replicate with bars representing standard deviations.
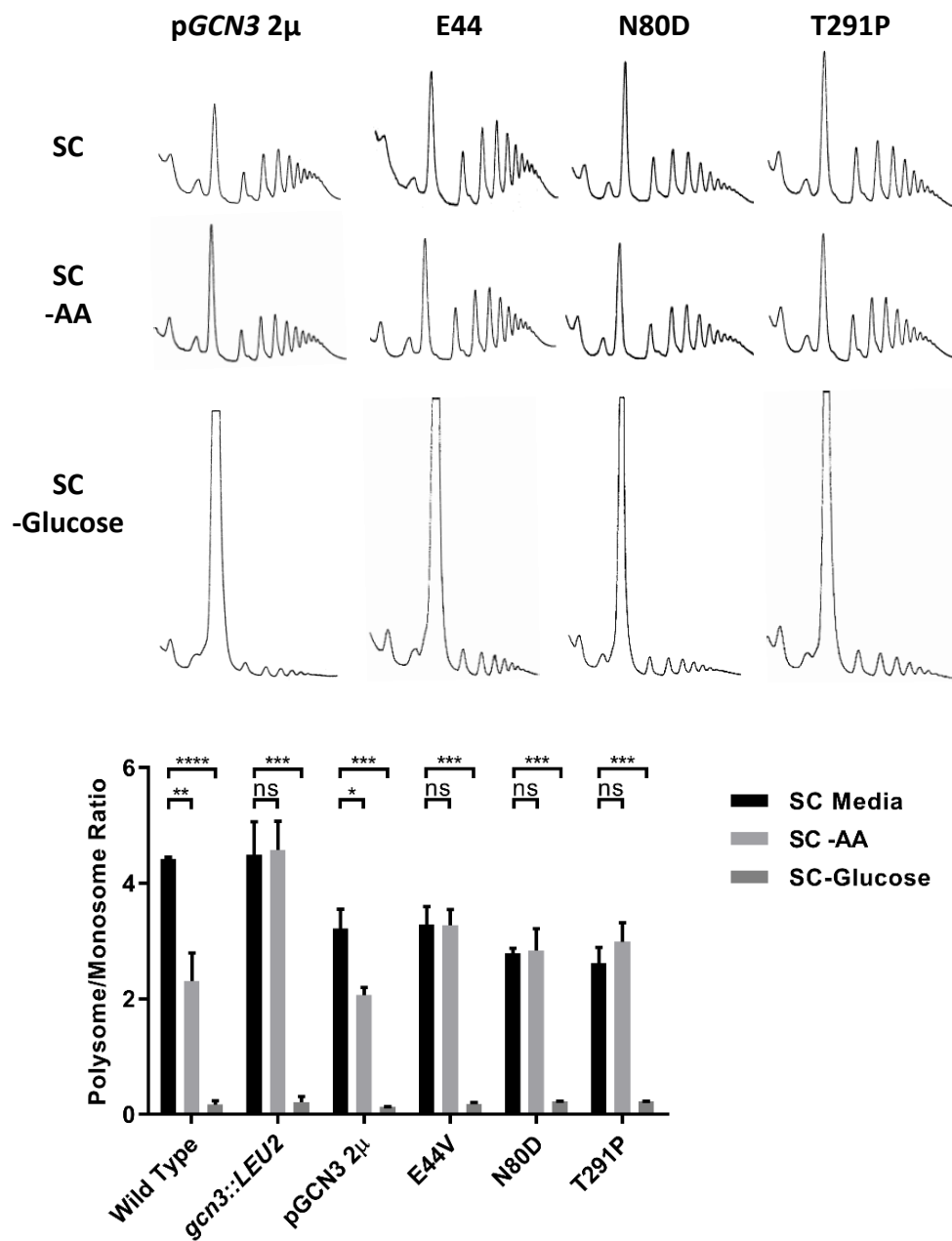
Figure 3.8 gcn3 regulatory mutants cannot respond to eIF2B-dependent regulation. (A) Polysome profiles of GCD1-yeGFP gcn3::LEU2 (yMK1402) exogenously expressing gcn3 regulatory mutants (E44V (pAV1109), N80D (pAV1112) and T291P (pAV1115)). (B) The area underneath the monosome peak and polysome peaks were quantified using ImageJ to find the polysome/monosome ratio. Overnight starter cultures were diluted to 0.2 OD_{600} in SCD media and incubated at 30°C with shaking until exponential growth was reached. Cultures were divided, pelleted and resuspended in media lacking amino acids or glucose, which were further incubated for 30 minutes and 10 minutes respectively. n=3, error bars are representative of SD, ns = not significant, * P=<0.05, ** P=<0.01, *** P=<0.001, **** P=<0.0001.

3.1.4.2. eIF2Bα regulatory mutants disperse eIF2B bodies

Combined, growth curves and polysome profiles confirmed the eIF2Bα regulatory mutants displayed similar phenotypes to previous data when expressed in our background strain (Pavitt et al., 1997). The mutations were next analysed for their impact on eIF2B body formation. Confocal microscopy was used to investigate whether eIF2B localisation would change in the presence of a *gcn3* regulatory mutation (**Fig. 3.9**). Live-cell images of wild-type cells containing exogenous *GCN3* expressed from a high copy plasmid, as well as the *gcn3* null strain are included for comparison (data from **Fig. 3.2**).

For all mutants analysed, eIF2B body formation was severely impaired (**Fig. 3.9A**) as indicated by a significant decrease in the number of cells forming eIF2B bodies. Accordingly, a significant increase was observed in the number of cells with dispersed eIF2B (**Fig. 3.9B**). Although there was a distinct lack of eIF2B body formation for most regulatory mutants, some eIF2B body formation (6.7 %) was apparent within the S293R mutant. Interestingly, the *gcn3* regulatory mutants seemed to mirror the *gcn3* null strain (**Fig. 3.2**), possibly suggesting a relationship between localisation and regulation of eIF2B.
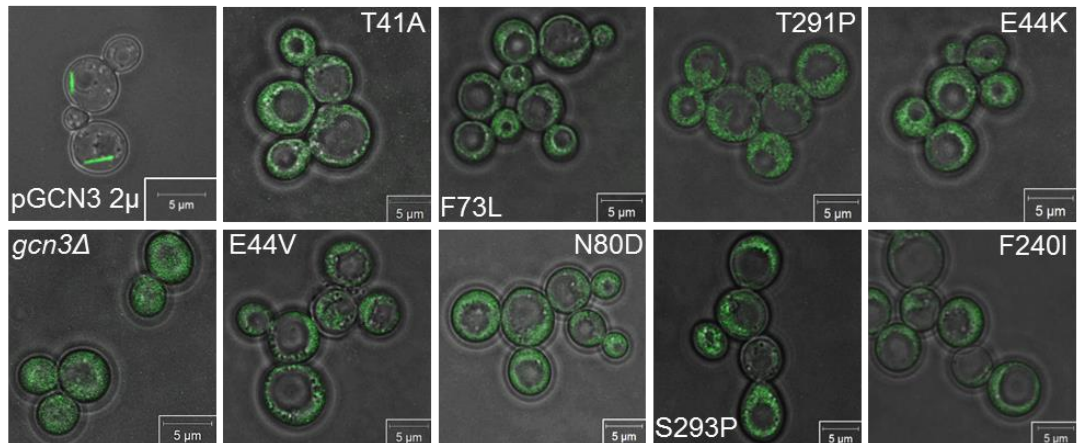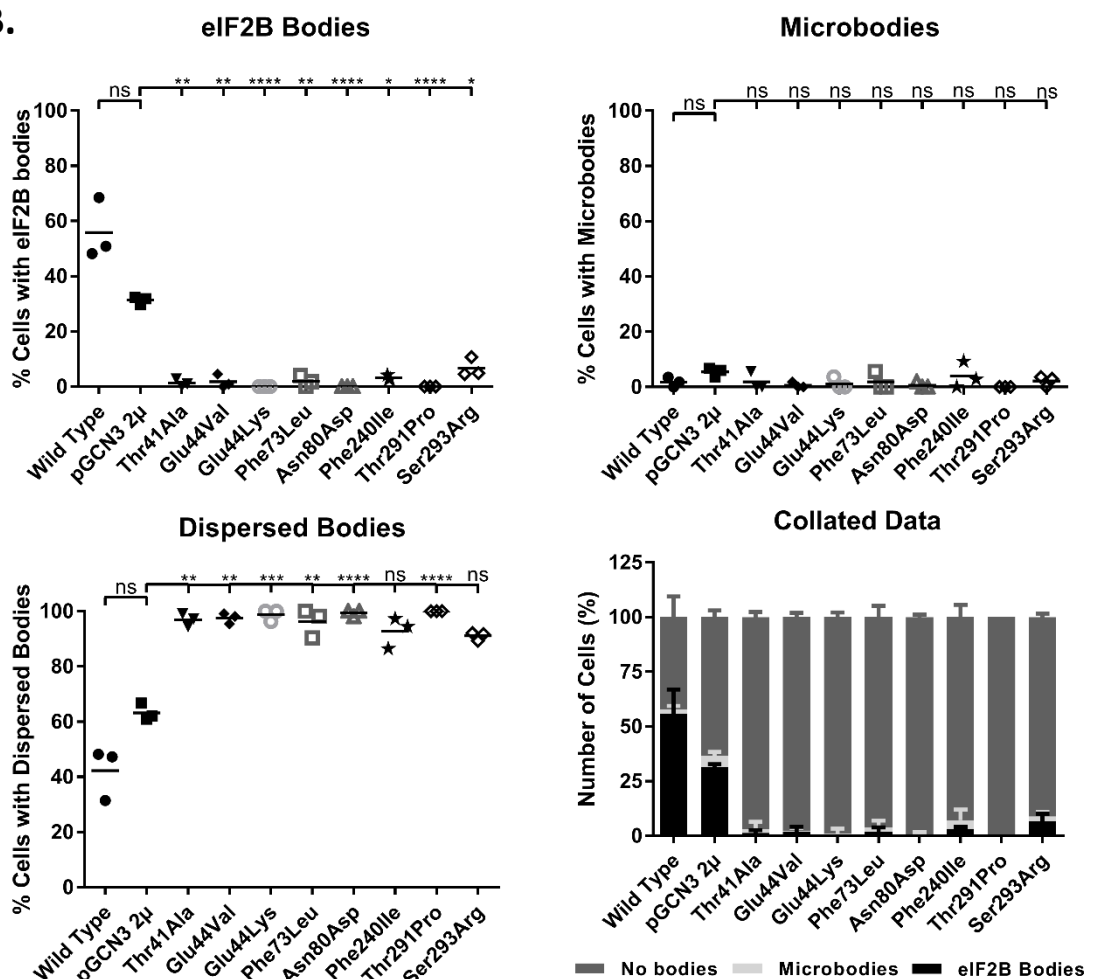
Figure 3.9 eIF2Ba regulatory mutants are unable to form eIF2B bodies. (A) Confocal microscopy of *GCD1-yeGFP gcn3::LEU2* (yMK1402) exogenously expressing Gcn⁻ mutations (pAV1108 – 13, 15 and 16), which were generated on the high copy 2μ WT *GCN3* plasmid (pAV1117). (B) A minimum of 100 cells were counted and assessed as to whether eIF2B bodies were present, dispersed or localised to microbodies. Overnight cultures were diluted in SCD media to 0.2 OD_{600} and incubated at 30°C with shaking until exponential growth was reached. n=3, error bars are representative of SD. ns = not significant, * P=<0.05, ** P=<0.01, *** P=<0.001, **** P=<0.0001.

3.1.4.3. Phenotypic confirmation of *gcn3* catalytic mutants

The *gcn3* catalytic mutants impair the GEF activity of eIF2B resulting in a reduction of GTP-bound-eIF2 and subsequently, reduced global protein synthesis (Hannig et al., 1990). To characterise the impaired catalytic phenotype within our background strain, growth curves and polysome profiles were generated for the three mutants AA25,26VV, E199K and AA 303//305Δ transformed into the *GCD1-GFP gcn3::LEU2* strain (yMK1402) (**Fig. 3.10A**).

As before, wild-type *GCN3* on a low-copy plasmid grew similarly to the deletion strain (**Fig. 3.10** and **Fig. 3.3**). AA25,26VV was the only mutant to exhibit slower growth, whilst E199K and AA 303//305Δ either grew at the same rate as the wild-type plasmid or faster.

A characteristic phenotype of eIF2B catalytic mutants is that they can grow in the presence of 3-amino-1,2,4-triazole (3-AT) due to derepression of *GCN4* (Hannig et al., 1990). 3-AT is a competitive inhibitor of the enzyme imidazoleglycerol-phosphate dehydratase, encoded by the *HIS3* gene. This drug therefore mimics an amino acid starvation stress. During such a starvation, the transcription factor *GCN4* is derepressed which in-turn upregulates *HIS3*, allowing cells to survive by outcompeting the toxic 3-AT. eIF2B therefore mimics the occurrence of cellular stress when a catalytic mutation is present. In contrast, cells are unable to respond to the 3-AT when a regulatory mutation is present, as eIF2B cannot bind eIF2-P. Thus, growth on agar containing 3-AT provides a simple qualitative method to establish catalytic mutants.

As stable expression of *HIS3* is required to analyse cellular growth in the presence of 3-AT, the strain ySC86, *gcn3::HIS3* was made. This *gcn3* deletion strain was generated via homologous recombination utilising the pRS423 plasmid. Three *gcn3*

catalytic mutations were chosen to establish the *gcn3* catalytic phenotype. AA25,26VV, E199K and AA 303//305Δ were all chosen as polysome profiles are yet to be published. To analyse growth in the presence of 3-AT, the three mutants were transformed into the *gcn3::HIS3* strain (ySC86).

In tandem with previously generated growth curves (**Fig. 3.10A**), AA25,26VV grew poorly on SCD agar, whilst AA 303//305Δ grew analogously to the wild-type *GCN3* Cen plasmid (**Fig. 3.10B**). A slight growth defect was observed for the E199K mutant when grown on solid media. When challenged with 3-AT the *gcn3* null strain was unable to derepress *GCN4*, indicated by the complete lack of growth (**Fig. 3.10B**). The addition of Gcn3p from a low copy plasmid allowed growth on 3-AT, but at a lower rate, indicating that Gcn3p is required to allow the cells to respond to the stress. Although the AA25,26VV and E199K grew poorly on SCD agar, their growth was not hindered by the presence of 3-AT, indicating higher levels of *GCN4* due to decreased levels of eIF2B activity. Whilst these results suggest AA25,26VV and E199K produce the catalytic phenotype, the AA 303//305Δ mutant grew slower in the presence of 3-AT, conflicting with previously published data where the mutants growth increased.

Previously published data has shown that catalytic mutations lead to instances of ribosomal 'run-off', subsequently resulting in a higher number of 80S monosomes (Warner et al., 1963, Jackson and Standart, 2015). Therefore, to further characterise the catalytic phenotype, polysome profiles were generated for the three mutants previously challenged with 3-AT, but in the *GCD1-GFP gcn3::LEU2* strain (**Fig. 3.11**). P:M ratios of the wild-type containing endogenous *GCN3* as well as the *gcn3* null strain are included for comparison. Under normal conditions, the three catalytic mutants exhibited exaggerated 80S monosome peaks, resulting in decreased P:M ratios under

steady-state growth. All three mutants were also able to respond to amino acid starvation as well as glucose starvation. These results recapitulate previous conclusions, whereby the presence of Gcn3p catalytic mutations do not hinder the regulation of eIF2B, but decrease the catalytic activity of eIF2B resulting in ribosomal run-off.
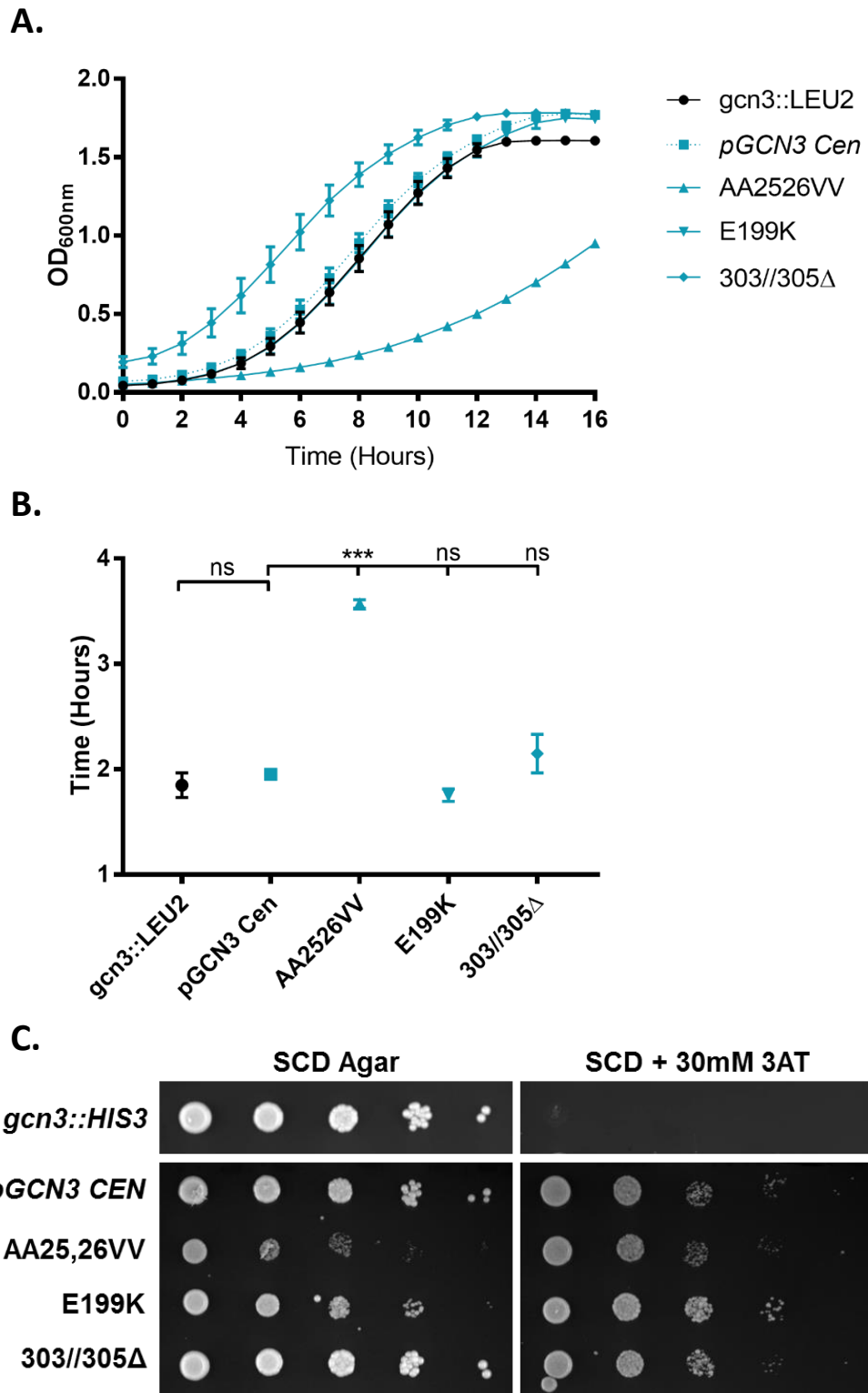
Figure 3.10 eIF2Bα catalytic mutants that grow slow grow better on 3-AT. (A) Overnight starter cultures were diluted to 0.1 OD_{600} in fresh SCD media before being incubated at 30°C with shaking. Growth was monitored over thirty hours in a 96-well plate; results shown are the mean of three values from one replicate, bars represent standard deviation. (B) Mutants were exogenously expressed in a gcn3::HIS3 (ySC86) strain. Starter cultures were backdiluted to 0.3 OD units before being serially diluted four times and spotted on to SCD agar as well as SCD agar containing 30 mM 3AT. Spot plates were incubated at 30 °C for 48 hours.
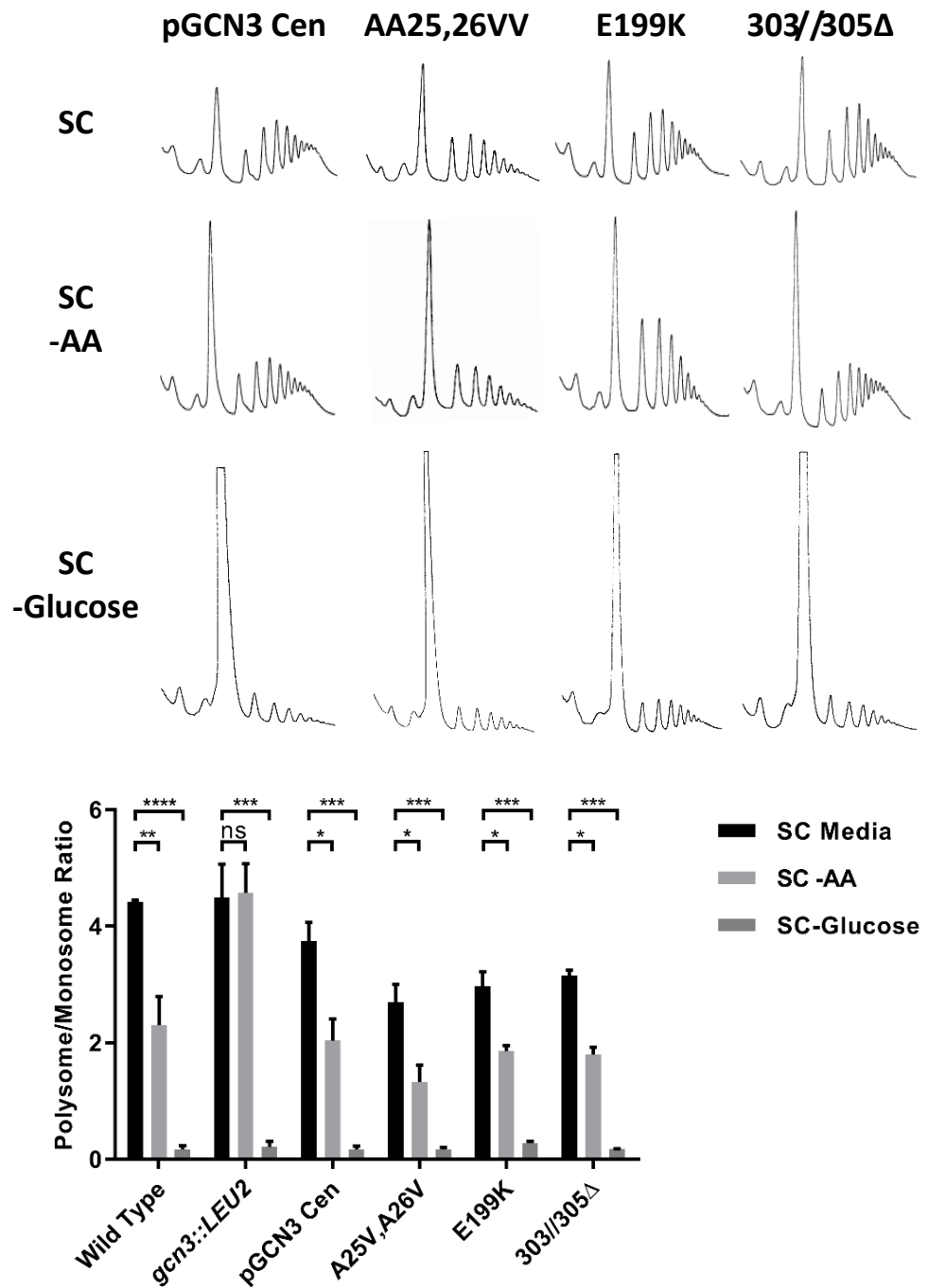
Figure 3.11 gcn3 catalytic mutants lead to an increase in 80S monosomes. (A) Polysome profiles of GCD1-yeGFP gcn3::LEU2 (yMK1402) exogenously expressing gcn3 Gcd[-] mutants (A25,26V (pAV1239), E199K (pAV1244) and 303//305Δ (pAV1268)). (B) The area underneath the monosome peak and polysome peaks were quantified using ImageJ to find the polysome/monosome ratio. Overnight starter cultures were diluted to 0.2 OD_{600} in SCD media and incubated at 30°C with shaking until exponential growth was reached. Cultures were divided, pelleted and resuspended in media lacking amino acids or glucose, which were further incubated for 30 minutes and 10 minutes respectively. n=3, error bars are representative of SD, ns = not significant, * P=<0.05, ** P=<0.01, *** P=<0.001, **** P=<0.0001.

3.1.4.4. eIF2Bα catalytic mutants form microbodies

Live-cell imaging via confocal microscopy was used to investigate eIF2B localisation in the presence of the *gcn3* catalytic mutations (**Fig. 3.12**). Intriguingly, all catalytic mutations caused eIF2B to localise to several smaller foci, which we termed microbodies (**Fig. 3.12A**). Analysis of a population of cells revealed eIF2B mainly localised to microbodies within most mutants (**Fig. 3.12B**). However, AA 303//305Δ was the only exception, where similar numbers of cells either dispersed eIF2B (33.5 %), formed microbodies (38.3 %) or eIF2B bodies (28.2 %). Interestingly, these data imply that the localisation of eIF2B may be important for GDP-GTP exchange on eIF2, which is required to initiate translation.
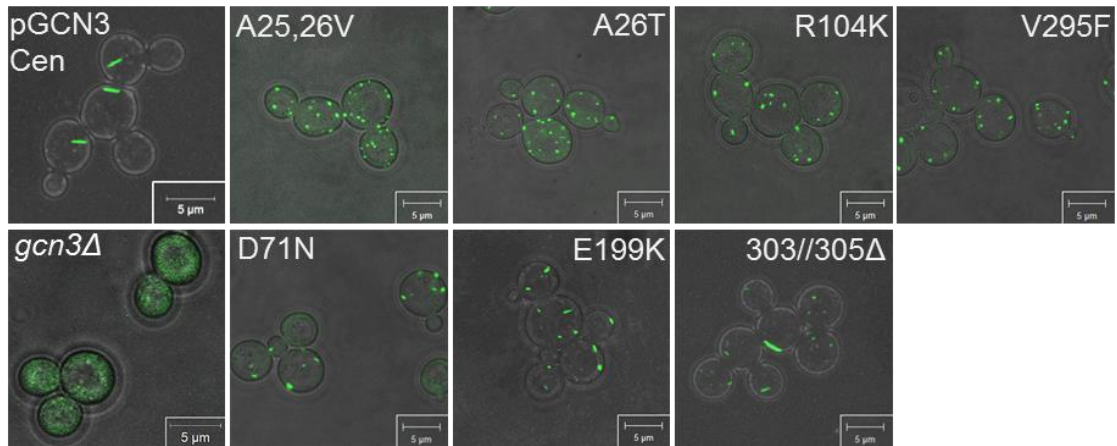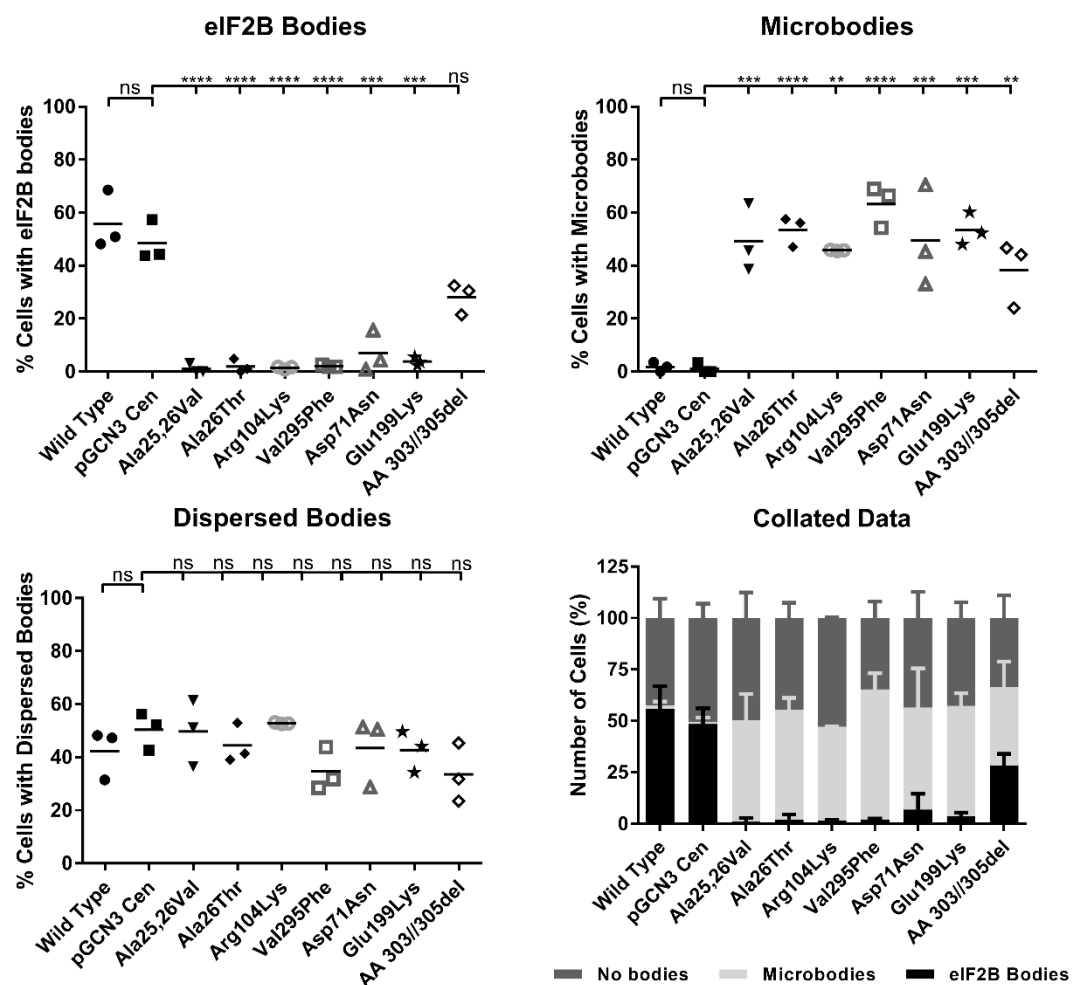
Figure 3.12 *gcn3* catalytic mutants localise eIF2B to multiple foci. Confocal microscopy of *GCD1-yeGFP gcn3::LEU2* (yMK1402) exogenously expressing *gcn3* Gcd⁻ mutations (pAV1239 – 44 and 68), which were generated on the low copy Cen *GCN3* plasmid (pAV1170). (B) A minimum of 100 cells were counted and assessed as to whether eIF2B was dispersed, localised to microbodies or formed eIF2B bodies. Overnight starter cultures were diluted in SCD media to 0.2 OD$_{600}$ and incubated at 30°C with shaking and allowed to reach exponential growth. *n*=3, error bars are representative of SD. ns = not significant, * *P*=<0.05, ** *P*=<0.01, *** *P*=<0.001, **** *P*=<0.0001.

3.1.5. Effect of *gcn3* VWM⁻ mutations on eIF2B localisation

Autosomal recessive mutations within any eIF2B subunit cause the human disease VWM (Leegwater et al., 2001). It was therefore valuable to characterise eIF2B function and localisation in the presence of a naturally occurring clinical mutation. Moreover, these analyses could also provide further insight to the pathogenesis of VWM, potentially helping with the elucidation of methods to ameliorate the fatal disease.

eIF2Bα contains the fewest VWM mutations amongst eIF2B subunits, with 1 frameshift, 1 deletion and 6 missense mutations reported so far (Pavitt and Proud, 2009). Mutated residues are mostly conserved between human and yeast, with the only exception being P278R (Q277 in *gcn3*). N208Y (N209Y in *gcn3*) represents the only VWM mutation to be analysed in yeast thus far (Richardson et al., 2004). These *gcn3* VWM missense mutations are shown modelled on the eIF2Bα homodimer crystal structure from *S. pombe* (**Fig. 3.13**). Interestingly, in contrast to the regulatory and catalytic Gcn3p mutations (see **Figure 3.6**), the VWM mutations are mostly present near the α-α dimer interface. Details of VWM mutations and their resulting phenotypes observed in humans are shown in **Table 3.1**.

To investigate if these mutations impact upon the function and localisation of eIF2B, site directed mutagenesis was performed to generate the VWM amino acid substitutions using the *GCN3 CEN6ARS4* low copy plasmid (pAV1769) as a template, as previously described (Richardson et al., 2004). Transformants were selected on LB agar containing 50 µg/ml carbenicillin overnight, before purified plasmids were sequenced gene-wide to ensure undesired mutations were not present.
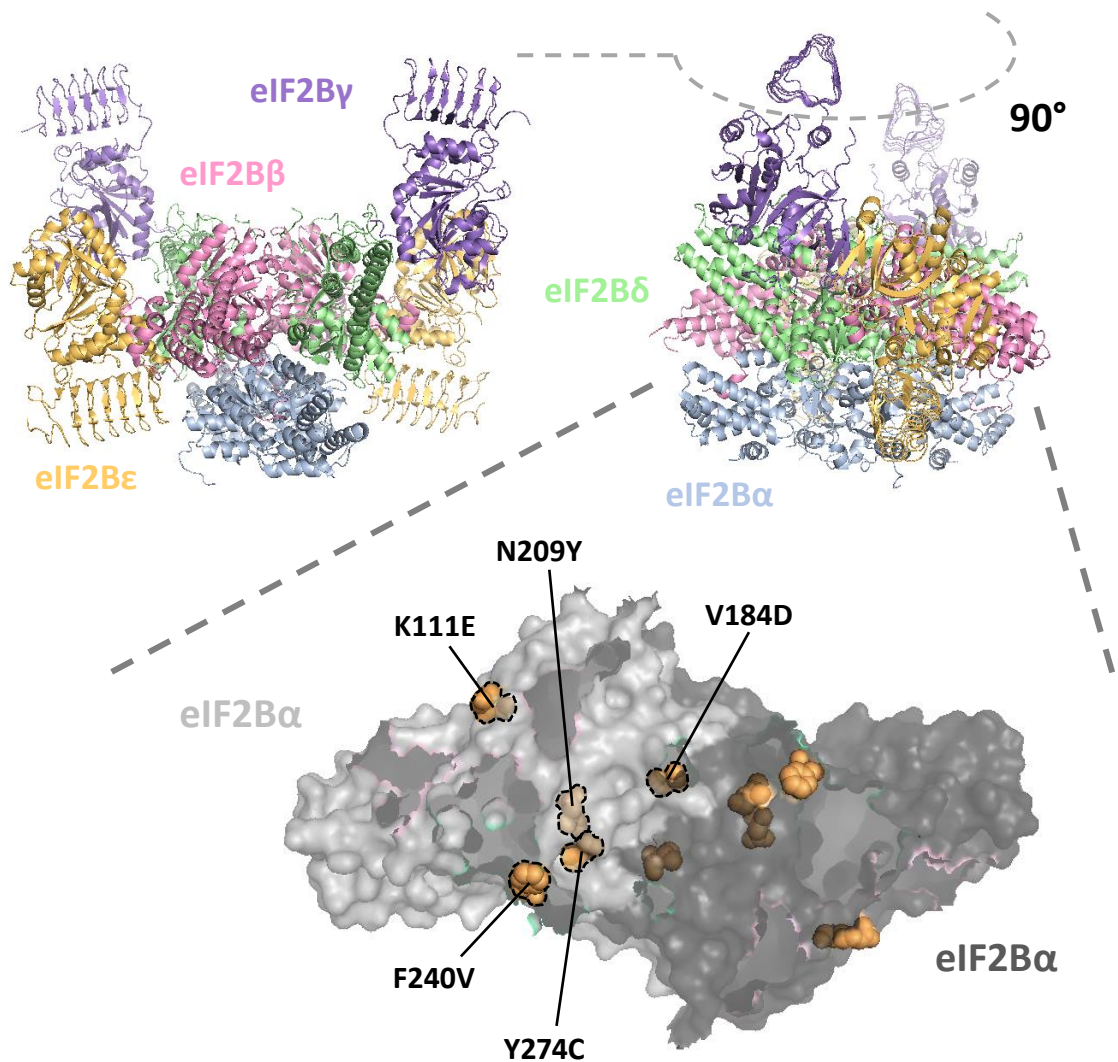
Figure 3.13 Structural schematic highlighting eIF2Bα VWM mutations. Five mutations, causative of the Human disease VWM, were generated by site directed mutagenesis to investigate their effect on eIF2B localisation and function. Mutated amino acids are modelled on crystal structure data derived from *Schizosaccharomyces pombe.*

Table 3.1 Genotypes and phenotypes of VWM missense mutations.

N/R: Not reported. IVS: Intervening sequence.

3.1.5.1. Phenotypic characterisation of eIF2Bα VWM mutations

To characterise their effect on eIF2B function and localisation, the VWM mutant plasmids were exogenously expressed in the *GCD1-GFP gcn3::LEU2* strain for live-cell imaging and the generation of growth curves and polysomes profiles. Moreover, to investigate *GCN4* depression, the plasmid-borne mutants were also transformed into the *gcn3::HIS3* strain to generate 3-AT spot plates.

As before, *GCN3* expressed from a low copy CEN6ARS4 plasmid (a different low copy plasmid to the Cen plasmid characterised in Section 3.2.1) grew similarly to the wild-type strain (**Fig. 3.14A**). All of the VWM mutants grew similarly to the wild-type plasmid, with slightly decreased growth rates for F240V and Y274C.

When challenged with 3-AT, cells containing the wild-type plasmid were able to grow suggesting that a stress response was possible (**Fig. 3.14B**). In the presence of 3-AT, growth was dramatically reduced for the *gcn3* VWM mutants V184D, N209Y and F240V. This suggested that these mutants were unable to derepress *GCN4*, indicative of a regulatory mutant phenotype. K111E and Y274C grew similar to wild-type.

Polysome profiles were generated to assess whether these VWM mutations in eIF2Bα resulted in a translation initiation defect (**Fig. 3.15**). Under normal steady state conditions all mutations produced a polysome trace similar to the wild-type, indicating no translational defect. However upon stress, the VWM mutations N209Y and F240V were unable to respond to amino acid starvation, as indicated by unaffected P:M ratios in comparison to normal conditions. These results were in-line with prior observations from 3-AT spot plates. The results of the V184D mutant were rather contradictory. Although V184D could not respond to 3-AT, P:M ratios decreased under amino acid starvation, suggesting that eIF2B dependent regulation was still possible. Polysome

profiles generated for K111E and Y274C were consistent with plasmid-borne wild-type and could respond to amino acid starvation. Although, P:M ratios were slightly exaggerated for Y274C under amino acid starvation, suggesting a slight hypersensitivity to eIF2B dependent regulation.

A.

B.

C.
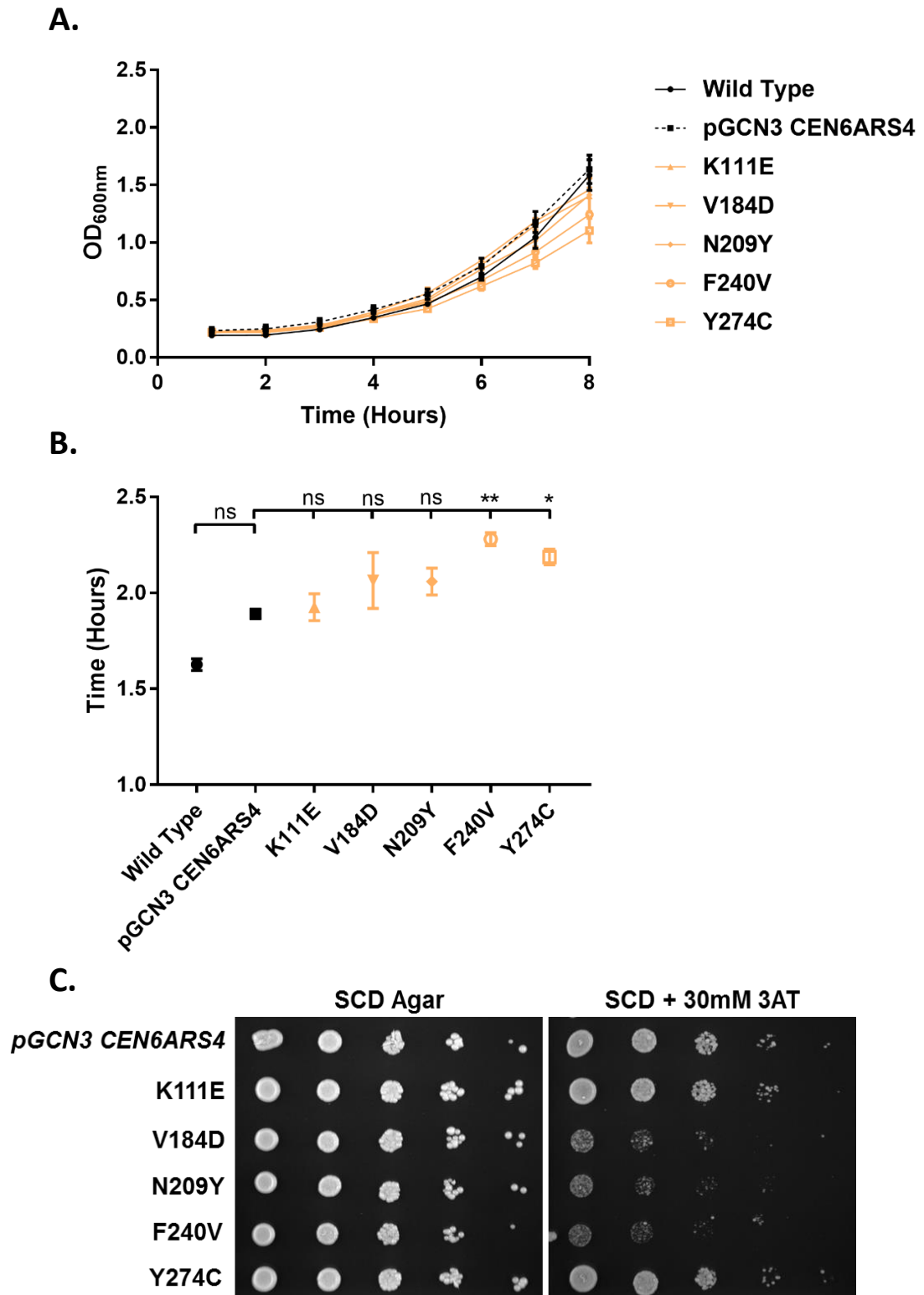
Figure 3.14 gcn3 VWM mutants growth on 3AT and growth curve. (A) Overnight starter cultures were diluted to 0.2 OD units in SCD media before being incubated at 30 °C with shaking. Growth was monitored over eight hours. n=3, error bars are representative of SD. (B) Mutants were exogenously expressed in a *gcn3::HIS3* (ySC86) strain. Starter cultures were backdiluted to 0.3 OD units before being serially diluted 4 times and spotted on to SCD agar plates as well as SCD agar containing 30 mM 3-AT. Spot plates were incubated at 30 °C for 48 hours.
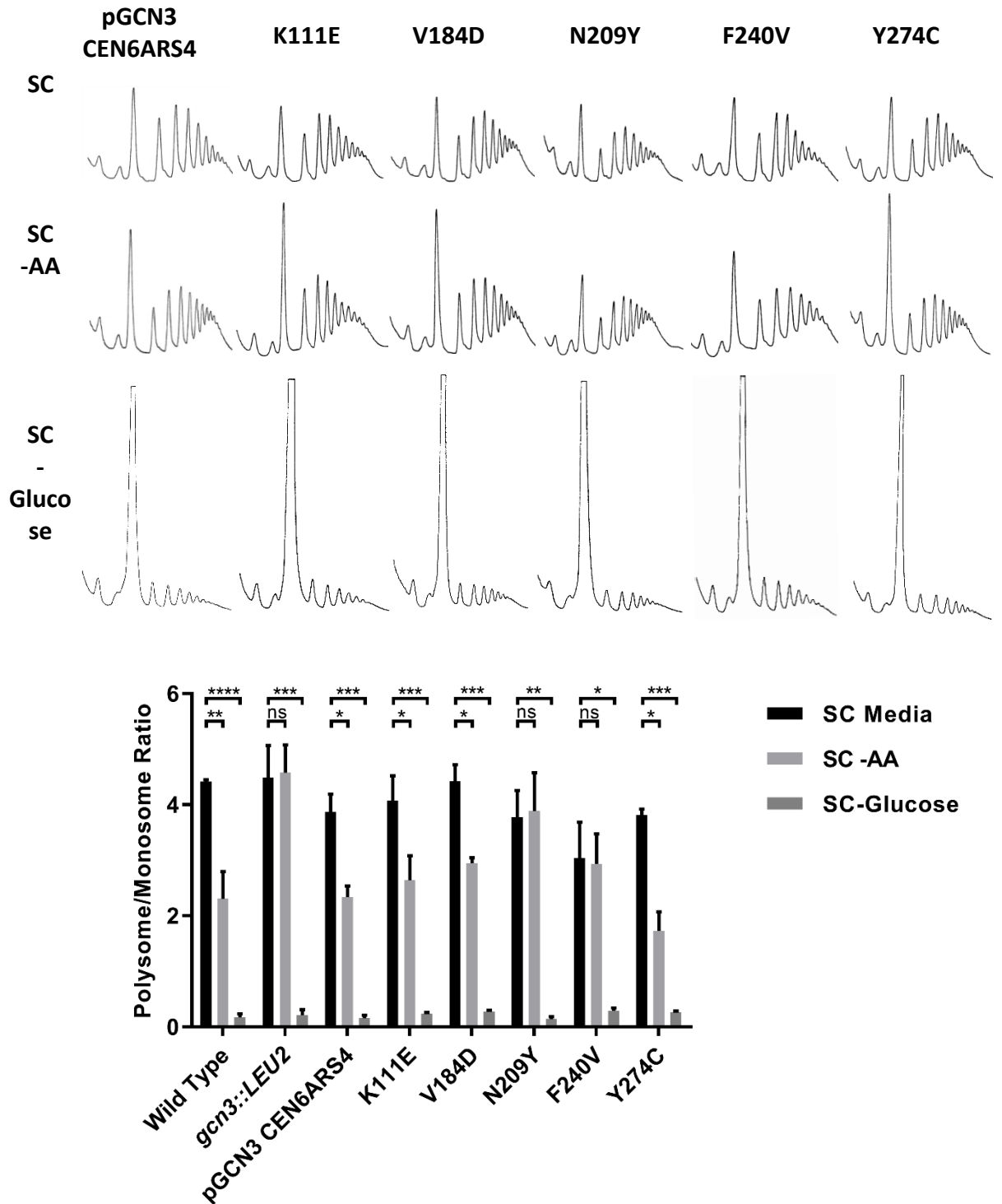
Figure 3.15 Polysome profiling of gcn3 VWM mutants. (A) Polysome profiles of *GCD1-yeGFP gcn3::LEU2* (yMK1402) exogenously expressing gcn3 VWM mutants (K111E (bSC116), V184D (bSC117), N209Y (pAV1778), F240V (bSC118) and Y274C (bSC119)), which were generated by site directed mutagenesis in the low copy CEN6ARS4 WT GCN3 plasmid. The area underneath the monosome peak and polysome peaks were quantified using ImageJ to find the polysome/monosome ratio. Overnight starter cultures were diluted to 0.2 OD_{600} in SCD media and incubated at 30°C with shaking until exponential growth was reached. Cultures were divided, pelleted and resuspended in media lacking amino acids or glucose, which were further incubated for 30 minutes and 10 minutes respectively. n=3, error bars are representative of SD, ns = not significant, * P=<0.05, ** P=<0.01, *** P=<0.001, **** P=<0.0001.

3.1.5.2.   eIF2Bα VWM mutations display varied eIF2B localisation

Overall, these results showed that both N209Y and F240V displayed phenotypic patterns consistent with them being regulatory mutants. Although the V184D mutant showed 3-AT data which suggested that it also displayed a regulatory phenotype, polysome analysis did not reflect this. K111E and Y274C were characteristically similar to wild-type, although Y274C displayed some abnormalities that were not consistent with either regulatory or catalytic phenotypes described previously.

To assess the impact of the VWM mutations on eIF2B localisation, live-cell images were taken via confocal microscopy (**Fig. 3.16**). N209Y was unable to nucleate eIF2B, consistent with regulatory mutations previously analysed (as in section 3.1.4.2). Whilst eIF2B body formation was absent from N209Y (0.26 %), some eIF2B bodies were visible within the F240V mutant (13.1 %). Y274C eIF2B body formation was impaired similar to F240V, with dispersed eIF2B being the dominant phenotype (19.9 % eIF2B bodies, 77.2 % dispersed eIF2B). V184D mostly localised eIF2B to microbodies (49.6 %) despite lacking any catalytic mutant characteristics (as in section 3.1.4.3). Localisation within the K111E mutant was somewhat similar to wild-type; however there was a decrease in the number of cells containing eIF2B bodies (28.8 %).
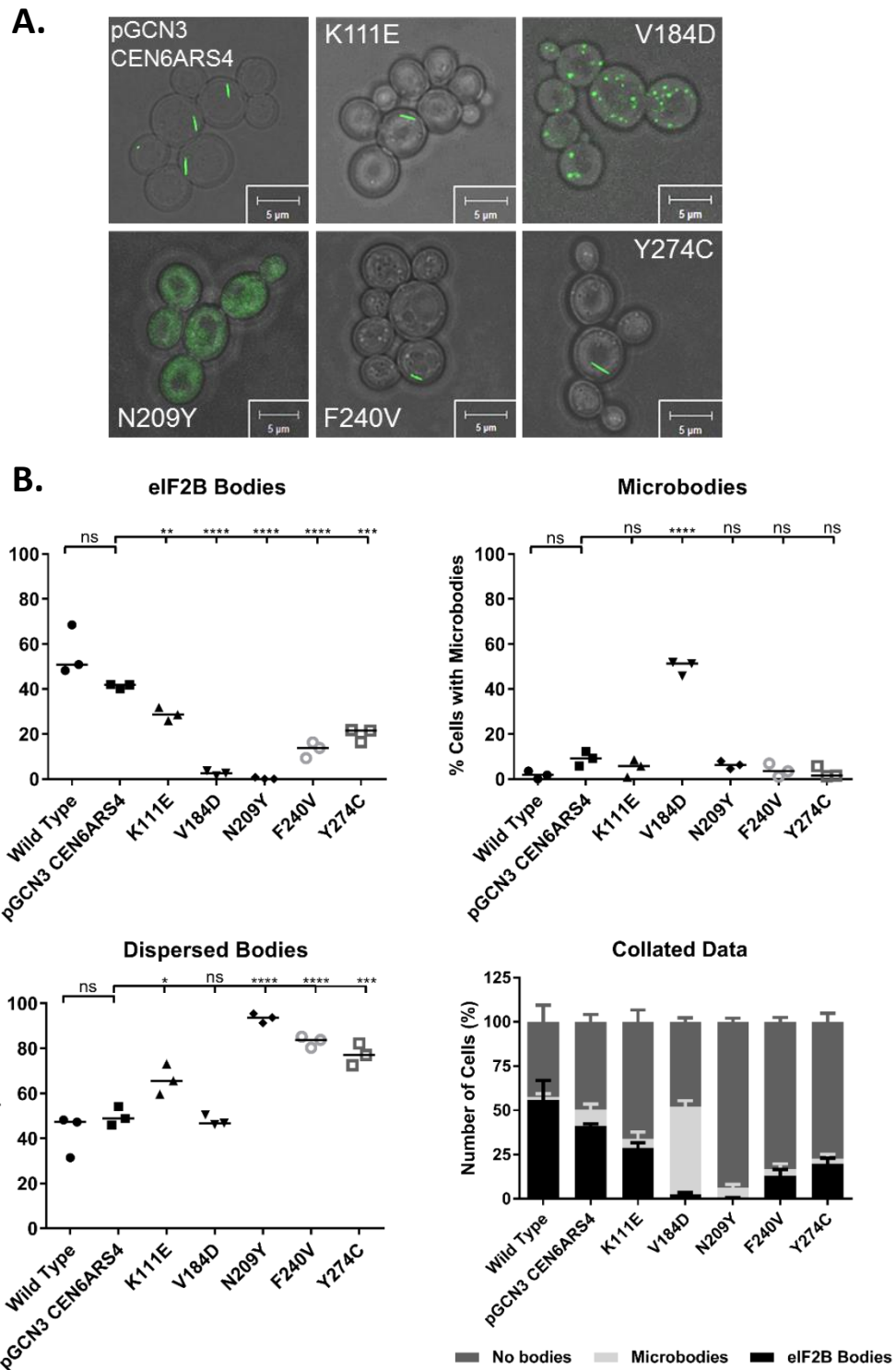
Figure 3.16 eIF2B localisation in the presence of gcn3 containing VWM missense mutations.
(A) Confocal microscopy of *GCD1-yeGFP gcn3::LEU2* (yMK1402) expressing *gcn3* VWM mutants as well as the low copy CEN6ARS4 WT *GCN3* plasmid. (B) A minimum of 100 cells were counted and assessed as to whether eIF2B was dispersed, localised to microbodies or formed eIF2B bodies. WT quantification from figure 3.1 included in graph for comparison. Overnight starter cultures were diluted in SCD media to 0.2 OD_{600} and incubated at 30°C with shaking until exponential growth was reached. N=3, error bars are representative of SD. Ns = not significant, * P=<0.05, ** P=<0.01, *** P=<0.001, **** P=<0.0001.

3.2. Discussion

3.2.1. eIF2Bα is required for the formation of eIF2B bodies

These results show for the first time that eIF2Bα is necessary for the formation of eIF2B bodies. In the absence of eIF2Bα, localisation was completely abolished, exclusively dispersing eIF2B throughout the cytoplasm (**Fig. 3.2**). Consistent with previous data, cells could not respond to eIF2B-dependent regulation when eIF2Bα was deleted (**Fig. 3.5**). The dispersal of eIF2B bodies and inability to regulate eIF2B activity suggests the two phenotypes may be linked.

eIF2B crystal structure data derived from *S. pombe* represents the most complete structure of eIF2B to-date (Kashiwagi et al., 2016). Whilst *S. cerevisiae* regulatory, catalytic and VWM mutations have been investigated within this chapter, a substantial proportion of the mutated residues are conserved within *S. pombe*, potentially highlighting the importance of these residues to eIF2Bα's structure and function (**Fig. 3.17**). Crystal structure data from *S. pombe* showed eIF2Bα contains several β and δ binding pockets (**Fig. 3.18**). It is therefore plausible that dispersed Gcd1-GFP is representative of tetrameric εγδβ complexes, as previous data showed holocomplex destabilisation when eIF2Bα is absent (Wortham et al., 2014). However, it should be noted that these studies used overexpressed eIF2B subunits purified from *E. coli* and may not represent subcomplexes *in vivo*.

Figure 3.17 eIF2Bα sequence alignment between Human, *S. pombe* and *S. cerevisiae*. The majority of regulatory (purple), catalytic (blue) and VWM (orange) mutations characterised herein are conserved between species, with the only major exceptions being N80D and 303//305Δ. Asterisks highlight conserved amino acids, whilst : and . represent amino acids that are highly or somewhat similar, respectively.
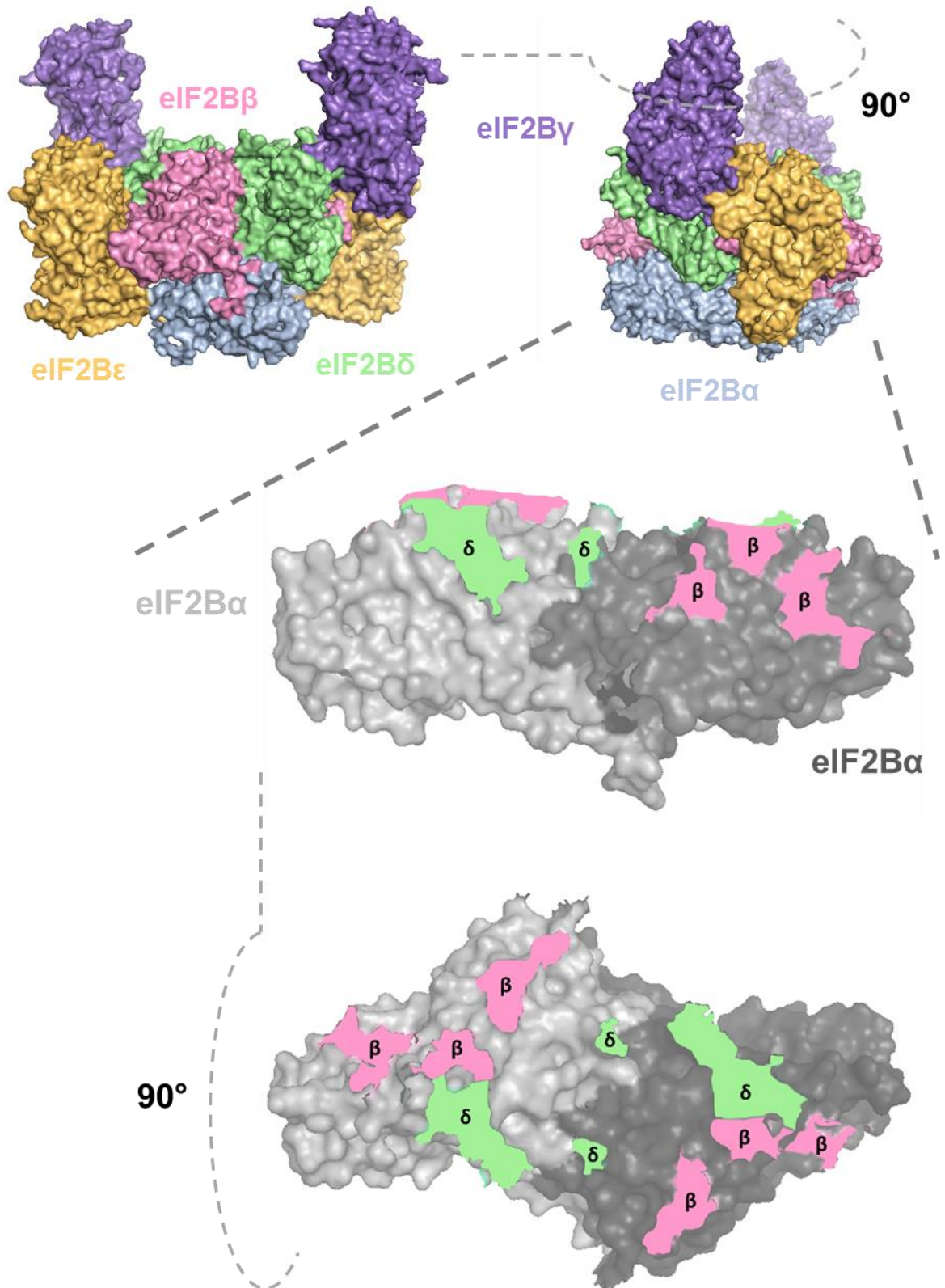
Figure 3.18 eIF2Bα contains eIF2Bβ/δ docking sites important for decameric stabilisation. The eIF2Bα homodimer stabilises two eIF2Bεγδβ heterotetramers through various pockets on the eIF2Bα distal face, which interact with eIF2Bβ (pink) and eIF2Bδ (green).

3.2.2. Insights into eIF2B body formation from regulatory mutations

eIF2Bα regulatory mutants were studied to determine their impact on eIF2B localisation when eIF2B could not be regulated. The phenotypical characteristics of these mutants found within this chapter are summarised in Table #. The regulatory mutants used in this study were unable to respond to amino acid starvation (**Fig. 3.8**). This could either be due to eIF2α-P being unable to bind and interact with eIF2Bα or eIF2Bα could be absent from the holocomplex, rendering any interaction redundant. Data derived from the regulatory mutants were strikingly similar to the null strain, as they were unable to form eIF2B bodies and instead, resulted in eIF2B being dispersed throughout the cytoplasm (**Fig. 3.9**). Growth rates were different between the regulatory mutants and the null strain (**Fig. 3.7**), although this could be attributed to the overexpression vector with which the regulatory mutations are present on (Yoshikawa et al., 2011). Considering the phenotypic similarities between the null strain and the regulatory mutants, eIF2Bα's ability to bind tetrameric complexes may be compromised in the regulatory mutants tested in this chapter.

Crystal structure data derived from *S. pombe* highlighted that some regulatory mutations are present on the distal face of eIF2Bα. As β and δ binding pockets are present here, mutations located on the distal face could explain why eIF2Bα is unable to incorporate itself into the holocomplex, subsequently preventing eIF2B localisation. The F240I substitution may affect interactions with eIF2Bδ, whilst the mutants T291P and S293R may detrimentally influence interactions with both β and δ (**Fig. 3.19**). Interestingly however, other regulatory mutations do not seem to affect β and δ interactions or even span across the distal face. F73L and N80D appear to be near a β binding pocket, but only intra-protein interactions seem to be present. These two

residues may be important for eIF2Bα's folding and substituting these amino acids may result in a conformational change that prevents nearby α-β interactions.

Although T41A and E44K/V may also be important for intra-protein interactions and therefore protein folding, they are not present along α-β or α-δ interfaces. Whilst there is no evidence to suggest a reason why E44V/K may affect the ability of eIF2Bα to incorporate itself into the holocomplex, the converse may be true for T41A. Previous work investigating translational control in response to butanol highlighted Gcn3p amino acid substitutions that influence *S. cerevisiae's* response to butanol (Taylor et al., 2010). Butanol is a potent inhibitor of translation initiation which leads to the derepression of *GCN4*. Whilst butanol resistance and sensitivity were originally attributed to various alleles of Gcd1p/eIF2Bγ (Ashe et al., 2001), mutations in Gcn3p were also identified which conferred resistance to butanol. In the study by Taylor *et al.,* (2010), a T41K mutation was identified which increased resistance to butanol, whilst the wild-type and *gcn3* null strains remained sensitive to the translation inhibition caused by butanol. Although the small alanine (A) and the basic lysine (K) are characteristically dissimilar, both T41A and T41K Gcn3p mutants were unable to localise eIF2B and resulted in eIF2B being dispersed throughout the cytoplasm. Another explanation for the lack of localisation within the T41A mutant is that the threonine residue is directly involved in aggregating eIF2B. Although, this would also mean that there is some relationship between localisation and regulation, which remains to be elucidated.

Table 3.2- Phenotypes observed from characterised *gcn3* regulatory mutants

	Wild Type	*gcn3::LEU2*	p*GCN3* 2μ	gcn3 Regulatory Mutants							
				T41A 2μ	E44V 2μ	E44K 2μ	F73L 2μ	N80D 2μ	F240I 2μ	T291P 2μ	S293R 2μ
Growth Rate[1]	++++	++++	++	N/A	N/A	+	N/A	+	N/A	+	N/A
Translational Regulation[2]	Yes	No	Yes	N/A	N/A	No	N/A	No	N/A	No	N/A
eIF2B Localisation[3]	eIF2B Bodies	Dispersed	eIF2B Bodies	Dispersed	Dispersed	Dispersed	Dispersed	Dispersed	Dispersed	Dispersed	Dispersed

N/A: Not analysed

[1]As determined by growth curves (see Figure 3.7)

[2]As determined by polysome profiling (see Figure 3.8)

[3]As determined by confocal microscopy (see Figure 3.9)
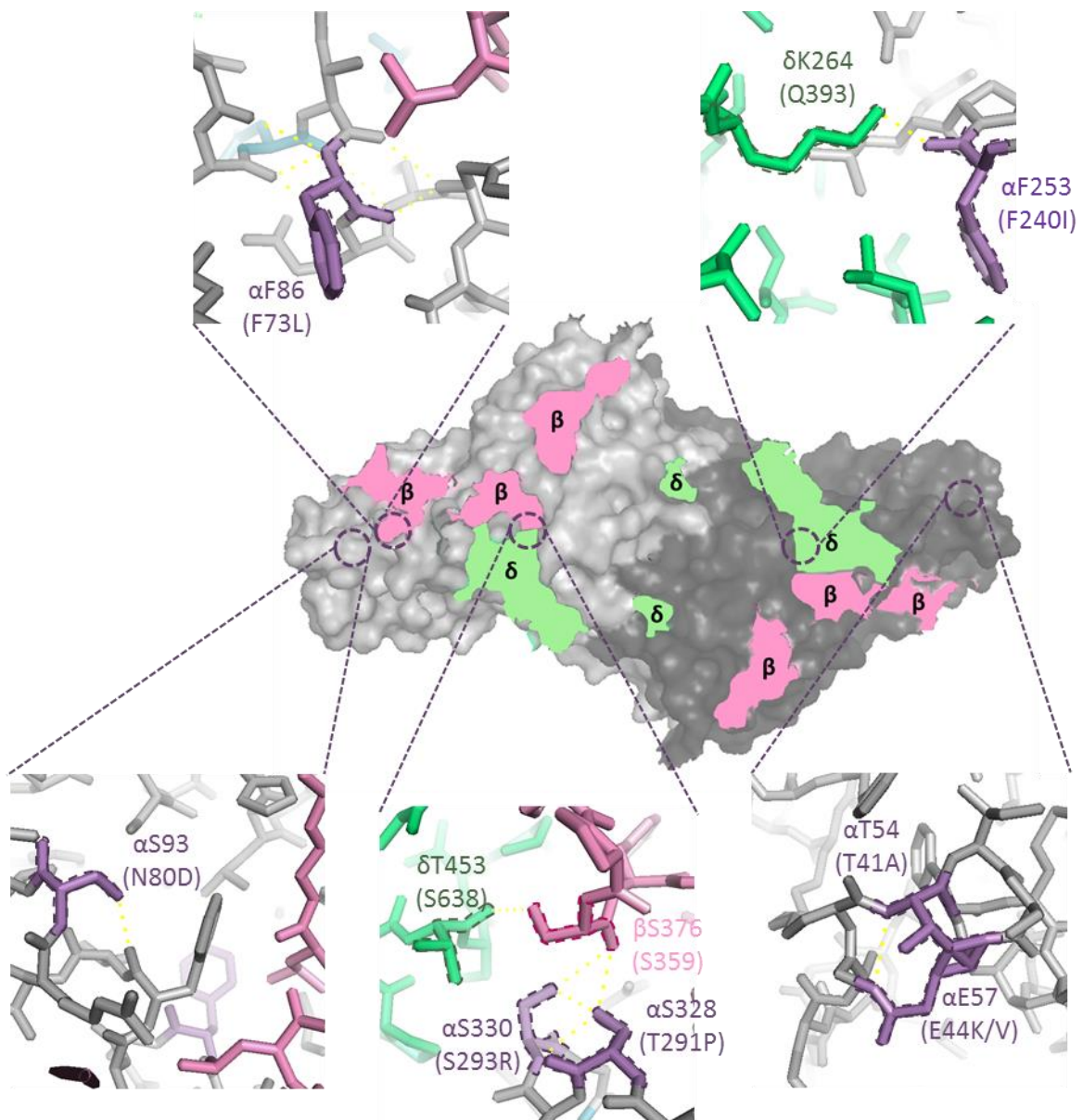
Figure 3.19 eIF2Bα regulatory mutants affect α-β and α-δ interactions, but not exclusively. Several eIF2Bα regulatory mutations (purple) are present on the distal face of eIF2Bα, therefore affecting important interactions with eIF2Bβ (pink) and eIF2Bδ (green). Other regulatory mutants are either in proximity of these pockets (i.e. F73L) or far away (i.e. T41A, E44K/V). *S. cerevisiae* amino acid residues are in brackets, whilst the *S. pombe* homologous residue are above.

3.2.3. Insights into eIF2B body formation from catalytic mutations

eIF2Bα catalytic mutants were also analysed to determine localisation when eIF2B GEF activity was hindered (Hannig et al., 1990). Catalytic mutants were unable to fully form the singular eIF2B body and instead, localised eIF2B to multiple smaller foci termed microbodies (**Fig. 3.12**). As microbodies were rarely seen within the wild-type, it is possible microbody foci are intermediate eIF2B aggregates, whereby the catalytic mutations result in a conformational change that prevents eIF2B from fully localising. Interestingly, 303//305Δ contained subpopulations of all three phenotypes observed, where eIF2B was dispersed or localised to microbodies and eIF2B bodies. In this instance, there could be a decrease in the rate of eIF2B localisation, as most other catalytic mutants predominantly formed microbodies, indicating that they cannot localise eIF2B beyond this intermediary structure. Although 303//305Δ had some characteristics indicative of a catalytic mutant, such as higher levels of 80S monosomes (a consequence of translation being initiated less frequently) (**Fig. 3.11**), 303//305Δ did not display any increases in tolerance and instead, grew analogously to wild-type (**Fig. 3.10B**). Considering the contradiction between polysome analyses and 3-AT spot plates, it is possible that alleles elsewhere in the eIF2B complex (within the background strain) may be affecting *GCN4* expression. Although amino acid substitutions in one eIF2B subunit have been shown to affect other subunits, therefore influencing eIF2Bs characteristics, a mechanism that affects *GCN4* expression without affecting eIF2B catalytic activity remains to be found.

eIF2B microbody formation has been previously observed when Ifa38p was deleted (Browne et al., 2013). Ifa38p is an enzyme involved in the very long fatty acid chain (VLFA) synthesis pathway with no current evidence to suggest a role in

translation initiation or translational control. However, upon deletion of *ifa38* the eIF2B body became fragmented into several smaller cytoplasmic foci. Interestingly, the change in localisation did not impact upon eIF2Bs catalytic or regulatory functions and did not disperse eIF2B throughout the cytoplasm completely, possibly indicating that the interaction between eIF2Bε/γ and Ifa38p may be required for the stability of eIF2B bodies. In contrast to our study, microbody formation correlates with a decrease in eIF2B activity, which is likely to be caused by direct influences on the conformation of eIF2B. Catalytic mutations could result in a conformational change that impedes interactions with Ifa38p as well as other unidentified proteins that may interact with eIF2B, which may affect the localisation, function and regulation of eIF2B.

Structurally, the catalytic mutants appear to be positioned in different regions to the regulatory mutants (**Fig. 3.20**). Although most catalytic mutations are located on eIF2Bα's distal face, they do not seem to directly interact with the β or δ subunits. Instead, most amino acid residues affected seem to be important for intra-protein interactions, therefore affecting the conformational structure of eIF2Bα. The only exception to this is R104K, which may be able to form hydrogen bonds with L125 within eIF2Bβ. R104K does not produce a regulatory phenotype because the arginine is substituted for a lysine. As both amino acids are characteristically similar and are usually favoured substitutions, it is possible that the lysine can still interact with the leucine within eIF2Bβ.

Table 3.3 - Phenotypes observed from characterised *gcn3* catalytic mutants

	Wild Type	*gcn3::LEU2*	pGCN3 Cen	AA25,26VV Cen	A26T Cen	D71N Cen	R104K Cen	E199K Cen	V295F Cen	303//305Δ Cen
				gcn3 Catalytic Mutants						
Growth Rate[1]	++++	++++	++++	++	N/A	N/A	N/A	++++	N/A	++++
Growth on 3AT	N/A	None	Inhibited	++	N/A	N/A	N/A	+++	N/A	Inhibited
Translational Regulation[2]	Yes	No	Yes	Yes	N/A	N/A	N/A	No	N/A	Yes
eIF2B Localisation[3]	eIF2B Bodies	Dispersed	eIF2B Bodies	Microbodies	Microbodies	Microbodies	Microbodies	Microbodies	Microbodies	eIF2B Bodies/ Microbodies

N/A: Not analysed

[1]As determined by growth curves (see Figure 3.10)

[2]As determined by polysome profiling (see Figure 3.11)

[3]As determined by confocal microscopy (see Figure 3.12)
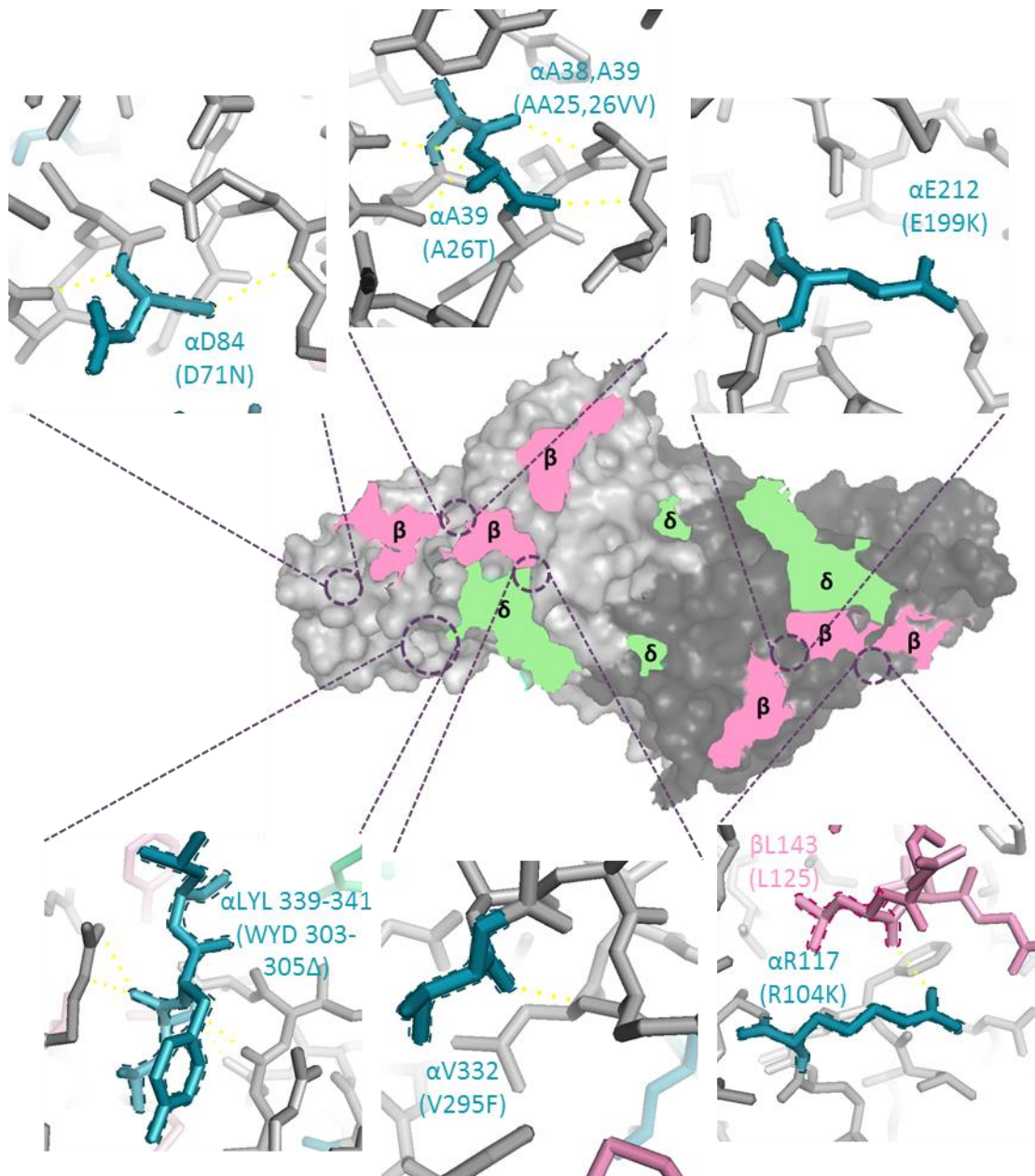
Figure 3.20 eIF2Bα catalytic mutants may affect intra-protein interactions. For the most part, the eIF2Bα catalytic mutations (blue) seem to affect intra-protein interactions, accounting for a conformational change that hinders eIF2Bs GEF activity. The R104K mutation however, seems to interact with the beta subunit (pink). S. cerevisiae amino acid residues are in brackets, whilst the S. pombe homologous residue are above.

3.2.4. Insights into eIF2B body formation and function from VWM mutations

The eIF2Bα regulatory and catalytic mutations were originally selected based on the potency of their phenotypes and may represent extreme situations. Naturally occurring missense mutations causative of the human disease VWM were investigated to determine their effect on the localisation of eIF2B. Although phenotypical correlations were identified between eIF2B localisation and either regulatory mutations (where eIF2B is dispersed) or catalytic mutations (where eIF2B localises to microbodies), some VWM mutations seem to be more complex.

Previous characterisation of the N209Y mutation identified the substitution acted analogously to the null strain, thus representing a regulatory mutant (Richardson et al., 2004). Polysome profiles (**Fig. 3.15**) and 3-AT spot plates (**Fig. 3.14B**) in addition to the dispersed eIF2B localisation (**Fig. 3.16**) supported these conclusions. F240V also resulted in a similar regulatory phenotype, although intriguingly localisation was not completely dispersed as a small subset of cells formed eIF2B bodies (**Fig. 3.16**). The V184D mutant also gave unexpected results with the 3-AT plates suggesting a regulatory mutant phenotype while the polysome analysis resulted in a wild-type response to the stress. These results were additionally confounded by the localisation data, which resulted in the formation of microbodies; a characteristic associated with a decrease in catalytic activity. Currently, there is no evidence to support a reason behind these contradicting phenotypes, thus further investigation is warranted. The remaining VWM mutations did not share any similarities with either phenotypes that previously affected eIF2B localisation, even though a slight decrease in the number of eIF2B bodies was observed for K111E, which was exacerbated in Y274C.

Whilst N209Y and F240V clearly produced regulatory phenotypes, how K111E, V184D and Y274C affect eIF2B leading to the pathogenesis of VWM remained elusive. Structurally, most VWM mutations (apart from K111E) are distinctively different from the regulatory/catalytic mutants and are in close proximity to the α-α interface (**Fig. 3.21**), possibly providing an explanation for the varied phenotypes in the V184D or the lack of phenotypical differences from Y274C. The VWM mutant F240V mirrored the regulatory mutant F240I, thus similar interactions with Q393 within eIF2Bδ may be perturbed. N209Y resides within a hydrophobic pocket responsible for binding phosphorylated serine 51 within eIF2α in response to cellular stress. Subsequently, previously published data suggests eIF2-P cannot interact with eIF2Bα (Kashiwagi et al., 2014). Considering that the N209Y mutant dispersed the localisation of eIF2B, data presented here also suggests an unknown link between regulation and localisation, as eluded to previously. Conversely, experiments performed using HEK293 cells showed eIF2B could still bind eIF2-P in the presence of the N208Y (human) mutation (Wortham and Proud, 2015). Moreover, the mutation increased eIF2Bs GEF activity by 40 %. Although notable differences between yeast and human eIF2B could explain these phenotypical differences, it should be noted that these experiments were conducted using transiently transfected cells where overexpressed proteins were combined with wild-type versions, and therefore may not represent eIF2B complexes *in vivo*. The VWM mutant V184D may interact with Q228 on the opposing eIF2Bα subunit, thus representing a unique mutation within this study. Considering the conflicting phenotypes observed, it is possible the α-α interaction may be perturbed producing either pentameric complexes ($εγδβα$) or nonameric complex ($ε_2γ_2δ_2β_2α$). In addition to eIF2B nonamers being previously observed, data generated using HEK293 cells showed V183D reduced interaction of eIF2Bα with the complex, albeit only moderately

(Wortham and Proud, 2015). K111E and Y274C do not seem to be involved in any subunit-subunit interactions and may only be required for intra-protein interactions or protein folding, possibly explaining why eIF2B function/regulation did not seem to be impaired. Whilst K111E analyses are novel to this study, Y274C produced similar observations in human HEK293 cells.

A clear correlation seems to exist between localisation, the type of mutation (*i.e.* regulatory or catalytic) and where the mutated residue exists. Indeed, the regulatory mutants seem to prevent eIF2B regulation, localisation and subsequently eIF2Bα incorporation. The catalytic mutants seem to affect intra-protein interactions, subsequently affecting the catalytic activity of eIF2B and localisation. The VWM mutations V184D and Y274C did not correlate with either of the aforementioned phenotypes. Hence, further analyses of these foci may provide novel observations that may help explain the molecular pathogenesis of VWM disease.

Table 3.4 - Phenotypes observed from characterised *gcn3* VWM mutants

	Wild Type	*gcn3::LEU2*	p*GCN3* CEN6ARS4	K111E	V184D	N209Y	F240V	Y274C
					***gcn3* VWM Mutants**			
Growth Rate[1]	++++	++++	++++	++++	++++	++++	+++	+++
Growth on 3AT	N/A	None	Inhibited	Inhibited	Severely Inhibited	Severely Inhibited	Severely Inhibited	Inhibited
Translational Regulation[2]	Yes	No	Yes	Yes	N/A	N/A	N/A	No
eIF2B Localisation[3]	eIF2B Bodies	Dispersed	eIF2B Bodies	eIF2B Bodies	Microbodies	Dispersed	[Reduced] eIF2B Bodies	[Reduced] eIF2B Bodies

N/A: Not analysed

[1]As determined by growth curves (see Figure 3.14)

[2]As determined by polysome profiling (see Figure 3.15)

[3]As determined by confocal microscopy (see Figure 3.16)
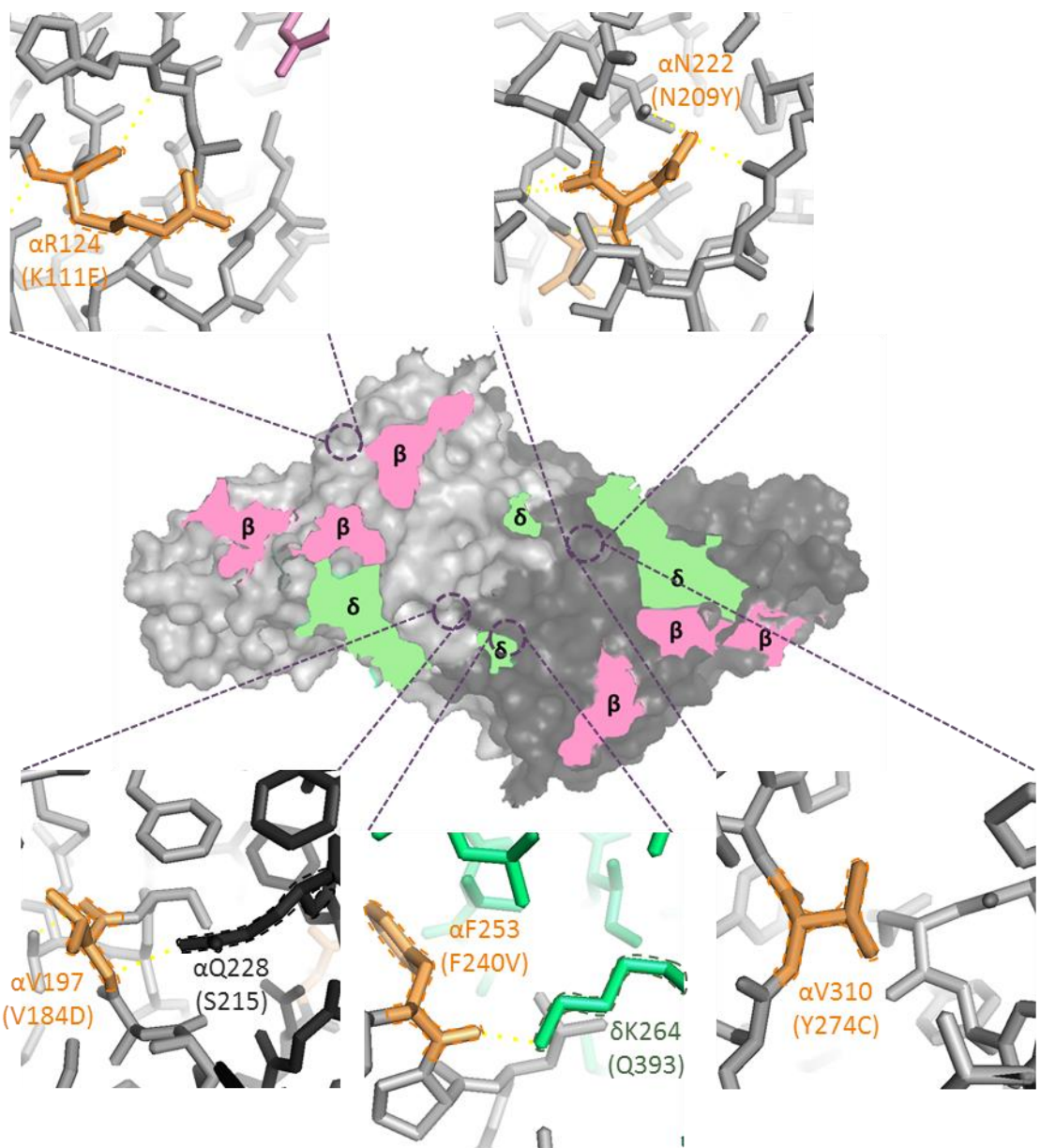
Figure 3.21 eIF2Bα VWM mutants are in close proximity of the α-α interface. With the exception of K111E, the eIF2Bα VWM mutations (orange) are in close proximity to the dimerization interface. F240V seems to interact with eIF2Bδ (green), whilst V184D may interact with the other α subunit (black). The remaining mutations may be important for intra-protein interactions, although no hydrogen bonding could be seen for Y274C. *S. cerevisiae* amino acid residues are in brackets, whilst the *S. pombe* homologous residue are above.

4. eIF2 shuttling is altered by mutations which disrupts the eIF2B body

4.1. Introduction

eIF2B is a complex enzyme unique amongst GEFs, comprising of multiple subunits that exert various functions (*i.e.* GEF and GDF) and is subject to regulation. To measure GEF activity, recombinant protein purified from bacterial expression systems is typically used in conjunction with isotopically or fluorescently labelled GTP (Jennings et al., 2013, Liu et al., 2011, Jennings and Pavitt, 2010, Wortham and Proud, 2015). Previous studies utilising this *in vitro* biochemical assay have produced valuable insights into several aspects of eIF2B, including the effects of VWM mutations (Liu et al., 2011, Wortham and Proud, 2015). It is generally accepted that VWM mutations decrease the catalytic activity of eIF2B, leading to the cell being in a constant state of stress with constitutive expression of stress-specific mRNA transcripts (*i.e. GCN4* in yeast, *ATF4* in humans) (Pavitt et al., 1997). However, some studies argue that this may not always be the case. For instance, analysis of eIF2Bα VWM mutations showed that N209Y increased eIF2B GEF activity by 40 % while the mutant P278R had no effect on eIF2B activity, holocomplex formation or eIF2/eIF2-P binding (Wortham and Proud, 2015). Moreover, Liu *et al.,* (2011) showed that catalytic deficits caused by VWM mutations do not correlate with the phenotypes observed within patients. It is possible that although the *in vitro* biochemical assay may be useful to analyse some mutations, it may not be informative for all mutations. Other proteins (*i.e.* Ifa38p) have also been shown to interact with eIF2B (Browne et al., 2013). Although the purpose behind eIF2B-Ifa38p interactions remain unclear, other interactors of eIF2B have been implicated, all of which are omitted during *in vitro* analysis (Babu et al., 2012). Thus, a method of analysing eIF2B activity *in vivo* is necessary, ensuring the accurate measurement of canonical eIF2B complexes in the presence of required co-factors.

Fluorescence recovery after photobleaching (FRAP) is a technique that analyses the movement of fluorescently tagged intracellular proteins. By irreversibly bleaching an area of interest, the movement of non-bleached molecules into the foci can be measured to gather valuable information, such as the ratio of mobile to immobile molecules and the half-time for fluorescence recovery (**Fig. 4.1**). During the original study describing eIF2B bodies, FRAP was highlighted as a novel method to measure eIF2B activity *in vivo* (Campbell et al., 2005). FRAP analyses of GFP tagged eIF2B and eIF2 subunits identified that the former remains resident within the discrete cytoplasmic foci, whilst the latter shuttled into and out of the eIF2B body. Using three different methods, Campbell *et al.,* (2005) highlighted that the shuttling of eIF2 throughout the eIF2B foci could potentially be used to measure the catalytic activity of eIF2B. Firstly, cells depleted for amino acids displayed reductions in mobile eIF2 and half-time recovery as well as a two-fold increase of eIF2 within the foci. These results correlated with an increase of eIF2α-P, which is known to bind eIF2B with high affinity, inhibiting GEF activity. Secondly, under amino acid stress Gcn2p phosphorylates S51 within eIF2α which then binds and inhibits eIF2B. Using two constitutively active Gcn2p mutants, eIF2 shuttling was shown to decrease in tandem with respective increases in eIF2α-P levels. Finally, using the Gcd6p (eIF2Bε) mutant F250L, the group highlighted eIF2 dynamics dramatically decreased in the presence of a mutation that decreased the catalytic activity of eIF2B. Together, these experiments provided strong evidence to suggest that eIF2 shuttling is dependent on eIF2B activity, whereby eIF2-GDP shuttles into the foci for GDP-GTP exchange to occur. Moreover, in-line with known mechanisms of eIF2B regulation, eIF2α-P was shown to remain resident within the eIF2B body as opposed to shuttling through it. Of importance to the present study, the authors showed FRAP could be utilised as an *in vivo* method to analyse the

catalytic activity of eIF2B in the presence of a mutated subunit. Thus, the main aim within this chapter was to analyse eIF2 dynamics within eIF2Bα/Gcn3p mutants characterised in the previous chapter.

Figure 4.1 Schematic of measuring eIF2B activity by analysing eIF2 recovery within foci, via FRAP. (A) A cell containing an eIF2B body is selected. The co-localised eIF2, which contains a yeGFP tag is bleached. Multiple images are then taken over time to measure the time needed for eIF2 to recover. (B) An example of a one-phase association graph depicting the different stages of FRAP as well as the various measurements that can be extrapolated. Marked in dashed lines; the t½ time defines the half-time for eIF2 to fully recover. Marked by a grey line; mobile eIF2 defines the amount of mobile eIF2 within the eIF2B body. Both values are important as a rate of recovery may be calculated.

4.2. Results

4.2.1. Amino acid starvation decreases the rate of eIF2 shuttling through eIF2B bodies

FRAP analysis was previously validated as a measurement of eIF2B activity by subjecting cells to amino acid starvation, leading to the phosphorylation of eIF2α that attenuates eIF2B activity and ultimately, the inhibition of translation initiation (Campbell et al., 2005). To ensure the background strain behaved similarly to data published previously, exponentially growing cultures of wild-type (yMK883) containing endogenously GFP tagged *SUI2* (eIF2α) were assessed in complete minimal media and media lacking amino acids. Following the bleaching step, eIF2 recovery was measured every 1.8 seconds over 25 cycles of recovery. For each eIF2B foci analysed, background fluorescence was subtracted from the fluorescent recovery, which was then normalised to total cellular fluorescence. Generated data was fitted to a one-phase association curve to find the percentage of eIF2 that was mobile, as well as half-time recovery. As fluctuations in the level of mobile eIF2 may influence the time required for eIF2 to recover, the rate of eIF2 recovery was calculated which took both measurements into consideration. eIF2α-P accumulates within eIF2B foci following cellular stress to reduce the catalytic activity of eIF2B (Campbell et al., 2005), therefore, total eIF2 content within eIF2B foci was measured to correlate decreases in eIF2 shuttling with eIF2α-P residency.

FRAP analysis was carried out on a Sui2p-GFP tagged strain, under normal conditions and under amino acid starvation for 30 minutes. Representative images of pre-bleach, post-bleach and recovery are shown in. **Fig 4.2A**, along with the one-phase

association curve used to determine percentage mobile eIF2 as well as half-time recovery. Under normal conditions, eIF2 recovery within the bleached region was rapid with a t½ of 2.3 seconds (**Fig. 4.2A** and **C**). eIF2 shuttling decreased following amino acid depletion for 30 minutes, with a prolonged t½ of 5.7 seconds (**Fig. 4.2A** and **C**). A slight decrease was observed in the amount of mobile eIF2, indicating that less eIF2 was shuttling into these foci (**Fig. 4.2B**). The rate of recovery was significantly reduced, decreasing by approximately 58 %, highlighting a dramatic reduction in the catalytic activity of eIF2B (**Fig. 4.2C**). In tandem with the reduction in mobile eIF2, total eIF2 content within eIF2B bodies increased, indicative of phosphorylated eIF2 taking residency within the foci, subsequently reducing eIF2Bs activity.
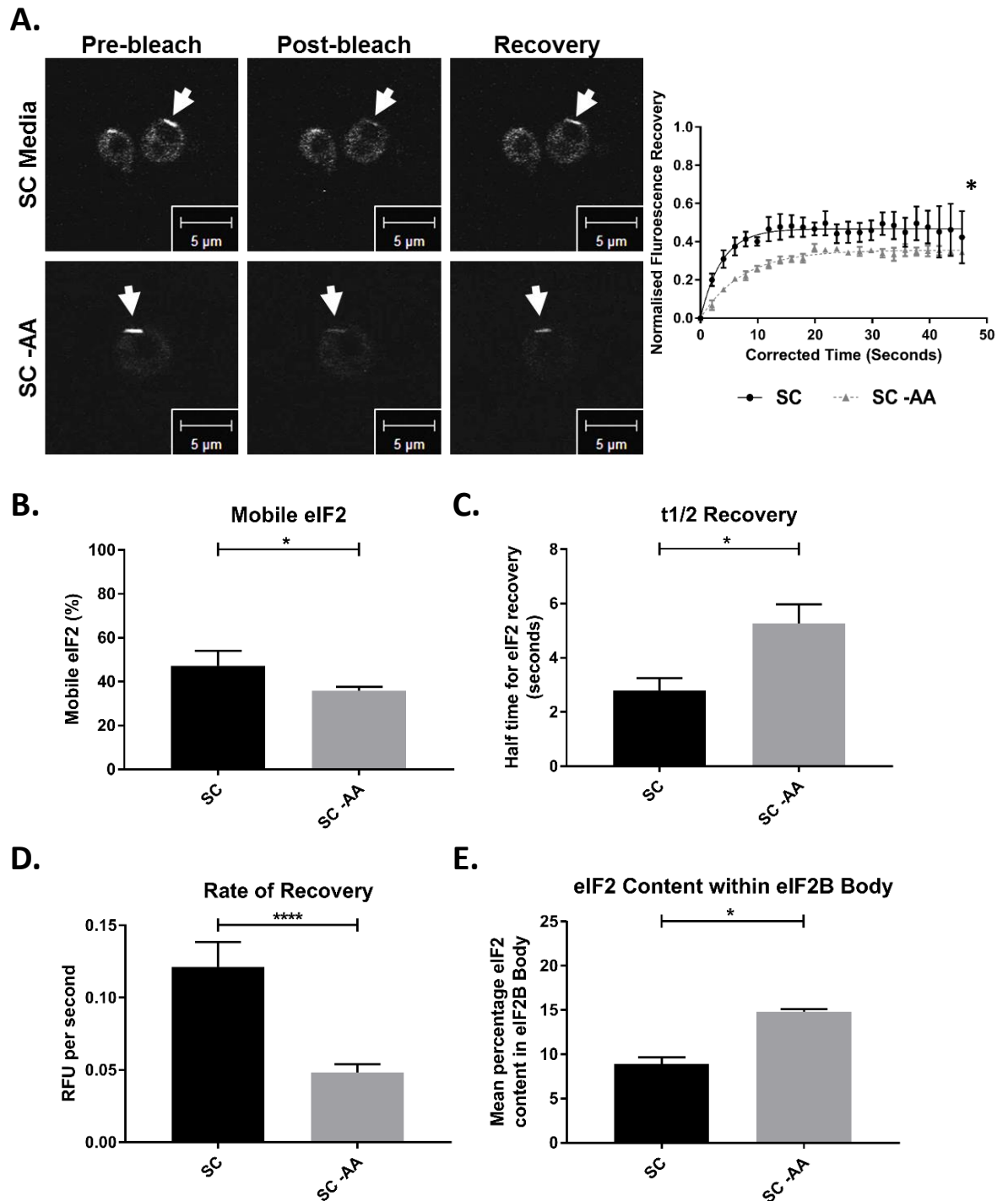
Figure 4.2 eIF2 recovery decreases following amino acid starvation. FRAP analysis of *SUI2-yeGFP* (yMK883) under amino acid starvation. (A) Live-cell images representing the pre-bleach, post-bleach and recovery stages as well as a graph displaying eIF2 recovery over time. A * denotes time at which the recovery image was from. (B) Bar chart representing the mobile eIF2 within the foci as a percentage. (C) Bar chart representative of half the time needed for eIF2 to fully recover. (D) Bar chart representing fluorescence recovery per second. (E) Bar chart representing eIF2 content within eIF2B foci. Starter cultures were diluted to 0.2 OD_{600} in SCD media and incubated at 30°C with shaking until exponential growth was reached. Cells were pelleted and resuspending in media without amino acids before being further incubated for 30 minutes. Data are representative of 25 cells, *n*=3, error bars are representative of SEM, ns = not significant, * P=<0.05, ** P=<0.01, *** P=<0.001, **** P=<0.0001.

4.2.2. Generation of GCN4-LacZ fusion strain to assess eIF2B activity

FRAP assesses the catalytic activity of eIF2B by exploiting the movement of eIF2 into and out of the body, presumably for GDP-GTP exchange. As this is a novel method for potentially measuring *in vivo* GEF activity, it was important to correlate the decrease in eIF2 shuttling with biochemical methods previously used to indicate reduced GEF activity. Sequestration of eIF2B activity derepresses *GCN4*, which is normally repressed under physiological conditions by the presence of four uORFs (see section 1.2.1.1.1) (Hinnebusch, 1985). To correlate eIF2B activity with *GCN4* repression, a strain was constructed that could analyse Gcn4p expression quantitatively via LacZ assay. An integration vector containing *GCN4-LacZ-TRP1* (pAV1729) was linearised by incubation with *SnaB*I, before being transformed into yMK467; a parental strain to the wild-type (yMK883) previously analysed by FRAP. Transformants were selected by incubation on SCD lacking tryptophan. Any transformants that were present will have genomically integrated the *GCN4-LacZ-TRP1* because the integration vector does not contain a yeast origin of replication (Dever et al., 1992). *gcn3* was deleted within the newly created strain by substitution with *HIS3* as previously described.

Exponentially growing cultures of *GCN4-LacZ-TRP1* (ySC87) and *GCN4-LacZ-TRP1 gcn3::HIS3* (ySC88) were subjected to amino acid starvation for 30 minutes before protein extracts were assayed to evaluate Gcn4p-LacZ expression levels. Amino acid starvation increased Gcn4p expression by 50 % within wild-type cells (**Fig. 4.3**). In contrast, the *gcn3* null strain could not derepress *GCN4* as no significant differences were observed between the two conditions. These results confirm that the exposure of cells to amino acid starvation induces the derepression of Gcn4p. Moreover, they

show a relationship between eIF2 shuttling and *GCN4* derepression, as both responded to amino acid starvation which is dependent upon eIF2B regulation. Therefore, these results validate analysing eIF2 dynamics as a measurement of eIF2B activity under similar conditions.
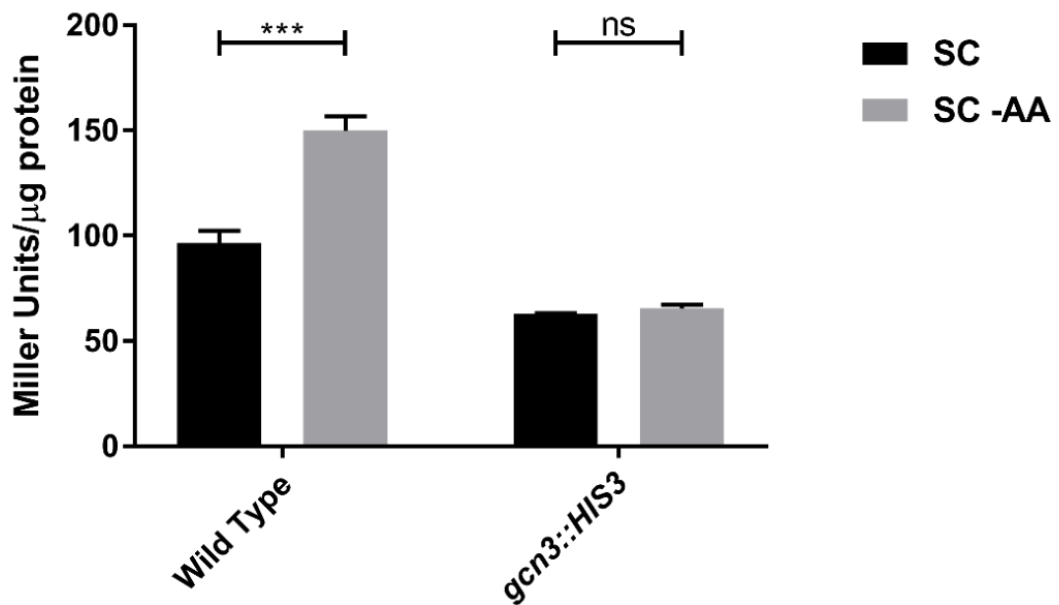
Figure 4.3 Gcn4p expression is derepressed during amino acid starvation. LacZ assay using *GCN4-LacZ* (ySC85) and *GCN4-LacZ gcn3::HIS3* (ySC86) to analyse Gcn4p expression in response to amino acid starvation. Starter cultures were diluted to 0.2 OD_{600} in SCD media and incubated at 30°C with shaking until exponential growth was reached. Cultures were halved, pelleted and one aliquot was resuspended in media without amino acids before being further incubated for 30 minutes. Following this, protein was extracted by bead beating and used *the β-galactosidase activity was measured to assess Gcn4p expression*. Protein was quantified by BCA assay. n=3, error bars are representative of SD, ns = not significant, * P=<0.05, ** P=<0.01, *** P=<0.001, **** P=<0.0001.

4.2.3. eIF2Bα catalytic mutants de-repress Gcn4p expression

In Chapter 3 data was presented which showed that *gcn3* catalytic mutants localised eIF2B to microbodies. As discussed in section 3.1.4.3, reduced eIF2B catalytic activity leads to the derepression of *GCN4,* which eventually results in the upregulation of genes involved in amino acid biosynthesis. To determine Gcn4p expression levels in the presence of a *gcn3* catalytic mutation, quantitative LacZ assays were carried out for the three mutants AA25,26VV, E199K and AA 303//305Δ. In addition to the plasmid-borne low-copy *GCN3* wild-type, the three mutants were exogenously expressed in the *GCN4-LacZ-TRP1, gcn3::HIS3* (ySC86) strain before protein extracts were used for LacZ assays.

The *gcn3* catalytic mutants AA25,26VV and E199K lead to significant increases in the levels of Gcn4p (**Fig. 4.4**). AA25,26VV produced a 7-fold increase in Gcn4p levels, whilst E199K lead to a 10-fold increase, possibly demonstrating differing reductions in eIF2B activity. Gcn4p levels failed to fluctuate significantly when the AA 303//305Δ mutation was present, implying eIF2B activity may be normal within this mutant. Overall, these results show that AA25,26VV and E199K reduce the catalytic activity of eIF2B, whilst AA 303//305Δ may not.
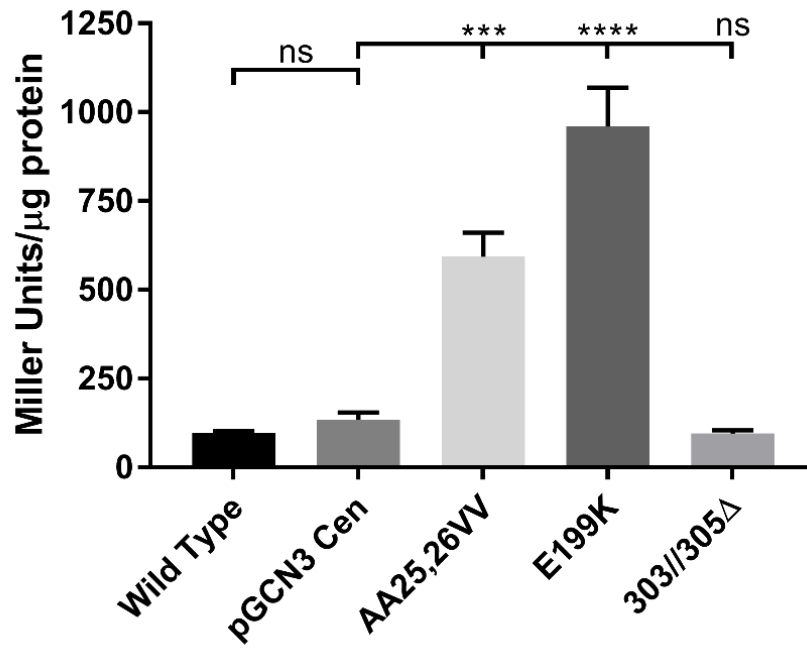
Figure 4.4 LacZ assay to assess Gcn4p expression in the presence of Gcd⁻ *gcn3* mutations. Three Gcd⁻ *gcn3* mutants were exogenously expressed in the *GCN4-LacZ, gcn3::HIS3* (ySC86) strain. Cultures were diluted to 0.2 OD_{600} and incubated at 30°C with shaking until exponential growth was reached. Total protein was extracted and the β-galactosidase activity was measured to assess Gcn4p expression. Protein concentration was determined via BCA assay. n=3, error bars are representative of SD, ns = not significant, * *P*=<0.05, ** *P*=<0.01, *** *P*=<0.001, **** *P*=<0.0001.

4.2.4. eIF2B microbodies display reduced eIF2 shuttling

As these catalytic mutants showed decreased eIF2B activity (via their increased Gcn4p levels) and displayed eIF2B microbodies, it was hypothesised that disruption of the large eIF2B body into microbodies may decrease the shuttling of eIF2 through eIF2B. To test this hypothesis, FRAP analysis was carried out on the mutants AA25,26VV, E199K and AA 303//305Δ. As the mutant AA 303//305Δ also formed eIF2B bodies as well as microbodies (see section; 3.1.4.4; **Fig. 3.12)**, this catalytic mutant represented a unique opportunity to investigate differences in the shuttling of eIF2 between the two types of eIF2B localisation. The plasmid-borne catalytic mutants, along with the corresponding wild-type *GCN3* low-copy Cen plasmid, were exogenously expressed in the *SUI2-GFP gcn3::LEU2* (ySC16). During FRAP analyses of eIF2B microbodies, eIF2 shuttling was measured within two or more microbodies and averaged per cell.

Representative images from the various stages of FRAP, as well as the individual one-phase association curves highlighting differences in eIF2 kinetics are shown in **Figure 4.5**. Analysis of these data sets showed that for all the mutants tested, eIF2 shuttling within microbodies was slower than eIF2 shuttling within eIF2B in wild-type cells (**Fig. 4.6**). Interestingly the percentage mobile eIF2 did not deviate significantly within any of the catalytic mutations tested, indicating similar amounts of mobile eIF2 between wild-type and mutants (**Fig. 4.6A**). AA25,26VV and E199K increased the half-time for eIF2 recovery by 2 seconds in comparison to the plasmid-borne wild-type *GCN3* (**Fig. 4.6B**). Expectedly, rates of recovery inversely correlated for both mutants, showing a 33.3 % decline in eIF2 recovery per second (**Fig. 4.6C**). Intriguingly, eIF2 shuttling through eIF2B bodies within the AA 303//305Δ mutant was

comparable to wild-type throughout, with no significant deviations observed. Conversely however, eIF2 shuttling through microbodies within the same mutant declined similarly to AA25,25VV and E199K. Total eIF2 content within eIF2B foci was not analysed for the catalytic mutants. Nonetheless, FRAP analyses of eIF2 dynamics herein suggest eIF2B localisation may affect the catalytic activity of eIF2B.
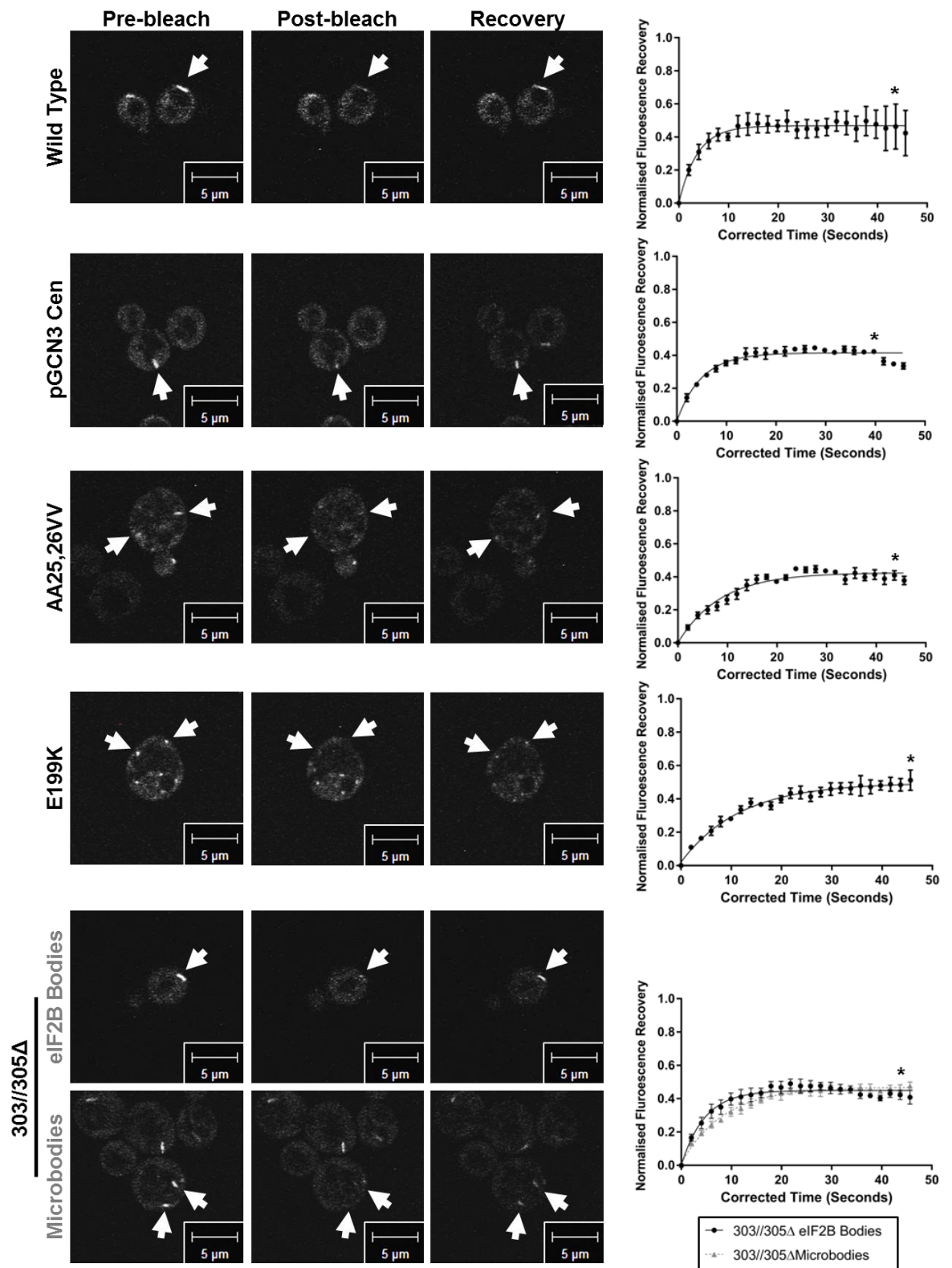
Figure 4.5 FRAP analysis of *gcn3* Gcd⁻ mutations. Three *gcn3* Gcd⁻ mutations (AA25,26VV (pAV1239), E199K (pAV1244) and 303//305Δ (pAV1268)) as well as the *GCN3 Cen* plasmid (pAV1170) were exogenously expressed in *SUI2-yeGFP gcn3::LEU2* (ySC16) to measure eIF2 recovery within eIF2B bodies. Both eIF2B body and microbody foci were analysed for the 303//305Δ mutant. Live-cell images representing the pre-bleach, post-bleach and recovery stages as well as a graph representing eIF2 recovery over time are shown. A * denotes time at which the recovery image was from. Data representative of 25 cells, *n*=3, error bars are representative of SEM.
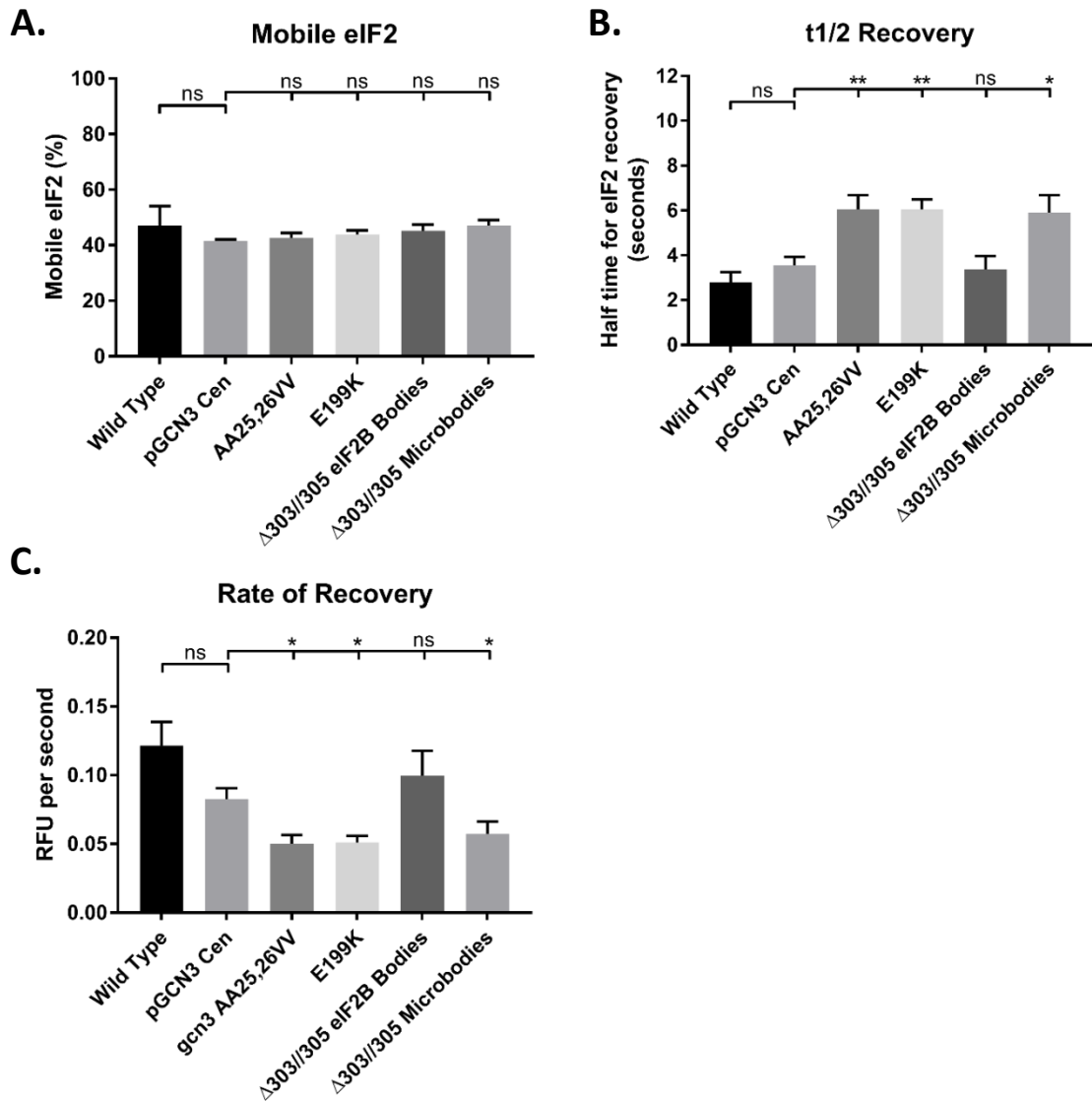
Figure 4.6 eIF2 shuttles slower through eIF2B microbodies in catalytic mutants. (A) Bar chart representing the mobile eIF2 within the foci as a percentage. (B) Bar chart representative of half the time needed for eIF2 to fully recover. (C) Bar chart representing eIF2 content within eIF2B foci. Data are representative of 25 cells, n=3, error bars are representative of SEM, ns = not significant, * P=<0.05, ** P=<0.01, *** P=<0.001, **** P=<0.0001.

4.2.5. The effect of eIF2Bα VWM mutants on Gcn4p levels

Within chapter 3, the impact of VWM missense mutations on eIF2B localisation was assessed, with a range of phenotypes observed. The VWM mutants V184D, N209Y and F240V were shown to be regulatory mutants, whilst K111E and Y274C were analogous to wild-type. Qualitative assessment of eIF2B catalytic activity via 3-AT spot plates indicated there were no deficits in the catalytic activity of eIF2B when any of the VWM mutations were present. However as this was not a quantitative assessment of the GEF activity of eIF2B, Gcn4p levels were investigated via the LacZ assay. In addition to the wild-type *GCN3 CEN6ARS4* low-copy plasmid, the VWM mutants were exogenously expressed in the *GCN4-LacZ-TRP1*, *gcn3::HIS3* (ySC86) before protein extracts from exponentially growing cultures were used for LacZ assays.

Interestingly, Gcn4p levels within the VWM mutations remained similar to wild type, with slight fluctuations from V184D and Y274C (**Fig. 4.7**). These results suggest that under steady state conditions the majority of the VWM mutations do not induce Gcn4p expression, with the exception of the Y274C mutant where a 20 % increase was observed.
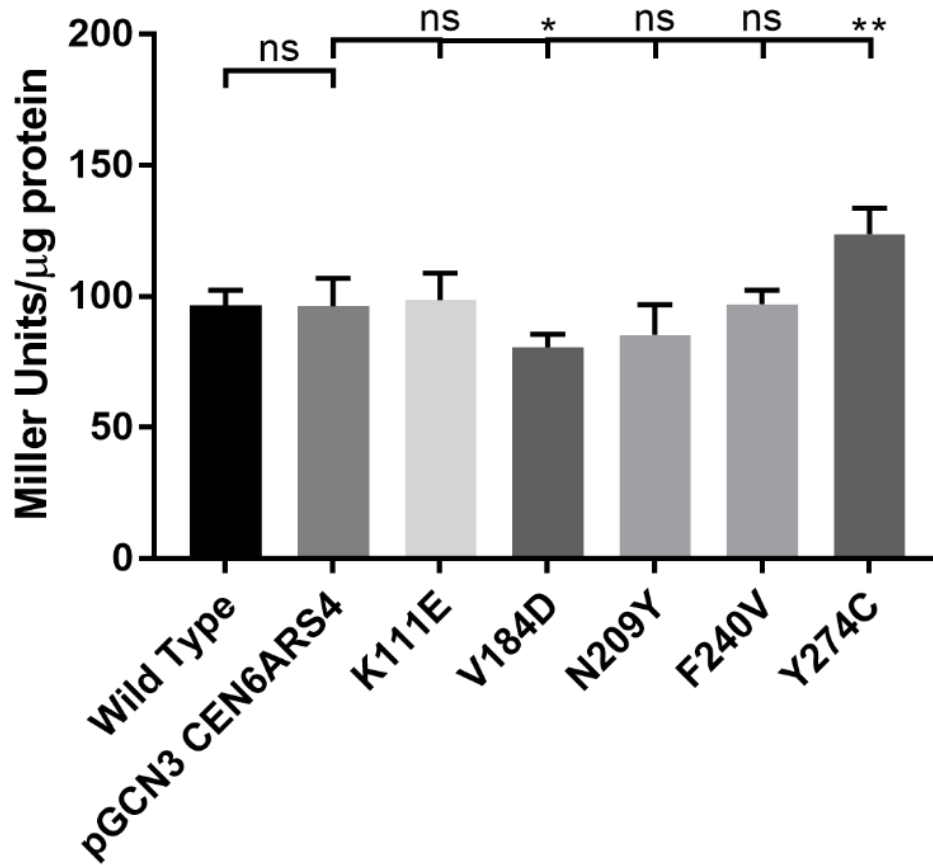
Figure 4.7 LacZ assay to assess Gcn4p expression in the presence of VWM _gcn3_ mutations.
Five _gcn3_ VWM mutants were, as well as the WT _GCN3 CEN6ARS4_ plasmid, were exogenously expressed in the _GCN4-LacZ, gcn3::HIS3_ (ySC86) strain. Cultures were diluted to 0.2 OD_{600} and incubated at 30°C with shaking until exponential growth was reached. Total protein was extracted and the β-galactosidase activity was measured to assess Gcn4p expression. Protein concentration was determined via BCA assay. _n_=3, error bars are representative of SD, ns = not significant, * _P_=<0.05, ** _P_=<0.01, *** _P_=<0.001, **** _P_=<0.0001.

4.2.6. FRAP analysis of eIF2Bα VWM mutations

During the analysis of eIF2B localisation in chapter 3, N209Y exclusively dispersed eIF2B throughout the cells, hence FRAP analysis was not performed on this mutant as there were no eIF2B cytoplasmic locus to focus on. However, the remaining mutations localised eIF2B either to microbodies (V184D) or to eIF2B bodies in varying numbers (K111E, F240V and Y274C) (see section 3.2.5.2; **Figure 3.16**). Although these mutations cause a range of disease severities in humans, under steady state growth in yeast, no decrease in cell growth was observed (**Fig. 3.14A**). FRAP was performed to investigate eIF2 dynamics when VWM mutations were present. In addition to the wild-type *GCN3* low-copy CEN6ARS4 plasmid, the VWM mutations were exogenously expressed in the *SUI2-GFP*, *gcn3::LEU2* (ySC16) strain for FRAP analysis.

Although eIF2B bodies were present within the mutants V184D and F240V, eIF2α-GFP did not localise to discrete cytoplasmic bodies and instead was dispersed throughout the cytoplasm (**Fig. 4.8**). Therefore FRAP analysis was not carried out on these mutant strains. This is despite eIF2B localising to microbodies when V184D was present, or eIF2B bodies when F240V was present, although F240 localised eIF2B at lower levels than wild-type (see section 3.2.5.2, **Fig. 3.16**).

However eIF2α-GFP did localise to eIF2B bodies in the presence of the mutants K111E and Y274C, therefore FRAP analysis was carried out to determine the rate of eIF2 shuttling in the presence of these mutations. Representative images from the various stages of FRAP are displayed in **Figure 4.10**, as well as one-phase association curves representing the recovery of eIF2 within eIF2B foci. Mobile eIF2 increased by 12 % when K111E was present, whilst the Y274C mutation increased by 24.6 % (**Fig. 4.11A**). Half-time recovery of eIF2 increased by 2.9 and 5.2 seconds for K111E and

Y274C respectively (**Fig. 4.11B**). Despite half-time recovery being dramatically increased, recovery rates of eIF2 per second decreased only slightly for both mutants (**Fig. 4.11C**). Interestingly, whilst no change was observed for the K111E mutant, eIF2 content within eIF2B foci increased by 4.5 % in the Y274C mutant (**Fig. 4.11D**). These results show that VWM mutations may affect the shuttling of eIF2 through the eIF2B body in different ways than the Gcn3p catalytic mutants analysed previously.

Gcd1p-GFP   **Sui2p-GFP**
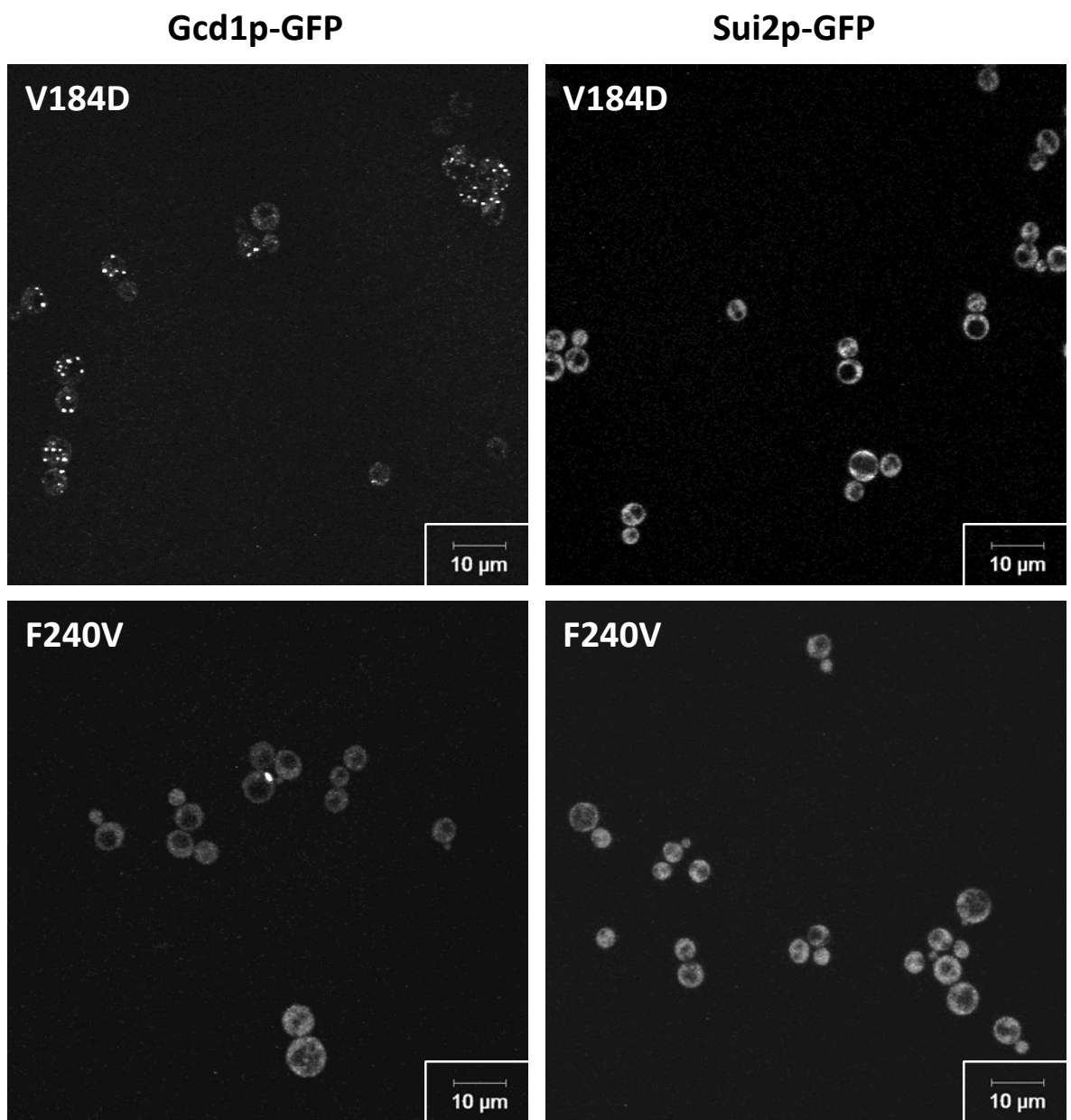
Figure 4.8 V184D and F240V do not localise eIF2 within eIF2B foci. Exponential cultures of *GCD1-GFP gcn3::LEU2* (yMK1402) and *SUI2-GFP gcn3::LEU2* (ySC16) containing the plasmid-borne V184D and F240V VWM mutants were live-cell imaged via confocal microscopy.
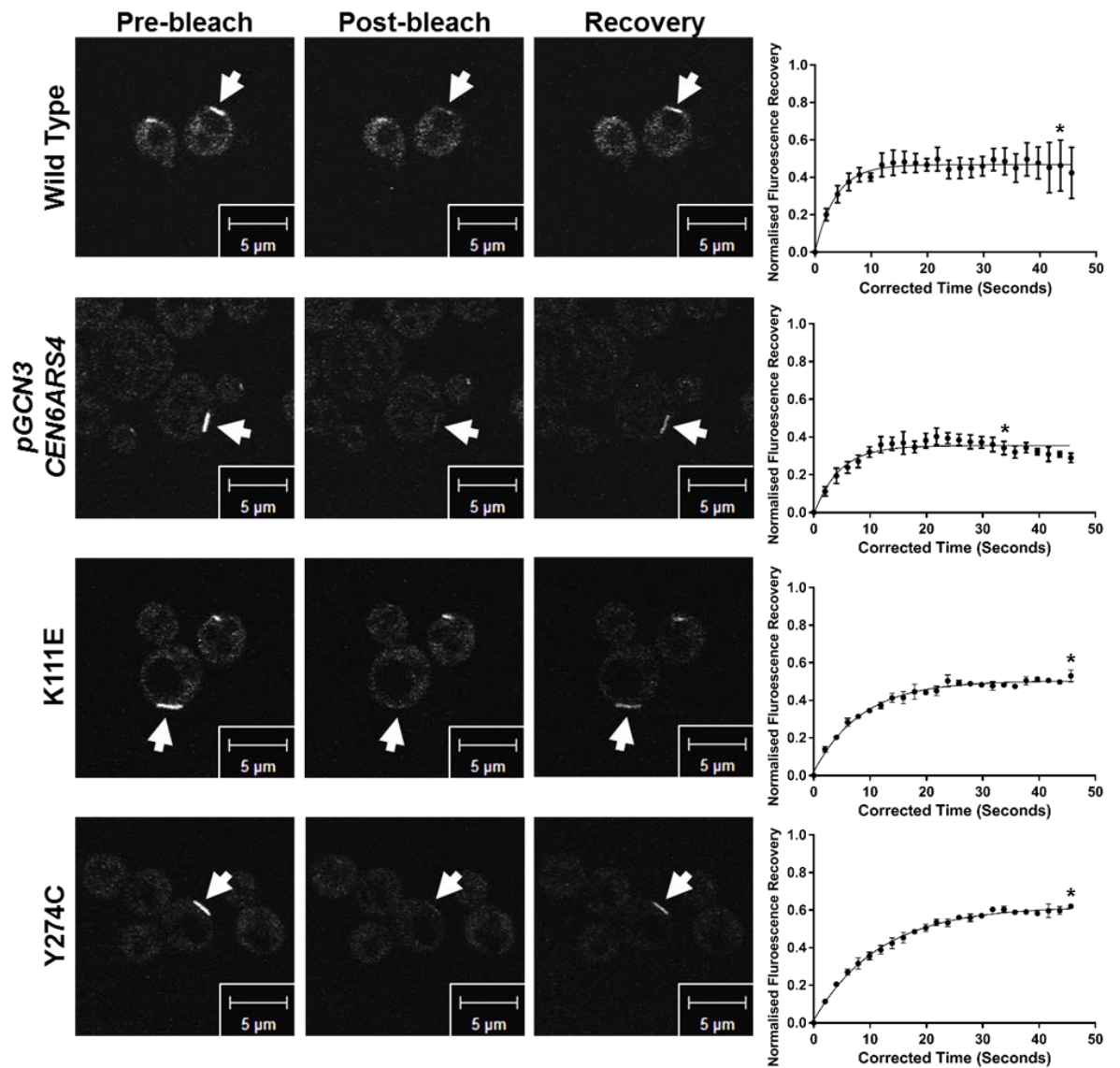
Figure 4.9 FRAP analysis of eIF2 cycling through eIF2B foci in the presence of a VWM gcn3 mutation. The VWM mutants K111E and Y274C were exogenously expressed in a *SUI2-yeGFP* strain lacking any *gcn3*. Live-cell images representing the pre-bleach, post-bleach and recovery stages as well as a graph representing eIF2 recovery over time. An * denotes time at which the recovery image was from. Data are representative of 25 cells, n=3, error bars are representative of SEM.
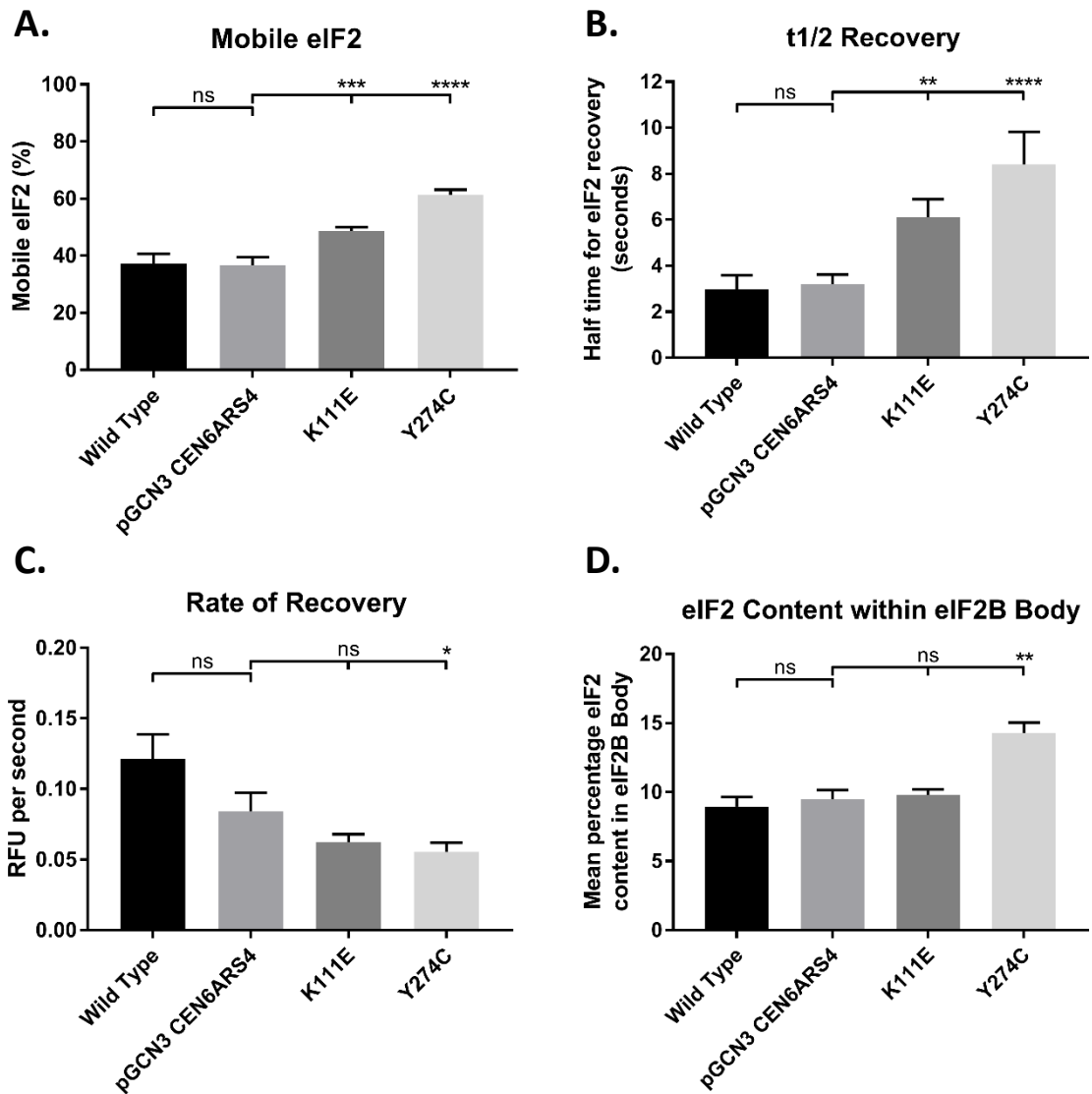
Figure 4.10 Analysis of eIF2 shuttling through eIF2B foci in the presence of a VWM gcn3 mutation. (A) Bar chart representing the mobile eIF2 within the foci as a percentage. (B) Bar chart representative of half the time needed for eIF2 to fully recover. (C) Bar chart representing eIF2 content within eIF2B foci. Data are representative of 25 cells, n=3, error bars are representative of SEM, ns = not significant, * P=<0.05, ** P=<0.01, *** P=<0.001, **** P=<0.0001.

4.2.7. Intracellular movement of eIF2B bodies may be important to eIF2B function

A characteristic of eIF2B bodies whose function remains unclear is the fact that eIF2B bodies are mobile within the cell. Interestingly, previous studies have shown that butanol, a potent inhibitor of translation initiation, inhibits eIF2B body movement (Taylor et al., 2010). Moreover, butanol has been shown to reduce eIF2 shuttling through the eIF2B body via FRAP analysis. During FRAP analyses of the catalytic and VWM *gcn3* mutations, noticeable differences were observed between eIF2B foci movement.

Figure 4.10 shows representative live-cell images highlighting eIF2B body movement over 45.7 seconds, during amino acid starvation conditions as well as when *gcn3* catalytic and VWM mutations are present. Intriguingly, eIF2B bodies were still motile following amino acid starvation for 30 minutes, possibly indicating that movement is not directly linked to eIF2B regulation. In comparison to the movement of eIF2B body foci from exogenously expressed plasmid-borne wild-type Gcn3p, AA25,26VV and E199K microbody foci remained still within the cytoplasm. The localised eIF2B from the VWM mutant K111E rarely moved, whilst Y274C eIF2B bodies remained still throughout. The catalytic and VWM mutants suggest a link between eIF2B activity and foci movement, although no significant catalytic defect has been found in the previous analyses for K111E.
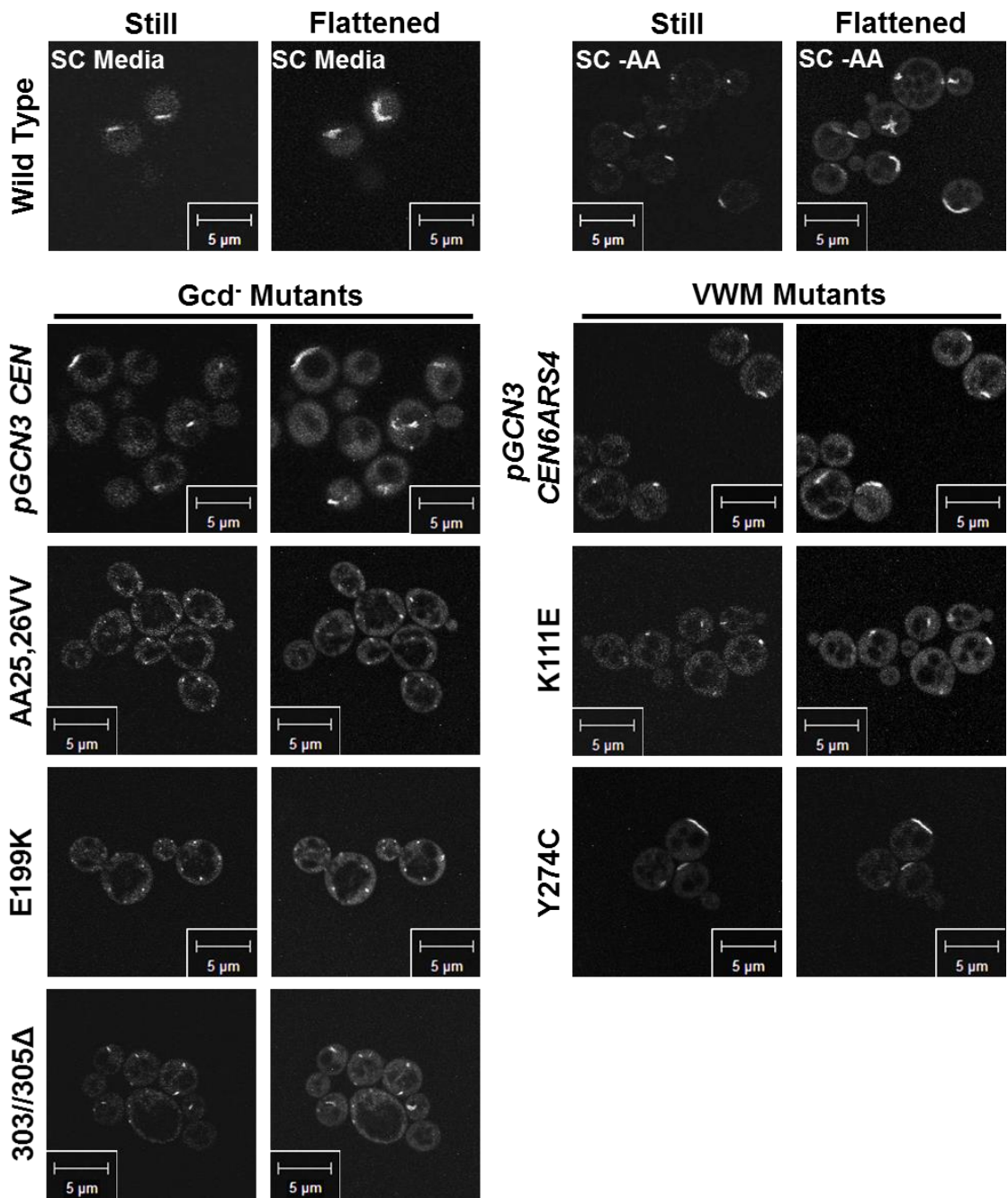
Figure 4.11 Representative images highlighting movement of eIF2B foci. Images were taken every 1.8 seconds over 25 cycles via confocal microscopy and flattened into one image using ImageJ to see the extent of eIF2B body movement. 'Still' images were the first image taken within that series.

4.2.8. Effect of *gcn3* mutations on Gcn3p expression

Previous studies investigating the functional consequences of eIF2B mutations have highlighted alterations in the steady-state levels of the mutated subunit. In 2004, Richardson *et al.,* showed that expression levels of the Gcn3p mutant, N209Y, decreased quite significantly from wild-type. In these instances, whether phenotypical differences are a result of the mutation or a decrease in expression will likely be unknown, therefore conclusions derived from observed phenotypes can be confounding. It was therefore important to investigate what impact the mutations had on Gcn3p expression levels. Cell extracts from the regulatory, catalytic and VWM mutants were compared to their respective wild types by Western blotting. The blots were probed for Gcn3p as well as Pab1p. The latter was used as a loading control and allowed quantitative analysis of Gcn3p expression by densitometry.

Expression levels of the Gcn3p regulatory mutants have not been documented thus far. In comparison to wild-type, the high-copy *GCN3* plasmid dramatically increased Gcn3p levels 20-fold (**Fig. 4.12A**). For most of the regulatory mutants, expression levels of Gcn3p decreased in comparison to the expression levels of the plasmid-borne wild-type. Although expression levels were lower, they remained higher than endogenous levels. The S293R mutant was the only mutant to increase Gcn3p levels.

Previously published data has shown that some catalytic mutants (AA25,26VV, A26T and V295F) decrease Gcn3p expression, whilst the AA 303//305Δ mutant increased Gcn3p levels (Hannig et al., 1990). In comparison to the plasmid-borne wild-type, the catalytic mutants AA25,26VV and E199K reduced Gcn3p levels by a third and two-thirds respectively (**Fig. 4.12B**). The mutant AA 303//305Δ increased expression

levels, although not as high as previously reported. The A26T substitution was the only mutant to remain similar to exogenous wild-type levels, whilst R104K, V295F and D71N increased levels by a factor of two or more.

As mentioned earlier, the N209Y mutation is the only eIF2Bα VWM mutant to be investigated in yeast prior to this study (Richardson et al., 2004). The N209Y mutant, along with the V184D and F240V mutations, substantially decreased Gcn3p levels in comparison to exogenously expressed wild-type levels (**Fig. 4.12C**). The Y274C mutant remained similar to wild-type, although K111E increased levels 1.5-fold. Interestingly, the K111E and V184D mutations seemed to exhibit slight differences in their molecular weight, as indicated by slight shifts in the Gcn3p band, in comparison to wild-type.
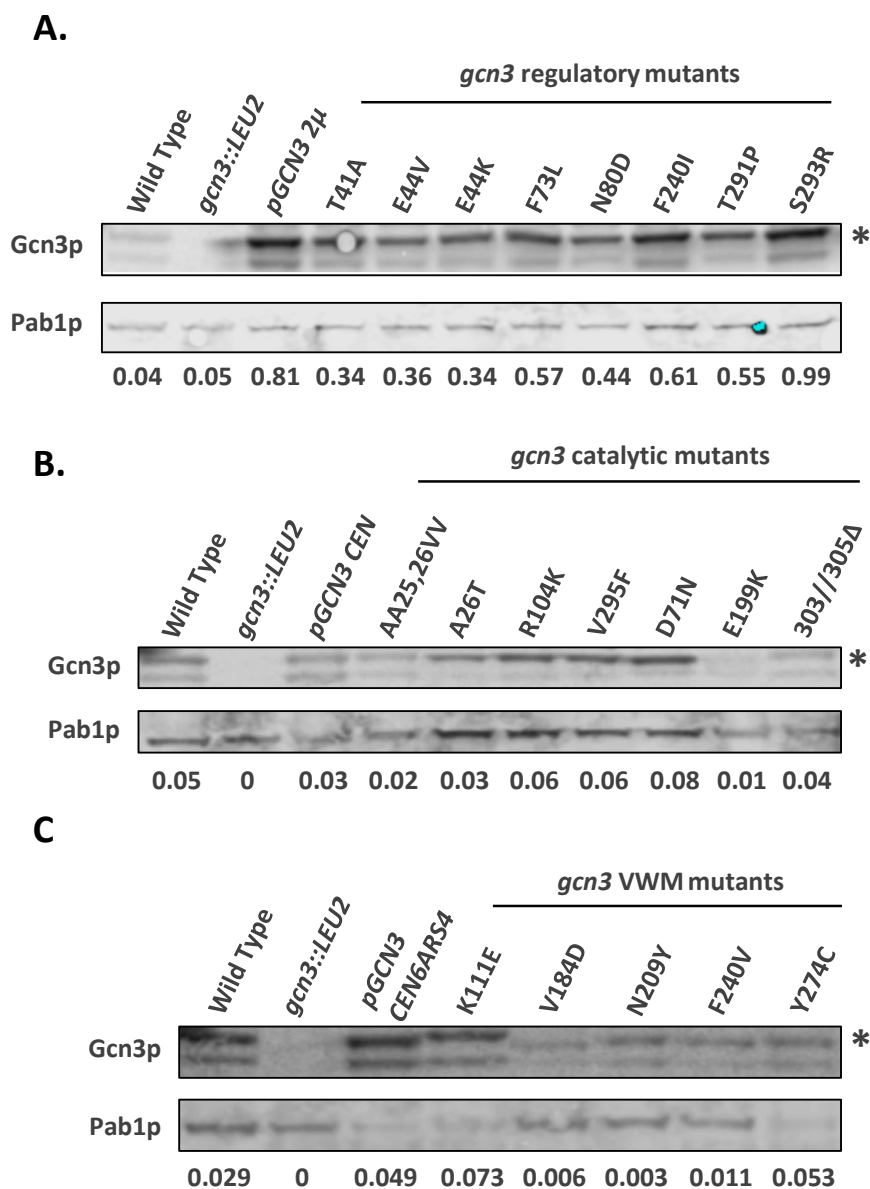
Figure 4.12 Western blotting analysis of *gcn3* Gcn⁻, Gcd⁻ and VWM mutants. Analysis of Gcn3p expression from *GCD1-yeGFP* (yMK880), *GCD1-yeGFP gcn3::LEU2* (yMK1402), as well as yMK1402 exogenously expressing *gcn3* regulatory (A), catalytic (B) and VWM (C) mutations. Cultures were grown to an OD_{600} of 1 before total protein was extracted via bead beating. Protein extract concentration was assessed via BCA assay. A total of 30µg protein extract was separated throughout a 4-20% SDS gel before being transferred onto a nitrocellulose membrane. The membrane was probed for Gcn3p and Pab1p using primary antibody concentrations of 1/1000 and 1/5000 respectively. Pab1p expression was utilised as a loading control and used to quantitatively assess Gcn3p expression by densitometry.

4.3. Discussion

eIF2B activity can be measured biochemically by using purified recombinant eIF2B, or by assessing expression levels of *GCN4* or *HIS3*. Although drawbacks to the former have already been noted, expression levels of *GCN4* or *HIS3* can only be used to infer defects in the catalytic activity of eIF2B and may be prone to downstream effectors. Thus, a more direct approach to measure GEF activity is necessary which maintains an *in vivo* environment. In keeping with this, FRAP analysis was employed which has shown promising results during the original study characterising eIF2B bodies. FRAP was previously validated as a measurement of eIF2B activity by analysing eIF2 shuttling following amino acid starvation, a stress which decreases eIF2B activity (Campbell et al., 2005). In this study, FRAP analysis was validated using similar conditions (**Fig. 4.2** and **4.3**). Whilst the original study correlated reduced eIF2 shuttling with an increase in eIF2α phosphorylation via immunoblotting, we correlated the decrease in eIF2 shuttling with the concomitant derepression of *GCN4* via LacZ assay (**Fig. 4.3**). Although these observations were expected, they reiterated conclusions from previously published FRAP analysis. In addition, these results validated the background strain to allow further functional analyses of the effects of eIF2Bα catalytic and VWM mutations on eIF2 shuttling and therefore, eIF2B activity.

4.3.1. eIF2B microbodies decrease the shuttling of eIF2

For the catalytic mutants, FRAP analyses correlated with Gcn4p expression levels in the presence of AA25,26VV and E199K Gcn3p mutations, with results indicating decreased eIF2B activity (**Fig. 4.4, 4.5** and **4.6**). Although Gcn4p levels were higher in the E199K than AA25,26VV, FRAP analyses indicated similar decreases between the two mutations. This suggested eIF2B was impaired more within E199K

than AA25,26VV. These differences can be explained by the differences in eIF2B measurement. FRAP is a direct real-time measurement of eIF2 cycling into (eIF2-GDP) and out of (eIF2-GTP) the eIF2B body. In contrast, *GCN4* accumulates throughout the cells lifespan and can be considered an endpoint assessment of eIF2B activity (see section 1.2.1.1.1). Thus, small variations of eIF2B activity may not be distinguished via FRAP but may be detectable by exacerbated Gcn4p levels. Nonetheless, measuring eIF2 dynamics is preferable considering the information that can be derived from such data which maintains an *in vivo* environment.

The 303//305Δ mutant previously displayed subpopulations of cells that either localised eIF2B to several small foci or the singular eIF2B body, therefore allowing the analysis of microbodies with the presence of eIF2B bodies serving as an internal control. The shuttling of eIF2 through 303//305Δ microbodies was decreased in comparison to 303//305Δ eIF2B bodies, which were analogous to wild-type (**Fig. 4.5** and **4.6**). These results suggest that GEF activity may be decreased when eIF2B localises to microbody foci and that the eIF2B body is necessary for the enzyme to elicit GEF activity to its fullest. Since eIF2B foci were completely absent from cells that were deleted for Gcn3p (see Chapter 3, Figure 3.2), the decameric holocomplex is likely to be complete when eIF2B localises to microbody foci. Therefore there may be additional factors required to fully form the eIF2B body. Although previous perturbation of Ifa38p-eIF2B interactions correlated microbody formation with no decreases of eIF2B GEF activity, other interactions with other proteins have been suggested (Browne et al., 2013).

During the analysis of eIF2Bα catalytic mutations, we observed an interesting correlation between foci movement and catalytic activity (**Fig. 4.11**). Previously, mean

square displacement (MSD) experiments showed that the eIF2B body moves via random diffusion throughout the cytoplasm (Taylor et al., 2010). In addition, MSD results also suggested that the body was tethered to a membrane; an observation that was reiterated by another study (Browne et al., 2013). In yeast eIF2 moves via diffusion, therefore eIF2B body movement could serve to encourage eIF2-GDP to enter the body for GTP exchange. How eIF2B moves around is currently unknown, although the regulation of eIF2B via eIF2-P did not seem to be a factor. Amino acid starvation did not seem to hinder movement, which is in-line with previous observations surrounding butanol. Although butanol leads to reduced eIF2B activity, increased Gcn4p levels and inhibits body movement, butanol's effects are independent of phosphorylated eIF2 (Taylor et al., 2010).

4.3.2. Impact of eIF2Bα VWM mutations on eIF2 shuttling

Further investigation of eIF2Bα VWM mutations resulted in observations that were distinct from the catalytic mutations. Characterisation of V184D and F240V previously showed characteristics of a regulatory mutant, yet eIF2B localisation resulted in the formation of microbodies and eIF2B bodies respectively. Rather surprisingly, eIF2 did not localise to these foci (**Fig. 4.8**). Mutational analyses in human eIF2Bα suggest these two mutations may affect eIF2B-eIF2 binding and this may possibly account for the lack of eIF2 within eIF2B bodies (Wortham and Proud, 2015).

For the most part, FRAP analyses of the VWM mutations K111E and Y274C indicated subtle fluctuations in the dynamics of eIF2 (**Fig. 4.9** and **4.10**). K111E increased eIF2 recovery time within eIF2B foci, however as more eIF2 was mobile within the foci, only a slight decrease in the rate of recovery was observed (**Fig. 4.10A, B** and **C**). This showed that eIF2B GEF activity may be enhanced as a consequence of

mutations, by allowing a higher amount of eIF2 to shuttle through the eIF2B body. Conversely, total eIF2 content did not increase within this mutant (**Fig. 4.10D**). If more eIF2 was allowed to shuttle through the eIF2B body, an increase in total eIF2 would be expected, therefore bringing these conclusions into question. The mutant Y274C displayed a similar pattern of recovery to the mutant K111E, whereby the half-time recovery showed a significant decline in tandem with increases in mobile eIF2, equating to a slight yet significant decrease in the rate of eIF2 recovery. Total eIF2 content within eIF2B bodies was significantly increased, therefore aligning with earlier ideas surrounding K111E. Whether this increase in eIF2 content was caused by the cycling of additional eIF2 or the influx of inhibitive eIF2-P is unknown. Considering slight increases in Gcn4p levels correlated with slight decreases in eIF2 shuttling, the presence of additional eIF2-P is unlikely.

4.3.3. *gcn3* regulatory, catalytic and VWM mutations may destabilise Gcn3p

Investigations into eIF2B mutations have highlighted numerous instances where missense mutations affect expression levels (Hannig et al., 1990, Richardson et al., 2004, Wortham and Proud, 2015). The very same observation was reiterated here from several Gcn3p mutants, although not all mutations decreased expression levels. For the majority of regulatory mutations, which were expressed on a high-copy plasmid, expression levels decreased in comparison to the exogenous wild-type Gcn3p (**Fig. 4.12A**). However, Gcn3p levels were still higher than the wild-type expressing endogenous *GCN3*. Since eIF2B bodies were formed within both wild-types (see section 3.2.1; **Fig. 3.2**), the change in expression level cannot solely account for the

dispersal of eIF2B but rather these missense mutations are likely to affect eIF2Bα incorporation.

Several catalytic mutants also reduced Gcn3p levels, but others remained similar to wild-type (**Fig. 4.12B**). In yeast, eIF2B tetramers (εγβδ) do not exhibit any catalytic deficiency when lacking eIF2Bα *in vitro* (Hannig et al., 1990). Lower levels of the subunit are therefore unlikely to cause the catalytic phenotype. Decreased expression of the catalytic mutants could produce two pools of eIF2B complexes with different configurations, including the tetrameric complex which exerts full catalytic activity and cannot be regulated, as well as the decameric ($\varepsilon_2\gamma_2\beta_2\delta_2\alpha_2$) complex which has decreased catalytic activity but can be regulated. Therefore, the full extent of eIF2B's decreased catalytic activity could be understated as there may be a larger pool of eIF2B complexes lacking the alpha subunit in comparison to wild-type cells. To determine the effects decreased expression levels had on the formation of decameric complexes, native cell extracts were analysed by immunoblotting (results not shown). Despite efforts to optimise the experiment by including different detergents in the lysis buffer, native immunoblots were unsuccessful as the eIF2B complexes were unable to separate through the polyacrylamide gel and seemed to aggregate in the well.

The VWM mutants V184D, N209Y and F240V, shown within this study to be regulatory mutants, decreased Gcn3p expression substantially (**Fig. 4.12C**). For these mutants, it is possible that regulation is not possible due to the lack of eIF2Bα. Therefore, eIF2B may exist as tetrameric complexes when these mutants are present. However, as some Gcn3p was still present, a Gcn3p-dose-dependent regulatory effect might be expected as opposed to a complete lack of regulation which was observed during polysome profiling (see section 3.2.4.1; **Fig 3.8**). To shed light on these

conflicting conclusions, additional experiments such as immunoprecipitation assays are required to investigate eIF2B complexes in the presence of VWM mutations.

Intriguingly, the VWM mutants K111E and V184D exhibited slight changes in the size of Gcn3p in comparison to wild-type (**Fig. 4.12C**). It is unlikely that the amino acid substitutions account for these shifts, as K111E decreases the mass of Gcn3p by 0.94 Da and V184D increases the mass by 2.06 Da. It is possible that the mutations have introduced (*i.e.* K111E) or abolished (*i.e.* V184D) post-translational modifications. The T291 residue within Gcn3p has been suggested to be phosphorylated (Albuquerque et al., 2008). Apart from the ubiquitinated K37 residue, the T291 residue currently represents the only amino acid within Gcn3p implicated for post-translational modification (Swaney et al., 2013). More investigations into these mutants are required, as these observations could have important implications for the pathogenesis of VWM.

Of the 20 mutants analysed, 12 resulted in decreased expression levels of Gcn3p. It is unlikely that the cause is due to codon biases, as such a large number of different mutations decreased Gcn3p levels. Nucleotide base changes could produce unstable mRNA transcripts (Russell et al., 1997). Similarly, amino acid substitutions could result in unstable Gcn3p (Tokuriki and Tawfik, 2009). Further experiments such as real-time qPCR or pulse-chase assays could elucidate why Gcn3p expression is low, which may shed light on why there are so few VWM mutations within eIF2Bα (Pavitt and Proud, 2009).

5. Characterisation of the interactions between eIF2B bodies and membrane proteins Mst27p, Erp4p and Sac1p

5.1. Introduction

Macromolecular structures containing aggregated protein often include additional co-factors to maintain structure as well as cytoplasmic location. For instance, the most characterised intracellular filamentous structure, F-actin, requires a host of actin-binding proteins to build a stable structure (Winder and Ayscough, 2005). Stress granules and P-bodies also require scaffold proteins to maintain structure, such as TIA-1 and GW182 respectively (Gilks et al., 2004, McDonald et al., 2011). Currently, the eIF2B body is known to comprise of eIF2B as well as the VLFA elongase enzyme Ifa38p (Browne et al., 2013). Previous studies suggest that the eIF2B body is tethered to a membrane, with Brown *et al.,* (2013) suggesting the endoplasmic reticulum (ER) (Campbell et al., 2005). Additional proteins, such as Mst27, Erp4p and Sac1p, have been shown to associate with eIF2B, but whether they are required for eIF2B body formation remains unknown.

A survey of 1590 TAP-tagged putative membrane proteins (MPs) showed that all five subunits of eIF2B co-precipitated with Mst27p, Erp4p and Sac1p (Babu et al., 2012). Proteins are known to be inherently 'sticky' and can sometimes interact non-specifically leading to false-positive protein-protein interactions (PPIs). Hence Babu *et al.,* took a multi-step approach to calculating confidence scores with an accuracy of 95.45%. The authors noted that the precision of their study was similar to high-quality data from large surveys of soluble PPIs. Although there was still a 1 in 22 chance of a false-positive PPI, several other studies have been published verifying observed interactions.

Specific roles for Mst27p and Erp4p within protein transport are yet to be described. Mst27p is predicted to contain two transmembrane domains (TMDs) with a short cytoplasmic domain (CD) at the N-terminus and a long CD at the C-terminus. Mst27p is known to form a heterodimer with its paralog Mst28p which interact with COPI and COPII coated vesicles (Sandmann et al., 2003). Erp4p is predicted to contain one TMD, a short 8 amino acid CD and a long non-cytoplasmic domain. Erp4p is a member of the p24 family which are a group of MPs responsible for regulating protein transport across the secretory system (Marzioch et al., 1999). To date, no report has linked Mst27p or Erp4p with translation initiation or translational control. Instead, these MPs are involved in vesicular mediated protein transport, potentially suggesting that the subcellular localisation of eIF2B bodies may play a role in their function. Endocytosed vesicular cargo contained within endosomes may be unpackaged in the Golgi and then transported to the ER by retrograde protein transport which utilises COPI coated vesicles. Newly folded proteins within the ER may be transported to the Golgi utilising COPII coated vesicles via retrograde protein transport. Proteins may also be secreted and are therefore transported from the Golgi apparatus to the plasma membrane. This process is reliant on steady state levels of phosphatidylinositol 4-phosphate (Ptdins(4)P) in the Golgi apparatus.

Sac1p is a phosphatidylinositol (PI) phosphate phosphatase (PI(4)P) responsible for regulating Ptdins(4)P levels within the Golgi apparatus. Ptdins(4)P is a membrane bound lipid important for actin cytoskeleton organisation, cell wall integrity and vesicular mediated protein transport (D'Angelo et al., 2008). In *S. cerevisiae*, two PI4 kinases (PI4K) exist; Stt4p and Pik1p (Audhya et al., 2000). Stt4p generates Ptdins(4)P at the plasma membrane whilst Pik1p maintains levels at the Golgi apparatus. Interestingly, temperature sensitive Stt4p/Pik1p mutants, which lead to 10-fold

Ptdins(4)P decrease, have been shown to impair translation initiation (Audhya et al., 2000, Cameroni et al., 2006). Whether Sac1p is involved in translation or whether it confers a similar translational response to abnormal PI4Ks remains to be elucidated.

Within this chapter, experiments were undertaken to provide further insights into the interactions between the MPs and eIF2B, as well as their role in translational control. We hypothesised that Mst27p, Erp4p and Sac1p may co-localise with the eIF2B body, either providing structural support or acted to tether the filamentous structure to a membrane.

5.2. Results

5.2.1. eIF2B localisation is unaffected within cells lacking Mst27p, Erp4p or Sac1p

All five eIF2B subunits previously co-precipitated with the TAP tagged putative membrane proteins (MPs); Mst27p, Erp4p or Sac1p (Babu et al., 2012). As all five subunits were identified, interactions could exist when eIF2B is in the decameric conformation. Therefore, we initially sought to determine whether the MPs were required for the formation of eIF2B bodies. Each MP was individually deleted in a strain (yMK880) containing GFP tagged *GCD1* (eIF2Bγ). *MST27* and *ERP4* were substituted with a *URA3* marker whilst *SAC1* was replaced with *LEU2*. Following confirmation of successful homologous recombination, the MP deletion strains underwent live-cell imaging via confocal microscopy to assess the impact of the deletion on eIF2B localisation.

Representative live-cell images are shown in **Figure 5.1A**. Quantitation of eIF2B localisation showed wild-type cells formed eIF2B bodies within 50 % of the cell population analysed, with rare instances of microbody formation (**Fig. 5.1B**). The MP deletion strains were similar to wild-type, although slightly higher levels of microbody formation were observed for *mst27Δ* and *erp4Δ*. However, these variations were not statistically significant. Although these results suggested that the MPs were not required for the formation of eIF2B bodies, they do not rule out a role in translation initiation or translational control.
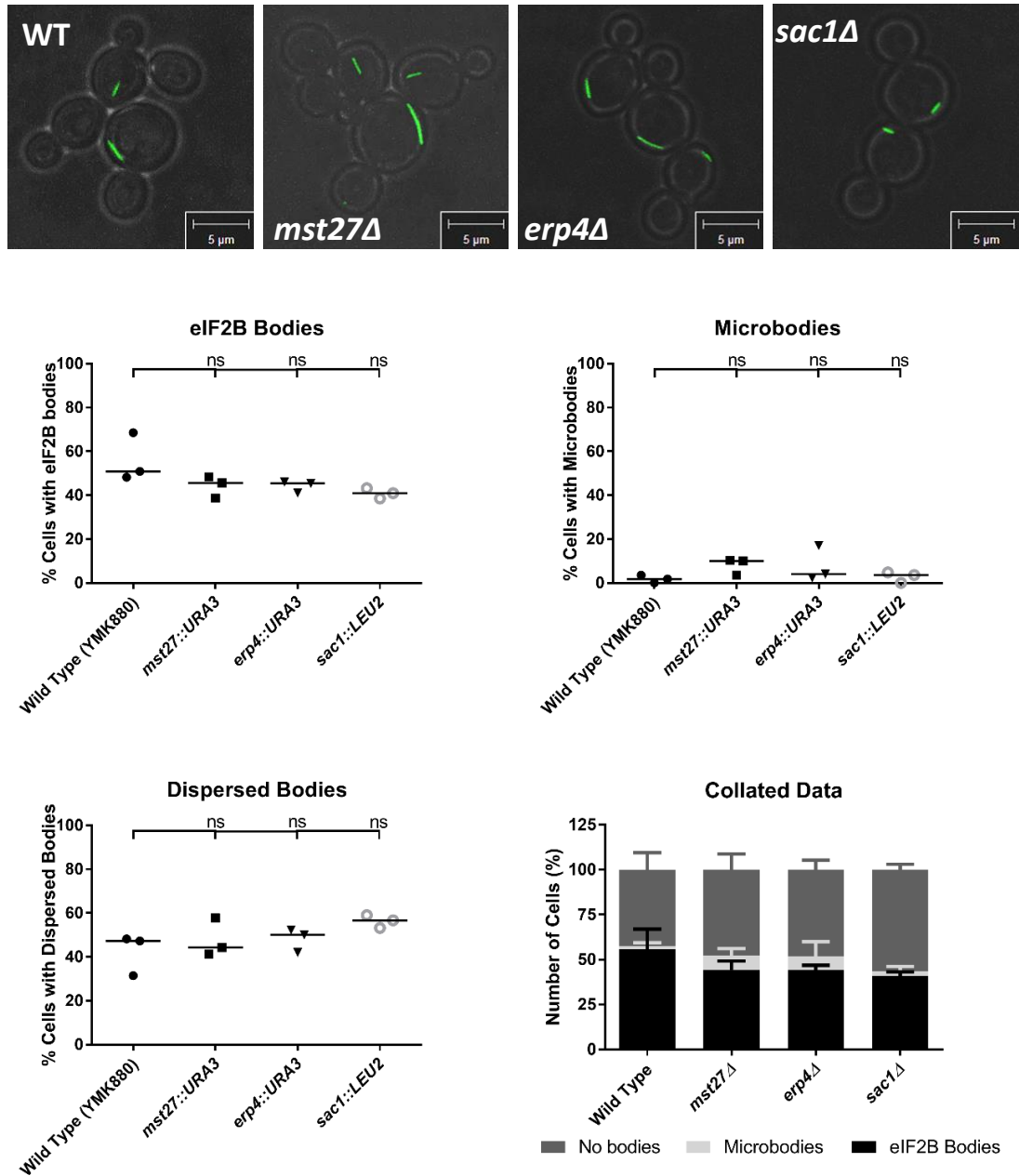
Figure 5.1 Deletion of mst27, erp4 or sac1 does not affect eIF2B localisation. *MST27, ERP4* and *SAC1* were individually deleted within a strain harbouring a genomically GFP tagged *GCD1* to visualise eIF2B localisation. (A) Representative live-cell images were taken via confocal microscopy. (B) A minimum of 100 cells were counted and assessed as to whether eIF2B was dispersed, localised to microbodies or formed eIF2B bodies. n=3, error bars are representative of SD. ns = not significant, * P=<0.05, ** P=<0.01, *** P=<0.001, **** P=<0.0001.

5.2.2. *sac1Δ* impairs translation initiation

Although there is little known about Mst27p and Erp4p, deletion of other enzymes within the phosphatidylinositol pathway that are linked to Sac1p (*i.e.* Pik1p) detrimentally affect rates of translation initiation, leading to ribosomal run-off and consequently increasing levels of 80S monosomes (Cameroni et al., 2006). Similarly, the effects of *mst27Δ* and *erp4Δ* on cellular growth are unknown, whilst *sac1Δ* has been shown to severely impair growth rates (Yoshikawa et al., 2011). To further characterise the MP deletion strains and ensure the *sac1Δ* mutant displayed similar growth patterns as previous, growth curves and polysome profiles were generated.

Growth rates were measured over 8 hours in SC media lacking appropriate amino acids at 30 ˚C (**Fig. 5.2**). *mst27Δ* and *erp4Δ* cells grew slightly faster than wild-type. In contrast, the *sac1Δ* mutant exhibited a severe growth defect, in agreement previously published data (Yoshikawa et al., 2011).

Polysome profiles were generated to determine whether deletion of the MPs affected translation initiation or translation regulation. As before (see section 3.2.3), cells were starved of amino acids for 30 minutes to elicit an eIF2B-dependent response, whereas glucose starvation for 10 minutes was included as an eIF2B-independent control. For the *mst27Δ* and *erp4Δ* mutants, similar responses to wild-type were observed for both amino acid and glucose starvation (**Fig. 5.3**). Both mutants were able to respond to amino acid starvation similar to wild-type, as indicated by increases in the 80S monosome peak, resulting in P:M ratios decreasing 2-fold. Interestingly, the *sac1Δ* strain exhibited a much higher 80S monosome peak than wild-type under normal conditions, producing a P:M ratio 2.5-fold lower than wild-type. Intriguingly *sac1Δ* cells were still able to respond to stress, but the generated

polysome profiles indicated *sac1Δ* cells may be hypersensitive to eIF2B-dependent stress, as the P:M ratio decreased by 75 %; a decrease 1.5-fold higher than similarly-stressed wild-type cells. Together, these results show Sac1p is required for efficient translation initiation and that the absence of Sac1p may exaggerate translational regulation to cellular stresses.
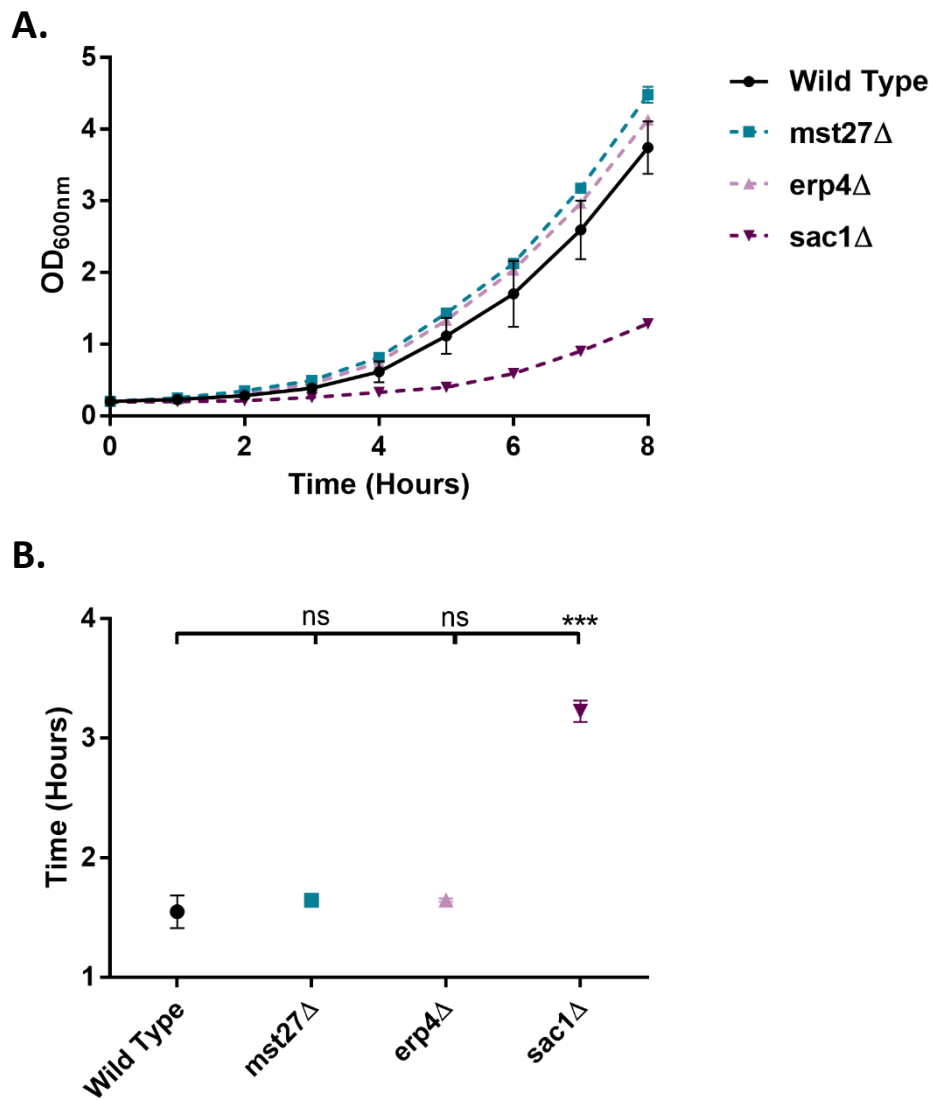
Figure 5.2 Growth curve of strains lacking Mst27p, Erp4p or Sac1p. Overnight starter cultures were backdiluted to 0.2 OD units in fresh media before being incubated at 30°C with shaking. Growth was monitored over eight hours, n=3, error bars are representative of SD.
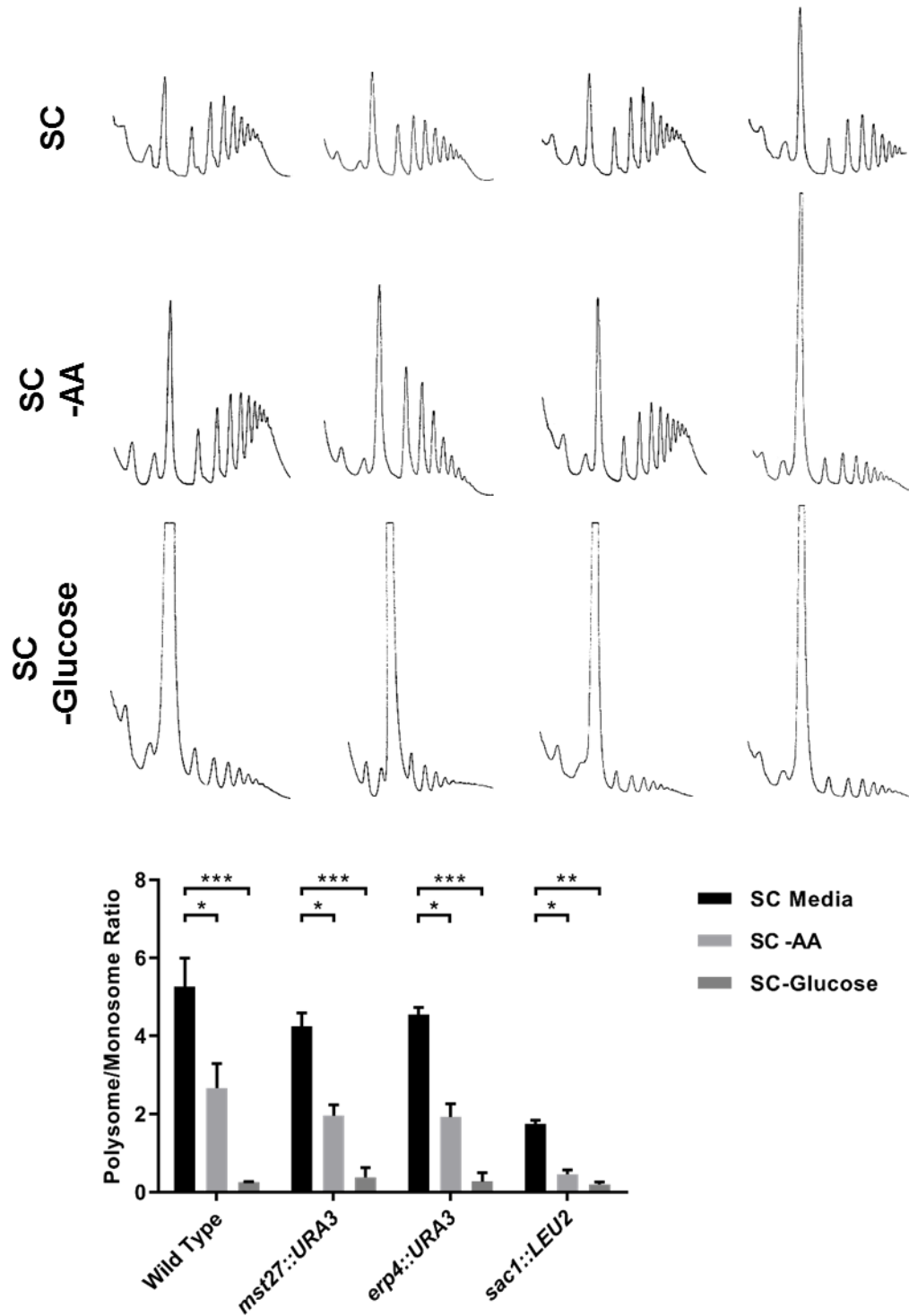
Figure 5.3 Polysome profiling of putative membrane protein deletes. Polysome profiling was used to assess whether eIF2B could respond to stress when Mst27p, Erp4p and Sac1p was absent. Amino acid starvation antagonises an eIF2B-dependent response, whilst glucose starvation antagonises an eIF2B-independent response. n=3, error bars are representative of SD, ns = not significant, * P=<0.05, ** P=<0.01, *** P=<0.001, **** P=<0.0001.

5.2.3. Analysis of co-localisation between eIF2B bodies and membrane proteins

In their study investigating interactors of putative membrane proteins, Babu *et al.,* (2012) used tandem affinity purification by virtue of endogenously TAP tagged proteins. To further investigate the observed interactions between eIF2B and the MPs, we investigated whether the MPs co-localised with the eIF2B body. To investigate co-localisation between the MPs and eIF2B, *MST27, ERP4* and *SAC1* were individually fused to *mKATE2*; a highly photostable monomeric RFP capable of withstanding high pHs indigenous to some organelles (Lee et al., 2013). Gene fusions were created by 'one-step' over-lap extension PCR (OE-PCR), which were purified by agarose gel electrophoresis before being cloned into a high-copy TOPO TA pYES2.1 vector containing a *GAL1* promoter (**Fig. 5.1**). Colony PCR was performed to find transformants that were positive for the *MP-mKATE2* insertion into the pYES2.1 vector. pYES2.1 plasmids containing *MST27/ERP4/SAC1-mKATE2* were Sanger sequenced gene-wide to ensure the gene fusion was in-frame and could therefore be exogenously expressed.

The newly generated plasmids (BSC87, 88 and 90) were transformed into their respective deletion strains. Expression was induced by incubating transformants in SC media containing 1 % (w/v) raffinose and 1 % (w/v) galactose overnight at 30 ˚C. Starter cultures were then diluted in SC media containing 2 % (w/v) galactose, before undergoing live-cell imaging via confocal microscopy (**Fig. 5.2A**).

Mst27p and Sac1p appeared to localise to the ER or the plasma membrane, while Erp4p seemed to localise to the Golgi apparatus. Quantitation of cells indicated that Erp4p lacked any co-localisation with eIF2B, whilst few instances of co-localisation

were observed for Mst27p. Data suggested that Sac1p may transiently co-localise with eIF2B, with 30 % of cells displaying Sac1p localisation within the eIF2B foci. As limited numbers of cells could be found expressing *MST27/ERP4-mKATE2,* over-expression of Mst27p/Erp4p may be detrimental to cells, leading to suppressor mutations.
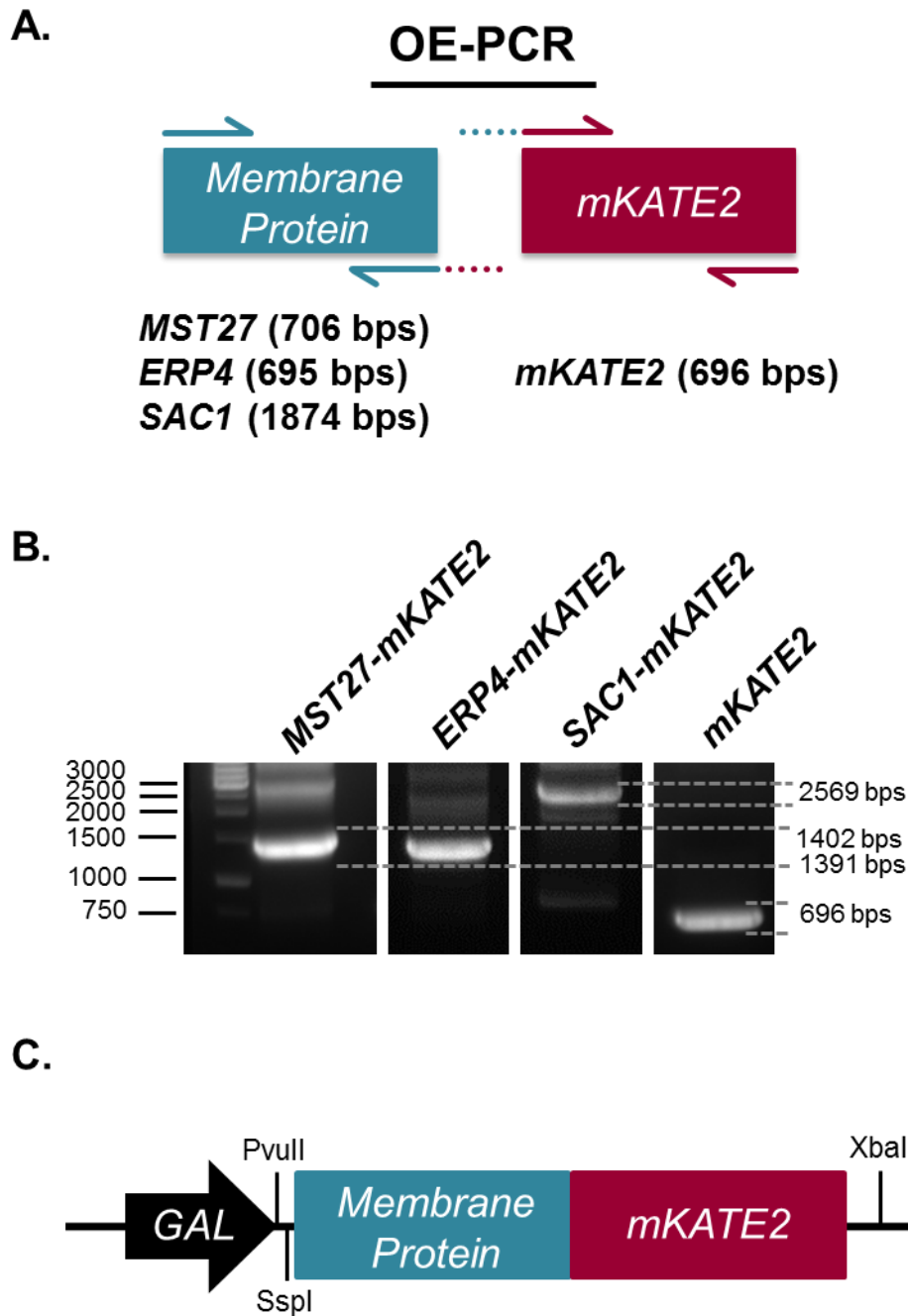
Figure 5.4 Schematic of OE-PCR and cloning to produce mKATE2 tagged membrane proteins.
(A) Diagram to show positioning of primers (half arrows), as well as the primers that contained homologous sites to the other gene (dotted lines). (B) Agarose gel showing the membrane protein genes fused to the *mKATE2* gene via OE-PCR. (C) The membrane protein genes fused to *mKATE2* were then purified from the agarose gel and cloned into a TOPO TA pYES2.1 high copy vector, which contains an inducible galactose promoter.

A.

	Brightfield	eIF2B	Membrane Protein	Merged
Mst27p				
Erp4p				
Sac1p				

B.
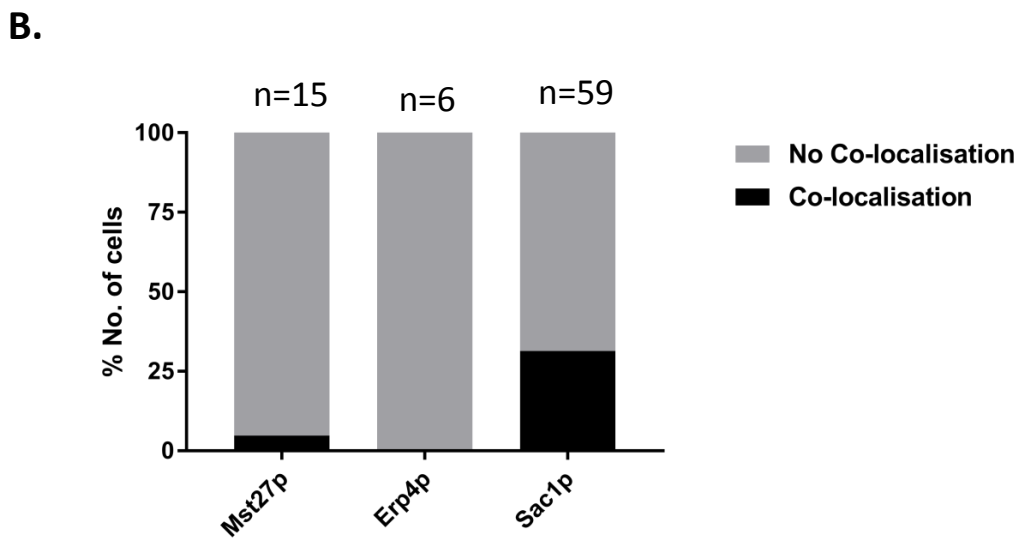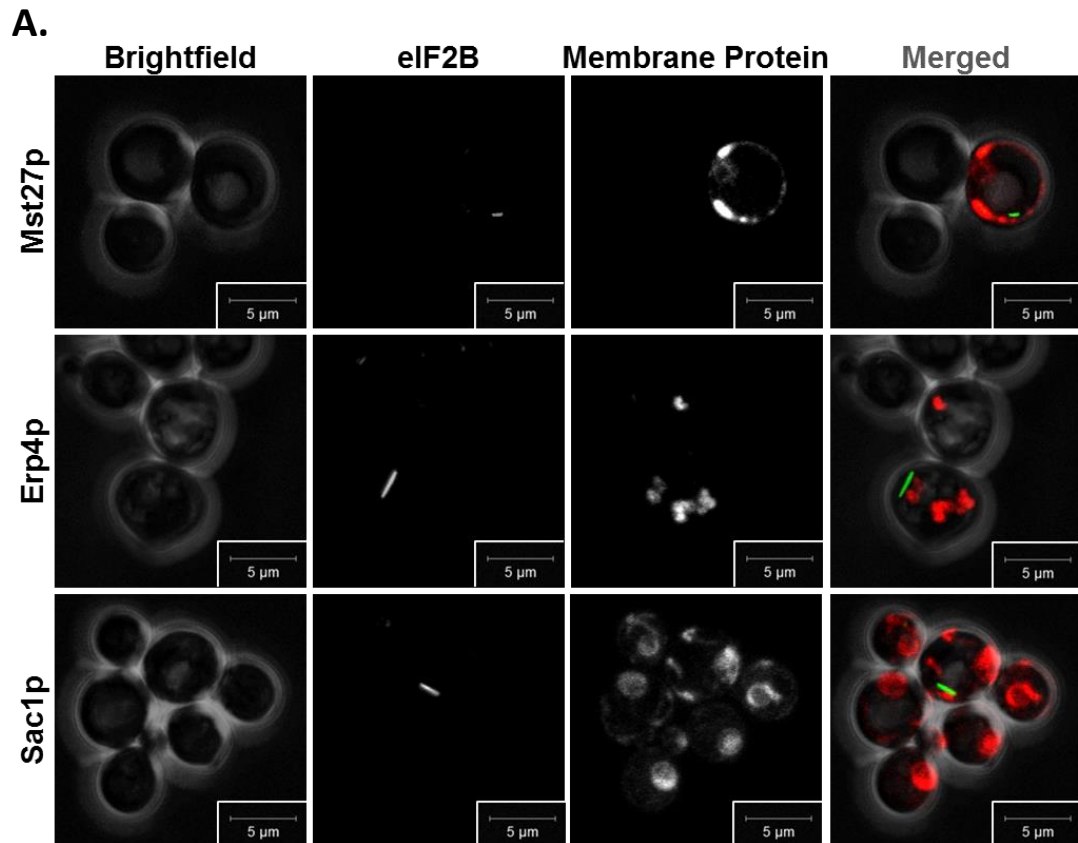
Figure 5.5 Co-localisation of putative membrane proteins and eIF2B. (A) Putative membrane proteins tagged with *mKATE2* were exogenously expressed in their respective deletion strains which already contained genomically yeGFP tagged GCD1 (see **figure 5.1**). To induce expression, starter cultures were made in SC media containing 1% raffinose and 1% galactose. Starter cultures were then backdiluted to 0.2 OD units in SC media containing 2% galactose. (B) A number of cells were imaged via confocal microscopy to see if any co-localisation with the eIF2B body occurred.

As polysome profiling showed a negative impact on translation initiation when Sac1p was absent and co-localisation studies showed transient co-localisation with eIF2B, Sac1p was the focus of further investigation.

To ensure the deletion of Sac1p caused the impaired translational effects observed earlier, a plasmid was required to complement the gene deletion. Considering different carbon sources can elicit different translational responses, the galactose induced pYES2.1 plasmid was not appropriate for this purpose (Ashe et al., 2000). Therefore, the *SAC1-mKATE2* was sub-cloned into a pSF1 low-copy *CEN6ARS4* vector containing a constitutively active *TEF1* promoter. The *SAC1-mKATE2* cassette was isolated from the pYES2.1 vector (BSC90) by *Ssp*I and *Xba*I restriction digest, before being purified by agarose gel electrophoresis. Purified *SAC1-mKATE2* was recombined into a pSF1-TEF1-CEN6ARS4 vector (**Fig. 5.6A**). Transformants were screened by colony PCR for the presence of recombinant DNA. Purified plasmids were Sanger-sequenced gene-wide to ensure an in-frame insertion.

The newly generated *TEF1-SAC1-mKATE2* plasmid (BSC128) was exogenously expressed in the *sac1Δ* strain. Localisation was reassessed to determine whether Sac1p co-localised with the eIF2B body or whether the transient co-localisation observed earlier was due to over-expression. Representative images of Sac1p-mKate2 and eIF2B-GFP are shown in **Figure 5.6**. Sac1p appeared to mainly localise to the ER or the plasma membrane. The eIF2B body occasionally co-localised with Sac1p, suggesting transient co-localisation.

To ensure growth defects as well as the impaired translational effects were caused by the lack of Sac1p, growth curves and polysome profiles were generated utilising the *TEF1-SAC1-mKATE2* plasmid. Under normal conditions, complementation

of Sac1p fused with mKate2 produced polysome profiles similar to wild-type; confirming that earlier translational defects were caused by a lack of Sac1p (**Fig. 5.7A**). Cells were also able to respond to amino acid and glucose starvation, although hypersensitivity to amino acid starvation was still apparent, as indicated by a heightened 80S monosome peak in comparison to wild-type (**Fig. 5.7B**). Whilst polysome profiles returned similar to wild-type under normal conditions, growth rates remained lower than wild-type (**Fig. 5.7B**). Together, these results suggested that the *TEF1-SAC1-mKATE2* plasmid could rescue translation initiation defects under normal conditions. However, the exogenous Sac1p-mKate2 was unable to complement the decreased growth rate or hypersensitivity to eIF2B-dependent cellular stresses, potentially due to low expression or C-terminal mKate2 fusion hindering phosphatase activity.
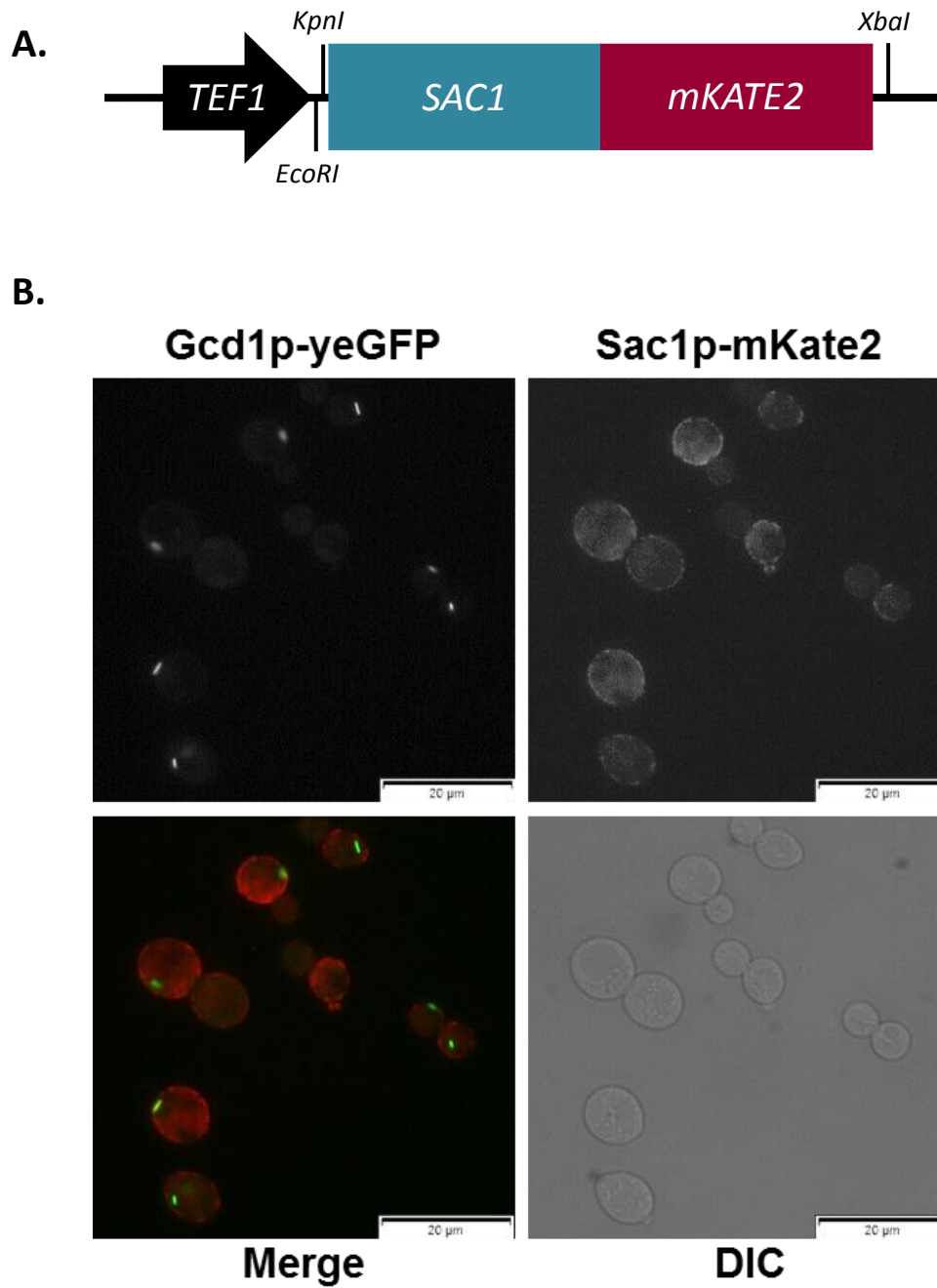
Figure 5.6 Co-localisation of Sac1p and the eIF2B body. (A) The constitutive *SAC1-mKATE2* expression cassette. (B) *SAC1-mKATE2* was exogenously expressed in the deletion strain to assess co-localisation with Gcd1p-GFP. Live-cell images were taken via fluorescence microscopy.

Figure 5.7 Complementation *of* the *Δsac1* phenotype. (A) Polysome profiling was performed to see whether the plasmid could rescue the *sac1Δ* phenotype (see **figure 5.3**). (B) Growth was monitored over eight hours to see whether the plasmid could rescue sac1Δ's growth deficit, *n*=3, error bars are representative of SD.

5.2.4. *sac1Δ* impairs translation initiation independent of eIF2B

Since co-localisation experiments only indicated transient interactions between Sac1p and eIF2B bodies, investigations focused on the impaired translation initiation conferred by the absence of Sac1p. Previously, Cameroni *et al.,* (2006) suggested that translation initiation may be liable to regulation in response to varying Ptdins(4)P levels. Results from experiments showed translation initiation was impaired when cells lacked Pik1p; an essential PI 4-kinase (PI4K) responsible for maintaining Ptdins(4)P in the Golgi apparatus. Within this study, a similar translational response was discovered in cells deficient for Sac1p; a non-essential phosphatase responsible for regulating Ptdins(4)P levels in the Golgi apparatus. Temperature sensitive Pik1p mutants have been shown to decrease Ptdins(4)P levels 10-fold, whilst *sac1Δ* cells increase levels 10-fold (Foti et al., 2001, Audhya et al., 2000). These observations suggest that an optimal concentration of Ptdins(4)P may be required for cellular homeostasis. Temperature sensitive Pik1p mutants have already been shown to affect translation initiation independent of eIF2B. However, whether a similar mechanism is instigated in the absence of Sac1p remains unknown.

To determine whether translation is regulated independent of eIF2B in the absence of Sac1p, additional strains were generated to investigate translational control without *gcn3* (eIF2Bα). As mentioned earlier (see section 3.2.3), eIF2Bα contains the binding site for eIF2α-P, thus cells lacking eIF2Bα will be unresponsive to eIF2B-dependent stresses. The *Mat a*, *sac1::LEU2 GCD1-GFP* (ySC18) strain was crossed with *Mat α, gcn3::HIS3 GCN4-LacZ-TRP1* (ySC86). Diploid cells were selected and sporulated, before tetrads were dissected and isolated on solid rich media. To determine genotypes, tetrads were replicated onto solid SC media individually lacking

leucine, histidine or tryptophan. Four new strains were created: *GCN4-LacZ-TRP1* (ySC99), *gcn3::HIS3 GCN4-LacZ-TRP1* (ySC100), *sac1::LEU2 GCN4-LacZ-TRP1* (ySC97) and *sac1::LEU2 gcn3::HIS3 GCN4-LacZ-TRP1* (ySC98).

To investigate whether the absence of Sac1p resulted in the downregulation of translation initiation via eIF2B-dependent regulation, growth curves and polysome profiles were generated using *sac1Δ gcn3Δ* (ySC98) cells to test whether deleting eIF2Bα would complement the absence of Sac1p. In comparison to wild-type under normal conditions, *sac1Δ gcn3Δ* cells exhibited reduced rates of translation initiation, as shown by a larger 80S monosome peak (**Fig. 5.8A**). As this observation was reminiscent of *sac1Δ* cells, additional deletion of *gcn3* did not impact upon this phenotype. Expectedly, *sac1Δ gcn3Δ* cells could not respond to amino acid starvation (see section 3.2.3), with an 80S monosome peak similar to normal conditions. A growth curve for the *sac1Δ gcn3Δ* mutant is shown in **Figure 5.8B**, wild-type data from **Figure 5.7B** is included for comparison. In line with generated polysome profiles, *sac1Δ gcn3Δ* cells exhibited slower growth. Together, these results suggest translation initiation is regulated independent of eIF2B when Sac1p is absent. Moreover, these results suggest that the translational regulation observed in *sac1Δ* cells is the same translational control mechanism previously observed in the Pik1p temperature sensitive mutant (Cameroni et al., 2006).

A.
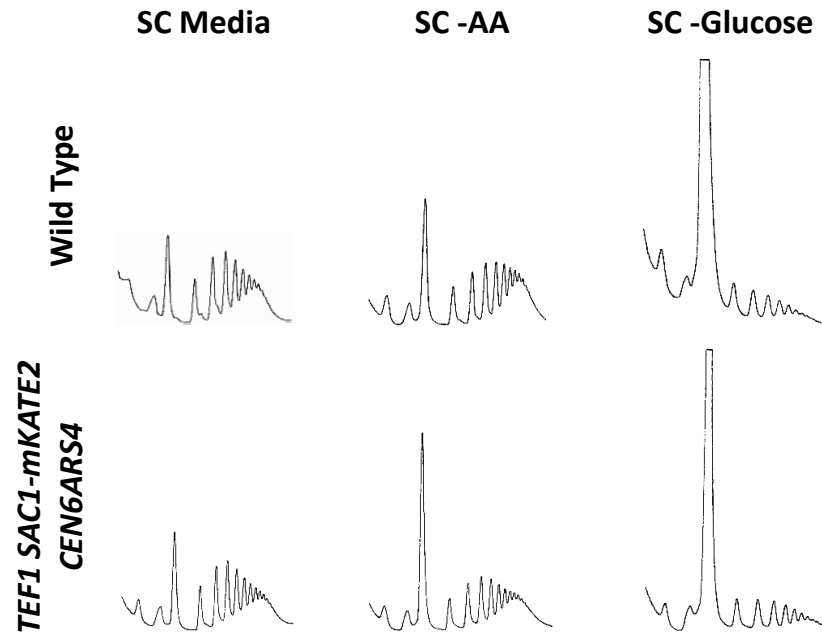
B.
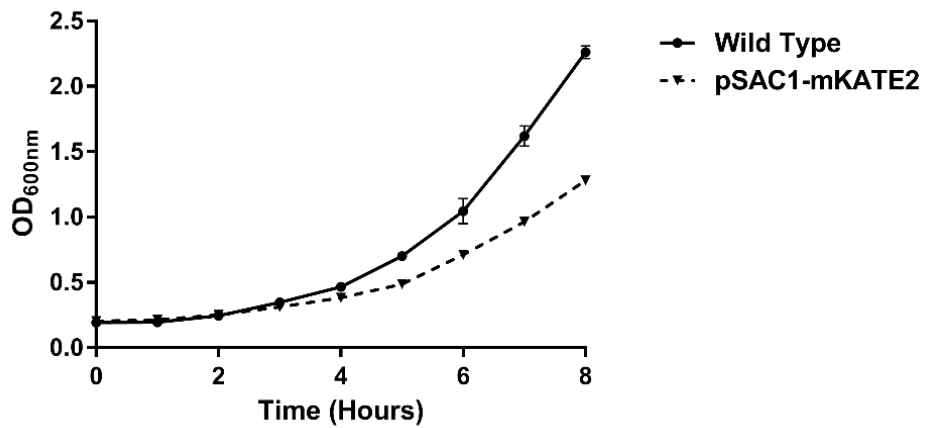
Figure 5.8 Complementation of *SAC1*. A *sac1::LEU2, gcn3::HIS3* strain was produced to see whether the *sac1* null phenotype could be rescued by deleting *gcn3*. (A) Polysome profiling. (B) Growth was monitored over eight hours to see whether deleting *gcn3* could rescue *sac1Δ*'s growth deficit. n=3, error bars are representative of SD. ns = not significant, * P=<0.05, ** P=<0.01, *** P=<0.001, **** P=<0.0001.

As mentioned in section 4.2.2; the transcription factor *GCN4* is derepressed when eIF2B activity is downregulated, conferred by the binding of phosphorylated eIF2 or a catalytic mutation in eIF2B. Generated polysome profiles of a *sac1Δ gcn3Δ* double-deletion under normal conditions remained similar to *sac1Δ* cells. Correspondingly, we hypothesised that Gcn4p levels in *sac1Δ* cells would remain comparable to wild-type cells. We also hypothesised that the *sac1Δ gcn3Δ* double-deletion would remain similar to *gcn3Δ* cells. To investigate this hypothesis, *GCN4-LacZ-TRP1* (ySC99), *gcn3::HIS3 GCN4-LacZ-TRP1* (ySC100), *sac1::LEU2 GCN4-LacZ-TRP1* (ySC97) and *sac1::LEU2 gcn3::HIS3 GCN4-LacZ-TRP1* (ySC98) cells were depleted of amino acids for 30 and 60 minutes at 30 ˚C to instigate the derepression of *GCN4*, before protein extracts were analysed via LacZ assay (**Fig. 5.8A**). Expectedly, wild-type cells increased Gcn4p levels 2-fold following amino acid starvation for 30 minutes. Gcn4p levels additionally increased following amino acid starvation for 60 minutes. As expected, *gcn3Δ* cells exhibited lower Gcn4p levels under normal conditions and were unable to respond to amino acid stress. Although *gcn3Δ* cells slightly increased Gcn4p levels following amino acid depletion for 60 minutes, the increase remained insignificant. In-line with our hypothesis, *sac1Δ* cells in the absence of stress did not increase levels of Gcn4p. Unexpectedly however, levels of Gcn4p seemed to be reduced similar to cells lacking Gcn3p, suggesting Gcn4p was actively repressed in the absence of Sac1p. *sac1Δ* cells were also unresponsive to amino acid depletion for 30 minutes, as no significant changes were observed. Gcn4p levels increased following 60 minute amino acid starvation, although the response still seemed weak in comparison to wild-type. Considering cells individually deleted for *sac1Δ* and *gcn3Δ* decreased Gcn4p levels under normal conditions, results indicating increased Gcn4p expression in the *sac1Δ gcn3Δ* double-deletion were intriguing. Interestingly, *sac1Δ gcn3Δ* increased Gcn4p

levels slightly higher than wild-type under normal conditions. Although, as expected; *sac1Δ gcn3Δ* cells were unresponsive to amino acid starvation. The double-deletion was subsequently spotted onto solid SC media containing 10 mM 3-AT and incubated at 30 ˚C for 48 hours (**Fig. 5.8B**). Slight growth was observed, reiterating the slight increase in Gcn4p levels.

These data further reiterate that translation is regulated by a mechanism that is independent of eIF2B within *sac1Δ* cells as Gcn4p was not expressed. Moreover, the expression of Gcn4p seemed to be actively repressed by a mechanism that is dependent upon eIF2B as Gcn4p levels increased in the *sac1Δ gcn3Δ* mutant. Interestingly, this suggests that these regulatory mechanisms of global translation may intersect with each other, reducing the levels of Gcn4p under specific conditions.

A.
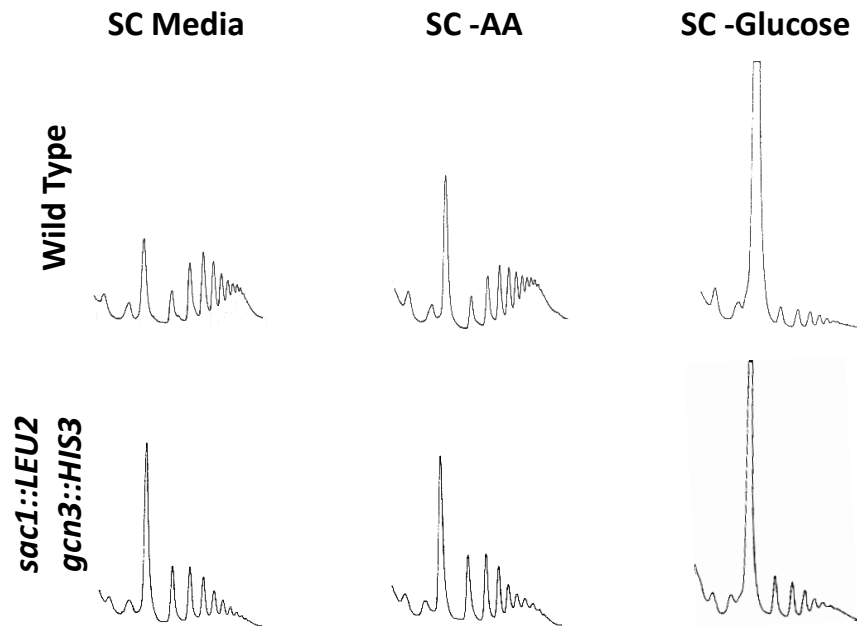
B.
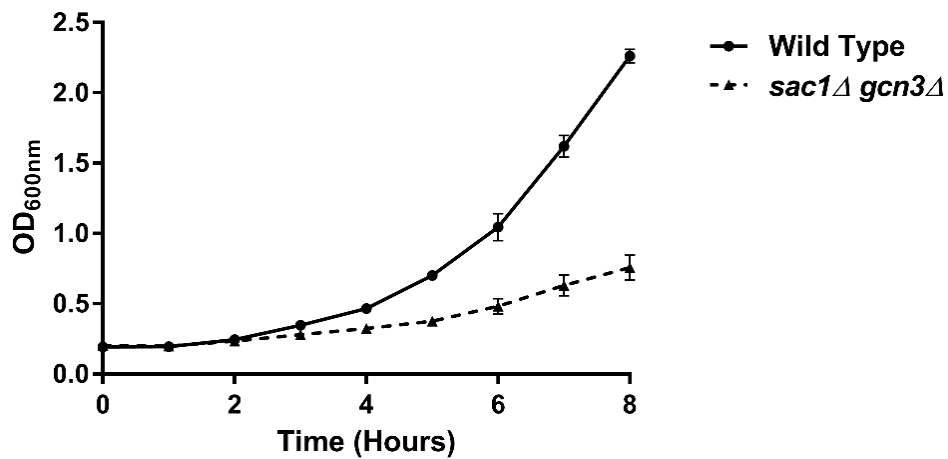
Figure 5.9 Gcn4p expression is repressed when sac1 is deleted, which is dependent on Gcn3p. (A) To assess whether the loss of *sac1* derepresses the expression of *GCN4*, as well as *GCN3*'s influences in this, a *sac1::LEU2* strain harbouring a genomically LacZ tagged *GCN4*, with and without *GCN3*, were used to perform a LacZ assay. Starter cultures were backdiluted to 0.2 OD and allowed to reach exponential growth before the cultures were divided and starved of amino acids for either 30 or 60 minutes. n=3, error bars are representative of SD. ns = not significant, * P=<0.05, ** P=<0.01, *** P=<0.001, **** P=<0.0001. (B) Starter cultures were backdiluted to 0.3 OD units before being serially diluted 4 times and spotted on to SCD agar plates as well as SCD agar containing 30 mM 3AT. Spot plates were incubated at 30°C for 48 hours.

5.3. Discussion

5.3.1. Mst27p and Erp4p are not involved in translation initiation.

Although associations between eIF2B and the putative membrane proteins Mst27p, Erp4p and Sac1p were previously observed by pull-down methods, individual gene deletions suggested that they are not required for the formation of eIF2B bodies (**Fig. 5.1**). Cellular growth was also found to be normal in *mst27Δ* and *erp4Δ* cells, as was translation initiation and translational control (**Fig. 5.2** and **5.3**). Although very little is known about Mst27p and Erp4p, with phenotypical characteristics mostly suggested from large-scale surveys, Mst27p is known to heterodimerise with its paralog Mst28p (Sandmann et al., 2003). Taking into account the similarities between Mst27p and Mst28p, it is possible that Mst28p homodimerises in the absence of Mst27p, thereby functionally complementing the loss of Mst27p. This hypothesis could be tested by a double deletion of Mst27p and Mst28p.

Previous work by Browne *et al.,* suggested the eIF2B body may be tethered to the endoplasmic reticulum (ER). Under normal conditions, Mst27p and Erp4p localises to the ER and the Golgi apparatus respectively. Sac1p mainly localises to the Golgi apparatus, but can also localise to the plasma membrane and ER. The ER localisation of Sac1p has been shown to occur under carbon limiting conditions; however the function behind this translocation remains unknown (Faulhammer et al., 2005). Co-localisation studies showed that Mst27p and Erp4p do not co-localise with the eIF2B body (**Fig. 5.5**), and that Sac1p displays only transient co-localisation (**Fig. 5.6**). Co-localisation studies are typically performed using fluorescently tagged

endogenous proteins, whilst exogenously expressed proteins lacking canonical promoters was utilised within this study. It should be noted that Discosoma RFP (dsRFP) was genomically incorporated with *SAC1*, but no fluorescent signal was observed, leading to the generation of plasmids instead. Whilst these experiments should be repeated, preliminary results suggest that Mst27p, Erp4p and Sac1p do not co-localise with the eIF2B body.

5.3.2. Sac1 may be involved in the control of translation initiation

There are two pools of Ptdins(4)P within yeast cells, present at the plasma membrane and the Golgi apparatus (D'Angelo et al., 2008). Ptdins(4)P is required for anterograde protein transport between the ER and the Golgi apparatus, as well as retrograde transport and the secretion of vesicular cargo at the plasma membrane (D'Angelo et al., 2008). The PI(4)K Stt4p is responsible for the production of Ptdins(4)P at the plasma membrane (Audhya and Emr, 2002), whilst Pik1p maintains a concentration gradient of Ptdins(4)P across the Golgi apparatus (Strahl et al., 2005). Temperature sensitive variants of either PI4K were shown to dramatically reduce Ptdins(4)P levels at their respective locations (Strahl et al., 2005, Audhya and Emr, 2002). In a later study, temperature sensitive PI(4)K mutants were found to impair translation initiation leading to the suggestion that translation may be regulated in response to Ptdins(4)P fluctuations (Cameroni et al., 2006). The PI phosphatase Sac1p is responsible for the regulation of Ptdins(4)P levels at the Golgi apparatus (Roy and Levine, 2004). Analysis of cells lacking Sac1p resulted in similar polysome profiles to the temperature sensitive PI4K mutants, presenting with larger 80S monosome peaks than wild-type under normal conditions (**Fig. 5.3**). This novel

result suggests high levels of Ptdins(4)P potentiates a translational response. Therefore, an optimal concentration of Ptdins(4)P must be present at the Golgi apparatus for cellular homeostasis.

To ensure the translational response was caused by the absence of Sac1p, *sac1Δ* cells were complemented by exogenously expressed Sac1p-mKate2 via a constitutively active *TEF1* promoter. The low-copy *CEN6ARS4* plasmid was utilised to prevent over expression that may be conferred by a constantly active promoter. The exogenous Sac1p was able to recover the translational defect under normal conditions, but was unable to recover the growth defect as well as hypersensitivity to amino acid stress. This could be due to low expression levels of Sac1p because of the low-copy vector. Additionally, the integration of mKate2 to the C-terminus of Sac1p could be hindering phosphatase activity. Although these experiments should be repeated whereby Sac1p is expressed through its canonical promoter which responds to Ptdins(4)P levels, the exogenous expression of *SAC1-mKATE2* did restore translation initiation under normal conditions (**Fig. 5.7**) (Knodler et al., 2008). This supports the hypothesis that the translational defect was indeed caused by the lack of Sac1p.

5.3.3. Ptdins(4)P translational response is controlled independent of eIF2B.

A translational control mechanism in response to Ptdins(4)P fluctuations was originally identified by a study investigating the specific target of wortmannin. Wortmannin is a natural molecule produced by the fungus *Penicillium funiculosum* and was found to primarily target Stt4p in *S. cerevisiae* (Cameroni et al., 2006).

Interestingly, temperature sensitive Pik1p mutants exhibited a resistant phenotype to wortmannin. By mutating the residue in eIF2α (S51A) that is phosphorylated in response to cellular stress, the group showed translation was downregulated independent of eIF2B. Similar results were observed here with *sac1Δ* cells lacking Gcn3p (**Fig. 5.8**). Under normal conditions, polysome profiles did not change when Gcn3p was absent; confirming the *sac1Δ* translational response was independent of eIF2B. This result also indicated that the absence of the PI4 phosphatase is likely to result in the same translational response when an abnormal PI4 kinase is present.

In addition to eIF2B, global protein synthesis is subject to regulation by eIF4E-binding proteins (4E-BPs), which competitively bind eIF4E preventing the assembly of the eIF4F complex, subsequently attenuating translation initiation. Two 4E-BPs exist in yeast: Eap1p and Caf20p. During a genetic screen of knock-out mutants; *sac1Δ* cells were shown to be hypersensitive to wortmannin, whilst cells lacking Eap1p were resistant (Zewail et al., 2003). Corresponding with results presented here, Eap1p may be responsible for translational control in response to varying Ptdins(4)P levels. 4E-BPs do not result in the derepression of *GCN4.* As the translational response in *sac1Δ* cells was shown to be independent of eIF2B, it was hypothesised that Gcn4p levels would remain unchanged. Interestingly, quantitative analyses of Gcn4p expression showed levels decreased, indicating *GCN4* repression (**Fig. 5.9A**). This provides further evidence for a role for Eap1p in the translational regulation of Sac1p, as the 4E-BP can attenuate Gcn4p expression when the target of rapamycin (TOR) is inactivated following a cellular stress (Matsuo et al., 2005). How Eap1p attenuates Gcn4p expression is unknown. Unexpectedly, Gcn4p levels increased when Gcn3p was absent from *sac1Δ* cells, suggesting eIF2Bα is required

for Eap1p-dependent *GCN4* repression. As there is no evidence directly showing Eap1p attenuates translation in response to varying Ptdins(4)P levels, more investigations are warranted. Nonetheless, results presented here suggest a novel mechanism independent of eIF2B. Gcn4p expression was also repressed, insinuating cross-talk between the two mechanisms of global translational control.

6. General Discussion

6.1. General Discussion

eIF2B is a complex GEF essential for initiating and controlling protein synthesis that localises to discrete cytoplasmic foci (Campbell et al., 2005). The macromoleular filamentous eIF2B body aggregate comprises all five subunits. In addition other proteins such as the VLFA enzyme Ifa38p has been reported to associate with eIF2B (Browne et al., 2013). Published data has highlighted that these discrete cytoplasmic foci are sites of GEF exchange for eIF2B's substrate eIF2, as well as sites of regulation where eIF2α-P binds to attenuate eIF2B activity (Campbell et al., 2005). Although a number of characteristics and features have already been described surrounding eIF2B bodies, how the eIF2B complex forms these large aggregates is unknown. Therefore, the main aim within this study was to investigate how eIF2B bodies are formed.

6.2. eIF2Bα localises eIF2B in a controlled two-step process

The eIF2B body contains all five subunits of eIF2B; it was therefore predicted that the formation of decameric complexes would precede localisation. In this study demonstrated eIF2Bα to be essential for the formation of eIF2B bodies; as eIF2B was dispersed throughout the cytoplasm when eIF2Bα was absent. Recent mass spectrometry analyses and crystallography have highlighted that the regulatory subunit eIF2Bα is integral to forming the eIF2B decamer; where eIF2Bα$_2$ homodimers stabilise two eIF2Bεγβδ tetrameric subcomplexes (Wortham et al., 2014). It is therefore reasonable to hypothesise that localised eIF2B represents decameric eIF2B complexes, whereas dispersed eIF2B represents tetrameric complexes.

Analysis of eIF2Bα mutations indicated that localisation was important for the regulation and catalytic activity of eIF2B. Similar to the deletion strain, regulatory mutants dispersed eIF2B throughout the cytoplasm whereas catalytic mutants formed microbodies. Sub-populations of cells were observed within wild-type cultures that displayed dispersed eIF2B, formed microbodies or formed eIF2B bodies. Subsequently, it is hypothesised that eIF2B bodies may be formed in two steps: firstly, tetrameric eIF2B is dispersed throughout the cytoplasm before eIF2Bα$_2$ stabilises eIF2B decameric complexes which congregate to form several smaller foci, secondly, eIF2B microbodies further aggregate together to form the singular filamentous eIF2B body. In support of this model, FRAP analysis of eIF2 cycling through eIF2B microbodies showed decreased rates of shuttling in comparison to eIF2B bodies, thus eIF2B may only be able to elicit full GEF activity when fully localised. This two-step accumulation has also been shown for the formation of aggregation of other translational components. Stress granules firstly form a core of untranslated mRNAs congregate before forming a shell, which aggregates further to produce a fully mature biphasic stress granule (Wheeler et al., 2016).

Intriguingly, analysis of eIF2B localisation within populations of cells from all wild-type variants, catalytic mutants, some VWM mutants and the MP deletion strains indicated that eIF2B may localise in a controlled manner. Irrespective of microbody or eIF2B body formation, the number of cells localising eIF2B was mostly consistent throughout. Moreover, the number of cells displaying dispersed eIF2B was consistent across all wild types, catalytic mutants and MP deletion strains. As cultures were analysed under exponential growth, it is plausible that the cell cycle could be a driving factor that dictates eIF2B localisation. In support of this and in-line

with published data (Campbell et al., 2005), eIF2B body formation was mainly limited to the mother cell. However, unique to the catalytic mutants A26T, D71N and V295F (**Fig. 3.13A**), as well as the VWM mutant V184D (**Fig. 3.17B**), were observations of microbodies within daughter cells. Whilst these mutants seemed to lack control of eIF2B localisation, others seemed unable to induce localisation. For instance, K111E/Y274C resulted in decreases in the number of foci, possibly suggesting an inability to induce localisation. Further investigation is warranted, as the elucidation of influencing factors that drive eIF2B localisation may provide novel insights into the role of eIF2B bodies.

6.3. The role of the eIF2B body in the control of translation initiation

Based on data from this study, it appears that two pools of eIF2B exist within the cell: the unregulatable tetrameric complexes that are dispersed; and regulatable decameric complexes localised to microbodies or eIF2B bodies. Hence a relationship seems to exist between localisation and regulation. However, eIF2B body formation has been shown to occur irregardless of eIF2α-P interaction (Campbell et al., 2005)**.** One possible reason for localising regulatable eIF2B may be to prime the cell for stress, which may be able to attenuate the catalytic activity of eIF2B more promptly. As mentioned earlier, deletion of eIF2Bα and the eIF2Bα regulatory mutations all displayed dispersed eIF2B localisation, suggesting that these regulatory mutant eIF2Bα subunits may be absent from the eIF2B holocomplex. In contrast however, there are some inconsistencies between particular eIF2Bα regulatory mutants and their resistance to butanol (*i.e.* T41K; see section 3.2.2), which attenuates eIF2B independent of eIF2α-P (Taylor et al., 2010). If eIF2Bα regulatory mutants cannot

interact with eIF2B tetramers, how do these specific mutants affect eIF2B activity in the presence of butanol? It is plausible butanol resistant eIF2Bα regulatory mutations could form the decameric complex without localising to eIF2B bodies. Correspondingly, there may also be a connection between localisation and eIF2B sequestration that is independent of eIF2α-P. Further experiments could shed light on these ideas, such as the immunoprecipitation of eIF2Bγ subunit to test whether eIF2Bα is associated with the eIF2B complex.

An association was also observed between localisation and catalytic function, whereby eIF2Bα catalytic mutations lead to the formation of microbodies, thereby reducing rates of eIF2 cycling. Additional co-factors may be required for the transition between the intermediary microbody and the fully localised eIF2B body, possibly enhancing GEF activity. In support of this, eIF2Bα catalytic mutations produce conformational changes that detrimentally affect the catalytic subunits, which are known to interact with Ifa38p (Browne et al., 2013). The absence of Ifa38p leads to two effects that were also common to eIF2Bα catalytic mutants; the formation of microbodies as well as reduced polysome:monosome ratios, indicative of decreased GEF exchange. Despite this, it was concluded that the catalytic activity of eIF2B remained unaffected based on *GCN4-LacZ* assays. It should be noted, however, that the authors did not investigate the rate of eIF2 cycling through microbody foci, which we found to be slower in comparison to eIF2B bodies (discussed further in section 4.3.1). The MPs Mst27p, Erp4p and Sac1p were previously shown to associate with eIF2B. However, within this research a specific interaction and role in eIF2B body formation could not be established (Babu et al., 2012). Further investigations studying the differences between eIF2B microbodies

and eIF2B bodies could uncover additional eIF2B co-factors required to fully localise eIF2B.

Although there seems to be relationships between localisation and the catalytic activity and regulation of eIF2B, the specific mechanism(s) that explains these associations remains unknown. One hypothesis is cooperative binding, which is a common feature of multimeric proteins and has been shown to occur within the ADP-glucose-pyrophosphorylase, a distant relative of eIF2B that shares homology with the ε and γ subunits (Gomez and Pavitt, 2000). In the decameric form, eIF2B has the capacity to bind two eIF2-GDP substrates or two eIF2α-P inhibitors. It is plausible that eIF2-GDP or eIF2α-P interaction within one binding domain could influence the other, potentially increasing affinity for either substrate or inhibitor. In-line with this idea, the catalytic activity of human eIF2B is reduced by 50% in the absence of eIF2Bα, which destabilises the decamer into two tetramers (Wortham et al., 2014)(Williams et al., 2001). Furthermore, several small molecules have been shown to allosterically regulate eIF2B activity, including NADPH and AMP-PNP (Bogorad et al., 2017). Cooperative binding has even been shown to occur within protein aggregates. Thus when eIF2B is localised, positive or negative cooperativity could influence nearby eIF2B complexes (Curtain et al., 2001). Although cooperativity is yet to be shown within eIF2B, this is currently the best theory to unite eIF2B catalytic and regulatory activities with eIF2B body formation.

6.4. The impact of eIF2Bα VWM mutants on eIF2B localisation

Inherited autosomal mutations within eIF2B cause the fatal disease VWM. The localisation of eIF2B with eIF2Bα VWM missense mutations was inconsistent

with correlations made from eIF2B catalytic and regulatory mutants. For instance, V184D localised eIF2B to microbodies, yet catalytic activity was not measurable as eIF2 did not co-localise to these foci. The VWM mutations could be hindering eIF2Bα homodimerisation, as the majority of affected residues reside within the α-α interface. Recent crystallography data from human eIF2B also suggests that the eIF2Bα$_2$ dimer must form prior to the stabilisation of two eIF2B tetramers, therefore perturbation of eIF2Bα dimerisation could lead to other unknown effects and subsequently, variable phenotypes (Zyryanova et al., 2018, Tsai et al., 2018).

The VWM mutations K111E and Y274C exhibited decreased eIF2 shuttling and eIF2B body formation. Interestingly, the Y274C eIF2B bodies contained higher amounts of total eIF2 within the foci. Although it is unknown whether-or-not the additional eIF2 was phosphorylated, it would explain why the catalytic activity of eIF2B was decreased. Whilst the underlying mechanism explaining this phenomenon is unknown, it could be explained by cooperative binding as described earlier. Upon amino acid starvation, Y274C exhibited hypersensitivity to the stress, hinting additional eIF2α-P may be able to enter the foci. Future experiments into these hypotheses could help explain why VWM sufferers suddenly deteriorate following intercurrent trauma that antagonises an eIF2B stress response (Pavitt and Proud, 2009).

The VWM mutants N209Y and F240V largely lead to the dispersal of eIF2B throughout the cytoplasm, correlating with a regulatory phenotype. Intriguingly, the N209Y mutation in human eIF2Bα does not affect eIF2α-P binding or eIF2Bα incorporation (Wortham and Proud, 2015). Regulation of eIF2B is not only important

to neutralise cellular stresses but is also vital for the development of cells, particularly in the brain (Marom et al., 2011). These observations within yeast are therefore likely to be reminiscent of severe VWM mutations which may be incompatible with life. The VWM mutation G204Δ (G205 in *S. cerevisiae*) abolishes eIF2Bα incorporation and affects eIF2Bα-eIF2-P interaction, possibly simulating the regulatory phenotype (Wortham and Proud, 2015). However, G204Δ may be incompatible with life, as it is yet to be found in the homozygous state and is usually heterozygous with another mutation (*i.e.* Y274C). These severe phenotypes may be ameliorated by compound heterozygosity, a layer of complexity which has not been investigated within yeast thus far. Integration vectors could be used to generate VWM mutations in haploid yeast cells which could be crossed to produce compound heterozygous diploid cells. FRAP analysis on these strains could provide novel and fascinating observations which may help elucidate underlying mechanisms of VWM disease.

6.5. eIF2 shuttling as a measure of *in vivo* GEF activity

The eIF2B body represents 40 % of a cell's total eIF2B, with the remainder of eIF2B dispersed throughout the cytoplasm (Campbell et al., 2005). Data presented within this study suggests that there are two pools of eIF2B subcomplexes present within cells. However, *in vitro* biochemical assays assume that eIF2B subunits are present in equimolar ratios and therefore do not account for this extra layer of *in vivo* complexity (Jennings and Pavitt, 2010, Wortham et al., 2014). To assess the GEF activity of eIF2B foci, FRAP analysis was employed to measure the efficiency of eIF2 cycling. Biochemical assays measuring *GCN4/HIS3* expression, as well as FRAP

analysis indirectly measure GEF activity whilst maintaining an *in vivo* environment, but under the proposed model of localisation, the latter analyses both complexes whilst the former scrutinises decameric complexes exclusively. *In vivo* analysis of GEF activity may therefore require careful consideration depending on the eIF2B subunit under investigation. Nonetheless, based on these conclusions, both experiments should be undertaken to ensure a comprehensive examination of eIF2B.

6.6. The impact of altering the levels of cellular Ptdins(4)P on translational control

Two independent studies reported that the eIF2B body may be membrane bound (Campbell et al., 2005, Browne et al., 2013). In light of the observed interactions between eIF2B and Mst27p, Erp4p and Sac1p, it was expected that these putative membrane proteins may tether the eIF2B body to an organelle. To investigate this, gene fusions were produced between the MPs and the monomeric RFP, mKate2. Exogenously expressed mKate2-tagged MPs did not specifically co-localise with eIF2B. Absence of a single MP did not affect the formation of eIF2B bodies. Therefore, in this study, we conclude that eIF2B does not have stable associations with Mst27p, Erp4p or Sac1p.

Interestingly, deletion of the PI(4) phosphatase Sac1p led to similar effects of temperature sensitive PI(4)K Pik1p and Stt4p mutants, which lead to the accumulation of 80S monosomes (Cameroni et al., 2006). In this instance, there is strong evidence to suggest translation is attenuated independent of eIF2B. Upon dephosphorylation, eIF4E binding proteins (4E-BPs) can also regulate global protein synthesis by attenuating the interaction between eIF4E and the 5' cap structure on

mRNA. In line with published data, we propose the phosphorylation status of the 4E-BP Eap1p is dependent upon Ptdins(4)P levels, attenuating protein synthesis under high or low cellular concentrations. Concentrated at the Golgi and plasma membrane, Ptdins(4)P is required for a host of cellular processes including actin-cytoskeleton arrangement, protein trafficking and the secretory system. Abnormal Ptdins(4)P levels may cause a back-log of protein cargo that require transporting, which may then trigger a translational response to inhibit protein production in an attempt to clear the back-log. In line with this idea, defective secretory (Sec) proteins were shown to downregulate translation initiation in an Eap1p-dependent manner (Deloche et al., 2004). Disorganisation of the actin-cytoskeleton has also been suggested to inhibit translation at the initiation stage, although the specific mechanism remains uncertain. Inhibition of G-actin polymerisation through the drug Latrunculin A does not induce eIF2α-P, thus a 4E-BP such as Eap1p may be responsible for attenuating translation instead (Cameroni et al., 2006).

There is a substantial body of evidence to suggest Eap1p is responsible for attenuating translation initiation in response to fluctuating levels of Ptdins(4)P. However a direct link between Eap1p and Sac1p, Stt4p and Pik1p remains to be shown. Addition analysis of double-deletion strains may be an effective approach to elucidate this novel translational control pathway.

7. Conclusions

The work within this thesis has highlighted the importance of eIF2Bα in the formation of eIF2B bodies. We hypothesise that eIF2Bα associates with tetrameric eIF2B complexes to form eIF2B bodies in a two-step process. Mutational analyses highlighted that the localisation of eIF2B is integral for function. Although the localisation of VWM mutants was surprisingly variable, this potentially recapitulated the variability in VWM disease. Intriguingly, data presented here suggests that eIF2B localises to two pools where only one may be subject to regulation. In conclusion, this work further underlines how important eIF2Bα is as the master regulator of eIF2B, and possibly explains why eIF2Bα contains the least VWM mutations out of all eIF2B subunits.

Although the putative membrane proteins Mst27p, Erp4p and Sac1p were shown to associate with eIF2B, a role in the formation of eIF2B bodies was not found. Surprisingly however, the PI(4)P Sac1p was shown to be required for efficient translation initiation. We conclude that the loss of Sac1p is likely to trigger a translational response dependent upon the 4E-BP Eap1p in response to altered Ptdins(4)p content at the Golgi apparatus.

8. References

ABELSON, J. N., SIMON, M. I., GUTHRIE, C. & FINK, G. R. 2004. *Guide to yeast genetics and molecular biology*, Gulf Professional Publishing.

ALBUQUERQUE, C. P., SMOLKA, M. B., PAYNE, S. H., BAFNA, V., ENG, J. & ZHOU, H. 2008. A multidimensional chromatography technology for in-depth phosphoproteome analysis. *Mol Cell Proteomics,* 7**,** 1389-96.

ANAND, M., CHAKRABURTTY, K., MARTON, M. J., HINNEBUSCH, A. G. & KINZY, T. G. 2003. Functional interactions between yeast translation eukaryotic elongation factor (eEF) 1A and eEF3. *J Biol Chem,* 278**,** 6985-91.

ASANO, K., CLAYTON, J., SHALEV, A. & HINNEBUSCH, A. G. 2000. A multifactor complex of eukaryotic initiation factors, eIF1, eIF2, eIF3, eIF5, and initiator tRNA(Met) is an important translation initiation intermediate in vivo. *Genes Dev,* 14**,** 2534-46.

ASHE, M. P., DE LONG, S. K. & SACHS, A. B. 2000. Glucose depletion rapidly inhibits translation initiation in yeast. *Mol Biol Cell,* 11**,** 833-48.

ASHE, M. P., SLAVEN, J. W., DE LONG, S. K., IBRAHIMO, S. & SACHS, A. B. 2001. A novel eIF2B-dependent mechanism of translational control in yeast as a response to fusel alcohols. *Embo j,* 20**,** 6464-74.

AUDHYA, A. & EMR, S. D. 2002. Stt4 PI 4-kinase localizes to the plasma membrane and functions in the Pkc1-mediated MAP kinase cascade. *Dev Cell,* 2**,** 593-605.

AUDHYA, A., FOTI, M. & EMR, S. D. 2000. Distinct roles for the yeast phosphatidylinositol 4-kinases, Stt4p and Pik1p, in secretion, cell growth, and organelle membrane dynamics. *Mol Biol Cell,* 11**,** 2673-89.

BABU, M., VLASBLOM, J., PU, S., GUO, X., GRAHAM, C., BEAN, B. D., BURSTON, H. E., VIZEACOUMAR, F. J., SNIDER, J., PHANSE, S., FONG, V., TAM, Y. Y., DAVEY, M., HNATSHAK, O., BAJAJ, N., CHANDRAN, S., PUNNA, T., CHRISTOPOLOUS, C., WONG, V., YU, A., ZHONG, G., LI, J., STAGLJAR, I., CONIBEAR, E., WODAK, S. J., EMILI, A. & GREENBLATT, J. F. 2012. Interaction landscape of membrane-protein complexes in Saccharomyces cerevisiae. *Nature,* 489**,** 585-9.

BASHKIROV, V. I., SCHERTHAN, H., SOLINGER, J. A., BUERSTEDDE, J. M. & HEYER, W. D. 1997. A mouse cytoplasmic exoribonuclease (mXRN1p) with preference for G4 tetraplex substrates. *J Cell Biol,* 136**,** 761-73.

BAUMANN, N. & PHAM-DINH, D. 2001. Biology of oligodendrocyte and myelin in the mammalian central nervous system. *Physiol Rev,* 81**,** 871-927.

BEN-SHEM, A., JENNER, L., YUSUPOVA, G. & YUSUPOV, M. 2010. Crystal structure of the eukaryotic ribosome. *Science,* 330**,** 1203-9.

BERTRAM, G., BELL, H. A., RITCHIE, D. W., FULLERTON, G. & STANSFIELD, I. 2000. Terminating eukaryote translation: domain 1 of release factor eRF1 functions in stop codon recognition. *Rna,* 6**,** 1236-47.

BERTRAND, E., CHARTRAND, P., SCHAEFER, M., SHENOY, S. M., SINGER, R. H. & LONG, R. M. 1998. Localization of ASH1 mRNA particles in living yeast. *Mol Cell,* 2**,** 437-45.

BOESEN, T., MOHAMMAD, S. S., PAVITT, G. D. & ANDERSEN, G. R. 2004. Structure of the catalytic fragment of translation initiation factor 2B and identification of a critically important catalytic residue. *J Biol Chem,* 279**,** 10584-92.

BOGORAD, A. M., LIN, K. Y. & MARINTCHEV, A. 2017. Novel mechanisms of eIF2B action and regulation by eIF2alpha phosphorylation. *Nucleic Acids Res,* 45**,** 11962-11979.

BOGORAD, A. M., XIA, B., SANDOR, D. G., MAMONOV, A. B., CAFARELLA, T. R., JEHLE, S., VAJDA, S., KOZAKOV, D. & MARINTCHEV, A. 2014. Insights into the architecture of the eIF2Balpha/beta/delta regulatory subcomplex. *Biochemistry,* 53**,** 3432-45.

BROWNE, C. M., SAMIR, P., FITES, J. S., VILLARREAL, S. A. & LINK, A. J. 2013. The yeast eukaryotic translation initiation factor 2B translation initiation complex interacts with the fatty acid synthesis enzyme YBR159W and endoplasmic reticulum membranes. *Mol Cell Biol,* 33**,** 1041-56.

BRYKSIN, A. V. & MATSUMURA, I. 2010. Overlap extension PCR cloning: a simple and reliable way to create recombinant plasmids. *Biotechniques,* 48**,** 463-5.

BUGIANI, M., BOOR, I., POWERS, J. M., SCHEPER, G. C. & VAN DER KNAAP, M. S. 2010. Leukoencephalopathy with vanishing white matter: a review. *J Neuropathol Exp Neurol,* 69**,** 987-96.

BUGIANI, M., BOOR, I., VAN KOLLENBURG, B., POSTMA, N., POLDER, E., VAN BERKEL, C., VAN KESTEREN, R. E., WINDREM, M. S., HOL, E. M., SCHEPER, G. C., GOLDMAN, S. A. & VAN DER KNAAP, M. S. 2011. Defective glial maturation in vanishing white matter disease. *J Neuropathol Exp Neurol,* 70**,** 69-82.

CAMERONI, E., DE VIRGILIO, C. & DELOCHE, O. 2006. Phosphatidylinositol 4-phosphate is required for translation initiation in Saccharomyces cerevisiae. *J Biol Chem,* 281**,** 38139-49.

CAMPBELL, S. G., HOYLE, N. P. & ASHE, M. P. 2005. Dynamic cycling of eIF2 through a large eIF2B-containing cytoplasmic body: implications for translation control. *J Cell Biol,* 170**,** 925-34.

CASTELLI, L. M., LUI, J., CAMPBELL, S. G., ROWE, W., ZEEF, L. A., HOLMES, L. E., HOYLE, N. P., BONE, J., SELLEY, J. N., SIMS, P. F. & ASHE, M. P. 2011. Glucose depletion inhibits translation initiation via eIF4A loss and subsequent 48S preinitiation complex accumulation, while the pentose phosphate pathway is coordinately up-regulated. *Mol Biol Cell,* 22**,** 3379-93.

CASTELLI, L. M., TALAVERA, D., KERSHAW, C. J., MOHAMMAD-QURESHI, S. S., COSTELLO, J. L., ROWE, W., SIMS, P. F., GRANT, C. M., HUBBARD, S. J., ASHE, M. P. & PAVITT, G. D. 2015. The 4E-BP Caf20p Mediates Both eIF4E-Dependent and Independent Repression of Translation. *PLoS Genet,* 11**,** e1005233.

CHRISTIANSON, T. W., SIKORSKI, R. S., DANTE, M., SHERO, J. H. & HIETER, P. 1992. Multifunctional yeast high-copy-number shuttle vectors. *Gene,* 110**,** 119-22.

COUGOT, N., BABAJKO, S. & SERAPHIN, B. 2004. Cytoplasmic foci are sites of mRNA decay in human cells. *J Cell Biol,* 165**,** 31-40.

CRIDGE, A. G., CASTELLI, L. M., SMIRNOVA, J. B., SELLEY, J. N., ROWE, W., HUBBARD, S. J., MCCARTHY, J. E., ASHE, M. P., GRANT, C. M. & PAVITT, G. D. 2010. Identifying eIF4E-binding protein translationally-controlled transcripts reveals links to mRNAs bound by specific PUF proteins. *Nucleic Acids Res,* 38**,** 8039-50.

CURTAIN, C. C., ALI, F., VOLITAKIS, I., CHERNY, R. A., NORTON, R. S., BEYREUTHER, K., BARROW, C. J., MASTERS, C. L., BUSH, A. I. & BARNHAM, K. J. 2001. Alzheimer's disease amyloid-beta binds copper and zinc to generate an allosterically ordered membrane-penetrating structure containing superoxide dismutase-like subunits. *J Biol Chem,* 276**,** 20466-73.

D'ANGELO, G., VICINANZA, M., DI CAMPLI, A. & DE MATTEIS, M. A. 2008. The multiple roles of PtdIns(4)P -- not just the precursor of PtdIns(4,5)P2. *J Cell Sci,* 121**,** 1955-63.

DELOCHE, O., DE LA CRUZ, J., KRESSLER, D., DOERE, M. & LINDER, P. 2004. A membrane transport defect leads to a rapid attenuation of translation initiation in Saccharomyces cerevisiae. *Mol Cell,* 13**,** 357-66.

DEVER, T. E., FENG, L., WEK, R. C., CIGAN, A. M., DONAHUE, T. F. & HINNEBUSCH, A. G. 1992. Phosphorylation of initiation factor 2 alpha by protein kinase GCN2 mediates gene-specific translational control of GCN4 in yeast. *Cell,* 68**,** 585-96.

DEVER, T. E., KINZY, T. G. & PAVITT, G. D. 2016. Mechanism and Regulation of Protein Synthesis in Saccharomyces cerevisiae. *Genetics,* 203**,** 65-107.

DEY, M., TRIESELMANN, B., LOCKE, E. G., LU, J., CAO, C., DAR, A. C., KRISHNAMOORTHY, T., DONG, J., SICHERI, F. & DEVER, T. E. 2005. PKR and GCN2 kinases and guanine nucleotide exchange factor eukaryotic translation initiation factor 2B (eIF2B) recognize overlapping surfaces on eIF2alpha. *Mol Cell Biol,* 25**,** 3063-75.

DUNN, E. F., HAMMELL, C. M., HODGE, C. A. & COLE, C. N. 2005. Yeast poly(A)-binding protein, Pab1, and PAN, a poly(A) nuclease complex recruited by Pab1, connect mRNA biogenesis to export. *Genes Dev,* 19**,** 90-103.

EDEN, A., VAN NEDERVELDE, L., DRUKKER, M., BENVENISTY, N. & DEBOURG, A. 2001. Involvement of branched-chain amino acid aminotransferases in the production of fusel alcohols during fermentation in yeast. *Appl Microbiol Biotechnol,* 55**,** 296-300.

EYSTATHIOY, T., JAKYMIW, A., CHAN, E. K., SERAPHIN, B., COUGOT, N. & FRITZLER, M. J. 2003. The GW182 protein colocalizes with mRNA degradation associated proteins hDcp1 and hLSm4 in cytoplasmic GW bodies. *Rna,* 9**,** 1171-3.

FAULHAMMER, F., KONRAD, G., BRANKATSCHK, B., TAHIROVIC, S., KNODLER, A. & MAYINGER, P. 2005. Cell growth-dependent coordination of lipid signaling and glycosylation is mediated by interactions between Sac1p and Dpm1p. *J Cell Biol,* 168**,** 185-91.

FERRAIUOLO, M. A., BASAK, S., DOSTIE, J., MURRAY, E. L., SCHOENBERG, D. R. & SONENBERG, N. 2005. A role for the eIF4E-binding protein 4E-T in P-body formation and mRNA decay. *J Cell Biol,* 170**,** 913-24.

FOGLI, A., SCHIFFMANN, R., BERTINI, E., UGHETTO, S., COMBES, P., EYMARD-PIERRE, E., KANESKI, C. R., PINEDA, M., TRONCOSO, M., UZIEL, G., SURTEES, R.,

PUGIN, D., CHAUNU, M. P., RODRIGUEZ, D. & BOESPFLUG-TANGUY, O. 2004a. The effect of genotype on the natural history of eIF2B-related leukodystrophies. *Neurology, 62***,** 1509-17.

FOGLI, A., SCHIFFMANN, R., HUGENDUBLER, L., COMBES, P., BERTINI, E., RODRIGUEZ, D., KIMBALL, S. R. & BOESPFLUG-TANGUY, O. 2004b. Decreased guanine nucleotide exchange factor activity in eIF2B-mutated patients. *Eur J Hum Genet, 12***,** 561-6.

FOGLI, A., WONG, K., EYMARD-PIERRE, E., WENGER, J., BOUFFARD, J. P., GOLDIN, E., BLACK, D. N., BOESPFLUG-TANGUY, O. & SCHIFFMANN, R. 2002. Cree leukoencephalopathy and CACH/VWM disease are allelic at the EIF2B5 locus. *Ann Neurol, 52***,** 506-10.

FORTES, P., INADA, T., PREISS, T., HENTZE, M. W., MATTAJ, I. W. & SACHS, A. B. 2000. The yeast nuclear cap binding complex can interact with translation factor eIF4G and mediate translation initiation. *Mol Cell, 6***,** 191-6.

FOTI, M., AUDHYA, A. & EMR, S. D. 2001. Sac1 lipid phosphatase and Stt4 phosphatidylinositol 4-kinase regulate a pool of phosphatidylinositol 4-phosphate that functions in the control of the actin cytoskeleton and vacuole morphology. *Mol Biol Cell, 12***,** 2396-411.

FUJIMURA, K., SASAKI, A. T. & ANDERSON, P. 2012. Selenite targets eIF4E-binding protein-1 to inhibit translation initiation and induce the assembly of non-canonical stress granules. *Nucleic Acids Res, 40***,** 8099-110.

GHAEMMAGHAMI, S., HUH, W. K., BOWER, K., HOWSON, R. W., BELLE, A., DEPHOURE, N., O'SHEA, E. K. & WEISSMAN, J. S. 2003. Global analysis of protein expression in yeast. *Nature, 425***,** 737-41.

GIETZ, R. D. 2014. Yeast transformation by the LiAc/SS carrier DNA/PEG method. *Methods Mol Biol, 1205***,** 1-12.

GILBERT, W. V., ZHOU, K., BUTLER, T. K. & DOUDNA, J. A. 2007. Cap-independent translation is required for starvation-induced differentiation in yeast. *Science, 317***,** 1224-7.

GILKS, N., KEDERSHA, N., AYODELE, M., SHEN, L., STOECKLIN, G., DEMBER, L. M. & ANDERSON, P. 2004. Stress granule assembly is mediated by prion-like aggregation of TIA-1. *Mol Biol Cell, 15***,** 5383-98.

GOMEZ, E., MOHAMMAD, S. S. & PAVITT, G. D. 2002. Characterization of the minimal catalytic domain within eIF2B: the guanine-nucleotide exchange factor for translation initiation. *EMBO J, 21***,** 5292-301.

GOMEZ, E. & PAVITT, G. D. 2000. Identification of domains and residues within the epsilon subunit of eukaryotic translation initiation factor 2B (eIF2Bepsilon) required for guanine nucleotide exchange reveals a novel activation function promoted by eIF2B complex formation. *Mol Cell Biol, 20***,** 3965-76.

GORDIYENKO, Y., SCHMIDT, C., JENNINGS, M. D., MATAK-VINKOVIC, D., PAVITT, G. D. & ROBINSON, C. V. 2014. eIF2B is a decameric guanine nucleotide exchange factor with a gamma2epsilon2 tetrameric core. *Nat Commun, 5***,** 3902.

HAGHIGHAT, A., MADER, S., PAUSE, A. & SONENBERG, N. 1995. Repression of cap-dependent translation by 4E-binding protein 1: competition with p220 for binding to eukaryotic initiation factor-4E. *Embo j, 14***,** 5701-9.

HANNIG, E. M., WILLIAMS, N. P., WEK, R. C. & HINNEBUSCH, A. G. 1990. The translational activator GCN3 functions downstream from GCN1 and GCN2 in

the regulatory pathway that couples GCN4 expression to amino acid availability in Saccharomyces cerevisiae. *Genetics,* 126**,** 549-62.

HECTOR, R. E., NYKAMP, K. R., DHEUR, S., ANDERSON, J. T., NON, P. J., URBINATI, C. R., WILSON, S. M., MINVIELLE-SEBASTIA, L. & SWANSON, M. S. 2002. Dual requirement for yeast hnRNP Nab2p in mRNA poly(A) tail length control and nuclear export. *Embo j,* 21**,** 1800-10.

HINNEBUSCH, A. G. 1985. A hierarchy of trans-acting factors modulates translation of an activator of amino acid biosynthetic genes in Saccharomyces cerevisiae. *Mol Cell Biol,* 5**,** 2349-60.

HINNEBUSCH, A. G. 1997. Translational regulation of yeast GCN4. A window on factors that control initiator-trna binding to the ribosome. *J Biol Chem,* 272**,** 21661-4.

HODGSON, R. E., **VARANDA, B. A.**, **ASHE, M. P.**, **ALLEN, K. E.** & **CAMPBELL, S. G.** 2018. eIF2B subunits localise to distinct populations of eIF2B bodies that allow for differential regulation by the ISR. *Manuscript in prep.*

HOLZ, M. K., BALLIF, B. A., GYGI, S. P. & BLENIS, J. 2005. mTOR and S6K1 mediate assembly of the translation preinitiation complex through dynamic protein interchange and ordered phosphorylation events. *Cell,* 123**,** 569-80.

HOYLE, N. P. & ASHE, M. P. 2008. Subcellular localization of mRNA and factors involved in translation initiation. *Biochem Soc Trans,* 36**,** 648-52.

HOYLE, N. P., CASTELLI, L. M., CAMPBELL, S. G., HOLMES, L. E. & ASHE, M. P. 2007. Stress-dependent relocalization of translationally primed mRNPs to cytoplasmic granules that are kinetically and spatially distinct from P-bodies. *J Cell Biol,* 179**,** 65-74.

JACKSON, R. & STANDART, N. 2015. The awesome power of ribosome profiling. *Rna,* 21**,** 652-4.

JANG, S. K., KRAUSSLICH, H. G., NICKLIN, M. J., DUKE, G. M., PALMENBERG, A. C. & WIMMER, E. 1988. A segment of the 5' nontranslated region of encephalomyocarditis virus RNA directs internal entry of ribosomes during in vitro translation. *J Virol,* 62**,** 2636-43.

JENNINGS, M. D. & PAVITT, G. D. 2010. eIF5 has GDI activity necessary for translational control by eIF2 phosphorylation. *Nature,* 465**,** 378-81.

JENNINGS, M. D., ZHOU, Y., MOHAMMAD-QURESHI, S. S., BENNETT, D. & PAVITT, G. D. 2013. eIF2B promotes eIF5 dissociation from eIF2*GDP to facilitate guanine nucleotide exchange for translation initiation. *Genes Dev,* 27**,** 2696-707.

KACZOROWSKA, M., KUCZYNSKI, D., JURKIEWICZ, E., SCHEPER, G. C., VAN DER KNAAP, M. S. & JOZWIAK, S. 2006. Acute fright induces onset of symptoms in vanishing white matter disease-case report. *Eur J Paediatr Neurol,* 10**,** 192-3.

KAMATH, A. & CHAKRABURTTY, K. 1989. Role of yeast elongation factor 3 in the elongation cycle. *J Biol Chem,* 264**,** 15423-8.

KAMINSKI, A., HOWELL, M. T. & JACKSON, R. J. 1990. Initiation of encephalomyocarditis virus RNA translation: the authentic initiation site is not selected by a scanning mechanism. *Embo j,* 9**,** 3753-9.

KANTOR, L., HARDING, H. P., RON, D., SCHIFFMANN, R., KANESKI, C. R., KIMBALL, S. R. & ELROY-STEIN, O. 2005. Heightened stress response in primary fibroblasts

expressing mutant eIF2B genes from CACH/VWM leukodystrophy patients. *Hum Genet,* 118**,** 99-106.

KAPP, L. D. & LORSCH, J. R. 2004. The molecular mechanics of eukaryotic translation. *Annu Rev Biochem,* 73**,** 657-704.

KASHIWAGI, K., ITO, T. & YOKOYAMA, S. 2014. Structural insight into the eIF2-eIF2B interaction. *Acta Crystallographica Section A,* 70**,** C1390.

KASHIWAGI, K., TAKAHASHI, M., NISHIMOTO, M., HIYAMA, T. B., HIGO, T., UMEHARA, T., SAKAMOTO, K., ITO, T. & YOKOYAMA, S. 2016. Crystal structure of eukaryotic translation initiation factor 2B. *Nature,* 531**,** 122-5.

KEDERSHA, N., CHEN, S., GILKS, N., LI, W., MILLER, I. J., STAHL, J. & ANDERSON, P. 2002. Evidence that ternary complex (eIF2-GTP-tRNA(i)(Met))-deficient preinitiation complexes are core constituents of mammalian stress granules. *Mol Biol Cell,* 13**,** 195-210.

KEDERSHA, N. L., GUPTA, M., LI, W., MILLER, I. & ANDERSON, P. 1999. RNA-binding proteins TIA-1 and TIAR link the phosphorylation of eIF-2 alpha to the assembly of mammalian stress granules. *J Cell Biol,* 147**,** 1431-42.

KNODLER, A., KONRAD, G. & MAYINGER, P. 2008. Expression of yeast lipid phosphatase Sac1p is regulated by phosphatidylinositol-4-phosphate. *BMC Mol Biol,* 9**,** 16.

KOMAR, A. A. & HATZOGLOU, M. 2005. Internal ribosome entry sites in cellular mRNAs: mystery of their existence. *J Biol Chem,* 280**,** 23425-8.

LANDERS, S. M., GALLAS, M. R., LITTLE, J. & LONG, R. M. 2009. She3p possesses a novel activity required for ASH1 mRNA localization in Saccharomyces cerevisiae. *Eukaryot Cell,* 8**,** 1072-83.

LEE, S., LIM, W. A. & THORN, K. S. 2013. Improved blue, green, and red fluorescent protein tagging vectors for S. cerevisiae. *PLoS One,* 8**,** e67902.

LEEGWATER, P. A. J., VERMEULEN, G., KONST, A. A. M., NAIDU, S., MULDERS, J., VISSER, A., KERSBERGEN, P., MOBACH, D., FONDS, D., VAN BERKEL, C. G. M., LEMMERS, R. J. L. F., FRANTS, R. R., OUDEJANS, C. B. M., SCHUTGENS, R. B. H., PRONK, J. C. & VAN DER KNAAP, M. S. 2001. Subunits of the translation initiation factor eIF2B are mutant in leukoencephalopathy with vanishing white matter. *Nat Genet,* 29**,** 383-388.

LEFEBVRE, A. K., KORNEEVA, N. L., TRUTSCHL, M., CVEK, U., DUZAN, R. D., BRADLEY, C. A., HERSHEY, J. W. & RHOADS, R. E. 2006. Translation initiation factor eIF4G-1 binds to eIF3 through the eIF3e subunit. *J Biol Chem,* 281**,** 22917-32.

LIU, R., VAN DER LEI, H. D., WANG, X., WORTHAM, N. C., TANG, H., VAN BERKEL, C. G., MUFUNDE, T. A., HUANG, W., VAN DER KNAAP, M. S., SCHEPER, G. C. & PROUD, C. G. 2011. Severity of vanishing white matter disease does not correlate with deficits in eIF2B activity or the integrity of eIF2B complexes. *Hum Mutat,* 32**,** 1036-45.

LU, P., VOGEL, C., WANG, R., YAO, X. & MARCOTTE, E. M. 2007. Absolute protein expression profiling estimates the relative contributions of transcriptional and translational regulation. *Nat Biotechnol,* 25**,** 117-24.

MAROM, L., ULITSKY, I., CABILLY, Y., SHAMIR, R. & ELROY-STEIN, O. 2011. A point mutation in translation initiation factor eIF2B leads to function--and time-specific changes in brain gene expression. *PLoS One,* 6**,** e26992.

MARZIOCH, M., HENTHORN, D. C., HERRMANN, J. M., WILSON, R., THOMAS, D. Y., BERGERON, J. J., SOLARI, R. C. & ROWLEY, A. 1999. Erp1p and Erp2p, partners for Emp24p and Erv25p in a yeast p24 complex. *Mol Biol Cell,* 10**,** 1923-38.

MATSUO, R., KUBOTA, H., OBATA, T., KITO, K., OTA, K., KITAZONO, T., IBAYASHI, S., SASAKI, T., IIDA, M. & ITO, T. 2005. The yeast eIF4E-associated protein Eap1p attenuates GCN4 translation upon TOR-inactivation. *FEBS Lett,* 579**,** 2433-8.

MCDONALD, K. K., AULAS, A., DESTROISMAISONS, L., PICKLES, S., BELEAC, E., CAMU, W., ROULEAU, G. A. & VANDE VELDE, C. 2011. TAR DNA-binding protein 43 (TDP-43) regulates stress granule dynamics via differential regulation of G3BP and TIA-1. *Hum Mol Genet,* 20**,** 1400-10.

MCTIGUE, D. M. & TRIPATHI, R. B. 2008. The life, death, and replacement of oligodendrocytes in the adult CNS. *J Neurochem,* 107**,** 1-19.

MERRICK, W. C. 2004. Cap-dependent and cap-independent translation in eukaryotic systems. *Gene,* 332**,** 1-11.

MIYASAKA, H. 1999. The positive relationship between codon usage bias and translation initiation AUG context in Saccharomyces cerevisiae. *Yeast,* 15**,** 633-7.

MOHAMMAD-QURESHI, S. S., HADDAD, R., HEMINGWAY, E. J., RICHARDSON, J. P. & PAVITT, G. D. 2007. Critical contacts between the eukaryotic initiation factor 2B (eIF2B) catalytic domain and both eIF2beta and -2gamma mediate guanine nucleotide exchange. *Mol Cell Biol,* 27**,** 5225-34.

NATARAJAN, K., MEYER, M. R., JACKSON, B. M., SLADE, D., ROBERTS, C., HINNEBUSCH, A. G. & MARTON, M. J. 2001. Transcriptional profiling shows that Gcn4p is a master regulator of gene expression during amino acid starvation in yeast. *Mol Cell Biol,* 21**,** 4347-68.

NOVOA, I., ZENG, H., HARDING, H. P. & RON, D. 2001. Feedback inhibition of the unfolded protein response by GADD34-mediated dephosphorylation of eIF2alpha. *J Cell Biol,* 153**,** 1011-22.

PAUSE, A., BELSHAM, G. J., GINGRAS, A. C., DONZE, O., LIN, T. A., LAWRENCE, J. C., JR. & SONENBERG, N. 1994. Insulin-dependent stimulation of protein synthesis by phosphorylation of a regulator of 5'-cap function. *Nature,* 371**,** 762-7.

PAVITT, G. D. 2005. eIF2B, a mediator of general and gene-specific translational control. *Biochem Soc Trans,* 33**,** 1487-92.

PAVITT, G. D. & PROUD, C. G. 2009. Protein synthesis and its control in neuronal cells with a focus on vanishing white matter disease. *Biochem Soc Trans,* 37**,** 1298-310.

PAVITT, G. D., RAMAIAH, K. V., KIMBALL, S. R. & HINNEBUSCH, A. G. 1998. eIF2 independently binds two distinct eIF2B subcomplexes that catalyze and regulate guanine-nucleotide exchange. *Genes Dev,* 12**,** 514-26.

PAVITT, G. D., YANG, W. & HINNEBUSCH, A. G. 1997. Homologous segments in three subunits of the guanine nucleotide exchange factor eIF2B mediate translational regulation by phosphorylation of eIF2. *Mol Cell Biol,* 17**,** 1298-313.

PELLETIER, J. & SONENBERG, N. 1988. Internal initiation of translation of eukaryotic mRNA directed by a sequence derived from poliovirus RNA. *Nature,* 334**,** 320-5.

PESTOVA, T. V., HELLEN, C. U. & SHATSKY, I. N. 1996. Canonical eukaryotic initiation factors determine initiation of translation by internal ribosomal entry. *Mol Cell Biol,* 16**,** 6859-69.

PETROVSKA, I., NUSKE, E., MUNDER, M. C., KULASEGARAN, G., MALINOVSKA, L., KROSCHWALD, S., RICHTER, D., FAHMY, K., GIBSON, K., VERBAVATZ, J. M. & ALBERTI, S. 2014. Filament formation by metabolic enzymes is a specific adaptation to an advanced state of cellular starvation. *Elife*.

PHAM, F. H., SUGDEN, P. H. & CLERK, A. 2000. Regulation of protein kinase B and 4E-BP1 by oxidative stress in cardiac myocytes. *Circ Res,* 86**,** 1252-8.

PREIS, A., HEUER, A., BARRIO-GARCIA, C., HAUSER, A., EYLER, D. E., BERNINGHAUSEN, O., GREEN, R., BECKER, T. & BECKMANN, R. 2014. Cryoelectron microscopic structures of eukaryotic translation termination complexes containing eRF1-eRF3 or eRF1-ABCE1. *Cell Rep,* 8**,** 59-65.

PRONK, J. C., VAN KOLLENBURG, B., SCHEPER, G. C. & VAN DER KNAAP, M. S. 2006. Vanishing white matter disease: a review with focus on its genetics. *Ment Retard Dev Disabil Res Rev,* 12**,** 123-8.

PROUDFOOT, N. J., FURGER, A. & DYE, M. J. 2002. Integrating mRNA processing with transcription. *Cell,* 108**,** 501-12.

PYRONNET, S., IMATAKA, H., GINGRAS, A. C., FUKUNAGA, R., HUNTER, T. & SONENBERG, N. 1999. Human eukaryotic translation initiation factor 4G (eIF4G) recruits mnk1 to phosphorylate eIF4E. *Embo j,* 18**,** 270-9.

RICHARDSON, J. P., MOHAMMAD, S. S. & PAVITT, G. D. 2004. Mutations causing childhood ataxia with central nervous system hypomyelination reduce eukaryotic initiation factor 2B complex formation and activity. *Mol Cell Biol,* 24**,** 2352-63.

RODNINA, M. V., SAVELSBERGH, A., KATUNIN, V. I. & WINTERMEYER, W. 1997. Hydrolysis of GTP by elongation factor G drives tRNA movement on the ribosome. *Nature,* 385**,** 37-41.

ROWLANDS, A. G., PANNIERS, R. & HENSHAW, E. C. 1988. The catalytic mechanism of guanine nucleotide exchange factor action and competitive inhibition by phosphorylated eukaryotic initiation factor 2. *J Biol Chem,* 263**,** 5526-33.

ROY, A. & LEVINE, T. P. 2004. Multiple pools of phosphatidylinositol 4-phosphate detected using the pleckstrin homology domain of Osh2p. *J Biol Chem,* 279**,** 44683-9.

RUSSELL, J. E., MORALES, J. & LIEBHABER, S. A. 1997. The role of mRNA stability in the control of globin gene expression. *Prog Nucleic Acid Res Mol Biol,* 57**,** 249-87.

SAINT-GEORGES, Y., GARCIA, M., DELAVEAU, T., JOURDREN, L., LE CROM, S., LEMOINE, S., TANTY, V., DEVAUX, F. & JACQ, C. 2008. Yeast mitochondrial biogenesis: a role for the PUF RNA-binding protein Puf3p in mRNA localization. *PLoS One,* 3**,** e2293.

SALAS-MARCO, J. & BEDWELL, D. M. 2004. GTP hydrolysis by eRF3 facilitates stop codon decoding during eukaryotic translation termination. *Mol Cell Biol,* 24**,** 7769-78.

SANDMANN, T., HERRMANN, J. M., DENGJEL, J., SCHWARZ, H. & SPANG, A. 2003. Suppression of coatomer mutants by a new protein family with COPI and COPII binding motifs in Saccharomyces cerevisiae. *Mol Biol Cell,* 14**,** 3097-113.

SCHENCK, M., CARPINTEIRO, A., GRASSME, H., LANG, F. & GULBINS, E. 2007. Ceramide: physiological and pathophysiological aspects. *Arch Biochem Biophys,* 462**,** 171-5.

SCHIFFMANN, R., FOGLI, A., VAN DER KNAAP, M. S. & BOESPFLUG-TANGUY, O. 2012. Childhood ataxia with central nervous system hypomyelination/vanishing white matter.

SCHNEIDER-POETSCH, T., JU, J., EYLER, D. E., DANG, Y., BHAT, S., MERRICK, W. C., GREEN, R., SHEN, B. & LIU, J. O. 2010. Inhibition of eukaryotic translation elongation by cycloheximide and lactimidomycin. *Nat Chem Biol,* 6**,** 209-217.

SHETH, U. & PARKER, R. 2003. Decapping and decay of messenger RNA occur in cytoplasmic processing bodies. *Science,* 300**,** 805-8.

SHIMADA, S., SHIMOJIMA, K., SANGU, N., HOSHINO, A., HACHIYA, Y., OHTO, T., HASHI, Y., NISHIDA, K., MITANI, M., KINJO, S., TSURUSAKI, Y., MATSUMOTO, N., MORIMOTO, M. & YAMAMOTO, T. 2015. Mutations in the genes encoding eukaryotic translation initiation factor 2B in Japanese patients with vanishing white matter disease. *Brain Dev*.

SHOEMAKER, C. J. & GREEN, R. 2011. Kinetic analysis reveals the ordered coupling of translation termination and ribosome recycling in yeast. *Proc Natl Acad Sci U S A,* 108**,** E1392-8.

SIL, A. & HERSKOWITZ, I. 1996. Identification of asymmetrically localized determinant, Ash1p, required for lineage-specific transcription of the yeast HO gene. *Cell,* 84**,** 711-22.

SINGH, C. R., LEE, B., UDAGAWA, T., MOHAMMAD-QURESHI, S. S., YAMAMOTO, Y., PAVITT, G. D. & ASANO, K. 2006. An eIF5/eIF2 complex antagonizes guanine nucleotide exchange by eIF2B during translation initiation. *The EMBO Journal,* 25**,** 4537-4546.

SINGH, I., PAHAN, K., KHAN, M. & SINGH, A. K. 1998. Cytokine-mediated induction of ceramide production is redox-sensitive. Implications to proinflammatory cytokine-mediated apoptosis in demyelinating diseases. *J Biol Chem,* 273**,** 20354-62.

SKABKIN, M. A., SKABKINA, O. V., DHOTE, V., KOMAR, A. A., HELLEN, C. U. & PESTOVA, T. V. 2010. Activities of Ligatin and MCT-1/DENR in eukaryotic translation initiation and ribosomal recycling. *Genes Dev,* 24**,** 1787-801.

SMITH, R. W. P., ANDERSON, R. C., LARRALDE, O., SMITH, J. W. S., GORGONI, B., RICHARDSON, W. A., MALIK, P., GRAHAM, S. V. & GRAY, N. K. 2017. Viral and cellular mRNA-specific activators harness PABP and eIF4G to promote translation initiation downstream of cap binding. *Proc Natl Acad Sci U S A,* 114**,** 6310-6315.

SOKABE, M., FRASER, C. S. & HERSHEY, J. W. 2012. The human translation initiation multi-factor complex promotes methionyl-tRNAi binding to the 40S ribosomal subunit. *Nucleic Acids Res,* 40**,** 905-13.

STRAHL, T., HAMA, H., DEWALD, D. B. & THORNER, J. 2005. Yeast phosphatidylinositol 4-kinase, Pik1, has essential roles at the Golgi and in the nucleus. *J Cell Biol,* 171**,** 967-79.

SUDHAKAR, A., KRISHNAMOORTHY, T., JAIN, A., CHATTERJEE, U., HASNAIN, S. E., KAUFMAN, R. J. & RAMAIAH, K. V. 1999. Serine 48 in initiation factor 2 alpha

(eIF2 alpha) is required for high-affinity interaction between eIF2 alpha(P) and eIF2B. *Biochemistry,* 38**,** 15398-405.

SUKARIEH, R., SONENBERG, N. & PELLETIER, J. 2009. The eIF4E-binding proteins are modifiers of cytoplasmic eIF4E relocalization during the heat shock response. *Am J Physiol Cell Physiol,* 296**,** C1207-17.

SVITKIN, Y. V., PAUSE, A., HAGHIGHAT, A., PYRONNET, S., WITHERELL, G., BELSHAM, G. J. & SONENBERG, N. 2001. The requirement for eukaryotic initiation factor 4A (eIF4A) in translation is in direct proportion to the degree of mRNA 5' secondary structure. *Rna,* 7**,** 382-94.

SWANEY, D. L., BELTRAO, P., STARITA, L., GUO, A., RUSH, J., FIELDS, S., KROGAN, N. J. & VILLEN, J. 2013. Global analysis of phosphorylation and ubiquitylation cross-talk in protein degradation. *Nat Methods,* 10**,** 676-82.

TAKANO, K., TSUYUSAKI, Y., SATO, M., TAKAGI, M., ANZAI, R., OKUDA, M., IAI, M., YAMASHITA, S., OKABE, T., AIDA, N., TSURUSAKI, Y., SAITSU, H., MATSUMOTO, N. & OSAKA, H. 2015. A Japanese girl with an early-infantile onset vanishing white matter disease resembling Cree leukoencephalopathy. *Brain Dev,* 37**,** 638-42.

TARUN, S. Z., JR. & SACHS, A. B. 1996. Association of the yeast poly(A) tail binding protein with translation initiation factor eIF-4G. *Embo j,* 15**,** 7168-77.

TAYLOR, E. J., CAMPBELL, S. G., GRIFFITHS, C. D., REID, P. J., SLAVEN, J. W., HARRISON, R. J., SIMS, P. F., PAVITT, G. D., DELNERI, D. & ASHE, M. P. 2010. Fusel alcohols regulate translation initiation by inhibiting eIF2B to reduce ternary complex in a mechanism that may involve altering the integrity and dynamics of the eIF2B body. *Mol Biol Cell,* 21**,** 2202-16.

THARUN, S. & PARKER, R. 2001. Targeting an mRNA for decapping: displacement of translation factors and association of the Lsm1p-7p complex on deadenylated yeast mRNAs. *Mol Cell,* 8**,** 1075-83.

TOKURIKI, N. & TAWFIK, D. S. 2009. Stability effects of mutations and protein evolvability. *Curr Opin Struct Biol,* 19**,** 596-604.

TRIANA-ALONSO, F. J., CHAKRABURTTY, K. & NIERHAUS, K. H. 1995. The elongation factor 3 unique in higher fungi and essential for protein biosynthesis is an E site factor. *J Biol Chem,* 270**,** 20473-8.

TSAI, J. C., MILLER-VEDAM, L. E., ANAND, A. A., JAISHANKAR, P., NGUYEN, H. C., RENSLO, A. R., FROST, A. & WALTER, P. 2018. Structure of the nucleotide exchange factor eIF2B reveals mechanism of memory-enhancing molecule. *Science,* 359.

UNBEHAUN, A., BORUKHOV, S. I., HELLEN, C. U. & PESTOVA, T. V. 2004. Release of initiation factors from 48S complexes during ribosomal subunit joining and the link between establishment of codon-anticodon base-pairing and hydrolysis of eIF2-bound GTP. *Genes Dev,* 18**,** 3078-93.

URAKOV, V. N., VALOUEV, I. A., KOCHNEVA-PERVUKHOVA, N. V., PACKEISER, A. N., VISHNEVSKY, A. Y., GLEBOV, O. O., SMIRNOV, V. N. & TER-AVANESYAN, M. D. 2006. N-terminal region of Saccharomyces cerevisiae eRF3 is essential for the functioning of the eRF1/eRF3 complex beyond translation termination. *BMC Mol Biol,* 7**,** 34.

VAN DER KNAAP, M. S., BARTH, P. G., GABREELS, F. J., FRANZONI, E., BEGEER, J. H., STROINK, H., ROTTEVEEL, J. J. & VALK, J. 1997. A new leukoencephalopathy with vanishing white matter. *Neurology,* 48**,** 845-55.

VAN DER KNAAP, M. S., VAN BERKEL, C. G., HERMS, J., VAN COSTER, R., BAETHMANN, M., NAIDU, S., BOLTSHAUSER, E., WILLEMSEN, M. A., PLECKO, B., HOFFMANN, G. F., PROUD, C. G., SCHEPER, G. C. & PRONK, J. C. 2003. eIF2B-related disorders: antenatal onset and involvement of multiple organs. *Am J Hum Genet,* 73**,** 1199-207.

VAN DER LEI, H. D., VAN BERKEL, C. G., VAN WIERINGEN, W. N., BRENNER, C., FEIGENBAUM, A., MERCIMEK-MAHMUTOGLU, S., PHILIPPART, M., TATLI, B., WASSMER, E., SCHEPER, G. C. & VAN DER KNAAP, M. S. 2010. Genotype-phenotype correlation in vanishing white matter disease. *Neurology,* 75**,** 1555-9.

VAN DIJK, E., COUGOT, N., MEYER, S., BABAJKO, S., WAHLE, E. & SERAPHIN, B. 2002. Human Dcp2: a catalytically active mRNA decapping enzyme located in specific cytoplasmic structures. *Embo j,* 21**,** 6915-24.

VAN KOLLENBURG, B., VAN DIJK, J., GARBERN, J., THOMAS, A. A., SCHEPER, G. C., POWERS, J. M. & VAN DER KNAAP, M. S. 2006. Glia-specific activation of all pathways of the unfolded protein response in vanishing white matter disease. *J Neuropathol Exp Neurol,* 65**,** 707-15.

VATTEM, K. M. & WEK, R. C. 2004. Reinitiation involving upstream ORFs regulates ATF4 mRNA translation in mammalian cells. *Proc Natl Acad Sci U S A,* 101**,** 11269-74.

VISA, N., IZAURRALDE, E., FERREIRA, J., DANEHOLT, B. & MATTAJ, I. W. 1996. A nuclear cap-binding complex binds Balbiani ring pre-mRNA cotranscriptionally and accompanies the ribonucleoprotein particle during nuclear export. *J Cell Biol,* 133**,** 5-14.

VON DER HAAR, T. 2008. A quantitative estimation of the global translational activity in logarithmically growing yeast cells. *BMC Syst Biol,* 2**,** 87.

WACHTEL, C. & MANLEY, J. L. 2009. Splicing of mRNA precursors: the role of RNAs and proteins in catalysis. *Mol Biosyst,* 5**,** 311-6.

WALTER, P. & RON, D. 2011. The unfolded protein response: from stress pathway to homeostatic regulation. *Science,* 334**,** 1081-1086.

WANG, X. Q. & ROTHNAGEL, J. A. 2004. 5'-untranslated regions with multiple upstream AUG codons can support low-level translation via leaky scanning and reinitiation. *Nucleic Acids Res,* 32**,** 1382-91.

WANG, Z. & ZHANG, J. 2011. Impact of gene expression noise on organismal fitness and the efficacy of natural selection. *Proc Natl Acad Sci U S A,* 108**,** E67-76.

WARNER, J. R., KNOPF, P. M. & RICH, A. 1963. A multiple ribosomal structure in protein synthesis. *Proc Natl Acad Sci U S A,* 49**,** 122-9.

WELLS, S. E., HILLNER, P. E., VALE, R. D. & SACHS, A. B. 1998. Circularization of mRNA by eukaryotic translation initiation factors. *Mol Cell,* 2**,** 135-40.

WELSH, G. I., MILLER, C. M., LOUGHLIN, A. J., PRICE, N. T. & PROUD, C. G. 1998. Regulation of eukaryotic initiation factor eIF2B: glycogen synthase kinase-3 phosphorylates a conserved serine which undergoes dephosphorylation in response to insulin. *FEBS Lett,* 421**,** 125-30.

WHEELER, J. R., MATHENY, T., JAIN, S., ABRISCH, R. & PARKER, R. 2016. Distinct stages in stress granule assembly and disassembly. *Elife,* 5.

WILLIAMS, D. D., PRICE, N. T., LOUGHLIN, A. J. & PROUD, C. G. 2001. Characterization of the mammalian initiation factor eIF2B complex as a GDP dissociation stimulator protein. *J Biol Chem,* 276**,** 24697-703.

WINDER, S. J. & AYSCOUGH, K. R. 2005. Actin-binding proteins. *J Cell Sci,* 118**,** 651-4.

WOODS, Y. L., COHEN, P., BECKER, W., JAKES, R., GOEDERT, M., WANG, X. & PROUD, C. G. 2001. The kinase DYRK phosphorylates protein-synthesis initiation factor eIF2Bepsilon at Ser539 and the microtubule-associated protein tau at Thr212: potential role for DYRK as a glycogen synthase kinase 3-priming kinase. *Biochem J,* 355**,** 609-15.

WORTHAM, N. C., MARTINEZ, M., GORDIYENKO, Y., ROBINSON, C. V. & PROUD, C. G. 2014. Analysis of the subunit organization of the eIF2B complex reveals new insights into its structure and regulation. *FASEB J,* 28**,** 2225-37.

WORTHAM, N. C. & PROUD, C. G. 2015. Biochemical effects of mutations in the gene encoding the alpha subunit of eukaryotic initiation factor (eIF) 2B associated with Vanishing White Matter disease. *BMC Med Genet,* 16**,** 64.

WORTHAM, N. C., STEWART, J. D., HARRIS, S., COLDWELL, M. J. & PROUD, C. G. 2016. Stoichiometry of the eIF2B complex is maintained by mutual stabilization of subunits. *Biochem J,* 473**,** 571-80.

YOSHIKAWA, K., TANAKA, T., IDA, Y., FURUSAWA, C., HIRASAWA, T. & SHIMIZU, H. 2011. Comprehensive phenotypic analysis of single-gene deletion and overexpression strains of Saccharomyces cerevisiae. *Yeast,* 28**,** 349-61.

ZEWAIL, A., XIE, M. W., XING, Y., LIN, L., ZHANG, P. F., ZOU, W., SAXE, J. P. & HUANG, J. 2003. Novel functions of the phosphatidylinositol metabolic pathway discovered by a chemical genomics screen with wortmannin. *Proc Natl Acad Sci U S A,* 100**,** 3345-50.

ZHANG, H., DAI, L., CHEN, N., ZANG, L., LENG, X., DU, L., WANG, J., JIANG, Y., ZHANG, F., WU, X. & WU, Y. 2015. Fifteen novel EIF2B1-5 mutations identified in Chinese children with leukoencephalopathy with vanishing white matter and a long term follow-up. *PLoS One,* 10**,** e0118001.

ZHAO, J., HYMAN, L. & MOORE, C. 1999. Formation of mRNA 3' ends in eukaryotes: mechanism, regulation, and interrelationships with other steps in mRNA synthesis. *Microbiol Mol Biol Rev,* 63**,** 405-45.

ZIPOR, G., HAIM-VILMOVSKY, L., GELIN-LICHT, R., GADIR, N., BROCARD, C. & GERST, J. E. 2009. Localization of mRNAs coding for peroxisomal proteins in the yeast, Saccharomyces cerevisiae. *Proc Natl Acad Sci U S A,* 106**,** 19848-53.

ZYRYANOVA, A. F., WEIS, F., FAILLE, A., ALARD, A. A., CRESPILLO-CASADO, A., SEKINE, Y., HARDING, H. P., ALLEN, F., PARTS, L., FROMONT, C., FISCHER, P. M., WARREN, A. J. & RON, D. 2018. Binding of ISRIB reveals a regulatory site in the nucleotide exchange factor eIF2B. *Science,* 359**,** 1533-1536.